IDŐJÁRÁS

QUARTERLY JOURNAL
OF THE HUNGARIAN METEOROLOGICAL SERVICE

CONTENTS

VOL. 101 * NO. 1 * JANUARY–MARCH 1997

IDŐJÁRÁS

Quarterly Journal of the Hungarian Meteorological Service

Editorial Office: P.O. Box 39, H-1675 Budapest, Hungary or
Gilice tér 39, H-1181 Budapest, Hungary
E-mail: gmajor@met.hu or *antal@met.hu*
Fax: (36-1) 290-7387

Subscription by

mail: IDŐJÁRÁS, P.O. Box 39, H-1675 Budapest, Hungary;
E-mail: gmajor@met.hu or *antal@met.hu*; *Fax: (36-1) 290-7387*

IDŐJÁRÁS

Quarterly Journal of the Hungarian Meteorological Service
Vol. 101, No. 1, January–March 1997, pp. 1–15

A one-dimensional thermal numerical model of morning convective boundary layer development

R. Mitzeva, St. Evtimov and **S. Doychinska**

Department of Meteorology, Faculty of Physics, University of Sofia,
5, J. Bourchier, Sofia–1126, Bulgaria
E-mail: rumypm@phys.uni-sofia.bg

(Manuscript received 12 December 1995; in final form 13 November 1996)

Abstract—A one dimensional numerical model of the evolution of the morning *convective boundary layer* (CBL) is developed. The basic assumption is that heat in the CBL is transported mainly by discrete convective elements — thermals. A governing equation for the vertical profile of the horizontal-mean potential temperature is derived by partitioning the CBL at each level and at each moment in two domains, one covered with thermals and the other occupied by downdrafts. The problem is closed by assuming that the thermals evolve as individual ones interacting with the environmental air by buoyancy and entrainment mechanisms.

The model was tested for both simulated and measured initial temperature soundings. The calculations demonstrate a two-stage type formation of the CBL. During the first stage the potential temperature lapse rate gradually decreases and the temperature inversion erodes in a layer of growing thickness. The CBL is formed only in the second stage and it occupies at once the layer of the already destroyed inversion. After that only its height increases. The calculations with different magnitudes of the radiation heating indicate that the CBL formation is possible only if that magnitude exceeds a critical value. Sensitivity studies were performed for two types of size distribution of thermals at the earth's surface.

Key-words: convective boundary layer, thermals, numerical model, nocturnal ground temperature inversion.

1. Introduction

Analyzing his own atmospheric measurements of the *convective boundary layer* (CBL) *Telford* (1992) concluded that convective transport is a process where isolated thermal elements carry practically all the quantities such as heat and moisture from one level to another. Observational studies of *Lenschow* and *Stephens* (1982), *Young* (1988) and *Hunt et al.* (1988) clearly indicate a 'thermal-like' structure of the CBL. According to these measurements thermals

are buoyancy-driven convective eddies which generate most of the turbulence in the unstable atmospheric boundary layer. The CBL is composed of thermal updrafts and their compensating environmental downdraft. A number of numerical models of the CBL development (*Telford*, 1966; *Manton,* 1975; *Andreev* and *Ganev,* 1981; *Roisin,* 1982; *Chatfield* and *Brost* 1987) realized these concepts.

This paper presents a one-dimensional numerical model of the morning CBL evolution due to the heat transfer by thermals. The thermals originate near the earth's surface during the morning hours when the ground is strongly heated by the solar radiation. Therefore, the model describes the penetrative convection in presence of a time-dependent heating forcing. In this case the turbulence is buoyancy-driven and the model is valid in the case of strong insolation and absence of wind and clouds.

The theoretical background and the derivation of the governing equations of the model are given in Section 2. The numerical scheme is presented in Section 3. The results of the numerical simulations with the model are given in Section 4. They are discussed in the final section of the paper.

2. Model description

The basic idea of the model is that heat in the CBL is transfered by discrete convective elements (buoyant parcels or thermals) and compensating environmental downdrafts. It means that at the parametrization of the CBL with respect to the velocity field the CBL has to be separated into updrafts or thermals, which are convective elements originating near the surface, and downdrafts — a domain outside the updrafts with a compensating mean downward velocity. Similar separation is used for example in *Andreev* and *Ganev* (1981), *Roisin* (1982), *Chatfield* and *Brost* (1987).

The observations show that the updrafts have more velocity fluctuations while the downdraft velocity distribution is rather narrow and it has a mode approximately equal to the average downdraft velocity (*Lamb*, 1982). Thus, representing the downdraft velocity by a mean velocity which is a function of height and time should be a rather good approximation, while for the vertical velocity it is better to use thermals with various sizes. This separation should also be valid for the other CBL characteristics, because the velocity controls their spatial and temporal distributions. Thus, a horizontal area of the CBL $S(z,t)$ at a given level and at a given moment can be partitioned in two domains — the first one with area $S_T(z,t)$ covered with thermals and the second one with area $S_e(z,t)$ occupied by downdrafts of environmental air (see *Fig. 1*). Obviously the horizontal-mean value $\bar{A}(z,t)$

$$\overline{A}(z,t) = \frac{1}{S}\int_{S} A(x,y,z,t)\,dx\,dy \tag{1}$$

of some CBL characteristic may be separated as

$$\overline{A} = \overline{A}_T + \overline{A}_e, \tag{2}$$

where

$$\overline{A}_T = \frac{1}{S}\int_{S_T} A\,dx\,dy \quad \text{and} \quad \overline{A}_e = \frac{1}{S}\int_{S_e} A\,dx\,dy. \tag{3}$$

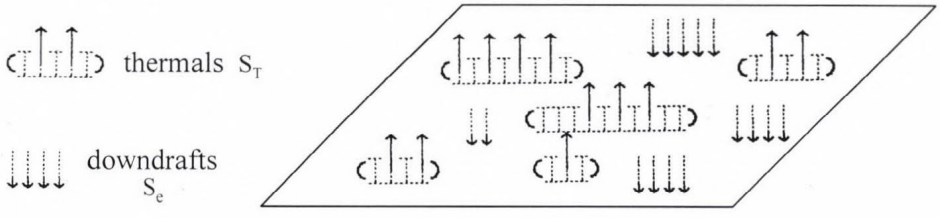

Fig. 1. Schematic illustration of the partition of CBL at a given level at a given time into thermals (updrafts) and downdrafts domains.

It has already been mentioned that the horizontal fluctuations of the downdraft characteristics are small. Therefore, approximately

$$\overline{A}_e = \frac{S_e}{S}A^*, \tag{4}$$

where A^* is a value of A in the environmental air, which is assumed to be horizontally uniform.

Following Eqs. (4) and (2) A^* may be expressed as

$$A^* = \frac{S}{S_e}\left(\overline{A} - \overline{A}_T\right). \tag{5}$$

It is supposed that the air is dry. Then after the application of the averaging given by Eq. (1) the continuity and heat equations for the atmospheric boundary layer become (*Matveev*, 1981) :

$$\frac{\partial}{\partial z}\,\overline{w} = 0, \tag{6}$$

$$\frac{\partial}{\partial t}\,\overline{\theta} = -\frac{\partial}{\partial z}\,\overline{w\theta}. \tag{7}$$

In Eq. (6) and Eq. (7) $\overline{w}$, $\overline{\theta}$ and $\overline{w\theta}$ are the horizontal-mean vertical velocity, potential temperature and vertical convective heat flux, respectively.

From Eq. (6) it follows that $\overline{w} = 0$, because at flat earth's surface the horizontal-mean vertical velocity vanishes. Eq. (5) gives

$$w^* = -\frac{S}{S_e}\,\overline{w}_T \quad \text{and} \quad \theta^* = \frac{S}{S_e}\left(\overline{\theta} - \overline{\theta}_T\right).$$

Now it can easily be obtained that

$$\overline{w\theta} = \left(\overline{w\theta}\right)_T - \frac{S}{S - S_T}\,\overline{w}_T\left(\overline{\theta} - \overline{\theta}_T\right),$$

and the heat Eq. (7) takes the final form

$$\frac{\partial}{\partial t}\,\overline{\theta} = -\frac{\partial}{\partial z}\left[\left(\overline{w\theta}\right)_T - \frac{S}{S - S_T}\,\overline{w}_T\left(\overline{\theta} - \overline{\theta}_T\right)\right]. \tag{8}$$

Let $f(R,z,t)$ be the number of thermals with radius R per unit area at level z and at time t. The fraction of the area occupied by rising thermals at fixed level and time is

$$\frac{S_T}{S} = \sum_R \pi R^2 f(R,z,t), \tag{9}$$

where the sum is over all thermals' radii.

Following Eq. (3) one can get for the updraft characteristics of the CBL

$$\overline{\theta}_T = \sum_R \pi R^2\,\theta\,(R,z,t) f(R,z,t),$$

$$\left(\overline{w\theta}\right)_T = \sum_R \pi R^2 W(R,z,t)\,\theta\,(R,z,t) f(R,z,t), \tag{10}$$

$$\overline{w}_T = \sum_R \pi R^2 W(R,z,t) f(R,z,t),$$

where $W(R,z,t)$ and $\theta(R,z,t)$ are the vertical velocity and the potential temperature of the rising thermals with radii R which are at level z at moment t.

Substituting Eq. (10) in Eq. (8) yields

$$\frac{\partial}{\partial t}\overline{\theta} + \frac{\partial}{\partial z}\left[B(z,t)\overline{\theta}\right] = C(z,t), \tag{11}$$

where

$$B(z,t) = -\frac{1}{1-(S_T/S)}\sum_R \pi R^2 Wf, \tag{11a}$$

$$C(z,t) = -\frac{\partial}{\partial z}\left[\frac{1}{1-(S_T/S)}\left(\sum_R \pi R^2 Wf\right)\left(\sum_R \pi R^2 \theta f\right) + \sum_R \pi R^2 W\theta f\right] \tag{11b}$$

and S_T/S is given by Eq. (9).

The temperature at the earth's surface follows the changes of the solar radiation and the lower boundary condition in the model is

$$\overline{\theta}(0,t) = \overline{\theta}_0(0) + k\sin(2\pi t/24), \tag{12}$$

where $\bar{\theta}_0(0)$ is the potential temperature at the earth's surface at the moment of sunrise, and k gives the increase of the earth's surface temperature in 6 hours. The parameters k and $\bar{\theta}_0(0)$ in Eq. (12) are varied in the numerical experiments.

At the limit of large z the initial potential temperature profile $\bar{\theta}_0(z)$ is unperturbed since the CBL has a finite depth during its evolution. Hence, the initial and upper boundary conditions in the problem are respectively:

$$\overline{\theta}(z,0) = \overline{\theta}_0(z), \quad \overline{\theta}(z,t) \to \overline{\theta}_0(z),$$

at large z.

The terms $B(z,t)$ and $C(z,t)$ in Eqs. (11a) and (11b) are unknown. They depend on the individual characteristics of the rising thermals with different radii and on the size statistics of the thermals. Therefore the problem is to evaluate the thermals' characteristics and their size distribution. Some additional

assumptions are needed for that purpose. The CBL is a composition of thermals and environmental air. The interaction between each thermal and the surrounding air is realized by the entrainment mechanism and the buoyancy effect due to the temperature excess. In the present model following *Andreev* and *Ganev* (1981) it is assumed that the thermals are spheres with radii R_i, vertical velocities W_i and potential temperatures θ_i and that they ascend as individual thermals. The time evolution of W_i and θ_i during the thermal's rising are given by (*see Andreev* and *Panchev*, 1975)

$$\frac{d}{dt}W_i = -\alpha W_i^2 + g\left[\frac{\theta_i - \bar{\theta}}{\bar{\theta}}\right], \tag{14}$$

$$\frac{d}{dt}\theta_i = -\alpha\left(\theta_i - \bar{\theta}\right)W_i, \tag{15}$$

and

$$\frac{d}{dt}z_i = W_i,$$

where g is the acceleration due to gravity and z_i is the coordinate of thermal's mass center, $R_i = R_{i0} + 0.2z_i$, R_{i0} is the thermal's radius near the earth's surface. The entrainment parameter α is

$$\alpha(z_i, R_i) = \frac{0.6}{R_i(z_i)}.$$

Some information on the thermal size distribution $f(R,z,t)$ is necessary for the closure of the problem. In the model $f(R,z,t)$ is numerically evaluated in the manner described in the next section.

3. Numerical scheme

Eq. (11) together with the initial and boundary conditions (Eqs. (12) and (13)) is solved numerically using an explicit finite-difference scheme.

It has been already mentioned that the problem is to evaluate the terms $B(z,t)$ and $C(z,t)$ in Eqs. (11a, 11b). The calculation of the sums in Eqs. (11a, 11b) requires some information about the characteristics of the rising thermals

and their size distribution at any level and at any moment. Numerical solutions of Eq. (14) to Eq. (16) for thermals with various initial radii R_{i0} provide the necessary information about W_i, θ_i and z_i at any time step. For the determination of the distribution function $f(R,z,t)$ the spherical thermals are transformed into cylinders with the same radius R_i and volume as the sphere. Thus the heights of the cylinders will be given by

$$H_i = \frac{3}{4} R_i. \tag{17}$$

It is supposed that at a given moment the thermal with radius R_i located at height z_i affects the levels between z_i and $z_i - H_i$. Hence the distribution function $f(R,z,t)$ for a given level z at a given moment t is the sum of the thermals with radii R_i affecting the level z. Obviously $f(R,z,t)$ depends on the size distribution of thermals at the earth's surface.

The level $z = 0$ in the model was set to be the level of the thermals starting.

The initial potential temperature profile $\bar{\theta}(z,0)$ is interpolated to determine the potential temperature at the vertical grid levels.

The evolution of potential temperature profiles for a time step is obtained as follows:

- The Eqs. (14) to (16) are numerically integrated by the Runge-Kutta method using $\bar{\theta}(z,t)$. Thus W_i, θ_i and z_i are calculated for a time step.
- The discrete size distribution function $f(R,z,t)$ is determined as the sum of the thermals with radii R_i which at a given moment t affect the levels z situated between z_i and $z_i - H_i$.
- The terms $B(z,t)$ and $C(z,t)$ are calculated from Eqs. (11a, 11b) and $\bar{\theta}(z,t + dt)$ is obtained from Eq. (11) by an explicit finite-difference scheme. For the levels not affected by the rising thermals at a given moment t, $f(R,z,t) = 0$ and $\bar{\theta}(z,t + dt) = \bar{\theta}(z,t)$.

These calculations are repeated until all the thermals reach the levels at which their velocities $W_i = 0$. In the model it is accepted that a new thermal group with a given distribution function starts at the earth's surface when the previous group stops, but not more often than every 15 minutes.

The calculations have been carried out using a time step $dt = 1s$ and a vertical grid length $dz = 50$ m. For the stabilization of the numerical scheme the potential temperature at each grid level z is recalculated as

$$\bar{\theta}(z,t) = \frac{1}{2}\left(\bar{\theta}(z + dz) + \bar{\theta}(z - dz)\right).$$

4. Numerical simulations and results

The purpose of the numerical simulations was to study the general behavior of the model, as well as its response to variation of the control parameters.

The model requires an initial sounding and initial size distribution, vertical velocities and temperature excesses of thermals at the earth's surface to be preassigned. Their values were chosen to be of the same order of magnitude as in the observations.

The measurements of *Warner* and *Telford* (1967) showed that thermals were typically 200–300 m in horizontal extent with an initial upward velocity of about 1 m/s and a temperature excess of about 1 K. The observations of *Vulfson* (1961) showed that the average size of the convective elements was 50–100 m. Various experimental estimates of the fraction of area covered with thermals are reported in the literature. *Warner* and *Telford* (1967) and *Frish* and *Businger* (1973) gave a value of 0.4, while *Lenschow* and *Stephens* (1980) recommended 0.25. *Young's* (1988) measurements showed that the fraction of area covered with thermals decreased with height up to the half of the CBL and then increased with height.

For all model simulations the starting velocities of the thermals were fixed to be 1 m/s and the temperature excess was set to be 1 K. Two types of size distribution (the number of thermals with a given diameter per km^2) at the earth's surface were used. The first type which will further be denoted as ST1 is presented in *Table 1*. *Andreev* and *Ganev* (1981) extracted that distribution from *Vulfson's* (1961) data. The second type of size distribution, ST2 is uniform — during the first six hours after sunrise there are 0.5 thermals per km^2 with diameters from 50 m to 250 m at intervals of 50 m. While ST1 is in accordance with some observations, ST2 is more or less speculative in order to test the sensitivity of the model to the type of the thermals' size distribution. In both cases the fraction of area covered with thermals was fixed to be 0.22 at the earth's surface. Four different values for $k(k = 5,6,7,8)$ were used in Eq. (12) to study the response of the model to the magnitude of the surface heating. These values allow to model adequately the real spring diurnal temperature variations in Sofia, Bulgaria.

The sensitivity to the initial sounding was tested by running the model from two initial temperature profiles, which were model inversions with constant lapse rates. They are given with solid lines on *Fig. 2* and *Fig. 3*. Being nocturnal ground inversions, the layers between 0 and 600 m had lapse rates $\gamma = -0.5$ K/100 m and $\gamma = -1$ K/100 m, respectively. The initial temperature profiles above 600 m were identical in both cases and they had temperature lapse rates of 0.5 K/100 m. The calculations were carried out at $k = 7$. The initial thermal size distribution was of type ST1.

Fig. 2 and Fig. 3 show that according to the model calculations the heat transfer by rising thermals and compensating downdrafts causes temperature

profile changes in the direction of decreasing air stability during the first hours. The CBL is not fully developed three hours after sunrise in both simulations, but the temperature inversion is eroded up to 350 m for the case with γ = –0.5 K/100 m (Fig. 2) and up to 250 m for the case with γ = –1 K/100 m (Fig. 3). The results show that the lapse rate of horizontal-mean potential temperature decreases gradually with the increase of solar radiation. Four hours after sunrise it is zero up to 400 m for the case with γ = –0.5 K/100 m (Fig. 2), i.e. at that moment the CBL is developed up to 400 m. For this case the CBL height increases up to 450 and 500 m five and six hours after sunrise, respectively (Fig. 2). For the case with stronger inversion (γ = –1 K/100 m) five hours after sunrise the CBL height is about 100 m lower compared to the case with γ = –0.5 K/100 m (see Fig. *2* and Fig. 3).

Table 1. The size distribution of the thermals at the earth surface named ST1 in the text. The statistics is extracted from *Vulfson's* (1961) data by *Andreev* and *Ganev* (1981).

Diameter of the thermals (m)	Number of the thermals per km^2	
	Hours after sunrise 0–3	Hours after sunrise 3–6
5	0.6	1.4
15	4.5	11.2
25	4.9	14.0
35	6.2	14.8
45	6.4	15.5
55	6.2	15.5
65	6.1	14.8
75	4.9	13.5
85	5.7	12.1
95	5.1	10.1
105	4.5	7.7
128	2.3	1.7

Further numerical simulations were carried out using a real temperature sounding observed on 4 May 1988 during the Sofia experiment (see *Brunzov et al.*, 1992). This sounding was selected because the wind had been weak (less than 3 m/s) and there had been no advection and clouds on that day. The initial potential temperature profile calculated from the data of *Brunzov et al.* (1992) is given as a solid line on *Fig. 4*. It can be seen that after sunrise there is a ground temperature inversion up to 250 m and a temperature isotherm between 250 m and 400 m.

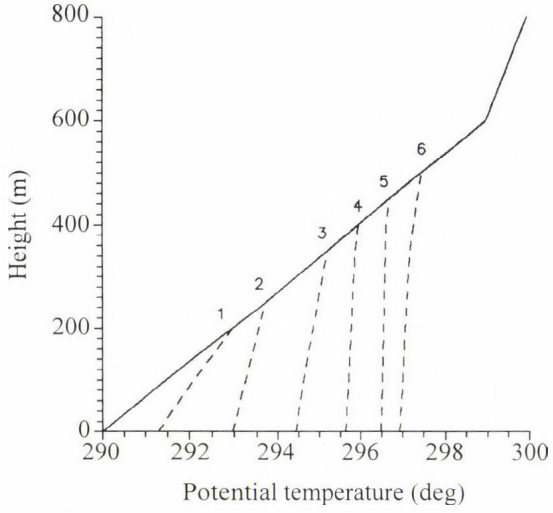

Fig. 2. Hourly vertical profiles of horizontal mean potential temperature (dashed lines). The numbers indicate hours after sunrise. The initial profile (solid line) represents temperature inversion with lapse rates γ = -0.5 K/100 m under 600 m and γ = -0.5 K/100 m above. The thermals have initial velocities 1 m/s, potential temperature excesses — 1 K and size distribution is of type ST1 (Table 1). The magnitude of radiation heating corresponds to k = 7.

The calculations show that if the parameter k is fixed to be k = 7, so that the surface temperature increases at a rate of 7 K/6 hours, and the initial thermal size distribution is of type ST1, there is no temperature inversion three hours after sunrise — the potential temperature lapse rate is 0.2 K/100 m up to 300 m. The CBL is fully developed four hours after sunrise up to 400 m and it rises with time up to 600 m six hours after sunrise (see Fig. 4). The measurements of *Brunzov et al.* (1992) indicate that the inversion is destroyed four hours after sunrise.

To test the response to the magnitude of solar heating the model was run with k = 5 (temperature increases at a rate of 5 K/6 hours), while the other parameters were unchanged. The calculation shows that in this case three hours after sunrise the temperature inversion is eroded up to 200 m, (potential temperature lapse rate is 0.33 K/100 m). As it is seen on *Fig. 5* the stability decreases gradually again, but the CBL is not developed even six hours after the beginning of the earth's heating.

The influence of the magnitude of radiation heating on the CBL development is clearly demonstrated on *Fig. 6a* and *Fig. 6b*. The potential temperature profiles four hours after sunrise are given on Fig. 6a. The same is plotted on Fig. 6b, but six hours after sunrise. The initial potential temperature profiles are plotted with solid lines. The parameter k, which controls the magnitude of radiation heating takes the values k = 5,6,7,8. The corresponding potential temperature profiles are plotted with asterisks and dashed lines with different sizes. The initial size distribution is of type ST1.

The results show that the stronger the heating is, the higher the convective boundary layer is developed. Obviously there is some threshold for the CBL development because while at $k = 5$ and $k = 6$ it is not developed at all, in the cases of $k = 7$ and $k = 8$ there are well developed convective mixed layers.

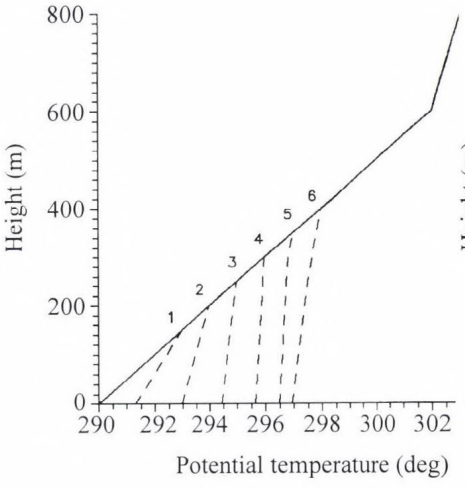

Fig. 3. As in Fig. 2 but for $\gamma = -1$ K/100 m.

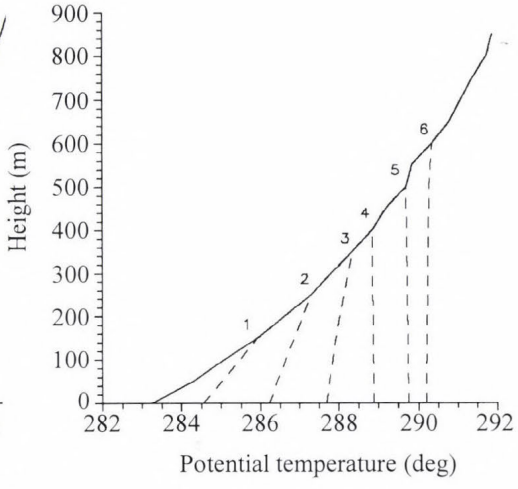

Fig. 4. As in Fig. 2 but the initial potential temperature profile is from real sounding (see *Brunzov et al.*, 1992).

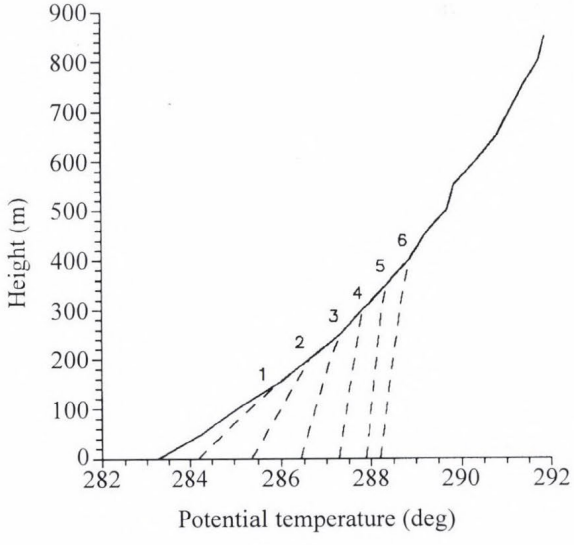

Fig. 5. As in Fig. 4 but for $k = 5$.

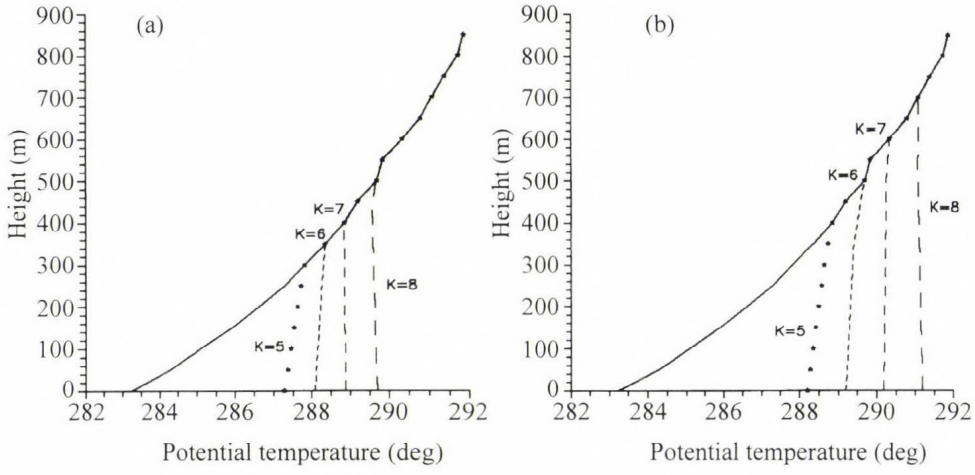

Fig. 6. Vertical profiles of horizontal-mean potential temperature for different magnitudes of radiation heating k = 5,6,7,8. (*a*) four hours after sunrise; (*b*) six hours after sunrise. The initial potential temperature profile, initial velocities, temperature excesses and size distribution of the thermals are as in Fig. 4.

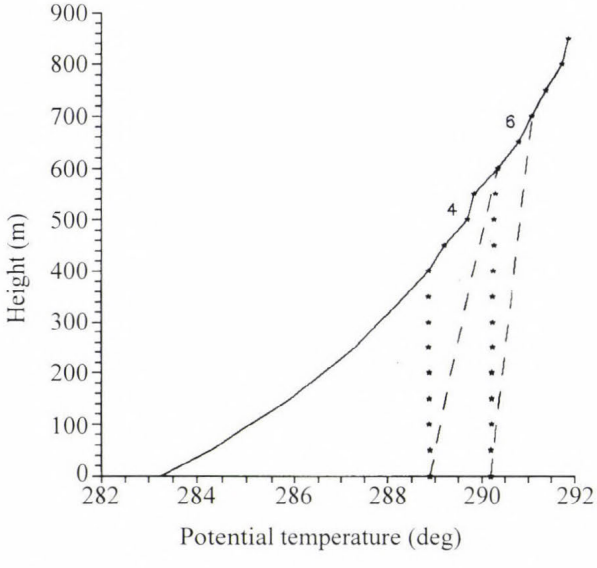

Fig. 7. Vertical profiles of horizontal-mean potential temperature for two types of size distributions of the thermals at the earth's surface 4 and 6 hours after sunrise. The type ST1 (asterisks) is given in Table 1 and type ST2 (dashed lines) — in the text. The initial potential temperature profile, initial velocities and temperature excesses of the thermals as well as the parameter k are as in Fig. 4.

To study the sensitivity of the model to the size distribution of thermals at the earth's surface the model was run for two types of size distributions — ST1 (see Table 1) and ST2. The results are presented on *Fig.* 7 where the calculated potential temperature profiles for four and six hours after sunrise are given. For the size distribution of type ST1, the potential temperature profiles are marked with asterisks, and for ST2 with dashed lines. In the case of the size distribution of type ST1, i.e. the heat is transported by thermals with diameters between 5 m and 128 m, for four and six hours after sunrise the potential temperature profiles are changed up to 400 m and 600 m, respectively. When the size distribution is of type ST2, i.e. the heat is transported by thermals with diameters 50–250 m, four and six hours after sunrise the changes in the potential temperature profile reach up to 600 m and 700 m, respectively. These results show that the bigger the ascending thermals initially are, the stronger they affect the initial temperature profile. This is due to the fact that larger thermals can ascend higher than smaller ones because the entrainment of the environmental air is smaller for them. The model results show that the CBL is not developed even six hours after sunrise in the case of the ST2 type distribution.

5. Summary and conclusion

A one-dimensional numerical model of evolving morning CBL has been developed. The basic idea of the model is that the heat in the convective mixed layer is transported by isolated buoyancy-driven turbulent eddies (thermals). Partitioning the CBL into 'updrafts' and compensating 'downdrafts' domains, the governing equation for the evolution of the horizontal-mean potential temperature was derived. This equation together with the initial and boundary conditions perform an unclosed initial value problem because its coefficients depend on unknown characteristics of the rising thermals as well as on their size distribution. The problem has been closed by assuming that thermals ascend as individual ones. Only vertical velocities, temperature excesses and size statistics of thermals at the earth's surface have to be given in order to compute numerically the evolution of the vertical profiles of the horizontal-mean potential temperature.

The model was run for two model initial temperature profiles in order to test its sensitivity to the initial sounding. These profiles correspond to nocturnal ground inversions. The calculations show that the CBL is formed in two stages. Initially the result of the increase of solar radiation is only the gradual decrease of the lapse rate of potential temperature and the gradual erosion of temperature inversion in a layer of growing thickness. During this stage — in the model two to three hours after sunrise — there is no CBL. The CBL as a layer with vanishing lapse rate of potential temperature is fully developed by four hours after sunrise and then its height grows. The CBL has the same type of evolution

for the case of a real initial sounding, too. Therefore the scenario of the convective mixed layer development qualitatively does not depend on the strength of the temperature inversion. The influence of the degree of the static stability of the initial temperature sounding changes only quantitatively the picture of evolution. As it could be expected, the stronger the initial temperature inversion, the lower the growth rate of the thickness of the layer affected by thermals in the first stage and the growth of CBL depth in the second stage. The same is valid for the heights of those layers a given time after sunrise.

A second type of numerical simulation was carried out by varying the parameter that controls the magnitude of radiation heating. The main result of the numerical tests is that there is a critical value of that parameter. When the magnitude of radiation heating is less than a critical value, the CBL is not formed, while when it takes values greater than the critical one there are fully formed convective mixed layers four hours after sunrise.

The model was run for two types of size distribution to study the sensitivity to the size statistics of thermals at the earth's surface. The calculation demonstrates physically adequate response of the model to the type of size statistics of thermals.

In conclusion, the numerical experiments indicate that in general the presented model gives reasonable results for the morning CBL evolution in the case of weak wind, absence of clouds and strong solar heating.

References

Andreev, V. and *Panchev, S.*, 1975: *Dynamics of Atmospheric Thermals* (in Russian). Gidrometeoizdat, Leningrad.

Andreev, V. and *Ganev, K.*, 1981: Model of convective heat exchange due to isolated thermals in the atmospheric boundary layer. *Boundary-Layer Meteorology 20,* 331-339.

Brunzov, H.T., Donev, E.H., Panchev, S., 1992: Experimental investigation of the structure and dynamics of temperature inversion and convective boundary layer above Sofia-area. Evaluation of the possibility of the apparatus available (in Bulgarian). *Ann. de L'Universite de Sofia 82,* 147-167.

Chatfield, R.B. and *Brost, R.A.*, 1987: A two-stream model of the vertical transport of trace species in the convective boundary layer. *J. Geophys. Res. 92,* 13263-13276.

Frish, S.A. and *Businger, J.A.*, 1973: A study of convective elements in the atmospheric surface layer. *Ibid. 2,* 301-328.

Hunt, J.C.R., Kaimal, J.C. and *Gaynor, J.E.*, 1988: Eddy structure in the convective boundary layer-new measurements and new concepts. *Quart. J. Roy. Meteorol. Soc. 114,* 827-858.

Lamb, R.G., 1982: Diffusion in the convective boundary layer. In *Atmospheric Turbulence and Air Pollution Modeling* (eds.: *F.T.M. Nieuwstadt* and *H. van Dop*). D. Reidel Hingham, Mass, 159-229.

Lenschow, D.H. and *Stephens, P.L.*, 1980: The role of thermals in the convective boundary layer. *Boundary Layer Meteorol. 19,* 509-532.

Lenschow, D.H. and *Stephens, P.L.*, 1982: Mean vertical velocities and turbulence intensity inside and outside thermals. *Atmos. Environ. 16,* 761-764.

Matveev, L.T., 1981: *Cloud Dynamics* (in Russian). Gidrometeoizdat, Leningrad.

Manton, M.J., 1975: Penetrative convection due to a field of thermals. *J. Atmos. Sci. 32*, 2272-2277.

Roisin, B., 1982: A theory of convection: Modeling by two buoyant interaacting fluids. *Geophys. Astrophys. Fluid Dynamics 19*, 35-59.

Telford, J.W., 1966: The convective mechanism in clear air. *J. Atmos. Sci. 23*, 652-666.

Telford, J.W., 1992: Clouds, noncloudy latent heat convection, entrainment, and horizontal averaging. *J. Atmos. Sci. 49*, 1848-1860.

Vulfson, N.T., 1961: *Convective Motion in a Free Atmosphere* (in Russian). Publ. Akad Nauk SSSR.

Warner, J. and *Telford, J.W.*, 1967: Convective below cloud base. *J. Atmos. Sci 24*, 374-382.

Young, G.S., 1988: Turbulence structure of the convective boundary layer. Part II; Phoenix 78 Aircraft Observations of Thermals and Their Environment. *J. Atmos. Sci 45*, 727-735.

IDŐJÁRÁS

Quarterly Journal of the Hungarian Meteorological Service
Vol. 101, No. 1, January–March 1997, pp. 17–31

Estimating probability density functions by kernel techniques

I. Matyasovszky

Department of Meteorology, Eötvös Loránd University,
Ludovika tér 2, H-1083 Budapest, Hungary; E-mail: matya@ludens.elte.hu

(Manuscript received 3 March 1996; in final form 4 October 1996)

Abstract—Kernel density estimation methods are discussed as flexible alternatives to traditional parametric methods for probability density estimation of climatological variables. Basic properties of such estimators are reviewed in this paper. The selection of the kernel function is outlined and attention is then focused on the bandwidth choice. Constant bandwidth and varying bandwidth kernel estimators are applied to daily mean temperature in Nebraska, USA. The histogram shows a possible complicated form of the probability density. The estimates are compared to each other and to a parametrically fitted binormal density. The results obtained demonstrate the usefulness of kernel estimators with local bandwidths.

Key-words: probability density function, kernel estimator, kernel function, bandwidth.

1. Introduction

Estimating probability distributions is a classical problem in meteorology. Parametric approaches which require an assumption on the type of the probability distribution are traditionally used for this purpose. Having a distribution type its parameters are estimated using one of several methods, like the maximum likelihood technique, or the method of moments. A review of frequently used distribution types can be found, for instance, in *Essenwanger* (1986).

Although well-developed statistical tests (e.g., the Kolmogorov-Smirnov test, or the chi-square test) can be used to check the fit of a selected distribution type, several important problems may arise. First, if a given distribution type fits observational data satisfactorily there is no guaranty that no other distribution type fits even better. In other words, since the true distribution is not known, just a best member of candidate distributions can be determined. However, it is not unusual that no particular distribution appears to be clearly

the best because the candidate distributions are close to each other and the goodness of fit measured by one of the common methods (e.g., chi-square norm, or entropy norm) cannot distinguish among those distributions. For instance, beside the two-parameter Weibull distribution (*Justus et al.*, 1976) the gamma and log-normal distributions (*Stewart* and *Essenwanger*, 1973) are generally used to model wind speed. A special case of this problem is when a distribution is compared with a more general class of distributions. For instance, the Rayleigh distribution having one parameter to be estimated is a special case of the Weibull distribution and under certain climate conditions the Rayleigh distribution can be used for wind speed (*Hennessey*, 1977). The necessity of a more general distribution can be analyzed by the likelihood ratio test, but frequently it is uncertain which type should be preferred.

Another problem is that a given meteorological element can follow different distributions depending on time. It is well-known that daily precipitation amount can be described by gamma distributions, but often, log-normal distributions are fitted for short time intervals (*Biondini*, 1975).

In several cases the variables in question appear to be poorly described by any of the distribution types discussed in even specialized statistical literature. For instance, hourly incoming global radiation was modeled by Weibull, log-normal, gamma, and chi-square distribution types (*Matyasovszky*, 1992), but none of these distributions could provide a fit consistent with observational data. In such cases transformations resulting in 'nicely behaving' variables can help the climatologist.

A further deficiency may be that standard distribution types (normal, log-normal, gamma, etc.) are unimodal, thus they cannot be applied to model multimodal distributions. A possibility to describe such distributions is to use mixtures of unimodal distributions. The probability density function $f(x)$ is then expressed as:

$$f(x) = \sum_{i=1}^{I} p_i f_i(x), \tag{1}$$

where p_i is the probability that the random variable comes from the ith distribution type and $f_i(x)$ is the probability density corresponding to that type. Using two-parameter distributions, which is the typical case, the number of parameters to be estimated is equal to $2I + (I - 1)$, a relatively large number even for small values of I.

The above mentioned difficulties establish the rationale of using non-parametric density estimators when no assumption is needed on the distribution to be estimated. The principle of these techniques introduced by *Rosenblatt* (1956) and *Parzen* (1962) is that each sample element x_i has a contribution to the density $f(x)$ and these contributions (weights) are proportional to the

distances between x and x_i. The weights are calculated through a so-called kernel function scaled by a smoothing parameter. This parameter controls how fast the weights decrease as the distances between x and x_i increase. An overall discussion of kernel density estimators can be found in *Silverman* (1986).

Mathematics of kernel density estimators have been mostly developed, but, according to our best knowledge, no meteorological application of these techniques has been reported. The purpose of this study is, therefore, to show the possibilities of this methodology. First the kernel density estimator is defined and its asymptotic properties are shown. The choice of a kernel and a smoothing parameter, key elements of applying kernel estimators, is discussed next. Since the role of the smoothing parameter seems especially crucial, we will focus on this question. Daily mean temperature in Nebraska, USA is used in Section 3 as an illustrative example for estimating bimodal distributions non-parametrically. Finally a brief section for discussion and conclusions is provided.

2. *Kernel density estimator*

The Parzen-Rosenblatt kernel density estimate $\hat{f}(x)$ from a sample $\{x_1, x_2, \ldots, x_n\}$ of size n is given by

$$\hat{f}(x) = \frac{1}{n}\sum_{i=1}^{n} \frac{1}{b} K\left(\frac{x - x_i}{b}\right), \tag{2}$$

where $K(z)$ is a so-called kernel function satisfying certain properties to provide an appropriate estimate of $f(x)$. The bandwidth b tends to zero as n tends to infinity.

A possibility for choosing the kernel is that $K(z)$ itself is a density function because $K(z)$ is required to integrate to unity. $K(z)$ with support [-1,1], i.e. $(K(z)_{[-1,1]})$ is called kernel of order k if the condition

$$\int_{-1}^{1} K(z) z^j dz = \begin{cases} 1, & j = 0, \\ 0, & 0 < j < k \end{cases} \tag{3}$$

is satisfied. Note that a density symmetric to zero is a second order kernel. The choice of $K(z)$ and b is discussed in the next section.

$\hat{f}(x)$ is an asymptotically unbiased and consistent estimate of $f(x)$ and the asymptotic mean square error (MSE) of the kernel density estimate Eq. (2) is given by

$$MSE[\hat{f}(x)] = E[(\hat{f}(x) - f(x))^2] = u^2(x) + v^2(x), \tag{4}$$

where the asymptotic bias is equal to

$$u(x) = E[\hat{f}(x) - f(x)] = B\frac{h^k}{k!}f^{(k)}(x) \tag{5}$$

and the asymptotic variance is

$$v^2(x) = Var[\hat{f}(x)] = E[(\hat{f}(x) - E(\hat{f}(x))^2] = \frac{V}{nb}f(x), \tag{6}$$

while

$$B = \int_{-1}^{1} K(z)z^k dz, \qquad V = \int_{-1}^{1} K^2(z)dz. \tag{7}$$

E denotes the expectation and $f^{(k)}$ is the kth derivative which is assumed to be finite. The dependence of the MSE on the density and its kth derivative, the kernel, and the bandwidth is clearly shown by Eqs. (3) to (6). The bias Eq. (5) is higher in areas where $f^{(k)}$ is higher, and the variance Eq. (6) is higher where $f(x)$ is large. The bias term penalizes oversmoothing, and the variance term penalizes undersmoothing. Thus an optimal b that recognizes this trade-off must exist. The optimal b minimizing MSE at a point x is

$$b_{opt} = \left(\frac{f(x)V}{(f^{(k)})^2 nB^2}\right)^{1/(2k+1)} \tag{8}$$

and the convergence rate of $\hat{f}(x)$ to $f(x)$ in terms of the integrated MSE (IMSE)

$$IMSE = \int_{-\infty}^{\infty} E\left[(\hat{f}(x) - f(x))^2\right]dx = \int_{-\infty}^{\infty} (u^2(x) + v^2(x))dx \tag{9}$$

is proportional to $n^{-2k/(2k+1)}$. The fastest convergence can be achieved by using b_{opt} which, however, cannot be determined in practice because it needs the knowledge of $f(x)$. The bandwidth, therefore, should be estimated from the sample.

One could think that the choice of b is not a difficult problem by using the bandwidth which delivers, in some sense, a best fit to the sample available,

while the choice of k and K seems to be highly arbitrary. However, the situation is just the contrary. A class of optimal kernel functions is known, and several simulation and real data studies suggest that a small variability in k does not considerably affect the resulting density. Generally, a relatively small value of k, say $k = 2$ can be chosen. In contrast, the choice of b has a great importance, and therefore we will focus principally on this question.

3. Kernel and bandwidth choice

3.1 Kernel choice

The choice of kernels is based on asymptotic properties Eqs. (5) and (6). The solutions of the variational problem

$$\int_{-1}^{1} K^2(z)\,dz \rightarrow \min \tag{10}$$

are called minimum variance kernels since they minimize the asymptotic variance Eq. (6). Such kernels can be found in *Gasser et al.* (1985). The minimum variance kernels are polynomials of even orders. For instance, for $k = 2$ and $k = 4$ the kernels are $K(z) = 1/2_{[-1,1]}$ and $K(z) = 3/8(3 - 5z^2)_{[-1,1]}$, respectively. *Müller* (1984) discussed a more general class of kernel functions which minimizes the asymptotic variance of the μth ($\mu \geq 0$) derivative of the kernel estimate. One of the most frequently used kernel is

$$K(z) = \frac{3}{4}(1 - z^2)_{[-1,1]} \tag{11}$$

with $k = 2$, $\mu = 1$. The above kernels, however, may be used just in the case when $f(x)$ is defined on the interval $(-\infty, \infty)$, unless the kernels are modified near the endpoints. *Gasser* and *Müller* (1979) defined boundary kernels with asymmetric support satisfying moment conditions necessary to maintain the order of unbiasedness in boundary intervals. Minimum variance kernels were derived by *Gasser et al.* (1985). *Müller* (1991) has developed a very general formulation to have kernels for any $x \in (m, M)$ and for any k, $\mu \geq 0$, where (m, M) denotes the support of $f(x)$. Let K_+ and K_- be functions with support [0, 1] $\times$ [-1, q] and [0, 1] $\times$ [-q, 1], respectively and with some smoothing requirements (*Müller*, 1991, p. 523). Then, kernels at a point x are given by

$$K_x(z) = \begin{Bmatrix} K_+(1,z), & b/(M-m) \le z \le 1 - b/(M-m) \\ K_+((x-m)/b,z), & 0 \le z < b/(M-m) \\ K_-((M-x)/b,z), & 1 - b/(M-m) < z \le 1 \end{Bmatrix},$$

where $K_-(q, z) = K_+(q, -z)$ and $q = 1$ for $x \epsilon [m + b, M - b]$ (interior), $q = (x - m)/b$ for $m \le x < m + b$ (left boundary region), $q = (M - x)/b$ for $M - b < x \le M$ (right boundary region). Eq. (7), necessary to calculate the asymptotic bias and variance, essentially holds, but now B and V depend on q (see *Müller*, 1991, p. 523). For $k = 2$, $\mu = 1$, and in the interior region of the support of $f(x)$ ($q = 1$) $K_x(z)$ becomes Eq. (11).

3.2 Bandwidth choice

Constant bandwidth. In parametric density estimation the parameters are estimated by maximum likelihood, least squares, or other methods. A natural way to estimate bandwidth is, therefore, to use these concepts for kernel estimators.

A direct application of the maximum likelihood principle is unsuccessful, since the degenerate choice of $b = 0$ maximizes the likelihood function. Therefore, a maximum likelihood cross-validation (MLCV) version developed by *Habbema et al.* (1974) can be offered for this purpose. The bandwidth b is chosen by maximizing a cross-validated likelihood function defined as

$$\prod_{i=1}^{n} \hat{f}_i(x_i),$$

where $\hat{f}_i(x_i)$ is the kernel density estimate at x_i with the x_i omitted. Substituting $\hat{f}_i(x_i)$ into the likelihood function, the

$$MLCV = \prod_{i=1}^{n} \left[\frac{1}{n-1} \sum_{j \neq i}^{n} \frac{1}{b} K\left(\frac{x_i - x_j}{b} \right) \right] \tag{12}$$

is obtained to be maximized with respect to b. A major theoretical study of the properties of MLCV is presented in *Hall* (1987).

The least square method for estimating b based on a minimization of the IMSE was suggested by *Rudemo* (1982). Given an estimator $\hat{f}(x)$, the IMSE can be written as

$$\int_{-\infty}^{\infty}(\hat{f}(x) - f(x))^2 dx = \int_{-\infty}^{\infty}\hat{f}^2(x)\,dx - 2\int_{-\infty}^{\infty}\hat{f}(x)f(x)\,dx + \int_{-\infty}^{\infty}f^2(x)\,dx.$$

The last term of the above equation does not depend on b and the first term can be estimated directly from the estimate $\hat{f}(x)$. It can be shown that the expectation of the second term is equal to

$$2/n \sum_{i=1}^{n} \hat{f}_i(x_i).$$

The data-based LSCV to be minimized to choose b is then

$$LSCV = \int_{-\infty}^{\infty}\hat{f}^2 dx - 2/n \sum_{i=1}^{n} \hat{f}_i(x_i),$$

which is generally approximated by

$$LSCV = 1/n \sum_{i=1}^{n} \hat{f}^2(x_i) - 2/n \sum_{i=1}^{n} \hat{f}_i(x_i), \tag{13}$$

where

$$\hat{f}_i(x_i) = \frac{1}{n-1} \sum_{j \neq i} \frac{1}{b} K\left(\frac{x_i - x_j}{b}\right).$$

Hall and *Marron* (1987) demonstrated the optimality of LSCV for density estimation in terms of IMSE. They showed that no other cross-validation bandwidth selection procedure can deliver smaller IMSE than LSCV. This is the reason why LSCV is preferred in almost every application. However, even this best bandwidth estimator has serious limitations. Specifically, the relative convergence rate of the estimated bandwidth to the optimal bandwidth is only proportional to $n^{-1/10}$ (*Hall* and *Marron*, 1987). For this reason, considerable effort has been put forth to find more accurate practical methods (see e.g. *Marron*, 1989). An important class of improved bandwidth selectors includes the so-called plug-in methods. A plug-in estimator is constructed in two steps: first, an initial estimate $\hat{f}(x)$ called pilot estimate is calculated using a bandwidth obtained from LSCV (Eq. 13); then, this estimate is plugged into IMSE (Eq. 9) substituting $f(x)$ and $f^{(k)}(x)$ by $\hat{f}(x)$ and $\hat{f}^{(k)}(x)$, respectively and IMSE is minimized with respect to b. $\hat{f}^{(k)}(x)$ can be approximated numerically

from $\hat{f}(x)$ using a finite difference scheme. Such an estimator can reach a relative convergence rate of $n^{-1/2}$ (e.g. *Hall et al.*, 1991), the fastest possible convergence rate of bandwidth estimation (*Hall* and *Marron*, 1987). Another class of improved bandwidth selectors utilizes frequency domain representation of LSCV. A modification of LSCV using some cut-off frequency filters the high frequencies out from the estimator and delivers a relative convergence rate of $n^{-1/2}$ (*Chiu*, 1992).

Plug-in estimators suggest the use of local bandwidths, because instead of minimizing IMSE a minimitazion of MSE for every particular x results in locally varying bandwidths.

Local bandwidth ($b(x)$). MSE of $\hat{f}(x)$ is governed by $f(x)$ and $f^{(k)}(x)$ (Eqs. (4) to (7)). This fact motivates the choice of locally varying bandwidths. A smaller bandwidth near the peaks of $f(x)$ reduces the bias and a larger bandwidth in the flat regions of $f(x)$ reduces the variance. Therefore, it may be expected that a good strategy for choosing local bandwidth $b(x)$ yields smaller IMSE than the IMSE of ordinary bandwidth selection for global bandwidth b.

In general, the construction of a local bandwidth estimator entails a two-step procedure. The first step produces a pilot estimator using a fixed bandwidth and the second step yields the local bandwidth estimator. This second step requires a reformulation of Eq. (2). Since the bandwidth b may depend on either x or x_i two versions of kernel estimators are discussed

$$\hat{f}_1(x) = \frac{1}{n} \sum_{i=1}^{n} \frac{1}{b(x)} K\left(\frac{x - x_i}{b(x)}\right) \tag{14}$$

$$\hat{f}_2(x) = \frac{1}{n} \sum_{i=1}^{n} \frac{1}{b(x_i)} K\left(\frac{x - x_i}{b(x_i)}\right). \tag{15}$$

An important disadvantage of the first estimator is that $\hat{f}_1(x)$ typically does not integrate to unity and thus is usually not itself a density. A further disadvantage is that no specification of $b(x)$ can be stated automatically. The second estimator is used in a form $b(x_i) = hf^{-1/2}(x_i)$ because this choice eliminates the asymptotic bias of Eq. (15). Then $\hat{f}_2(x)$, called Abramson estimator (*Abramson*, 1982), is equal to

$$\hat{f}_2(x) = \frac{1}{n} \sum_{i=1}^{n} \frac{f^{1/2}(x_i)}{h} K\left(\frac{(x - x_i) f^{1/2}(x_i)}{h}\right), \tag{16}$$

where h is a parameter to be estimated. The asymptotic IMSE of $\hat{f}_1(x)$ and $\hat{f}_2(x)$ is expected to be smaller than or at most equal to IMSE of fixed bandwidth estimators. Indeed, a frequently used version of $\hat{f}_1(x)$ was found to

be more efficient than the fixed bandwidth estimator, but it allows very little improvement (*Terrel* and *Scott*, 1992). $\hat{f}_2(x)$ exhibits larger asymptotic IMSE than the fixed bandwidth estimator, because the estimate at a point x can be strongly influenced by points x_i far from x. In spite of this fact the Abramson estimator is preferred in practice because it enjoys a significant reduction of IMSE for small and moderate sample sizes. Such sample sizes represent the typical case in climatology. The efficiency of the Abramson estimator over fixed bandwidth estimators seems to disappear only for sample sizes of ten thousands (*Terrel* and *Scott*, 1992).

The parameter h in Eq. (16) can be estimated by cross-validation as described by *Hall* (1992). The quantity to be minimized to choose h is

$$CV = 1/n \sum_{i=1}^{n} \tilde{f}_2^2(x_i) - 2/n \sum_{i=1}^{n} \tilde{f}_2(x_i), \tag{17}$$

where

$$\tilde{f}_2(x) = \frac{1}{n} \sum_{j=1}^{n} \frac{\check{f}_j^{1/2}(x_j)}{h} K\left(\frac{(x_i - x_j)\check{f}_j^{1/2}(x_j)}{h} \right) \tag{18}$$

is the Abramson estimate at x_i with a cross-validated constant bandwidth pilot estimate

$$\check{f}_i(x_i) = \frac{1}{n-1} \sum_{j \neq i} \frac{1}{b} K\left(\frac{x_i - x_j}{b} \right). \tag{19}$$

However, as the performance of cross-validation for estimating fixed bandwidth is relatively poor, so is for estimating h. *Müller* and *Wand* (1990) and *Müller* and *Zhou* (1991), therefore, proposed the following procedure. The bias $u(x)$ and the variance $v^2(x)$ of the estimator (14) can be rewritten as:

$$u(x) = \int_{-\infty}^{\infty} K(z) f(x - b(x)z)\, dz - f(x) \tag{20}$$

$$v^2(x) = \frac{1}{nb(x)} \int_{-\infty}^{\infty} K^2(z) f(x - b(x)z)\, dz. \tag{21}$$

The local bandwidth is estimated by minimizing the expression

$$MSE(x) = u^2(x) + v^2(x) \tag{22}$$

with substituting $f(x)$ in Eqs. (20) and (21) by a pilot estimate. This minimization of (22), referred to as Müller estimator, does not use asymptotic expressions, but rather the exact MSE is estimated and then minimized. It was shown in *Müller* and *Wang* (1990) that, for a large range of pilot bandwidths, the estimated local bandwidth converges to the optimal local bandwidth in terms of MSE.

4. Example

Daily mean temperature in Nebraska, USA for January is examined using a data set for the period from 1950 to 1989. To analyze the probability distribution a statistically independent sample is needed, but daily temperatures are serially correlated. Therefore, a temperature subset has been created picking up each fifth temperature value from the original data set, since autocorrelations for lags larger than four or five days are quite small (*Fig. 1*). Thus, an approximately independent sample of size $n = 280$ is available for daily mean temperature.

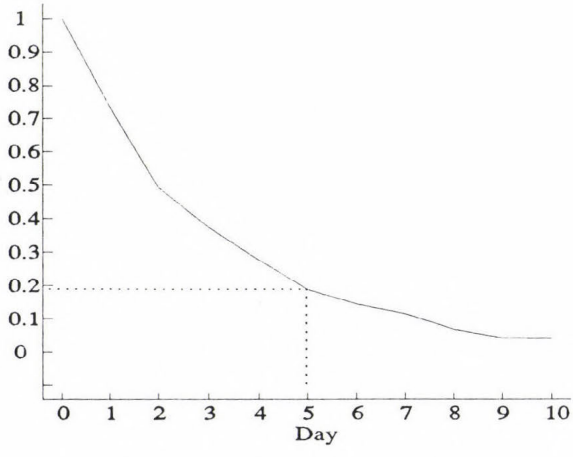

Fig. 1. Autocorrelations of daily mean temperature at Grand Island, U.S. in January.

Fig. 2 shows the histogram of this subsample of daily mean temperature at Grand Island. Even a visual examination suggests that a normal distribution commonly used to describe temperatures does not fit. Indeed, either a Chi-square test or a Kolmogorov-Smirnov test rejects the hypothesis that the temperature follows a normal distribution even at the 99% significance level. The distribution seems to be quite asymmetric or even bimodal. One mode of the histogram appears at relatively high temperatures, while the second and smaller

mode corresponds to very low temperatures. This second mode is associated with strong northern advection of cold air masses ('North Pole Express').

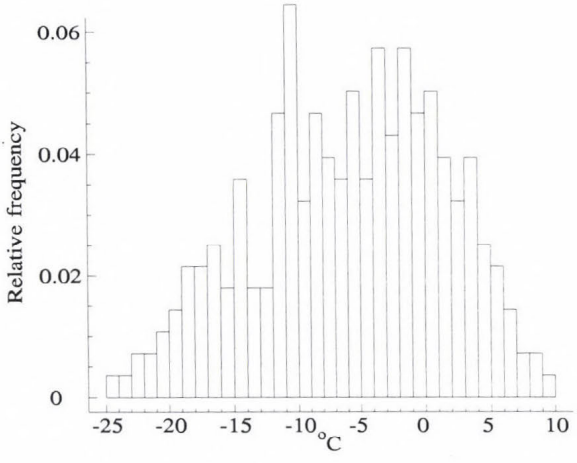

Fig. 2. The histogram of daily mean temperature at Grand Island, U.S. in January.

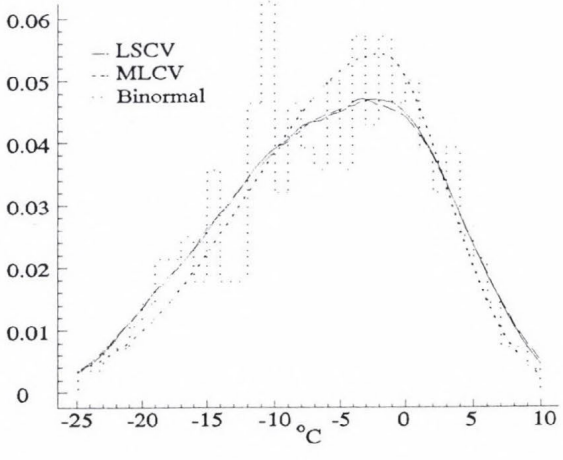

Fig. 3. Probability density function of daily mean temperature estimated with maximum likelihood (MLCV) and least square (LSCV) cross-validated bandwidths.

First the MLCV and LSCV techniques have been used with kernel Eq. (11) and nearly the same bandwidths have been obtained. According to the bandwidths $b = 5.4°C$ (LSCV) and $b = 5.9°C$ (MLCV) the corresponding densities are almost identical as it is seen in *Fig. 3*. In an earlier examination

(*Matyasovszky et al.*, 1994), a binormal distribution has been used to model daily mean temperature in Nebraska. The binormal distribution is similar to the Gaussian except for its symmetry as discussed in *Toth* and *Szentimrey* (1990). This density function indicated in Fig. 3 differs substantially from the two nonparametric estimates. This may be a consequence of the inadequacy of the binormal distribution model, or the inadequacy of using constant bandwidths for nonparametric estimation. Nonparametric estimates look overestimated at flat regions of $f(x)$, and underestimated at the peak regions.

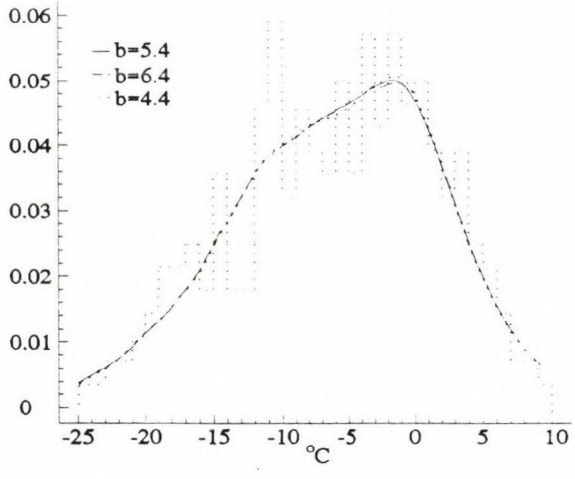

Fig. 4. Probability density function of daily mean temperature estimated by the Abramson method

A deeper analysis, therefore, should apply local bandwidths. *Fig. 4* shows the Abramson estimate of the probability density using pilot estimate with the bandwidth ($b = 5.4$°C) obtained from LSCV. Two other curves are indicated corresponding to pilot bandwidths somewhat larger and smaller than the LSCV-selected bandwidth. The three density functions seem identical which demonstrates the robustness of the Abramson estimator in view of different pilot estimates. The asymmetry of the density is considerably larger than in the constant bandwidth case. The location of the maximum corresponds to the expected principal mode, and a relatively strong increase of the curve is experienced at temperatures –15 to –10 °C, but no second mode has appeared. The Müller estimates show a finer structure of the underlying density, the second mode has formed clearly (*Fig. 5*).

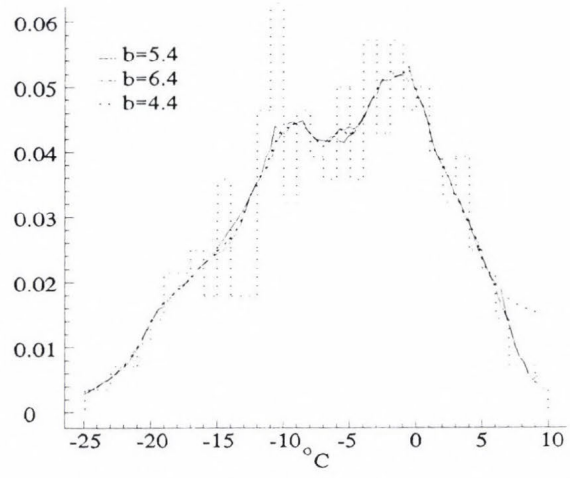

Fig. 5. Probability density function of daily mean temperature estimated by the Müller method.

5. Discussion and conclusions

First, two classical bandwidth selectors, namely the maximum likelihood and least square cross-validation were used to estimate probability density of daily mean temperature at Grand Island, Nebraska in January. The obtained densities are close to each other, but considerably different from a parametrically fitted binormal density (Fig. 2). Nonparametric estimates look overestimated at the flat regions of the density, and underestimated at the peak regions. Therefore, stabilized ($n^{-1/2}$ convergent) constant bandwidth selectors were not applied here since the use of local bandwidths seemed more promising. Figs. 3 and 4 strengthen the theoretical finding, namely: the Abramson and Müller estimators are robust in respect to the bandwidths used in pilot estimates. The only but important drawback to the present application example is that the two above techniques resulted in substantially different estimates. Which estimate can be rather believed ?

To answer this question a stronger knowledge of the properties of nonparametric density estimators is necessary. Three important and useful tools for understanding the behavior of these estimators include the asymptotic analysis, simulation and numerical calculation of one of the error criteria, like IMSE. The strength of asymptotic analysis is that it gives general results for each possible density. It is not known, however, how a given sample size is close to sizes where the behavior of a specific estimate can be substituted by the asymptotic behavior. By simulating samples of size n corresponding to a given density and by calculating kernel estimate for each simulated sample, the

properties of the estimator can be evaluated. The weakness of this process is that the results obtained are applicable only to the densities and sample sizes used in the simulation. The numerical calculation of error criteria seems to be the most promising approach to analyze the behavior of kernel estimators. The main idea is the exact calculation of error criteria for special classes of examples which make the calculation tractable, but at the same time represent a broad base of cases. *Marron* and *Wand* (1992) defined several classes of densities as mixtures of normal densities. The family of normal mixture densities is very flexible and the formulae derived allow exact analysis for a wide variety of density shapes. One of the most important findings is that the practical importance of higher order kernels is surprisingly small. This is the reason why only the order $k = 2$ was applied in this paper. Another important result is that the usual asymptotic approximation to IMSE can be quite inaccurate, especially when the underlaying density is not 'too smooth'. These conclusions were drawn for constant bandwidths, but similar, although less general findings have been obtained for local bandwidth case (*Terrel* and *Scott*, 1992; *Hall*, 1992).

Considering the above facts, my feeling is that the Müller estimator provides the better estimate in the present application case since the Müller estimate is based on an exact expression of MSE, while the choice of $b(x_i)$ in Eq. (15) resulting in the Abramson estimator Eq. (16) is based on the asymptotics of Eq. (15).

Acknowledgements—Much of this work was completed while the author was at the Department of Civil Engineering, University of Nebraska, NE 68588. Research leading to this paper has been partly supported by grants from the U.S. National Science Foundation, EAR-9205717, and the Great Plains Regional Center of the National Institute for Global Environmental Change.

References

Abramson, I.S., 1982: On bandwidth estimation in kernel estimators — A square root law. *Ann. Statist. 10*, 1217-1223.

Biondini, R.W., 1975: The log-normal distribution and cumulus clouds. *Proc. Fourth Conf. on Prob. and Stat. in Atm. Sci.*, 76-79.

Chiu, S.T., 1992: An automatic bandwidth selector for density estimation. *Biometrika 79*, 771-782.

Essenwanger, O.M., 1986: *General Climatology, 1B: Elements of Statistical Analysis. World Survey of Climatology*. Elsevier, Amsterdam-London-New York-Tokyo.

Gasser, T. and *Müller, H.G.*, 1979: Kernel estimation of regression functions. *Lecture Notes in Mathematics 757*, 23-68.

Gasser, T., Müller, H.G. and *Mammitzch, V.*, 1985: Kernels for nonparametric curve estimation. *Quart. J. Roy. Statist. Soc. B. 47*, 238-252.

Habbema, J.D.F., Hermans, J. and *Broek, V.D.*, 1974: A stepwise discrimination program using density estimation. In *Compstat* (ed.: *G. Bruckman*). Physica Verlag, Vienna.

Hall, P., 1987: On Kullback-Leibler loss and density estimation. *The Annals of Statistics 15*, 1491-1519.

Hall, P. and *Marron, J.S.*, 1987: Extent to which least squares cross-validation minimizes integrated squared error in nonparametric density estimation. *Prob. Theory Rel. Fields 74*, 567-568.

Hall, P., Sheather, S.J., Jones, M.C. and *Marron, J.S.*, 1991: On optimal data-based bandwidth selection in kernel density estimation. *Biometrika 78*, 263-269.

Hall, P., 1992: On global properties of variable bandwidth density estimators. *The Annals of Statistics 20*, 762-778.

Hennessey, J.J. 1977, Some aspect of wind power statistics. *J. Appl. Met. 16*, 119-128.

Justus, C.G., Hargraves, W.R. and *Yaclin, Y.*, 1976: Nationwide assessment of potential output from wind power generators. *J. Appl. Met. 15*, 673-678.

Marron, J.S., 1989: Automatic smoothing parameter selection: a survey. *Empir. Econ. 13*, 187-208.

Marron, J.S. and *Wand, M.P.*, 1992: Exact mean integrated squared error. *The Annals of Statistics 20*, 712-736.

Matyasovszky, I., 1992: Simulation of hourly incoming global radiation. In *Constructing a Typical Meteorological Year* (ed.: *G. Major*) (in Hungarian). *OMSZ Series*, 68, Budapest, Hungary.

Matyasovszky, I., Bogardi, I., Bardossy, A. and *Duckstein, L.*, 1994: Local temperature estimation under climate change. *Theor. Appl. Climatol. 50*, 1-13.

Müller, H.G., 1984: Smooth optimum kernel estimates of densities, regression curves and modes. *The Annals of Statistics 12*, 766-774.

Müller, H.G., 1991: Smooth optimum kernel estimators near endpoints. *Biometrika 78*, 521-530.

Müller, H.G. and *Wang, J.L.*, 1990: Locally adaptive hazard smoothing. *Prob. Theor. Rel. Fields 85*, 523-538.

Müller, H.G. and *Zhou, H.*, 1991: Comments on *Transformations in Density Estimation* by *M.P. Wand, J.S. Marron* and *D. Ruppert. J. Am. Stat. Assoc. 86*, 356-358.

Parzen, E., 1962: On the estimation of probability density function and mode. *Ann. Math. Statist. 33*, 1065-1076.

Rosenblatt, M., 1956: On some nonparametric estimates of a density function. *Ann. Math. Statist. 27*, 832-837.

Rudemo, M., 1982: Empirical choice of histograms and kernel density estimators. *Scand. J. Stat. 9*, 65-78.

Silverman, B.W., 1986: *Density Estimation for Statistics and Data Analysis*. Chapman and Hall, London.

Stewart, D.A. and *Essenwanger, O.M.*, 1973: Frequency distribution of wind speed near the surface. *J. Appl. Met. 17*, 1633-1642.

Terrell, G.R. and *Scott, D.W.*, 1992: Variable kernel density estimation. *The Annals of Statistics 20*, 1236-1265.

Toth, Z. and *Szentimrey, T.*, 1990: The binormal distribution: A distribution for representing asymmetrical but normal-like weather elements. *J. Climate 3*, 128-136.

IDŐJÁRÁS

Quarterly Journal of the Hungarian Meteorological Service
Vol. 101, No. 1, January–March 1997, pp. 33–43

Air quality simulation models in Poland

Anna Madany

Warsaw University of Technology,
ul. Nowowiejska 20, 00-653 Warsaw, Poland
E-mail: madany@jowisz.iis.pw.edu.pl

(Manuscript received 1 August 1996; in final form 17 October 1996)

Abstract—The paper is a review of the air pollution dispersion models developed and used in Poland over the recent 15 years. Information about these models has been collected on an inquiry basis. Characteristics of these models, input data, problems of model verification and uncertainty of modeling are extensively described and presented in a Polish paper (*Madany* and *Bartochowska*, 1995). This article presents a brief summary of the most essential information about these models as a supplement to *Szepesi*'s Compendium (*Szepesi*, 1989).

Key-words: environmental protection, air pollution model, air pollution control, meteorological modeling uncertainty, dispersion model classification.

1. Introduction

Mathematical models of air pollution dispersion have been developed worldwide for over three decades now. Apart from their analytical aspect, models are essential environmental quality management instruments. They are used, for example, in developing warning systems and in identifying areas of risk in case of random emission occurrence, such as nuclear explosions or failure of nuclear power plant. Recently they have been incorporated into the so-called 'integrated models' geared to analyses of specific scenarios of pollution emission abatement and to cost and environmental impact analyses including *(Juda-Rezler et al.* 1996). Modeling with the use of the so-called influence function are also of substantial importance since they allow the identification of sources — even distant ones — which contribute most to the contamination of a specific, usually protected area (*Uliasz,* 1993).

The Compendium of Regulatory Air Quality Simulation Models of *Szepesi* (1989) presents about 700 papers from all over the world, but models from Poland are not comprised therein. This fact was the reason for writing this article. Information about models developed and used in Poland has been

collected by means of inquiries sent out to interested parties. Responses were returned by 12 centers, which presented 29 models developed by as much as 50 persons. The authors mainly are scientists of Polish Universities: Warsaw University of Technology, Jagiellonian University of Cracow, Warsaw University, Military University of Technology and large public institutions: Polish Academy of Sciences, Institute of Meteorology and Water Management, Central Laboratory of Radiation Protection and several private companies. (*The respondents' addresses are available from the author, Warsaw University of Technology, ul. Nowowiejska 20, 00-653 Warsaw, Poland.*)

Air pollution modeling is performed by people of various educational backgrounds and profiles, biased by a specific recognition of the phenomena and processes described. However, this problem branch requires the co-operation of various experts representing various scientific disciplines.

2. General model characteristics

A comprehensive description of a large number of models requires ranking under an adopted classification. This is not simple since the models differ from each other in various aspects: mathematical structure, the description (or a lack of that) of the physical state and physical processes within the gaseous medium of pollution dispersion, simplifications adopted in the modeling, the purpose, temporal and spatial scale, topographical conditions, quantity and quality of input data. Air pollution model classifications presented in the literature (*Sorbjan*, 1989; *Juda-Rezler,* 1991; *Szepesi,* 1989; *Venkatram* and *Seigneur*, 1993) differ substantially and simultaneously clarify the extensive diversity of the mathematical description of this problem. *Table 1* presents some basic information about the Polish models. This shall only become usable after discussing certain terms comprised therein. The temporal scale of modeling is of essential meaning, because short-term forecasting models, for computing instantaneous values of pollution concentrations 12 or 24 hours in advance, must differ in the level of detail and structure from a climatological model, defining monthly mean or annual mean concentrations. The spatial scale of the modeled area is also a distinguishing feature.

Commonly known as the *turbulent diffusion equation* is the basis for the majority of pollution dispersion models. It is derived from the mass conservation principle for pollutant concentration (C). In this equation variables C and V (wind) are averaged values depending on the averaging time. Atmospheric turbulence has a wide energy spectrum comprising various scales of movement. Therefore the interpretation of computation and survey results should account for this fact. One of the simplest ways of parameterization of turbulent fluxes from this equation by averaged variables is to adopt the hypothesis of proportionality of pollution mass turbulent flux $\overline{F}_c$ to concentration gradient:

$\vec{F}_c = -\hat{K}\nabla C$ where $\hat{K}$ is a tensor with nine components. This approximation (the so-called 'first-order-turbulent closure') defines the turbulent fluxes at the given point with the use of mean pollution concentration gradients (K-theory). In the majority of such models it is assumed that the $\hat{K}$ tensor has non-zero components only along the main diagonal. Sometimes it is also assumed that it is constant in time and space, but measurements show that K depends on the scale of turbulence, turbulent energy, the atmospheric equilibrium and land configuration. These models are useless for the description of dispersion during convection, strongly unstable conditions and within front areas.

The turbulent diffusion equation is a second-order parabolic partial differential equation. The adoption of a number of assumptions and approximations allows an analytical approach, exemplified by the Pasquill model of 1961, widely used in engineering practice. The model defines the so-called Gaussian Plume Model. Plume dispersion is defined by the dispersion coefficients σ_y and σ_z, depending on the distance traveled by molecules at atmospheric equilibrium state. It is determined in classes as a function of wind velocity at 10 m altitude and insolation. However, such approximation neglects the vertical structure of the atmosphere and comprises an excessive range of atmospheric conditions into the inert equilibrium and thus it is applicable for flat surface and horizontally homogeneous meteorological fields. It was further assumed that pollution does not undergo any chemical changes, there is no gravity fall, the plume reflects at the ground and is not absorbed thereby. These assumptions substantially reduce the extent of model applicability. The Gaussian Segmented Plume Model is a modification of the Pasquill equation for non-stationary emission and meteorological conditions (*Markiewicz,* 1994). The non-linear diffusion equation in full form (when the wind and turbulence coefficients are functions of the co-ordinates) requires numerical integration. Integration schemes using finite differences were most commonly used, however this method is only applicable for surface or volumetric emission sources of large sizes as compared with the numerical grid integration step. These obstacles can however be eliminated by a finite element scheme of integration of areas in the vicinity of point emission sources. Recently spectral methods have also been used in Polish models *(Bartnicki*, 1994).

Numerical integration of coupled diffusion equations allows two-variant source or receptor-oriented computations of pollution concentrations (*Uliasz,* 1993). This technique will be described as follows: modeling is geared to the determination of a certain characteristic of concentration at the given receptor $\phi(C)$, which may be generally defined as the $C(r,t)$ concentration integral in time and space of the modeled area:

$$\phi(C) = \int\int RC\,dt\,d\vec{r} = \int\int C^* Q\,dt\,\vec{dr}, \tag{1}$$

where C^* is the influence function, Q is the source output of pollutant emission, R is the receptor function (geometry and location of source). Traditional source-oriented computations consist of the forward integration of the diffusion equations in respect of time for given emission sources, to obtain a $C(r,t)$ concentration over the time and space modeling domain. The $C^*(r,t)$ influence function for a given receptor is obtained by the backward integration of the coupled diffusion equation in respect of time. C^* depends on the meteorological conditions, dry and wet deposition and transformations of pollution in the atmosphere, but it does not depend on the emission sources. It should be noted that the computative capacity of such an option is limited to linear dispersion models.

The *Eulerian model* is the most frequently used one in atmospheric dynamics; it presents the field of velocity $V = f(r,t)$, variables in space (r) and time (t) at each point of the studied area in a spherical or in a Cartesian coordinate system (x,y,z), fixed with respect to the ground. This model allows the incorporation of complex processes, e.g. non-linear chemical reactions. In Eulerian model assumptions the emission value is averaged within the grid cell, resulting in an overestimation of the concentration values in the vicinity of the emission source. *Lagrangian models* are based on relationships betwen coordinates of all considered particles and time and their initial location. *Lagrangian Particle Dispersion Models* (LPD) have recently become an important tool for pollution dispersion investigation. They are based on the assumption that atmospheric diffusion may be modeled with the use of Markov chains (*Uliasz,* 1993). It should be noted that mesoscale modeling of dispersion is much more difficult than modeling at local scale, since both the mean and turbulent flow characteristics are non-stationary and non-homogeneous in mesoscale. Such conditions exclude the use of small-scale diffusion models based on Gaussian distribution or probability mathematics. In LPD models dispersion is modeled by the simulation of the movement of a large number of molecules at amounts proportional to the pollutant emission concentrations. These molecules are simultaneously or successively transported by the wind. In these models wind velocity components u_i and its turbulent fluctuations u'_i are obtained from the meteorological model (preprocessor), complex enough to forecast turbulent components of velocity, variances, covariances and Lagrangian R_i correlations. The disadvantages of the Lagrangian methods are the inability to model nonlinear pollution change processes and the high cost of computer computations. For larger areas *hybrid Lagrangian-Eulerian models* are used *(Uliasz,* 1993).

The double stochastic model introduced by Polish mathematicians (*Kazimierczyk et al.*, 1993) forecasts the nitric oxides concentration fields. Nitric oxides (NO_x) undergo complex changes in the atmosphere, they disappear and reappear at random, hence $NO_{x\ molecule}$ trajectories are discrete. In this paper these phenomena are defined in two planes of calculus of probability, one for microscopic processes, the other for macroscopic ones.

Table 1. Collection and description of models

1	2	3	4	5	6	7	8	9	10	11	12
No.	Acronim	Model class	Model design	Dimen-sion, scale	Type of sources	Modeled pollutant	Physical & chemical processes	Meteorological data		Other input data	Refer-ences
								General inf.	Para-meters		
1.	AIREM	Gaus	diag	2D local	point volum	rad	wash, dep, chem	clima	v, H, γ, d	radde	[6]
2.	ALINA	grid, Eul	diag, exp-rep	1D local	area	cool.tower plume, dust	physical	prepr, own, mesurements	T, v, γ, p, f	emi, pars	[8]
3.	KZMA	Gaus	diag, prog	reg	point, area	SO_2	dep, chem	clima	v, γ	emi, pars, k	[10]
4.	MDMS	grid, Lgr, Eul	reas, diag, prog	3D reg	point, area, line	SO_2	dep	prepr	T, v, p, f, N, othem	emi, top, pars, z_o, veg, soil	[24] [25]
5.	MCHGIG	grid, Psq	diag, prog	3D reg	point, area, volum	rad-dust	dep	stand	T, v, γ, H, p, N	emi, imi, othes	[28]
6.	MKOAS	grid, Eul, Psq	prog, exp.rep	3D local,	point	dust, SO_2, NO_2	dep, chem	stand, clima	T, v, γ, H, p, N	emi, top, othin	[29]
7.	MOD	grid, Eul, 3lay	diag	2D, reg, local	point, area	SO_2, SO_4	dep, chem	prepr, stand, field	v, T, γ	emi, τ_d, pars, k, z_o, v_d	[11]

1	2	3	4	5	6	7	8	9	10	11	12
8.	SPM	Gaus, Psq, segpl	diag, reas	reg, local	point	dust, SO_2, NO_x	wash, dep, chem	stand, field	v, H, γ, T, d	emi, s_o, v_d pars, λ, z_o	[17]
9.	OSMA	grid, Eul, spect	diag, oper	3D macro	area	SO_2, SO_4	wash, dep, chem	prepr, stand	v, H, d	emi, k, λ, τ_d, v_d	[2]
10.	POLIGW	grid, Eul Psq	diag, prog	3D local	point, line	–	–	stand	T, v, γ	emi, imi, othin	[3]
11.	RAPFOS	grid, Lgr, Eul, two preproc.	diag, prog Izerskie Montain	3D reg	point, line, area	SO_2	dep, wash	prepr	T, p, v, N, f, d, othem	emi, pars, z_o, othin	[15]
12.	REGFOR3	grid, Eul	prog	2D reg, 3lay	point, line, area	SO_2, dust	wash, dep, chem	prepr	v, γ, H, d	emi, v_d, pars, s_o, k, z_o, top	[9]
13.	REGSIM	Gaus, Psq	exp-rep	reg	point, area	dust, SO_2, NO_x	wash, dep, chem	clima	T, v, γ, H, d	emi, z_o, k, pars, λ, v_d	[4]
14.	REMOTA	grid, Eul, spect	diag, oper	2D reg	point, line	hamet	wash, dep	stand	v, d	emi, λ, v_d	[7]
15.	SO2.ARX	stat	prog, oper	local	area	SO_2	–	prepr	T, v	imi	[18]
16.	SOXNOX	grid, Eul K-theory	diag	2D reg	point, area	SO_2, NO_x, NH_3, SO_4	wash, dep, chem	prepr, stand	H, v, d, T	pars, λ, v_d, z_o, s_o, τ_d, k	[1]
17.	DOUBLY STOCH	grid, doubstoch	prog, diag	3D reg	point, line, area	NO_x	wash, dep, chem	prepr, clima, stand, field	T, v, γ, H, d, N	emi, imi, k, v_d, top	[14]

1	2	3	4	5	6	7	8	9	10	11	12
18.	STOCH	grid, Eul, Kalm	prog, diag	3D, reg, local	point, area	SO_2	wash, dep, chem	prepr, clima, stand, field	T, v, γ, H, d	emi, imi, k, v_d, top	[23]
19.	URFOR2	Gaus, Psq	diag, reas	local	point, area	SO_2,	wash, dep, chem	field	T, v, γ, H, d	emi, pars, λ, k, v_d, z_o, s_o	[5]
20.	URFOR3	grid, Eul	prog	2D local 3lay	point, line, area	SO_2, dust	wash, dep, chem	prepr	v, γ, H, d	emi, pars, s_o, k, top, v_d, z_o	[9]
21.	WDSW2G	Gaus, Eul, Psq	diag exp-rep	3D local	point, line	-	-	stand	T, v, γ	emi, imi, othin	[3]

Symbols and denotations:

area - area; **chem** - chemical reactions; **clima** - climatological; **cool.tower plume** - cooling tower plume; **D** - dimensional, **d** - atmospheric precipitation; **dep** - dry deposition; **diag** - diagnostic; **doubstoch** - doubly stochastic; **dust** - dust; **emi** - emission data; **Eul** - Eulerian; **exp.rep** -expert's report; **f** - relative humidity; **field** - field experiment mesurements; γ - Pasquill classification; τ_d - deposition time; **Gaus** - Gaussian; **grid** - grid, numerical; **H** - mixing layer height; **hemet** - heavy metals; **imi** - imission data; **k** - chemical transformation rate; **Kalm** - Kalman filter; λ - scavenging ratio; **lay** - layers; **line** - line; **local** -local; **Lgr** - Lagrangian; **N** - cloud cover; **othem** - others meteorological parameters; **othes** - others sources parameters; **othin** - other input data; **oper** - operating; **p** - atmospheric pressure; **pars** - source parameters; **point** - point; **prepr** - from preprocessor; **prog** - forecasting, prognostic; **Psq** - Pasquill; **rad** - radioactivity; **radde** - radioactive decay; **rad-dust** - radioactive dust; **reas** - researching; **reg** - regional; s_o - concentration background of pollutions; **segpl** - segmented plume; **soil** - soil thermal and wetness parameters; **spect** - spectral; **stand** - standard measurements; **stat** - statistical; **T** - temperature; **top** - topography, **wash** - washout; **veg** - vegetation cover; **v** - wind; v_d - dry deposition velocity; **volum** - volume; z_o - surface roughness coefficient; **[-]** - no information;

Numerous models applied in engineering practice use otherwise known regressive models, such as multiple regression and time series analysis. ARIMA — the Auto Regressive Integrated Moving Average is a model in which concentration forecast at a fixed point or mean for an area is expressed as a linear combination of concentrations in the past period and a purely random term (white noise). ARX-*A*uto *R*egressive with e*X*ogeneous input is an ARIMA model with an external input *(Morawska-Horawska* and *Tumidajski*, 1988). Pollution concentration in a given time interval is expressed here by a linear combination of past concentrations and external meteorological parameter values plus a random term. This model use is justified solely in climates with high weather pattern persistency, since synoptic and seasonal atmospheric variability cannot be avoided.

3. Model input data

The sets of input data for dispersion models may be divided into four groups:

- modeled area parameters defining characteristic features of the modeled area (roughness, vegetation, hypsometry, soils). These are prerequisite to numerical models; in analytical models, surface is usually defined solely by the roughness parameter,
- parameters defining the emission source — most often very difficult to obtain,
- parameters defining chemical changes occurring in pollution in the atmosphere — they are usually insufficiently identified. A complete description of pollution chemistry in the model should comprise about 1,000 reactions occurring between hundreds of various substances. Constant values defining the rate of reactions depend on numerous factors, i.e.: season of the year, part of the day, air humidity, presence of other substances which may act as catalysts,
- meteorological data.

The complex structure of a dispersion model accounting for a wide range of physical processes occurring in the atmosphere as well as chemical and/or nuclear changes requires information about meteorological variables, their spatial fields and transformations in time. Such data may be obtained from the so-called meteorological preprocessors only. These are primarily meteorological numerical models in macro or regional scale, operating in national or continental centers. Such a preprocessor may also be constituted by a numerical model of the atmospheric boundary layer on local, meso or regional scale, which generates a set of meteorological data exclusively for a specific diffusion model. Preprocessors are also the simple integral models of the mixing layer developed in Denmark (*Sorbjan,* 1989) and the uncomplicated models using the

similarity theory of the surface layer or boundary layer. Numerous models use standard data from meteorological synoptic stations; however they mainly include wind measurements at 10 m altitude, temperature measurements at 2 m altitude and cloud cover. Meteorological measurement data introduced into dispersion models should be *representative* of the modeling area with respect to the adopted averaging period (*Pruchnicki*, 1987). Current or historical measurement data should be controled and assimilated in accordance with the currently adopted techniques. Meteorological data processing may include interpolation to grid nodes. In case of winds for scales other than local a diagnostic model is required, satisfying the continuaity equation. The computation of Pasquill equilibrium classes is also included into the processing. Pollution emission measurements belong to the model input data set. These primarily come from monitoring networks and other gauge stations, registering pollution concentrations systematically at fixed times or automatically on a continuous basis.

4. Model evaluation problem

Authors of models developed in Poland only in a few cases provide information about verification against measurement data. A field experiment was organized in Cracow MONAT'84 *(Nowicki*, 1985) for models URFOR2, MOD and SPM. Dispersion models LPD and EGD, incorporated into the atmospheric mesoscale dispersion modeling system MDMS (*Uliasz*, 1993) package were verified against the mesoscale meteorological and dispersion experiment organized over Øresund strait on Baltic Sea. The Kalman filter model *(Twardowska,* 1989) was verified in Uppsala Silesia Industrial District against monitoring data TEST-88.

The model evaluation problem is too extensive to be discussed in this review, we shall just list the sources and types of modeling uncertainties. Difficulties in the mathematical definition of the atmospheric processes as well as measurement problems are the main reasons of model inadequacies. The atmosphere is highly variable in time and space, hence the models should be verified against measurement data in various weather conditions. Insufficient identification of chemical reactions affecting pollution in the atmosphere may have an essential impact on modeling outputs. Even the best diffusion model with high class meteorological preprocessor shall fail to provide results in line with the measurements if we overlook the natural decomposition of pollution or creation of a given compound in the atmosphere in various circumstances outside the emission source.

Uncertainty of modeling dispersion in the atmosphere (*Venkatram*, 1988) primarily results from the stochastic structure of atmospheric turbulence, but it is also related to the possibility of the comparison of results obtained in various models. This is linked with the notion of averaging over ensemble and with

random process realization. *Inherent* relates to the mean deviation between the concentration measured during one (of many) realization and the concentration averaged over the ensemble. The main problem resides in that the definition of 'ensemble' is not precise enough against real measurements. Modeling uncertainty also comprises errors in input data, errors in formulating the ensemble average (these are systematic errors): Model uncertainty analysis may to a certain extent become its means of evaluation.

Recapitulating, we can say that numerous dispersion models have been developed in Poland; modeling methods and levels are highly diverse. The majority of models were neither verified nor evaluated in terms of modeling outputs. The position of Poland in this field is noticeable. Many of the herein presented models are of high international standard, some of theme are unique *(Kazimerczyk et al.,* 1993).

Anna Madany asks the inquiry respondents for forgiveness: limited space in Időjárás publication did not allow the presentation of all the 84 publications of Polish model developers nor more extensive information about them, comprised in the article published in Polish by Madany and Bartochowska (1995).

References

[1] Abert, K., Budziński, K. and *Juda-Rezler, K.*, 1994: Regional air pollution models for Poland. *Ecological Engineering, Elsevier Science Publishers 3,* 225-244.

[2] *Bartnicki, J.*, 1994: Tree-dimensional long-range pseudospectral model for atmospheric transport of sulphur oxides. *Tech. Desc. Report of MSC-E*, Moscow.

[3] *Cibor, R., Rymarz, Cz.* and *Woźniak, M.*, 1984: Algorithm for computing local transport of chemical compounds with consideration for meteorological conditions. *Bull. MUT. XXX*, Warsaw (in Polish).

[4] *Chróściel, St. et al.*, 1984: Development of a computer software for REGSIM model. *Report PR8*, No. 7.2.3.3.b2, WUT Warsaw (in Polish).

[5] *Chróściel, St.* and *Markiewicz, M.*, 1985: Modeling of the atmospheric dispersion of sulphur dioxide in the urban Cracow agglomeration. *Envir. Prot. Engin.*, Vol. II, 65-72.

[6] *Dąbrowski, D.*, 1991: Assessment of radiological contamination model for nuclear power station. *Report Central Laboratory of Radiation Protection*. Warsaw (in Polish).

[7] *Hrehoruk, J. et al.*, 1993: Regional heavy metals of atmospheric transport model for Poland. *Reports of IMWM 3,* (in Polish).

[8] *Haman, K.E.* and *Malinowski, S.P.*, 1989: Observations of stack and cooling tower plumes and their comparison with plume model ALINA. *Atmos. Environ. 23*, 1223-1234.

[9] *Holnicki, P. et al.*, 1993: A multilayer computer model for air quality forecasting in urban/regional scale. *Control and Cybernetic 22,* No. 3, 5-28.

[10] *Jagusiewicz, A.*, 1980: *Methodics of Atmospheric Air Pollution Long-Term Forecasting*. Ed.: Environment Cultivation Institute, Warsaw (in Polish).

[11] *Juda-Rezler, K.*, 1986: Modelling of the air pollution in the Cracow area. *Atmos. Environ. 20,* 2449-2558.

[12] *Juda-Rezler, K.*, 1991: *Classification and Characteristics of Air Pollution Models Chemistry for Protection of the Environment*. Plenum Publishing Corporation, New York.

[13] *Juda-Rezler, K. et al.*, 1996: *Emission Abatement Strategies and the Environment Progress Report*. Copernicus, Warsaw University of Technology.

[14] *Kazimierczyk, P., Szabłowski, P.J.* and *Twardowska, K.*, 1993: Estimation and prediction of pollutant concentrations involved in nitrogen oxides cycles a doubly stochastic model. *Appl. Math. and Compt. Sci. 3,* 731-750.

[15] *Madany, A. et al.*, 1995: Numerical modeling of air pollution transport in Central Europe and preprocessing of meteorological data. *Proc. of Polish-British Conference.* Environmental Engineering, Warsaw, 16-18 Oct 1995, 142-148.

[16] *Madany, A.* and *Bartochowska, M.*, 1995: Review of Polish air pollution dispersion models. *Sc. Papers Warsaw Univ. of Technology 19*, 73-110 (in Polish).

[17] *Markiewicz, M.*, 1994: The Gaussian air pollution dispersion model with variabiliy of input parameters taken into account. Part I, II. *Envir. Prot. Engineering 1-4.*

[18] *Morawska-Horawska, M.* and *Tumidajski, T.*, 1988: Statistical models of mean daily SO_2 concentration in Cracow. *Reports of IMWM, Vol. IX,* No. 3 (in Polish).

[19] *Nowicki, M.*, 1985: MONAT 84, Experimental study for the needs of air pollution control in Cracow, Poland. *Environ. Protect Eng. 11*, No. 2, 11-15.

[20] *Pruchnicki, J.*, 1987: Methods of climatological data elaboration. *Polish Sc. Public.*, Warsaw, 203 (in Polish).

[21] *Sorbjan, Z.*, 1989: *Structure of the Atmospheric Boundary Layer.* Prentice Hall.

[22] *Szepesi, D.J.*, 1989: *Compendium of Regulatory Air Quality Simulation Models.* Akadémiai Kiadó, Budapest.

[23] *Twardowska, K.*, 1989: The stochastic processes and filtering theory in the prediction of air pollution in the Silesian district. *Proc. of the 28th SICE Annual Conference*, Vol. II., July 25–27, 1989 Matsuyama.

[24] *Uliasz, M.*, 1990: Development of the mesoscale dispersion modeling system using personal computers. Part I: Models and computer implementation. *Z. Meteor. 40,* 104-114, Part II, 285-298.

[25] *Uliasz, M.*, 1993: The atmospheric mesoscale dispersion modeling system. *J. Appl. Meteor. 32*, 139-149.

[26] *Venkatram, A.* 1988: Inherent uncertainty in air quality modeling. *Atmos. Environ. 22*, 1211-1227.

[27] *Venkatram, A.* and *Seigneur, Ch.*, 1993: Review of mathematical models for health risk assessment: II Atmospheric chemical concentrations. *Envir. Software 8*, 75-99.

[28] *Winnicki, J.*, 1989: Air pollution dispersion model in the atmospheric boundary layer. *Report 02/072/WAT.KOAS.* Military University of Technology, Warsaw (in Polish).

[29] *Winnicki, J.*, 1990: Theoretical basis for development of a pollution dispersion model in the atmospheric surface layer with orography in generalised Philips coordinates. *Report 01 KOAS.* Military University of Technology, Warsaw (in Polish).

IDŐJÁRÁS

Quarterly Journal of the Hungarian Meteorological Service
Vol. 101, No. 1, January–March 1997, pp. 45–54

Influence of the foundry plant operation on the heavy metal level in the air of New Belgrade in the reduced production regime

Dragana Đorđević[1], **Dušan Jovanović**[2], **Zorka Vukmirović**[3] and **Dragan Veselinović**[4]

[1]*Holding Co., Workers Safety, Fire and Environmental Protection, Deskaševa 7, YU-11000 Belgrade, Yugoslavia*
[2]*IChTM-Institute of Catalysis and Chemical Engineering, Njegoševa 12, YU-11000 Belgrade, Yugoslavia; E-mail: dusanmj@hf01.chem.bg.ac.yu*
[3]*Institute of Physics, Pregrevica 118, YU-11080 Zemun, Yugoslavia*
[4]*Faculty of Physical Chemistry, Studentski trg 12-14, YU-11000 Belgrade, Yugoslavia*

(Manuscript received 13 November 1995; in final form 19 February 1996)

Abstract—Due to their extensively deteriorating influence on biosphere, heavy metals in the human environment have been intensively monitored during the recent years. From September 1992 to September 1993, we continually monitored the content of heavy metals in the air of the New Belgrade industrial zone. We proved that the operation of the foundry BCF (Belgrade Casting Factory) influenced the heavy metal content in the air of its surroundings. BCF is an industrial complex located within an urban, densely populated area of New Belgrade. It has also been recorded that other sources were influencing the heavy metal content in the air, primarily the local wind re-suspension of soil particles, wind-transport from distant locations, etc.

Key-words: human environment, heavy metal monitoring, wind re-suspension.

1. Introduction

Heavy metals are emitted into the environment due to various human activities. They are widely used in industry and in the course of the smelting and combustion processes they are emitted mainly to the atmosphere. The main emission sources are:

- metal-processing industry,
- energy production, and
- road traffic.

Heavy metals are significant for their contribution to air pollution. In recent years their presence has been monitored all over Europe. From them As, Be,

Cd, Co, Cr, Cu, Hg, Mn, Ni, Pb, Sb, V, Zn, Se and Zr are of particular interest. The above mentioned metals' negative influence on the biosphere attracts an increased attention of researchers (*Guthner*, 1989; *Kurfurst*, 1989; *Santroch*, 1989). From September 1992 to December 1995 the economic sanctions influenced the production level and the continuity of the New Belgrade foundry plant operation. That enabled us to monitor the content of some heavy metals in the air in the conditions of the reduced production, as well as during the operation shut-downs, including the influence of the previous soil-pollution on the pollution during the mentioned period of time.

2. Database

2.1 Sampling site and period

This study has been aimed at the investigation of the heavy metal content in the air surrounding the foundry plant as influenced by its operation. The testing was made at five measuring spots that were located from 100 to 400 meters from the emission source, in different directions (as shown in *Fig. 1*) and positioned in a manner that enabled the monitoring of the heavy metal spreading.

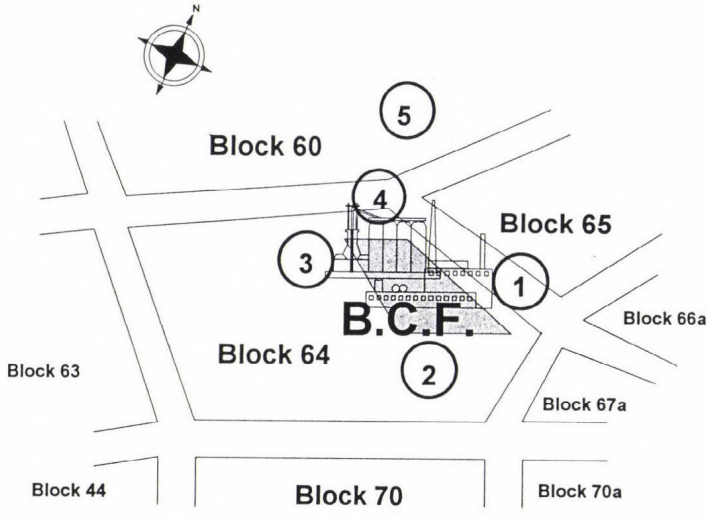

Fig. 1. Position of the Belgrade Casting Factory (BCF) with the positions of the measuring spots (1–5) as marked.

The Belgrade Casting Factory — BCF (Fabrika odlivaka Beograd — FOB) in New Belgrade was built in 1947 and the new foundry plant became

operational in 1977. It is located at the territory of the residential Block 64 (New Belgrade). It is a unique example of a newly constructed foundry plant within a residential area (Fig. 1). The foundry is located at the City of Belgrade territorial grounds (at the geographic latitude of 44°48'20''N and the geographic longitude of 20°25'30''E).

To the west of BCF there is the metalworking industrial complex (IMT) and to the southeast there is the Central City Heating Plant; one closer and the other further, respectively. Around the mentioned plants and between the residential blocks there are heavy-traffic arteries.

The basic source of the metal pollution in a smelting process is the furnace. The complexity of the technological process in a foundry is increased by a large number — more than 50 — of basic raw materials. The material is smelted and homogenized, and it leaves the furnace at the temperature of 1520°C–1550°C. The smelting process causes the rise and separation of different gases and waste materials.

The capacity of the foundry is about 1,000 tons of castings a month. In the last few years, i.e. from 1988 on, the production level was about 3,500 tons/month, with a drop in 1991 but with no interruptions. All the way through December 1992, the foundry continued to operate, although with a further drop of the production level, and then it shut down its operation. At the end of March 1993 the furnaces were started again and the reduced production process continued all through August 1993, the next shut-down. *Fig. 2* presents the production level in the period from September 1992 to September 1993.

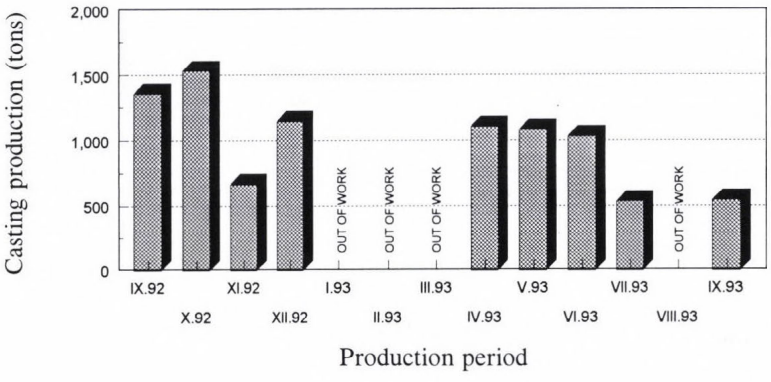

Fig. 2. Belgrade Casting Factory production level: September 1992–September 1993.

From September 1992 to September 1993, the samples were taken at the five designated (and mentioned) measuring spots, and in April 1993 an

additional measuring spot (measuring spot No. 6) was introduced. It is located within the eco-meteorological station at Ušće — New Belgrade.

At the onset of our investigations we monitored the Fe, Cu, Ni, Pb, Cd and Cr concentrations in the air surrounding the foundry complex, and since April 1993, in addition to the above mentioned metals, the concentrations of Mn, Zn and As were monitored as well.

2.2. The sample-taking process

The sampling system consists of a controlled-flow (app. 1 dm^3/min) membranous pump, a membranous PTFE filter of 1.0 μm and 0.22 μm pore openings, a gas meter and a probe mounted at 1.5 m above the ground with its opening facing downwards. In these conditions, and in a no-wind situation, we performed sampling of the particles of a diameter <20.0 μm (*Katz*, 1977; *Marendić-Miljković et al.*, 1989). The analysis of the investigated metals was done by the method of Atomic Absorption Spectrometry (AAS) using the VARIAN SpectrAA-20 Plus device. The standardizing of a solution for AAS analysis was performed through a precise measuring-up of the previously dried-up salt (at 105°C to constant mass) of the corresponding metal and by its diluting in the HNO_3/HCl solution in a normal dish. The arsenic was determined by a so-called hydride technique. The skimming of deposits off the membranous filter was done through a quantitative diluting in the HNO_3/HCl mixture, after which the solution was analyzed on AAS referred to as the 'blank' test. The standard AAS solutions were made by the usual analytical technique with adequate diluting. A calibration curve in the optimal measuring range was made for each individual metal.

3. Results and discussion

The average concentration data for Fall 1992, Winter 1992/93, Spring 1993 and Summer 1993, for each element (ng/m^3) and measuring position spot (Pos. 1.–Pos. 5), with the corresponding wind rose, are presented in the tables below (*Table 1–Table 4*).

The data clearly show that the copper concentrations, used for computing the average seasonal concentrations in summer, are below the detection limit for the given sampling conditions. Also, the average nickel and chromium concentrations in summer are below the detection margin for the given sampling conditions, while the average manganese concentrations are within the instrument's detection range for the given sampling conditions.

There are no reliable conclusions for the copper, nickel, chrome and manganese concentrations in spring and summer.

Table 1. Average concentrations (ng/m^3) and the wind rose for Fall 1992

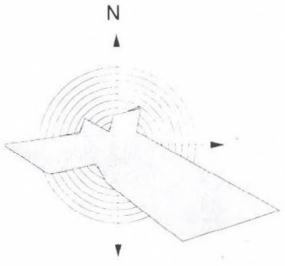

	Pos. 1	*Pos. 2*	*Pos. 3*	*Pos. 4*	*Pos. 5*
Cd	55	35	-	66	45
Cr	1400	360	50	900	550
Cu	78	82	140	157	79
Fe	460	280	-	410	230
Ni	110	240	-	500	450
Pb	490	430	940	760	640

Table 2. Average concentrations (ng/m^3) and the wind rose for Winter 1992/1993

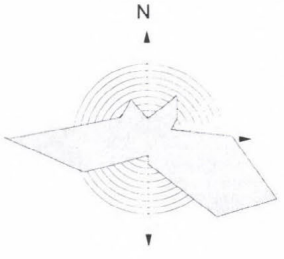

	Pos. 1	*Pos. 2*	*Pos. 3*	*Pos. 4*	*Pos. 5*
Cd	24	18	10	43	21
Cr	70	50	50	80	60
Cu	24	50	18	60	28
Fe	330	160	320	240	150
Ni	70	60	60	120	70
Pb	160	100	110	190	120

Table 3. Average concentrations (ng/m^3) and the wind rose for Spring 1993
(dl – detection limit)

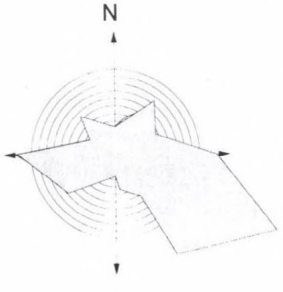

	Pos. 1	*Pos. 2*	*Pos. 3*	*Pos. 4*	*Pos. 5*
Cd	16	10	10	20	10
Cr	220	210	500	390	190
Cu	< dl	< dl	< dl	10	< dl
Fe	550	350	680	560	450
Ni	< dl	< dl	< dl	< dl	< dl
Pb	160	120	130	200	100
As	90	118	336	87	98
Mn	60	60	30	140	30
Zn	55	89	56	225	62

Table 4. Average concentrations (ng/m^3) and the wind rose for Summer 1993 (dl – detection limit)

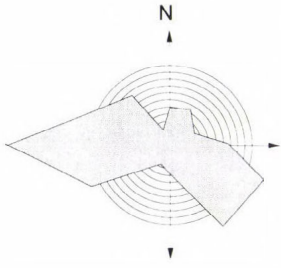

	Pos. 1	*Pos. 2*	*Pos. 3*	*Pos. 4*	*Pos. 5*
Cd	24	16	68	24	15
Cr	< dl	< dl	< dl	< dl	< dl
Cu	< dl	< dl	< dl	< dl	< dl
Fe	200	80	300	170	170
Ni	< dl	< dl	< dl	< dl	< dl
Pb	150	100	370	200	150
As	8	18	13	12	12
Mn	40	30	20	20	20
Zn	32	20	44	15	26

It is interesting to compare the measurements obtained in Milan, Vienna, Budapest and the regional K-puszta station (which is about 100 km southeast off Budapest, Hungary) with the concentration values (see *Table 5*) (*Molnár et al.*, 1993).

Table 5. Six-month (July-December 1991) average concentrations of metals in the air of the urban zones of the surrounding countries and the regional K-puszta station, in ng/m^3

	Milan	K-puszta	Budapest	Vienna
Cu	100.0	4.4	20.0	22.0
Cr	10.0	4.8	9.8	6.5
As	20.0	3.7	22.0	-
Zn	800.0	21.8	136.0	50.0
Mn	9.1	3.4	13.0	19.0
Ni	10.0	1.9	6.1	11.0
Fe	5,000.0	194.0	715.0	520.0
Pb	500.0	10.4	203.0	83.0

It is interesting to note that the individual elements' concentrations (Fe, Pb, As, Mn and Zn) taken in the industrial part of New Belgrade, where the metal-processing industry is located, in spring and summer, are close to the ones taken in Milan, Budapest and Vienna. The Zn concentrations in summer are close to those measured at the regional K-puszta station in Hungary which is far away from any urban zone.

The economic sanctions introduced in June 1992 caused the reduction of both the industrial production and the highway traffic frequency (due to the motor vehicle gas import embargo). The effect of the sanctions was the most

severe in spring and summer 1993. It caused the shut-down of almost all industrial facilities and reduced the traffic to a minimum. One of the consequences was a drop of the heavy metal concentration in the air of the New Belgrade industrial zone. In the course of the sampling BCF operated at about 15% of its capacity and with occasional shut-downs. Such conditions did not enable the monitoring of the factory's influence on the heavy metals in the air, since there were other sources that probably contributed to it; local wind re-suspension, primarily; aerosol transport from the highly contaminated distant locations; mechanical re-suspension, as well as the trash incineration (the probable source of Cr and As contained in the dyes).

The heavy metal content in the air in the measuring period was most probably very highly influenced by the local wind re-suspension of the particles that precipitated into the soil due to the foundry plant operation in the course of the years.

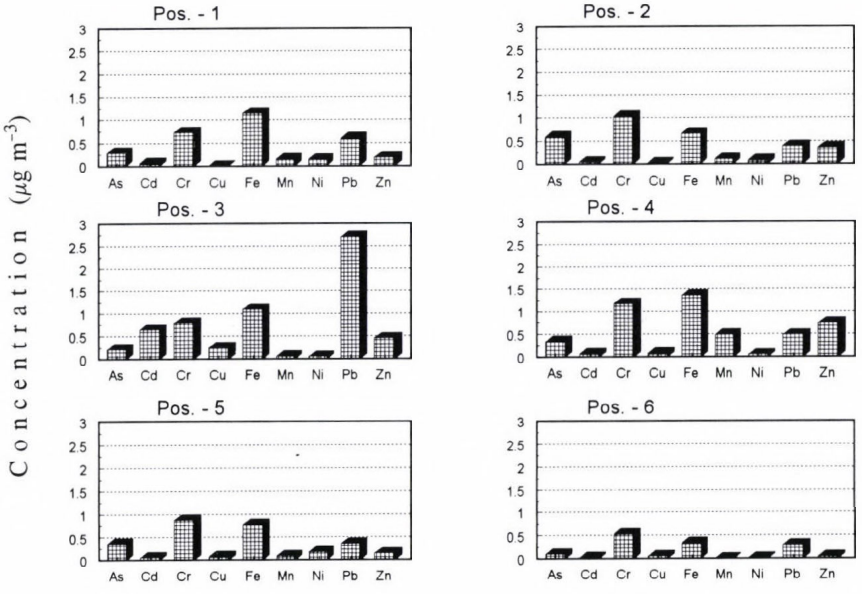

Fig. 3. Histograms of the maximal element concentrations measured at all the measuring positions including the position spot No. 6 (Ušće), for the period from April 1993–September 1993.

The histograms (*Fig. 3*) show that the maximal concentrations measured around the plant are considerably higher that those measured at Ušće. In the conditions of the significantly low operation regime (throughout the measuring

period), no significant differences were to be expected as Ušće is quite far (about 3,000 m) from the monitored emission source, and because the sampling included particles with long atmospheric residence time that were easily transported to large distances. Upon analyzing these values and having in mind that the production regime was very low and that the measuring spot No. 6 (Ušće) is above the grass, where the re-suspension effect is negligible, it is possible to claim that the re-suspension process is dominant in the vicinity of the plant. This conclusion is supported by the results obtained by averaging the concentration of the investigated metals over the period when the foundry did not work (January–March 1993 and August 1993), as shown in *Tables 6* and *7*.

Table 6. Average metal concentration values in the air around the foundry from January to March 1993

	Pos. 1	Pos. 2	Pos. 3	Pos. 4	Pos. 5
Cd	21	16	10	38	18
Cr	80	60	370	210	110
Cu	<5	<5	<5	20	<5
Fe	2160	160	510	290	180
Ni	40	40	20	70	40
Pb	130	60	130	120	60

Table 7. Average metal concentration values in the air around the BCF plant in August 1993 (dl – detection limit)

	Pos. 1	Pos. 2	Pos. 3	Pos. 4	Pos. 5
Cd	52	24	15	43	28
Cr	<dl	<dl	<dl	<dl	<dl
Cu	<dl	<dl	<dl	<dl	<dl
Fe	200	60	210	200	110
Ni	<dl	<dl	<dl	<dl	<dl
Pb	140	50	80	130	50

After reviewing the series of individual data and choosing the statistical distribution functions that describe the influence of the emission source, we tried to define the empirical functions through theoretical functions. Two theoretical functions were chosen: log-normal, best describing the influence of a constant emission source, and Weibull's theory that is best for describing the wind re-suspension. The Kolmogorov-test was used for fitting the empirical distributions with the theoretical functions. This analysis did not yield a good

match, which implies that the problem is complex due to the influence of a larger number of various processes on the heavy metal content in the air. Only the series of data pertaining to iron gives a proximate match with the theoretical function of the log-normal distribution, which implies that for this element the Casting Plant (BCF) is indeed a dominant emission source (*Garger et al.*, 1994; *Vukmirović*, 1989). The mis-match of the empirical and theoretical functions is indicative of the existence of a large number of equally dominant emission sources, except for iron. This is due to the fact that the added metal content in a casting charge is changed in dependence of the quality requirements, while the percentage of iron is fairly constant.

The Hydrometeorological Institute of the Republic of Serbia provided us with wind roses (seasonal and annual) for the period September 1992–September 1993 from the Surčin Meteorological Station, which is most representative for the New Belgrade territory. For this territory, the dominant wind courses are from the east and west-southwest direction, marked as prolonged acute angles of the polygons in such directions. The wind data were necessary to define the correlation between the dominant wind courses and the metals' concentration level in those directions. The measuring spot No. 3 was located to the east and the measuring spot No. 1 was located to the west-southwest. It has been found that the iron follows this correlation in winter, spring and summer, while the cadmium follows it in summer only. The other elements do not follow the dominant wind courses.

4. Conclusion

In the second measuring period the sampling conditions were unfavorable for defining the level of copper, nickel, chrome and manganese. High concentrations in the first measuring period (Fall–Winter) could be explained by their high concentrations in the particles originating from the wind re-suspension. With the foundry shut-down, in the course of time and especially after the seasonal rainfalls, these metals have been diluted, washed-down and migrated into the soil, which, in turn, reduced their level in the re-suspended particles.

In addition to the Casting Plant (BCP), there are other sources of heavy metal emission into the air, from which the most probable one is the re-suspension off the soil, except for iron for which the casting plant is a dominant source.

During that period the heavy metal concentration in the air did not drastically differ from the concentrations of the neighboring countries' urban zone air, with the Zn concentrations being in the order of magnitude of the ones measured at the regional K-puszta station.

The results of this study are significant for the environment restoration strategy, since they indicate that the metals are present around the industrial sources even after a drastic reduction in their emission.

References

Garger, E., Kashpur, V., Gurgula, B., Paretzke, H. and *Tschiersch, J.*, 1994: Statistical characteristics of the activity concentration in the surface layer of the atmosphere in the 30 km zone of Chernobyl. *J. Aerosol Sci. 25*, 767-777.

Guthner, G., 1989: Remarks on control of heavy metal emission in the Federal Republic of Germany. First Meeting 'Heavy Metal Emissions', Vol. 1, Prague, 24-26 Oct 1989.

Katz, M., 1977: *Methods of Air Sam-pling and Analysis*. APHA, Washington.

Kurfurst, J., 1989: ECE Project 'Heavy Metals Emissions', First Meeting 'Heavy Metal Emissions', Vol. 1, Prague, 24-26 Oct 1989.

Marendić-Miljković, J., Marković, D., Vukelić N. and *Vukmirović, Z.*, 1989: Trace metal deposition in the complex orographic conditions. *Proc. XIV International Conference on Carpathian Meteorology*, Sofia, 25-30 Sep 1989.

Molnár, Á., Mészáros, E., Bozó, L., Borbély-Kiss, I., Koltay, E. and *Szabó, Gy.*, 1993: Elemental composition of atmospheric aerosol particles under different conditions in Hungary. *Atmos. Environ. Part A, 27A*, 2457-2461.

Santroch, J., 1989: Heavy metals in atmospheric aerosol and deposition. First Meeting 'Heavy Metal Emissions', Vol. 1, Prague, 24-26 Oct 1989.

Vukmirović, Z., 1989: Lognormal distribution application for air-quality assessment. *J. Serb. Chem. Soc. 54*, 373-381.

IDŐJÁRÁS

Quarterly Journal of the Hungarian Meteorological Service
Vol. 101, No. 1, January–March 1997, pp. 55–64

Characteristic global and diffuse solar radiation values for Serbia

Miroslava Unkašević

Faculty of Physics, Institute of Meteorology, University of Belgrade,
11001 Belgrade, P.O. Box 550, Yugoslavia
E-mail: itosic@rudjer.ff.bg.ac.yu

(Manuscript received 13 November 1995; in final form 19 February 1996)

Abstract—Monthly mean global and diffuse solar radiation values recorded by the radiation network of the Serbian Meteorological Service were analyzed in order to derive characteristic elements of the solar climate from seven typical Serbian locations. The diffuse solar radiation was estimated for the stations where such data were not available by means of formulae relating the measured data to the 'clearness index' K, which is expressed as a function of the global and extraterrestrial solar radiation, and to the sunshine index I, which depends on the sunshine ratio n/N, where n is the monthly mean daily value of bright sunshine hours and N is the maximum possible value of sunshine hours. The relationship between the diffuse and global radiation leads to the conclusion that the 'clearness index' does not adequately describe all the climate variables. It can be stated that individual formulae based on the direct regression analysis of the measured data are necessary for different climatic and geographic areas.

Key-words: global and diffuse radiation, 'clearness' and sunshine indexes, correlation.

1. Introduction

The only available data of solar radiation from a number of locations are measurements of global radiation on a horizontal surface. Diffuse solar radiation data, which are necessary to design solar energy collecting systems, are usually not available.

Many studies dealing with the global solar radiation at various locations and regions of Southern Europe were made in the past (e.g. *Elena et al.*, 1981; *Pasquale*, 1987; *Santamouris* and *Katsoulis*, 1989; *Katsoulis et al.*, 1991), whereas *Katsoulis* (1991) has carried out a comparison of several diffuse solar radiation models for Greece.

The purpose of the present work is to investigate the solar radiation in Serbia and to test the applicability of a correlation model for the estimation of diffuse radiation at one site, Belgrade-Zeleno Brdo (φ = 44°47'N, λ = 20°23'E, h = 243 m asl). Only two stations in Serbia have relatively long-term records of global and diffuse radiation (Belgrade-Zeleno Brdo and Sjenica), whereas five stations can measure only the global radiation on the horizontal plane. Therefore, an estimate of the ratio of diffuse to global radiation would increase the usefulness of the existing data. There are several statistically-based correlation models relating global radiation G and its diffuse component D. The models accepted for estimating the horizontal diffuse solar radiation are of two types (*Lewis*, 1987). The first type is based on the expression of the monthly mean daily diffuse radiation ratio, D/G, as a function of the monthly mean daily 'clearness index' $K = G/G_0$ (G_0 is the extraterrestrial solar radiation). The second type, which is applied here as it correlates better with the measured values, is based on the expression of the ratio D/G or D/G_0 as a function of the sunshine index I (*Pasquale*, 1987), which is defined by the monthly mean daily value of bright sunshine hours, n, and the maximum possible sunshine N.

2. *Analysis of global solar radiation*

The measurements of global and diffuse solar radiation in Serbia began during the 1957–1958 International Geophysical Year. The network consisted of seven radiation measuring stations (*Fig. 1*), whose geographical coordinates and recording periods are shown in *Table 1*. Four stations are located in urban areas (Novi Sad, Belgrade-Zeleno Brdo, Negotin and Priština), whereas three are located on high mountains (Sjenica, Zlatibor and Kopaonik). The global solar radiation is measured by Moll-Gorczynski pyranometers, while the diffuse radiation is measured by diffusographs consisting of the above pyranometers equipped with special shading devices whose purpose is to exclude the direct radiation from the sun.

The monthly mean values of the global radiation available on horizontal surfaces for each station are listed in *Table 2*. These values have been derived from the daily totals of each month of the periods shown in Table 1.

Although the periods of observation are not the same in all the stations, some general conclusions may be drawn from the data. Although the local effects may be considerable, the data of global solar radiation are related to the geographic latitude. In the urban areas G has maximum values in June–July, (22.04–23.83 MJ m^{-2} day^{-1}) and minimum values in December (3.31–4.85 MJ m^{-2} day^{-1}). The mountain stations, because of their high elevation, show in the colder part of the year higher global radiation. Here the maximum of G (21.44–22.26 MJ m^{-2} day^{-1}) is recorded in July, whereas the minimum (4.80–5.62 MJ m^{-2} day^{-1}) is again in December.

Fig. 1. Territory of Serbia (full circles showing recording network for solar radiation). The insert in the upper right-hand corner shows the region relative to the remaining parts of former Yugoslavia and surrounding countries.

The data from Belgrade-Zeleno Brdo and Negotin stations (similar geographical latitude) can be taken as an example of the local effects on the global radiation. Negotin receives in the colder part of the year a smaller amount of global radiation than Belgrade-Zeleno Brdo, whereas the global radiation is higher in the warmer part of the year. Negotin is located behind mount Deli Jovan, near river Danube, so that fogs are frequent during the colder part of the year, while the Belgrade-Zeleno Brdo station is located out of the town centre.

3. Analysis of diffuse solar radiation

In order to calculate the diffuse component of the global radiation on a monthly basis on a horizontal surface at stations where actual diffuse radiation data are not available (Novi Sad, Negotin, Kopaonik, Zlatibor and Priština), we have worked out an equation relating the D/G ratio to the 'clearness' parameter K, based on long-term data from the Belgrade-Zeleno Brdo station. Relevant meteorological and solar radiation data for Belgrade-Zeleno Brdo and Sjenica are given in *Tables 3* and *4*. Because of its high elevation and lower geographical latitude Sjenica receives during the year a higher diffuse radiation than Belgrade-Zeleno Brdo.

Table 1. Geographic coordinates of the stations and recording periods

No.	Station	Period	Measurement
1.	*Novi Sad* φ = 45°20'N λ = 19°51'E h = 84 m asl	1964–1986	global
2.	*Belgrade-Zeleno Brdo* φ = 44°47'N λ = 20°23'E h = 243 m asl	1957–1990	global, diffuse
3.	*Negotin* φ = 44°14'N λ = 22°33'E h = 42 m asl	1957–1990	global
4.	*Zlatibor* φ = 43°44'N λ = 19°43'E h = 1029 m asl	1957–1986	global
5.	*Kopaonik* φ = 43°17'N λ = 20°48'E h = 1711 m asl	1981–1990	global
6.	*Sjenica* φ = 43°16'N λ = 20°01'E h = 1015 m asl	1964–1974	global, diffuse
7.	*Priština* φ = 42°39'N λ = 21°09'E h = 573 m asl	1967–1990	global

Table 2. Global solar radiation data for stations in Serbia (MJ m^{-2} day^{-1})

Station	Jan	Feb	Mar	Apr	May	Jun	Jul	Aug	Sep	Oct	Nov	Dec
Novi Sad	4.89	7.58	11.72	16.01	19.74	22.09	22.02	19.18	14.37	9.88	5.11	3.31
Belgrade	5.22	7.90	12.68	16.56	20.17	22.37	22.29	19.93	15.36	10.52	5.73	3.77
Negotin	4.76	7.53	11.59	15.97	21.05	23.25	23.83	20.89	15.87	10.95	4.75	3.59
Zlatibor	5.83	8.68	12.20	15.70	18.63	20.88	21.44	19.23	14.90	10.50	6.28	4.80
Kopaonk	6.80	10.02	13.22	16.63	19.70	21.82	22.26	19.50	14.99	10.87	6.61	5.38
Sjenica	6.91	10.21	14.28	17.01	20.44	22.74	22.84	20.18	19.85	11.36	7.57	5.62
Priština	5.88	8.69	13.53	16.96	20.24	22.43	22.18	20.45	15.65	11.52	6.78	4.85

Table 3. Indexes *K* and *I* and measured and estimated values of diffuse solar radiation for Belgrade-Zeleno Brdo

Month	K	I	D′ measured (MJ m^{-2} day^{-1})	D′ estimated from equations (MJ m^{-2} day^{-1}) for Belgrade-Zeleno Brdo					
				(1)	(2)	(3)	(4)	(5,6,7)	(8)
Jan	0.42	0.25	3.16	2.99	2.74	2.32	2.99	4.75	3.00
Feb	0.44	0.33	4.68	4.18	3.95	3.53	4.34	6.75	4.45
Mar	0.49	0.41	6.16	5.91	5.59	4.82	6.21	9.84	6.40
Apr	0.50	0.47	8.23	7.58	7.28	6.14	8.01	12.50	8.25
May	0.51	0.50	9.34	9.09	8.46	7.32	9.32	14.70	9.35
Jun	0.54	0.55	9.95	9.80	8.82	7.61	9.72	15.56	9.51
Jul	0.55	0.63	9.17	9.73	8.41	7.38	9.00	14.67	8.26
Aug	0.56	0.64	7.99	8.70	7.32	6.44	7.87	13.28	7.14
Sep	0.54	0.58	6.40	6.73	6.03	5.22	6.55	10.46	6.28
Oct	0.51	0.49	4.62	4.74	4.45	3.82	4.91	7.73	4.94
Nov	0.41	0.31	3.24	3.34	3.07	2.61	3.38	5.15	3.46
Dec	0.35	0.24	2.52	2.75	2.30	1.98	2.61	3.82	2.61
RMSE				0.397	0.662	1.487	0.197	3.969	0.282

Table 4. Index *I* and measured and estimated values of diffuse solar radiation data for Sjenica

Month	I	D′ measured (MJ m^{-2} day^{-1})	D′ estimated from Eq. (8) (MJ m^{-2} day^{-1})
Jan	0.27	4.82	4.28
Feb	0.32	6.47	6.00
Mar	0.39	7.68	7.77
Apr	0.43	8.80	8.81
May	0.46	9.88	10.20
Jun	0.49	10.72	10.92
Jul	0.51	10.58	10.64
Aug	0.50	8.80	9.55
Sep	0.49	7.14	7.61
Oct	0.48	4.87	5.52
Nov	0.41	3.81	4.02
Dec	0.24	3.87	3.59
RMSE			0.408

Based on the Belgrade-Zeleno Brdo experimental data, the regression equation that represents best the relation between the D/G ratio and K is of the form:

$$D/G = 2.59 - 7.76K + 7.00K^2, \tag{1}$$

which is shown in *Fig. 2* for $0.35 \leq K \leq 0.56$. G_0 may be calculated from *Sellers* (1965) and *Robinson* (1966) using a value of 1368 W m^{-2} for the solar constant:

$$G_0 = 37.610\,(\bar{d}/d)^2\,(H \sin\varphi \sin\delta + \cos\varphi \cos\delta \sin H),$$

where $\bar{d}/d$ is the ratio of the mean to the instantaneous distance of the earth from the sun, φ is the latitude, δ is the declination angle, and H = arc cos (–tan φ tan δ) is the hour angle.

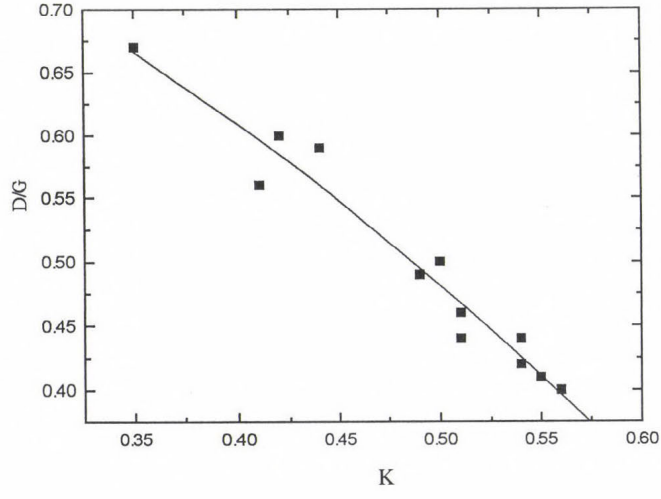

Fig. 2. D/G as a function of the 'clearness' index *K* based on Belgrade-Zeleno Brdo data (1957–1990).

The ratio of the daily diffuse to global radiation D/G was also examined by *Page* (1961) by means of data from ten locations in the belt between 40°N to 40°S. He derived the following relationship:

$$D/G = 1.00 - 1.13K. \tag{2}$$

Klein's (1977) mathematical expression for the same relation is expressed as follows:

$$D/G = 1.390 - 4.027K + 5.531K^2 - 3.108K^3, \quad \text{for } 0.4 \leq K \leq 0.5. \tag{3}$$

Using the Belgrade-Zeleno Brdo experimental data, the regression equation that represents better the relation between D/G_0 and the sunshine index I is:

$$D/G_0 = 0.208 + 0.198\,I - 0.277\,I^2, \tag{4}$$

which is shown in *Fig. 3*, for $0.25 < I < 0.64$.

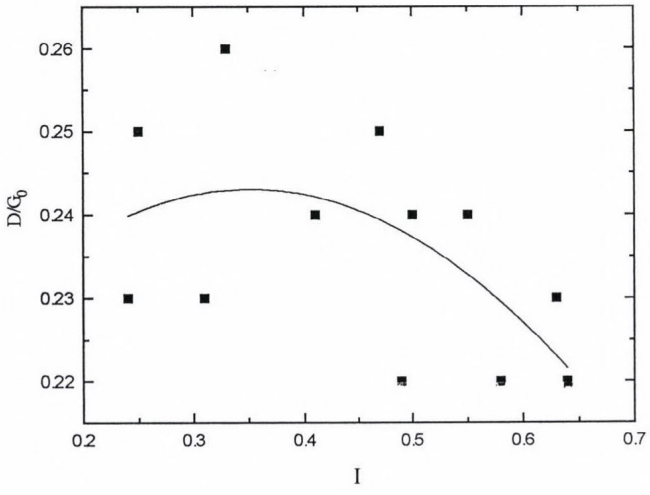

Fig. 3. D/G_0 as a function of the sunshine index I based on Belgrade-Zeleno Brdo data (1957–1990).

Hay (1965), analysing data from Canadian stations, proposed the following location-independent formulae:

$$G' = G\left\{1 + \alpha\left[\beta_0 I + \alpha_c(1 - I)\right]\right\}, \tag{5}$$

$$D'/G' = 0.9702 + 1.6688(G'/G_0) - 21.3030(G'/G_0)^2 + 51.2880(G'/G_0)^3$$
$$- 50.0810(G'/G_0)^4 + 17.5510(G'/G_0)^5 \tag{6}$$

and

$$D = D' + G\alpha\,[\beta_0 I + \alpha_c(1 - I)], \tag{7}$$

where G' and D' are the global and diffuse components of the solar radiation incident on a horizontal surface, α is the albedo (0.2) and β_0 and α_c are constants with values of 0.60 and 0.25, respectively. *Iqbal* (1979) used also data from three locations in Canada to propose the following equation:

$$D/G = 0.791 - 0.635\,I. \tag{8}$$

In order to calculate D accurately, the procedure was based on estimating D from Eqs. (1) to (8) for each month and then comparing its values with the data of Belgrade-Zeleno Brdo. The accuracy of the estimated values from the six models was tested by calculating the root mean square error (*RMSE*), which is defined as:

$$RMSE = \left\{ \frac{\left[\sum (D_{ci} - D_i)^2\right]}{12} \right\}^{\frac{1}{2}}, \tag{9}$$

where D_{ci} is the i-th calculated and D_i is the i-th measured value. Generally, lower *RMSE* records indicate that the model gives more accurate and realistic values.

The obtained results of the applied models are presented in Tables 3 and 4 with computations of *RMSE* and measured values of D for Belgrade-Zeleno Brdo and Sjenica. It can be seen that the data agree better with models (4) and (8), which include the sunshine index I, than with models (1), (2) and (3) which include the 'clearness' index K. For this reason, the values of D were calculated for Sjenica from Eq. (8) and compared with the measured values (Table 4). The calculated *RMSE,* similarly to the case of Belgrade-Zeleno Brdo indicates a good agreement between the measured and calculated values.

From the comparison of the measured values and predicted results given in Tables 3 and 4, it turns out obviously that the deviation from *Hay*'s (1965) formula is very high. Among the remaining results, the equations of *Page* (1961) show lower *RMSE* than that of *Klein*'s (1977) expression.

As there is a good agreement between the measured and calculated values of D for Belgrade-Zeleno Brdo and Sjenica stations, *Iqbal*'s (1979) equation (8) was also used to calculate the diffuse radiation at the stations where only global radiation was measured. The obtained results are presented in *Fig. 4*.

The estimation of the monthly average daily diffuse radiation D for five sites of Serbia shows that the above equation is valid for the region where the sunshine index was obtained. Also, it is very simple to use. However, *Katsoulis*'s (1991) study indicates that the diffuse solar radiation on a horizontal surface in Athens can be better estimated by using formulae proposed by *Page* (1961) and *Hay* (1965). Therefore, at moderate latitudes the local climate may have a markedly dominant effect.

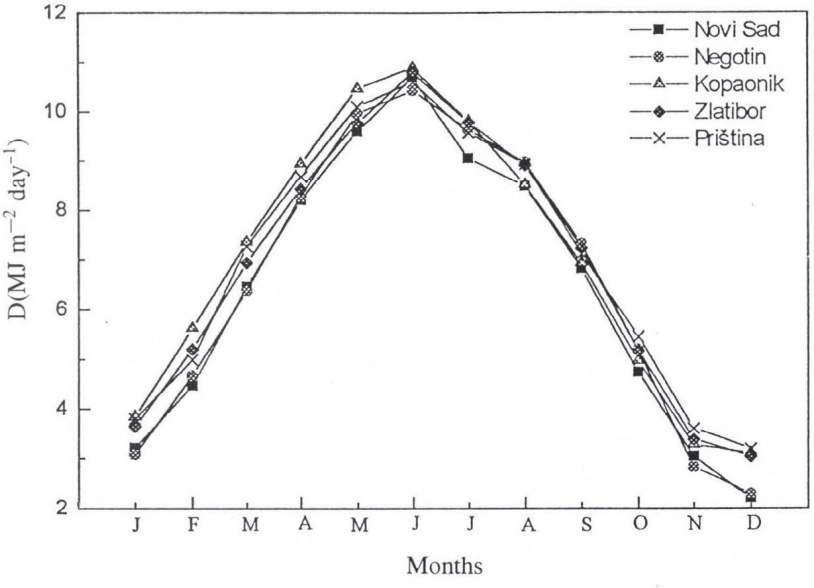

Fig. 4. Estimated annual variation of daily diffuse radiation for different stations in Serbia.

4. Conclusion

The yearly solar global and diffuse radiation in Serbia obviously depends both on the solar elevation and on the prevailing weather conditions. Based on the Belgrade-Zeleno Brdo data, the regression equations between D/G and K and D/G_0 and I lead to the conclusion that individual expressions are required for different climatic and geographic regions (see *Pasquale*, 1987).

The main conclusion of the study is that the diffuse solar radiation on horizontal surfaces in Serbia can be better estimated from formulae which include the sunshine index I, as proposed by Iqbal (1979) than from those which include the 'clearness' index K. However, the use of equations of this type is complicated by the effect of the different types of clouds as well as by significant errors in the duration of the sunshine recording.

References

Elena, A., Flocchini, G. and *Pasquale, V.*, 1981: Solar global radiation and climate at Genova, Italy. *Arch. Met. Geoph. Biol., Ser. B, 29*, 129-135.

Hay, J.E., 1965: Calculation of monthly mean solar radiation for horizontal and inclined surfaces. *Solar Energy 9*, 301-307.

Iqbal, M., 1979: A study of Canadian diffuse and total solar radiation data. *Solar Energy 22,* 81-86.

Katsoulis, B., 1991: A comparison of several diffuse solar radiation models for Greece. *Theor. Appl. Climatol. 44*, 181-186.

Katsoulis, B.D, Retalis, D.A. and *Nikolakis, D.I.*, 1991: Some solar radiation statistic for Greece. *Ann. Geophysicae 9*, 309-318.

Klein, S.A., 1977: Calculation of monthly average insolation on titled surfaces. *Solar Energy 19*, 325-329.

Lewis, G., 1987: The applicability of diffuse solar radiation model to Huntsville, Alabama. *Solar Energy 38*, 55-57.

Page, J.K., 1961: The estimation of monthly mean values of daily total short-wave radiation on vertical and inclined surfaces, from sunshine records for latitudes 40°N to 40°S. *Proc. of UN Cont. on New Sources of Energy*, Rome, Italy.

Pasquale, V., 1987: Solar irradiance in NW Italy. *Theor. Appl. Climatol. 38*, 85-92.

Robinson, N., 1966: *Solar Radiation*. Elsevier, New York.

Santamouris, M. and *Katsoulis, B.*, 1989: Solar radiation over the northwest part of Greece. *Solar and Wind Technology 6*, No. 1, 79-84.

Sellers, W.D., 1965: *Physical Climatology*. University of Chicago Press, Chicago.

BOOK REVIEWS

Hervé Le Treut (ed.): **Climate Sensitivity to Radiative Perturbations. Physical Mechanisms and Their Validation.** Srpinger-Verlag 1996. ISBN 3-540-60434-0. NATO Advanced Science Institutes Series Vol. 34. pp. 330, price 378 DEM.

This book gathers many of the papers, both invited and contributed, which were presented during the NATO Advanced Research Workshop on *'Climate Sensitivity to Radiative Perturbations'*, held in Paris, July 1994. A workshop dedicated to the FANGIO (Feedback Analysis of General Circulation Models for Intercomparison and Observation) programme was embedded within the NATO workshop, and some of the papers presented in the book correspond to this programme.

Section 1 contains contributions which are not dedicated to the study of one model but address more general or methodological issues. Many of the questions raised in this section receive answers, directly or indirectly, within the papers of Section 2 and 3 which concern individual models. In Section 1 presented are details of investigations on the Atmospheric Model Intercomparison Project including results concerning radiative forcing calculated by means of 25 different models, absorption of solar radiation by clouds, evaluation of variability of tropical convection in GCMs by using geostationary satellite data, impact of volcanic eruption on global temperature, stochastic models to represent the temporal variability of global average radiation budget and temperature.

Section 2: 'Cloud and water vapour feedbacks in atmospheric models' presents many details of results obtained from research on warm pool heat budget by different versions of the ECHAM model developed at the Max Planck Institute, Hamburg; GCM implications for mechanism determining cloud and water vapour feedbacks, comparison of convection parameterisations in an atmospheric GCM, sensitivity of the simulated climate to parameterisation of cloud optical properties in GCM, the role of cloud-radiative interactions in the sensitivity of the ECMWF model, water vapor and cloud feedback in Atmospheric General Circulation Models, cloud feedbacks in the UKMO unified model etc.

Section 3: 'Feedbacks in coupled ocean-atmosphere models' contains papers concerning the climate sensitivity and cloud-albedo feedback in a global coupled ocean-atmosphere GCM, cloud effects on the ocean surface energy budget, feedback processes in the GFDL (Geophysical Fluid Dynamics Laboratory) R 30–14 level GCM, aerosol and greenhouse gases forcing, analysis of the monsoon response to radiative perturbations in GCM simu-

lations, large scale atmosphere-ocean interaction and climate, a 65–70 year oscillation in observed surface temperatures.

Altogether 43 researchers and lecturers from 12 countries and at least 20 institutions took part in the meeting.

G. Koppány

C.D. Schönwiese: **Klimaänderungen. Daten, Analysen, Prognosen.** Springer-Verlag, 1995, ISBN 3-540-59096-X. pp. 226, 58 figures, several colour photos, 16 tables.

The author has been a professor of meteorology at the University of Frankfurt/Main since 1981 and director of the Environment Research Centre at the same University since 1994. He is well known as an excellent expert in the field of climate variation and a skilled investigator concerning global change. He is a scientific adviser at WMO, as well.

This book comprises the most important elements of climatology including the term or definition of climate, the time scales of the atmospheric phenomena, the survey of the climate system (Chapter 1), the sources of climate data including paleoclimatic information, e.g. historical data, glacier expansions, pollen analyses etc. (Chapter 2). Statistical methods most frequently applied in climatology (Chapter 3), a very good summary of methods and results of paleoclimatology (Chapter 4), the natural factors causing climate changes (Chapter 5), some features of climate models (Chapter 6), the consequences of human activity in global change (Chapter 7), and the possible future of climate (Chapter 8). The simple survey of subjects discussed in individual chapters may convince the reader that is this book one can find elementary knowledge on climatology as well as up-to-date information on the past climate of the earth including some methods of paleoclimatology, the recent assessments on the future of our climate making use of the newest climate models. The didactics of the book's construction is so good that the reader is attracted to read over all the chapters one after the other from the first to the last one. In addition to the newest knowledge, this book presents several color photos, one of them made by a satellite.

Finally the author attaches the symbols and abbreviations used most frequently in the book as well as the list of additional recent works concerning the relevant topic. About 130 books and papers are cited.

G. Koppány

ATMOSPHERIC ENVIRONMENT

an international journal

To promote the distribution of Atmospheric Environment *Időjárás* publishes regularly the *contents* of this important journal. For further information the interested reader is asked to contact *Prof. P. Brimblecombe,* School for Environmental Sciences, University of East Anglia, Norwich NR4 7TJ, U.K. E-mail: atmos_env@uea.ac.uk

Volume 31 Number 1 1997

Volume 31 Number 2 1997

Volume 31 Number 3 1997

The Dutch Aerosol Project (1992–1994)
Plus Regular Papers

M.W. Gallagher, K.M. Beswick, J. Duyzer, H. Westrate, T.W. Choularton and *P. Hummelshøj:* Measurements of aerosol fluxes to Speulder Forest using a micrometeorological technique, 359-373.

A.T. Vermeulen, G.P. Wyers, F.G. Römer, N.F.M. Van Leeuwen, G.P.J. Draaijers and *J.W. Erisman:* Fog deposition on a coniferous forest in The Netherlands, 375-386.

G.P.J. Draaijers, J.W. Erisman, N.F.M. Van Leeuwen, F.G. Römer, B.H. Te Winkel, A.C. Veltkamp, A.T. Vermeulen and *G.P. Wyers:* The impact of canopy exchange on differences observed between atmospheric deposition and throughfall fluxes, 387-397.

W. Ruijgrok, H. Tieben and *P. Eisinga:* The dry deposition of particles to a forest canopy: a comparison of model and experimental results, 399-415.

Regular Papers

M.J. Ten Harkel: The effects of particle-size distribution and chloride depletion of sea-salt aerosols on estimating atmospheric deposition at a coastal site, 417-427.

M. Bennett and *G.C. Hunter:* Some comparisons of Lidar estimates of peak ground-level concentrations with the predictions of UK-ADMS, 429-439.

S. Parat, A. Perdrix, H. Fricker-Hidalgo, I. Saude, R. Grillot and *P. Baconnier:* Multivariate analysis comparing microbial air content of an air-conditioned building and a naturally ventilated building over one year, 441-449.

E. Weingartner, C. Keller, W.A. Stahel, H. Burtscher and *U. Baltensperger:* Aerosol emission in a road tunnel, 451-462.

C.-S. Chen and *C.-Y. Lin:* A numerical study of airflow over Taiwan Island, 463-473.

G.R. Carmichael, A. Sandu and *F.A. Potra:* Sensitivity analysis for atmospheric chemistry models via automatic differentiation, 475-489.

Z. Cvetnić and *S. Pepeljnjak:* Distribution and mycotoxin-producing ability of some fungal isolates from the air, 491-495.

B.C. Faust, K. Powell, C.J. Rao and *C. Anastasio:* Aqueous-phase photolysis of biacetyl (an α-dicarbonyl compound): a sink for biacetyl, and a source of acetic acid, peroxyacetic acid, hydrogen peroxide, and the highly oxidizing acetylperoxyl radical in aqueous aerosols, fogs, and clouds, 497-509.

Volume 31 Number 4 1997

M. Piringer, K. Baumann, H. Rötzer, J. Riesing and *K. Nodop:* Results on perfluorocarbon background concentrations in Austria, 515-527.

S.-O. Baek, Y.-S. Kim and *R. Perry:* Indoor air quality in homes, offices and restaurants in Korean urban areas—indoor/outdoor relationships, 529-544.

A. Virkkula: Performance of a differential optical absorption spectrometer for surface O_3 measurements in the Finnish Arctic, 545-555.

D. Brocco, R. Fratarcangeli, L. Lepore, M. Petricca and *I. Ventrone:* Determination of aromatic hydrocarbons in urban air of Rome, 557-566.

M.H. Hermanson, C.L. Monosmith and *M.T. Donnelly-Kelleher:* Seasonal and spatial trends of certain chlorobenzene isomers in the Michigan atmosphere, 567-573.

M. Gonzalez: Analysis of the effect of microscale turbulence on atmospheric chemical reactions by means of the p.d.f. approach, 575-586.

M. Z. Jacobson: Development and application of a new air pollution modeling system—Part III. Aerosol-phase simulations, 587-608.

T. Castro, L.G. Ruiz-Suárez, J.C. Ruiz-Suárez, M.J. Molina and *M. Montero:* Sensitivity analysis of a UV radiation transfer model and experimental photolysis rates of NO_2 in the atmosphere of Mexico City, 609-620.

Volume 31 Number 5 1997

Short Communications

Volume 31 Number 6 1997

Volume 31 Number 7 1997

NOTES TO CONTRIBUTORS

The purpose of *Időjárás* is to publish papers in the field of theoretical and applied meteorology. These may be reports on new results of scientific investigations, critical review articles summarizing current problems in certain subject, or shorter contributions dealing with a specific question. Authors may be of any nationality but papers are published only in English.

Papers will be subjected to constructive criticism by unidentified referees.

* * *

The manuscript should meet the following formal requirements:

Title should contain the title of the paper, the names(s) of the author(s) with indication of the name and address of employment.

The title should be followed by an *abstract* containing the aim, method and conclusions of the scientific investigation. After the abstract, the *key-words* of the content of the paper must be given.

Three copies of the manuscript, typed with double space, should be sent to the Editor-in-Chief: *P.O. Box 39, H-1675 Budapest,* Hungary.

References: The text citation should contain the name(s) of the author(s) in Italic letter or underlined and the year of publication. In case of one author: *Miller* (1989), or if the name of the author cannot be fitted into the text: *(Miller,* 1989); in the case of two authors: *Gamov* and *Cleveland* (1973); if there are more than two authors: *Smith et al.* (1990). When referring to several papers published in the same year by the same author, the year of publication should be followed by letters a,b etc. At the end of the paper the list of references should be arranged alphabetically. For an article: the name(s) of author(s) in Italics or underlined, year, title of article, name of journal, volume number (the latter two in Italics or underlined) and pages. E.g. *Nathan, K. K.,* 1986: A note on the relationship between photosynthetically active radiation and cloud amount. *Időjárás 90,* 10-13. For a book: the name(s) of author(s), year, title of the book (all in Italics or underlined with except of the year), publisher and place of publication. E.g. *Junge, C. E.,* 1963: *Air Chemistry and Radioactivity.* Academic Press, New York and London.

Figures should be prepared entirely in black India ink upon transparent paper or copied by a good quality copier. A series of figures should be attached to each copy of the manuscript. The legends of figures should be given on a separate sheet. Photographs of good quality may be provided in black and white.

Tables should be marked by Arabic numbers and provided on separate sheets together with relevant captions. In one table the column number is maximum 13 if possible. One column should not contain more than five characters.

Mathematical formulas and *symbols:* non-Latin letters and hand-written marks should be explained by making marginal notes in pencil.

The final text should be submitted both in manuscript form and on *diskette.* Use standard 3.5" or 5.25" DOS formatted diskettes for this purpose. The following word processors are supported: WordPerfect 5.1, WordPerfect for Windows 5.1, Microsoft Word 5.5, Microsoft Word 6.0. In all other cases the preferred text format is ASCII.

* * *

Authors receive 30 *reprints* free of charge. Additional reprints may be ordered at the authors' expense when sending back the proofs to the Editorial Office.

Published by the Hungarian Meteorological Service

Budapest, Hungary

INDEX: 26 361

HU ISSN 0324-6329

IDŐJÁRÁS

QUARTERLY JOURNAL
OF THE HUNGARIAN METEOROLOGICAL SERVICE

CONTENTS

****

http://www.met.hu/firat/ido-e.html

VOL. 101 * NO. 2 * APRIL–JUNE 1997

IDŐJÁRÁS

Quarterly Journal of the Hungarian Meteorological Service

Editorial Office: P.O. Box 39, H-1675 Budapest, Hungary or
Gilice tér 39, H-1181 Budapest, Hungary
E-mail: gmajor@met.hu or *antal@met.hu*
Fax: (36-1) 290-7387

Subscription by

mail: IDŐJÁRÁS, P.O. Box 39, H-1675 Budapest, Hungary;
E-mail: gmajor@met.hu or *antal@met.hu*; *Fax: (36-1) 290-7387*

IDŐJÁRÁS

Quarterly Journal of the Hungarian Meteorological Service
Vol. 101, No. 2, April–June 1997, pp. 73–92

The atmosphere as a colloidal medium: absorption of solar radiation

K. Ya. Kondratyev

Research Center for Ecological Safety
Nansen International and Remote Sensing Center,
18, Korpusnaya str., 197110 St. Petersburg, Russia
E-mail: nansen@sovam.com

(Manuscript received 20 December 1996; in final form 17 March 1997)

Abstract—An overview of recent studies on "excess" absorption of solar radiation by the atmosphere has been made. The main result of the overview is the demonstration of the multicomponent nature of shortwave radiation (SWR) absorption in the atmosphere. Clouds are significant absorbers of SWR and it is very important to take into account the 3-D spatial inhomogeneity of cloud cover as well as the cloud pollution due to both natural and anthropogenic sources of aerosol pollution. There are, however, other important contributors to SWR absorption. For example, contribution of water vapor is far from being adequately assessed. Much more reliable observations and assimilation techniques (to consider observation data from different sources) are necessary to avoid relevant biases. The unacceptably high level of the underestimation of SWR absorption in the atmosphere by the present-day climate models (the disagreement with observations is an order of magnitude larger than the enhancement of the atmospheric greenhouse effect due to CO_2 concentration increase) requires further research with the two principal purposes: (1) complex dedicated field experiments to study SWR absorption in real atmosphere; (2) more adequate radiation parameterization in models.

Key-words: absorption, solar radiation, clouds, spatial inhomogeneity, multiple scattering, climate models.

1. Introduction

As it is well known, cloud dynamics and cloud–radiation interaction belong to the basic uncertainties of present-day climate modeling (*Borisenkov* and *Kondratyev*, 1988; *Kondratyev*, 1992; *Ma et al.*, 1996; *Marchuk et al.*, 1986; *Ridout* and *Rosmond*, 1996 and many other publications including the three recent volumes of the Intergovernmental Panel on Climate Change reports). An issue of critical importance in this context is the existence of uncertainties

relevant to the redistribution of solar energy transformed by the atmosphere due to impacts of various optically active components: gases, aerosols, and clouds.

Li et al. (1995) have recently emphasized that "...after more than 40 years of work, both theory and observations of the absorption of solar radiation by clouds are still fraught with uncertainties" (see also *Crutzen* and *Ramanathan*, 1996). A new illustration to this conclusion is the very intensive discussion of the problem of so called "excess" or "anomalous" absorption of solar radiation by clouds. *Ramanathan et al.* (1996) are correct in their statement that there is no reason to talk about "anomalous absorption" but "...it is safe to consider this phenomenon as simply, 'excess absorption' to point out that there is excess solar absorption in cloudy atmospheric columns when compared with clear sky column absorption".

The basic problem under discussion is the relationship between absorption of shortwave radiation (SWR) by the atmosphere and the Earth's surface which has been obtained on the basis of observations and numerical modeling. *Cess et al.* (1995) have concluded that "globally, GCMs that constrain their planetary albedos with satellite data, may overestimate the solar energy reaching the surface by as much as 8% or equivalently 25 W/m^2" (*Ramanathan et al.*, 1996).

Wild et al. (1995) showed that the ECHAM 3 General Circulation Model (GCM) calculated global mean surface SWR absorption (around 165 W/m^2) is higher by 10–15 W/m^2 compared to observations from the Global Energy Balance Archive (GEBA) data. A similar or higher overestimate is present in several other GCMs. Deficiencies in the clear sky absorption of the ECHAM 3 radiation scheme under clear sky conditions have been assumed as contributors to the flux discrepancies. A stand-alone validation of the radiation scheme under clear sky conditions revealed overestimates of up to 50 W/m^2 for daily maximum values of incoming shortwave fluxes. The lack of shortwave absorption by model clouds contributes to the overestimation of surface absorbed SWR. There is, however, a compensation between the overestimation of shortwave and underestimation of incoming longwave radiation by 10–20 W/m^2, which results in realistic enough values of the calculated surface radiation budget.

This survey paper answers the question: why may models overestimate the solar energy reaching the surface? The answer to this question is not at all simple, especially because the problem has a number of aspects to be considered. It has long been known (*Arking*, 1991; *Kiehl* and *Briegleb*, 1993, *Kondratyev*, 1969, 1972, 1988a, 1992, 1996; *Kondratyev* and *Binenko*, 1984; *Marchuk et al.*, 1986; *Stephens et al.*, 1978; *Stephens* and *Tsay*, 1990) that models underestimate SWR absorbed by clouds, but it is just one aspect of the problem, the other aspect is the "excess" absorption in the clear atmosphere.

2. *Observational data*

The problem of reliability of observational data is fairly complex. What we need to know is SWR absorption by the atmosphere (SWRA) in order to determine, how much solar energy is absorbed by the surface. SWRA may be found from combined surface and satellite observations. While the latters are really of global scale, surface solar radiation measurements are rather fragmentary and the existing global data set can therefore not be considered as adequately representing the global distribution of SWR. Besides, different spatial scales of surface point observations and satellite data averaged over large territories complicate a combined analysis of such data (important comments in this respect have been made by *Arking et al.*, 1996).

What we need to determine is the difference of shortwave radiation balances — SWRB (net SWR) at the top of the atmosphere (TOA net SWR values) and at the surface. SWRB itself is the difference between upward and downward SWR fluxes (irradiances). Thus, a necessity arises to differentiate twice the measured values of SWR fluxes. Undoubtedly, it might lead to serious errors. Unfortunately, persuasive assessments of such errors do not exist as yet. Certain efforts have been made to estimate errors in case of aircraft and balloon observations of SWR vertical profiles in the atmosphere (*Hayasaka et al.*, 1996; *Kondratyev*, 1969; *Kondratyev et al.*, 1976; *Kondratyev* and *Binenko*, 1984; *Stephens et al.*, 1978; *Pilewskie* and *Valero*, 1995, 1996; and others).

In view of the absence of reliable enough estimates of observational errors we would like to emphasize here an urgent necessity of the careful consideration of this problem. An important aspect of the problem is the use of various assimilation techniques to process inhomogeneous (in space and time) data series, which also requires a critical analysis. An illustration of this problem is the determination of clear sky radiative forcing (RF) values which is unavoidably based on various kinds of extrapolation (see *Arking et al.*, 1996).

3. *Effect of clouds on atmospheric absorption of solar radiation*

The discussion of the redistribution of solar energy between the atmosphere and the surface was mainly focused on assessments of cloud impacts on the atmospheric absorption of solar radiation (*Cess et al.*, 1995; *Li* and *Moreau*, 1996, 1997; *Li et al.*, 1995; *Ramanathan et al.*, 1995), since models obviously underestimated cloud absorption. *Ramanathan et al.* (1996) correctly noted that "Some of the fundamental flaws of our radiation models, at least those used to assert the zero net cloud effect, is that they assume: (1) clouds are flat plates with horizontally homogeneous properties, (2) cloud drops and crystals are made of pure water; and, (3) the absorption is by Lorentzian lines with arbitrary specified wavelength cut-offs, and (4) poor treatment of aerosol

effect". One more important feature to be mentioned is 3-D spatial inhomogeneity of cloud cover.

To assess the SWR absorption by clouds *Cess et al.* (1995) have undertaken an analysis of the data of simultaneous satellite and surface observations of the SWR fluxes at four locations: American Samoa (14.25°S; 170.56°W), Barrow (71.32°N; 157°W), Boulder (40.05°N; 105.01°W), Cape Grim (40.67°S; 114.69°E), and at 11 stations located in the state of Wisconsin. The data of pyranometric observations of the upward and downward SWR fluxes make it possible to calculate the shortwave radiation budget (SWRB), and satellite data contain information on the outgoing shortwave radiation (OSWR). The SWRB and OSWR differences for real cloud conditions and clear sky cases characterize the shortwave radiative forcing $C_s(S)$ and $C_s(TOA)$ at the surface and at the top of the atmosphere, respectively (the satellite data were averaged over 1° × 1° or 2.8° × 2.8° latitude-longitude grid).

From the data for Boulder, mean diurnal $C_s(S) = -92.6$ W/m^2 and $C_s(TOA) = -63.2$ W/m^2, that is $C_s(S)/C_s(TOA) = 1.46$, whereas the calculated $C_s(S)/C_s\ (TOA) \approx 1$, from which it follows that the calculated SWR absorbed by the cloudy atmosphere is substantially underestimated (by $C_s(S) - C_s(TOA) = 30$ W/m^2).

In view of possible errors in the estimates, an alternative technique has been applied based on estimation (by linear regression) of the variable

$$\beta = \frac{-dA_{TOA}}{d(Q_s/Q_{TOA})}, \tag{1}$$

where A_{TOA} is the albedo of the surface-atmosphere system, Q is the insolation at the levels of surface (S) and at the top of the atmosphere (TOA). From the data of observations in Boulder, $\beta = 0.59$, whereas calculations with the ECMWF (the European Centre for Medium Range Weather Forecasts) and CCM2 (the National Center for Atmospheric Research Community Climate Model) models gave 0.79 and 0.81, respectively.

An agreement of the calculated β values with observations is only possible with the calculated absorption supposedly underestimated. It is obvious that

$$\frac{C_s(S)}{C_s(TOA)} = \frac{1 - A_s}{\beta}, \tag{2}$$

where A_s is the surface albedo. For the Boulder conditions ($A_s = 0.17$) the quantity $\beta = 1.41$ agrees well with the estimate given above. All the other locations are also characterized by underestimated calculated absorption (with an exception of the cases of high snow surface albedo).

Cess et al. (1995) believe that though the water vapor content in the cloudy atmosphere is greater than in the clear one, this circumstance, as illustrated by respective estimates, cannot explain the growth of the SWR absorption. The universal character of the considered "anomalous" ("excessive") absorption by clouds (its independence on the location of the observation point) prompts one to reject also a possible role of the aerosol effect on the optical properties of clouds in view of the strong spatial and temporal variability of the aerosol concentration and properties.

Thus the problem consists, presumably, of the inadequacy of the present ideas of the optical properties of clouds. With the mean global surface albedo assumed to be 0.1, the excess absorption of solar radiation by clouds not considered in present climate models turns out to be about 25 W/m^2, i.e. it exceeds the $2 \times CO_2$ — induced enhancement of the greenhouse effect by almost an order of magnitude (*Borisenkov* and *Kondratyev*, 1988). Therefore there is an urgent need to understand the nature of this absorption and its consideration in the numerical climate modeling. In accordance with *Cess et al.* (1995), the mean global mean annual value of the shortwave cloud-radiation forcing $C_s(TOA)$ characterizing the effect of clouds on the shortwave radiation budget of the surface – atmosphere system (the difference of the SWRB of the mean conditions of clouds and clear sky cases) varies from –45 to –50 W/m^2. The value

$$C_s(TOA) = C_s(S) + C_s(A) \tag{3}$$

is determined by the sum of the contributions from the surface (S) and atmosphere (A). If SWR absorption grows in the presence of clouds, then $C_s(A) > 0$.

To analyse the formation of $C_s(TOA)$, the observational data of the surface heat balance and heat transport in the ocean for the region of the "warm pool" (WP) in the western Pacific (140–170°E; 10°N–10°S) have been processed by *Ramanathan et al.* (1995). In this region the SST reaches a mean annual value of ~302.5K, maximum for the World Ocean. The WP region is characterized by a humid and cloudy atmosphere with a frequent occurrence of cumulus clouds (60% of cases). An unexpected feature of WP turned to be a small mean annual dynamical heat transport (D) out of the WP mixed layer due to horizontal advection and vertical diffusion: $0 \leq D \leq 20$ W/m^2, which constrains the long-term annual mean net downward surface heat flux (H) to small values, since over an annual cycle no net heating of the mixed layer should take place. This condition

$$H - D = 0 \tag{4}$$

is used to close the WP heat balance from the observational data. It turned out that the closing is only possible in the case of strong reduction of total radiation

by clouds (> 100 W/m^2) which, in its turn, requires high values of $C_s(A)$ (~ 35 W/m^2) in the region of the WP, i.e. an anomalously intensive SWR absorption by clouds.

The resulting heat flux H at the ocean surface is

$$H = S_c + C_s(S) - F - E - h, \tag{5}$$

where S_c is the clear sky SWRB, F is the net longwave radiation, E is the heat loss due to evaporation, h is the turbulent sensible heat flux. The mixed layer net heating $Q = H - D$ is determined by two components: horizontal advection in the mixed layer (D_a) and downward entrainment of heat into the thermocline zone below (D_e). From the available data of ship and satellite observations all the heat balance components of Eq. (5) can be estimated, except for $C_s(s)$, which is calculated as a residual term.

Calculations made by *Ramanathan et al.* (1995) show that the mean annual values of the components of Eq. (5) turned out to be: $S_c = 275$ W/m^2 (with possible variations within 270–280 W/m^2) and $F = -45$ W/m^2. In this case $C_s(S) = -100$ W/m^2 (80–135 W/m^2).

The following relationship corresponds to the optimal values of the components of Eq. (5)

$$f_s = C_s(S)/C_s(TOA) = 1.5, \tag{6}$$

whereas calculations give $f_s < 1.2$. The results obtained by *Ramanathan et al.* (1995) reveal the fundamental gap in the present understanding of the effects of clouds on the SWR transport mentioned above. The value $f_s = 1.5$ means an increase of absorption by the atmosphere in the WP region by 35 W/m^2, compared to 100 W/m^2 for the cloud-free atmosphere. The oceanic mixed layer heating due to solar radiation absorption is thus reduced by 35 W/m^2. All this means a change in the meridional energy transport by the ocean and the atmosphere from the tropics to mid-latitudes within 25–50%, which, of course, is of fundamental importance from the viewpoint of climate formation.

To check these results from the data of direct observations, *Pilewskie* and *Valero* (1995) carried out simultaneous aircraft pyranometric measurements of total upward and downward SWR fluxes (the wavelength interval is 0.3–4.0 μm) in the tropical Pacific (140–180°E; 0–15°S) using aircraft measurements at altitudes from 8 to 12 km as well as at about 20 km, near the tropical tropopause. The goal of these measurements was to obtain data on the contribution of clouds to the SWR absorption by the atmosphere between the two altitudes. Through an extrapolation, data for the whole atmosphere were obtained.

The analysis of the observational results revealed a strong SWR absorption by clouds: on the average, the SWR absorbed by clouds reached 165 W/m^2, whereas, according to calculations, it was negligible. These results agree well with the estimates from the data on the ocean heat balance mentioned above. Since the results of spectral measurements revealed only specific selectivity typical of water, a supposition of the possible explanation of absorption by cloud pollution cannot be accepted. Therefore *Pilewskie* and *Valero* (1995) believe that the nature of absorption remains unclear (probably, the effects of the broken cloud morphology causing an increase of the length of the free path of photons play some role).

The problem of "anomalous" absorption by clouds would not have been highlighted as has been done in some publications (*Cess et al.*, 1995; *Ramanathan et al.*, 1995) if their authors had been acquainted with the results of complex studies of cloud–radiation interaction carried out under the programs CAENEX (Complex Atmospheric Energetic Experiment), GAAREX (Global Atmospheric Aerosol Experiment), and FGGE (First GARP (Global Atmospheric Research Programme) Global Experiment) (*Kondratyev*, 1972, 1988, 1992; *Kondratyev et al.*, 1976, 1996a; *Marchuk et al.*, 1986), and with recent results of radiation transport calculations for overcast and partial cloudiness (*Kondratyev et al.*, 1996b). Here are some illustrations of the respective results. The vertical soundings of the cloudy (5 October, 1972) and cloud-free (6 October, 1972) atmosphere over the Azov Sea revealed a strong transformation of both total and spectral radiative characteristics of the atmosphere on these days, determined by the emission of aerosol from the industrial zone of the cities Donezk and Zaporozhye, where the aerosol optical thickness of the atmosphere according to actinometric measurements was $\tau_a = 0.35$. The analysis of aircraft spectral measurements in the cloudy atmosphere carried out during the CAENEX period (*Kondratyev* and *Binenko*, 1984) revealed: (1) the SWR absorption by clouds is close to neutral in the visible; (2) the cloud top plays an active role in the SWR absorption; (3) maximum wavelength dependence on absorption in the oxygen and water vapor absorption bands; (4) strong cloud aerosol-induced absorption at $\lambda = 0.5$ μm (up to 0.15) compared to more "clean" clouds over the Black Sea (10 April, 1971), when the relative absorption was 0.03 (the optical thickness of clouds was 25 and 19, respectively).

Simultaneous measurements of the attenuation coefficient ϵ and size distribution parameters of stratified clouds of 550 m (5 October, 1972) and 450 m (10 April, 1971) thickness revealed: (1) the cloud top (within 50–100 m) has maximum ϵ, maximum values of water content, number concentration and modal radius of droplets; (2) a possibility to estimate the average droplet radius r with the use of the dependence $r = 0.9\ w/\rho\epsilon$, where w is the water content, ρ is the water density, and $\epsilon = \sigma + \kappa$ is the volume attenuation coefficient expressed as a sum of scattering and absorption coefficients; (3) the characteristic feature of marine clouds compared to clouds over land, consisting in a

greater contribution of large particles into the size distribution spectrum and in water content which could result from the impact of industrial aerosol pollution of clouds over land.

Processing the data of measurements of the SWR total fluxes (0.3–3.0 μm) showed that the SWR absorbed by the layer 0.2–1.2 km in cloudless conditions (6 October, 1972) for the sun elevation 38° was 35 W/m^2 but for the same layer in the presence of clouds the absorbed SWR reached 91 W/m^2 (5 October, 1972). Thus the contribution of absorption due to the cloud (as a difference of these values) constitutes 56 W/m^2. If we estimate the residual absorption by cloud, both total (0.3–3.0 μm) and in the visible wavelength range, in the climatological terms of other studies (*Cess et al.*, 1995; *Ramanathan et al.*, 1995) for the atmospheric layer 0.2–8.5 km, then $C_s(S)/C_s(TOA) = 140/118 = 1.16$, and for $\lambda = 0.5$ μm: $C_s(S)/C_s(TOA) = 45/18 = 2.5$, which points to an excess absorption by clouds in the visible. Since the object of the study was very extended horizontally homogeneous stratified cloudiness (it should be reminded that an element of the sub-grid climatological analysis is 250 × 250 km^2), the results of local aircraft soundings of the atmosphere could be used to assess the radiative forcing of clouds in the layer up to 8.4 km. The same estimates for more clean clouds over the Black Sea at the sun elevation 53° gave values $f_s = C_s(S)/C_s(TOA) = 1.11$ and 1.18, respectively. The radiation measurements performed on clear and cloudy days over the industrial town of Rustavi (Georgia) enabled one to estimate the ratio $C_s(S)/C_s(TOA)$ at 1.07 from the data of pyranometric measurements and 1.33 for $\lambda = 0.5$ μm.

Complex measurements carried out under the GAAREX program over Zaporozhye at sun elevation of 50°, and outside the city (on the windward side) showed that the city intensified the SWR absorption by clouds over the city compared to conditions outside the city within 21 W/m^2 to 77 W/m^2 (depending on the optical thickness of clouds at the wavelength 0.5 μm varying from 16 to 38). Therefore the SWR absorption prevails over the cloud longwave cooling. The values of $C_s(S)/C_s(TOA)$ varied from 1.2 to 2.6, which reflects an intensifying effect of clouds and pollution aerosols on the SWR absorption. Analysis of the data of sounding of the cloudy atmosphere over the Ladoga Lake (sun elevation 26°, $\tau = 80$) gave $C_s(S)/C_s(TOA) = 1.13$ and 1.18 within the wavelength interval 0.5–1.8 μm and 1.8 for $\lambda = 0.5$ μm.

In case of high surface albedo (ice or snow) the $C_s(TOA)$ differences for clear and cloudy weather are small and therefore the relative errors in estimating the radiative flux divergence, cloud absorptance and the ratio $C_s(S)/C_s(TOA)$ can reach 60% and more. Thus, the estimates of the SWR absorption by clouds become unreliable.

Based on the use of measured values of spectral downward and upward radiation fluxes and asymptotic formulas of the theory of radiation transfer in clouds, the spectral dependencies of the coefficient of scattering σ and absorption κ for a polydisperse turbid medium have been retrieved. With the

use of analytical formulas the single scattering albedo $\omega_0 = \rho/(\rho + \kappa)$ and the imaginary part of the complex refraction index were estimated from the data of the aircraft soundings of the cloudy atmosphere mentioned above (*Kondratyev et al.*, 1996b).

The calculated values of ρ and κ agree with the measured values of the attenuation coefficients and cloud optical thickness. The results of calculations with account of multiple scattering (both molecular and on droplets) for $\rho = 30\ km^{-1}$ as well as with account of the mean aerosol absorption coefficient in the cloud ($0.08\ km^{-1}$) make it possible to explain the excess absorption of solar radiation by clouds in the spectral interval 0.4–0.7 μm by the effect of multiple scattering, which enhances aerosol and cloud droplet absorption (a certain contribution is, apparently, made by changing optical properties of dirty clouds). An excess SWR absorption by clouds in the visible occurs always, and the presence of aerosol in clouds enhances this effect depending on its scattering and absorbing properties (ρ and κ) and on the place of its location: between droplets (interstitial aerosol), inside them, or on the surface.

4. Further discussion

The results published by *Cess et al.* (1995) and *Ramanathan et al.* (1995) have stimulated a rather hot discussion concerning the reality of "excess absorption". The viewpoints supported by the results of both observations and numerical modeling varied from completely negative (clouds do not absorb solar radiation) to partly supportive and to fully recognizing the significance of cloud absorption of shortwave radiation.

For instance, *Stephens* (1996) has pointed out that "current understanding predicts that absorption of solar radiation by the entire atmospheric column containing clouds is only slightly enhanced over absorption by an equivalent clear sky column" and emphasized that "...this absorption occurs in place of rather than in addition to clear sky absorption".

In their reply *Cess* and *Zhang* (1996) have emphasized again that "differences between the current observations and models...are large and constitute a signal in excess of uncertainties associated with the measurements...the model's clouds are underpredicting cloud SW absorption by overestimating cloud-sky surface insolation relative to clear sky; we see no other plausible explanation".

Pilewskie and *Valero* (1996) have pointed out in their reply that they found several errors in Stephens' arguments and made relevant comments. Pilewskie and Valero have correctly noted, for instance, that only some cloud absorption occurs in place of clear sky absorption. They have substantiated the reliability of their observations.

Let us dwell now upon a number of recent publications discussing both observation and numerical modeling results.

Hayasaka et al. (1995) conducted simultaneous observations of upward and downward total shortwave radiation fluxes below and above stratocumulus clouds in the western Pacific with the help of two aircraft equipped with pyranometers. The results of observations compared with Monte Carlo calculations show that as a result of horizontal inhomogeneity of cloud cover and respective divergence or convergence of radiation fluxes an additional absorption seemed existing which actually did not exist. Relevant corrections to remove the influence of horizontal inhomogeneity has been suggested resulting in complete coincidence of measured and calculated (for horizontally homogeneous cloud layer) absorption values. It may be concluded that, in fact, excess absorption of shortwave radiation by clouds does not exist in reality. It has been pointed also out by *Hayasaka et al.* (1995) that observed variations of cloud droplet size distribution do not influence shortwave radiation absorption by clouds.

Pinkus et al. (*Abstracts..*, 1996) have accomplished aircraft observations (the University of Washington's C-131A cloud physics aircraft) with the help of the Cloud Absorption Radiometer (CAR) which measures the distribution of radiation at 13 wavelengths in the visible and near-infrared region as a function of zenith angle in a plane perpendicular to the aircraft flight track. The measured radiance distribution and *in situ* measurements of the droplet size distribution have been analysed using radiative transfer theory for optically thick clouds to determine the spectrally dependent optical thickness, similarity parameter, and single scattering albedo of the cloud droplets and water vapor. Cloud horizontal inhomogeneity has been taken into account.

O'Hirok and *Gautier* (*Abstracts..*, 1996) have demonstrated through model calculations that specific spatial distribution of solar radiation due to the effects of 3-D cloud structure acts to enhance atmospheric absorption. Monte-Carlo calculations have indicated that the plane-parallel assumption used in radiative transfer models contributes significantly to the discrepancy between measurements and theoretical estimates and that the exclusion of 3-D effects in standard radiative transfer models may be a partial explanation for enhanced absorption. The assessments of an impact of cloud cover spatial inhomogeneity on radiative transfer have also been made by *Kinne et al.* (*Abstracts..*, 1996) and *Georgdzhaev et al.* (*Abstracts..*, 1996) who accomplished Monte-Carlo simulations as well as by *Zuidema* and *Evans* (*Abstracts..*, 1996) who applied a stochastic radiative transfer approach.

New approaches to 3-D radiative transfer calculations have been recently suggested, including the spherical harmonic discrete ordinate method (*Evans*: *Abstracts..*, 1996) and the Lattice-Boltzmann method (*Caudill* and *Mozer*: *Abstracts..*, 1996).

Using a Monte-Carlo technique, *Batey* and *Harshvardhan* (*Abstracts..*, 1996) have studied the radiative properties of inhomogeneous cloud fields for typical near-infrared conditions. The results of calculations indicate that an in-

homogeneous cloud field is less absorbing as well as less reflecting when compared to the corresponding field having the same optical depth.

Várnai and *Davies* (*Abstracts..*, 1996) have undertaken an effort to establish a theoretical framework which allows to define and calculate the various processes through which cloud inhomogeneities influence solar radiation. Using satellite information on irregular cloud fields they have shown that even for overhead sun, the dominant 3-D effects of decreasing the albedo takes place which often results not from the flow of radiation from thick to thin areas (where photons can pass through the cloud layer more easily), but rather, from thin to thick areas. This is why counter-intuitive phenomena arise such as that both spatial averaging and the addition of an underlying plan-parallel cloud can strengthen 3-D radiative effects in decreasing cloud albedo, even if the sun is overhead and if no absorption occurs. The numerical modeling indicates that radiative properties change significantly if the horizontal optical thickness variations which are observed from satellites are attributed not to variations in the volume extinction coefficient (like it was done before), but to variations in geometrical cloud thickness (which is probably a more realistic attribution for many cumulus cloud fields).

Presence of low level stratocumulus clouds is a case of inhomogeneities in microphysical and radiative properties over a wide range of scales. *Taylor* and *Hignett* (*Abstracts..*, 1996) have used aircraft observations for such a case off the coast of Namibia to constrain 3-D Monte-Carlo model calculations of the reflectance of the cloud field through relevant intercomparison. The results obtained show a significant negative albedo bias when the inhomogeneous cloud is compared to a plan-parallel cloud with the same average liquid water content.

Liou et al. (*Abstracts..*, 1996) have applied 3-D inhomogeneous radiative transfer program based on successive-order-of scattering approach to study the effects of cirrus cloud geometry and inhomogeneity on the spectral reflection and absorption.

Absorption of solar radiation by optically thin clouds over highly reflective surface has been investigated by *Otterman* and *Fraser* (*Abstracts..*, 1996). The absorption of solar radiation by clouds, surface and gaseous atmosphere has been expressed as an explicit function of the cloud-absorption, fraction a_0 of the downleg flux and a_r of the upleg (surface-reflected) flux, cloud-backscattering, fraction b_0 of the downleg and b_r of the upleg, gaseous absorption and the surface spectral albedo A. It has been shown that in the explicit expression for R (the ratio of CF at the surface to that at the TOA) the parameter a_0 appears only in a ratio a_0/b_0 which both increase with the solar zenith angle Θ. Since the b_0 increase is stronger than that of a_0 (in case of b_0 an additional contribution of an enhancement of backscattering with Θ is substantial), at large Θ the value of R tends to be close to 1.0 for zero surface albedo A, and changes only slowly with A. In case of $\Theta = 0$ (the sun near the zenith) the upleg absorption is, by a factor of at least 2.0, higher than that of the downleg. *Otterman* and

Faser have emphasized that the factor of more the 3.0 by which the combined downleg and upleg absorption exceeds the absorption for a dark surface (sun near the zenith) may explain, to some extent at least, the anomalous cloud absorption. Since for many surfaces spectral albedo in the infrared is high, the use of albedo averaged over the solar spectrum can result in an erroneous assessment of the cloud absorption.

The reflection and transmission properties of spatially inhomogeneous water-cloud fields above a dark surface have been simulated by *Macke et al.* (*Abstracts..*, 1996) by means of a Monte-Carlo radiative transfer program. A three-dimensional broken cloud field was constructed by applying a cellular automation model for cloud formation.

Francis et al. (*Abstracts..*, 1996) have analysed aircraft measurements from the C-130 aircraft of the broadband and narrow-band radiation fields in and around different cloud types. These observation were made over a number of years in several different locations around the globe. An attempt to identify "enhanced" absorption as a result of increased condensed-phase water absorption in the infrared has not been successful. Therefore it has been concluded that the observational results "...can be explained much better, both qualitatively and quantitatively, by current accepted theory".

In this context *Li* (*Abstracts..*, 1996) has pointed out that contrary to some recent claims of cloud absorption anomaly, the systematic discrepancy is attributed primarily to the treatment of clear-sky radiative processes including the negligence of aerosol and the use of dated schemes for computing water vapor absorption. After assessing various estimates, Li has come to the conclusion that the following disposition of solar energy appears to best represent our current knowledge: 30% reflection to space, 25% absorption in the atmosphere and 45% at the surface on a global and annual mean basis. *Long* and *Ackerman* (*Abstracts..*, 1996) also believe (on the basis of the observational data for the tropical western Pacific warm pool) that the proposed anomalous SW cloud absorption does not exist. The same conclusion has been made by *Davis et al.* (*Abstracts..*, 1996) who have emphasized the significance of cloud horizontal inhomogeneity and relevant horizontal radiative fluxes for the interpretation of atmospheric absorption data in presence of clouds.

One more suggestion has been made by *Chen* and *Lu* (*Abstracts..*, 1996) who discussed a possibility of an impact due to the neglect of the variation of water refractive index with temperature.

Crisp and *Zuffada* (*Abstracts..*, 1996) used a sophisticated atmospheric radiative transfer model to compute solar fluxes and heating rates for clear sky and cloudy conditions (line-by-line approach was applied for molecular absorption calculations; non spherical water, ice and aerosol particles were taken into account; multilevel, multistream, discrete ordinate algorithm was used to solve the equation of radiative transfer). The results of calculations indicate that the model accounts for a large fraction of the anomalous

absorption. For example, a standard, mid-latitude summer model atmosphere with a single, horizontally uniform, stratocumulus cloud absorbs 20 to 30 W/m^2 more sunlight at altitudes within the cloud (1 to 1.5 km) than the associated clearsky case. However, the cloudy atmosphere absorbs about 12 W/m^2 less than the clear atmosphere at altitudes below the cloud base because the cloud reduces the amount of solar radiation available at these levels. Water vapor absorption above the cloud base account for most of the additional flux divergence associated with the cloud. This contribution to anomalous absorption is proportional to the water vapor abundance and the photon path lengths within the cloud, and inversely proportional to the solar zenith angle. Crisp and Zuffada have emphasized a necessity to also consider other factors of anomalous absorption, such as horizontal inhomogeneity of cloud abundance.

Line-by-line adding-doubling computations of solar radiation absorption by clouds made by *Ramanathan* and *Freidenreich* (*Abstracts..,* 1996) were made to assess the relative roles of water vapor and clouds.

An important field study of radiative effects of tropical clouds (convection in the tropical Pacific) has been accomplished by *Collins et al.* (1996) within the program of the Central Equatorial Pacific Experiment (CEPEX) from November 1992 to February 1993. Radiation fluxes at the tropopause level were measured from ER-2 aircraft between 18 and 20 km. The ship R/V "John Vickers" and Lockheed P-3 turboprop aircraft were used to measure surface fluxes. Calculations of radiative forcings indicate that at the tropopause SW and LW forcings are nearly equal and opposite, even on daily time-scales. Therefore the net effect of an ensemble of convective clouds is small compared to other radiative terms in the surface–troposphere heat budget. The heat budget at the tropopause is determined primarily by the sum of the clear sky SW and LW fluxes, and during the CEPEX observing period the net clear sky flux across the tropopause was approximately 120 W/m^2. At the surface the net effect of clouds is to reduce the radiant energy absorbed by the ocean. Under deep convective clouds the diurnally averaged reduction exceeds 150 W/m^2. Calculations of the flux divergence in the cloudy atmosphere indicate that the atmospheric cloud forcing is nearly equal and opposite to the surface cloud forcing. Being dependent on the frequency of convection, the atmospheric forcing approaching 100 W/m^2 was observed when the surface temperature was 303K. During the CEPEX period the surface net radiative cooling due to SW forcing increased at a rate of 22 W/m^2 K.

Taylor et al. (1996) made in situ observations of SW radiation fluxes from the UK Met. Office C–130 aircraft (three cases of clear sky and four cases where a liquid-water boundary-layer cloud was present). A comparison with calculations (a new two stream radiative-transfer formulation) has revealed in case of clearsky an agreement within 3%. In the cloudy cases the albedo and transmittance agree within $\pm$ 0.1 but the absorption in the model is higher than that observed, sometimes by a factor of two. *Taylor et al.* (1996) have

concluded that there is no evidence of anomalous absorption in the observations. The observed absorptions do not exceed 6% for the stratocumulus cases considered. It is important, however, to take into account cloud spatial inhomogeneity.

To continue a discussion of "balance of evidence" one has to point out (in the contradiction with the results just mentioned) conclusions made by *Ward* (1995) on the basis of a comparison of the monthly mean SW radiation budget (SRB) obtained from the World Climate Research Programme (WCRP) shortwave global dataset with that simulated by the National Center for Atmospheric Research Community Climate Model version 2.0 (CCM2). Large differences were found in monthly mean surface solar fluxes, the largest discrepancies being in the summer mid-latitude regions where CCM2 overestimates surface SW radiation fluxes relative to retrieved from satellite data by as much as 100 W/m^2. *Ward* (1995) believes that most of the differences are associated with deficiencies in CCM2's prediction of cloud optical properties and cloud amount. However significant differences also occur in clearsky fluxes and surface albedo. CCM2 was found to have larger clearsky surface insolation than retrieved from satellite data over nearly all land areas by more than 60 W/m^2 in some locations.

There are still a few examples of a combined analysis of simultaneous surface and satellite radiation budget data which allow to obtain information on atmospheric radiation budget and its components. In this context *Yamanouchi* and *Charlock* (1995) have considered such kind of data for the Antarctic with the main purpose to assess cloud radiative effects. Radiative fluxes at the top of the atmosphere (TOA) and the surface were compared at two Antarctic stations, Syowa and the South Pole, using Earth Radiation Budget Experiment (ERBE) data and surface observations for the time period from February 1987 to January 1988. Cloud amounts were derived from surface synoptic observations.

Throughout the year over the snow and ice covered Antarctic cloud radiation impact consisted in heating the surface and cooling the atmosphere. Cloud longwave (LW) effects were greater than cloud shortwave (SW) effects. Clouds have a negligible effect on the absorption of SW by the atmosphere in the interior and clouds slightly increase the absorption of SW by the atmosphere along the coast. The atmospheric SW heating due to Antarctic clouds is much smaller than the 25–40 W/m^2 SW cloud forcing which was inferred for other latitudes. At the TOA, the LW cloud effect was heating along the coast in summer and winter, heating in the interior during summer, and slight cooling in the interior during winter. This unique TOA cloud LW cooling was due to the extremely low surface temperature in the interior during winter. At the TOA, clouds induced SW cooling in the interior and along the coast. The comparison of the monthly averaged fluxes has shown that the atmospheric column loses net radiation energy through the year with an asymmetrical

seasonal variation. The largest cooling for the atmospheric column, about 140 and 125 W/m^2, appears in May at Syowa and in April at the South Pole, respectively. The loss of net radiation energy by the atmosphere is much larger than the loss by the surface.

A very important study has been accomplished by *Evans* and *Puckrin* (1996) who made spectral measurements of the solar flux in the near-infrared region (3,000–10,000 cm^{-1}) using FTIR spectrometer under clear and overcast sky conditions. These results also yielded information concerning the absorption of direct solar radiation by clouds. A comparison of the spectra of solar fluxes for clear and overcast sky measured from the ground for a northern mid-latitude location (Nova Scotia, Canada: 43.8°N; 66.2°W) in August and September 1995 indicates that about 118 W/m^2 of the solar radiation is absorbed preferentially by clouds in the spectral region mentioned. The cloud RF ratio was estimated to be 1.24. *Evans* and *Puckrin* (1996) believe that the absorption by cloud liquid water may contribute, in part, to the anomalous cloud absorption effect.

Summarizing some of the results discussed above and their own results of processing a four-year global record of solar flux observed from both space and the Earth's surface *Li et al.* (1995) have pointed out that f_s values are highly variable in the tropics with a median of about 1.1, and consistently less than 1.0 in polar regions. They have proposed that "large values and high variations of f_s may be related to the presence of absorbing aerosols and the uncertainties in both the observed and inferred solar flux data used here. Therefore, a substantial revision of our understanding of cloud absorption and its impact on the atmosphere's energy budget may not, after all, prove to be necessary if the effects of absorbing aerosols are properly incorporated" (unfortunately, like *Cess et al.* (1995), *Ramanathan et al.* (1995), *Li et al.* (1995) and some others have failed to refer to older publications on this subject by *Kondratyev* (1972, 1988a, b, etc.) as well as by *Kondratyev et al.* (1976, 1983), *Kondratyev* and *Binenko* (1984, etc.)).

The assumption made by *Li et al.* (1995) that $f_s > 1$ due to the impact of absorbing aerosol is based on the facts that in the tropics strong absorbing aerosols produced by biomass burning could play an important role, whereas in mid-latitudes maximum f_s values were obtained near Hamburg and the Rhine Valley i.e. in heavily polluted areas. In all cases for a sizable fraction of months $f_s < 1$ which may be the influence of cirrus clouds (backscattering by cirrus clouds leads to a reduction of absorption by aerosols located below the clouds). *Li et al.* (1995) have pointed out that although the observed variation of f_s has been explained by changes in solar zenith angle and aerosol effects, the potential dependence of f_s on cloud structure (morphology) also deserves examination. They conclude that their study "...does not rule out the existence of the cloud absorption anomaly, but rather indicates that its magnitude (if it exists) on a global scale may not be as large as suggested in some recent reports".

In a later study *Li* and *Moreau* (1996) have investigated two parameters employed in recent attempts to address cloud absorption anomaly: the ratio R discussed above and the slope s, of the regressional relationship between TOA albedo and atmospheric transmittance. Li and Moreau have emphasized that neither R nor s is a direct measure of cloud absorption: they both are sensitive to many factors, especially cloud height and surface condition. In spite of that, R can indicate the effect of clouds on the atmospheric absorption of solar radiation, if the clearsky conditions remain the same. However, modeled R exceeds 1.25, and modeled s is generally less than –0.7, except for bright surfaces. Observational values of R and s from the Earth Radiation Budget Experiment (ERBE) and the Global Surface Energy Balance Archive (GEBA) (four years worth of monthly mean data) demonstrate that R is highly variable with both location and season and also shows strong interannual variations. Low to moderate values of R tend to occur over relatively clean areas, while large R values appear to be associated with heavy pollution in the mid-latitudes or frequent occurrence of biomass burning in the tropics. The overall value of R obtained with the use of various approaches is about 1.1, which is in good agreement with model calculations. In general, $R < 1$ and > 1 over the polar and tropical regions, respectively. Thus, polar and tropical clouds have opposing effects on total atmospheric absorption, while midlatitude clouds have relatively little impact on absorption. *Li* and *Moreau* (1996) have pointed out, however, that large R values for the tropical areas are less reliable than the moderate values for midlatitude areas. *Li* and *Moreau* (1996) have repeated their earlier conclusion that their study does not rule out cloud absorption anomaly, but indicate, however, that its magnitude (if it exists) is not as large, and its occurrence is not as widespread, as suggested in some recent studies. In the most recent papers *Li et al.* (1997) have come to the conclusion that the difference between model calculations and observations is primarily due to deficiencies in clearsky calculations: the use of dated schemes for water vapor absorption and the neglect of absorbing aerosols.

Arking (1996) and *Arking et al.* (1996) have confirmed the conclusion that the present-day global climate models underestimate the amount of solar energy absorbed by the atmosphere within the range of up to 25–30 W/m^2 but suggested quite different explanation of this facts. *Arking* (1996) has found on the basis of both observations and models that clouds have little (~ 5 W/m^2) or no effect on atmosphere absorption. Therefore his conclusion is that "water is the dominant influence on atmospheric absorption, and improvements in our models lie in improving the parameterization of water vapor absorption and, perhaps discovering of additional absorption in the clear atmosphere".

Chou et al. (1995) have pointed out in this context that for the ratio of cloud forcing at the surface to that at the top of the atmosphere to reach 1.5, cloud specific absorption would be required to increase by a factor of about 40 beyond what has been determined by in situ aircraft measurements.

The discussion on the nature of excess absorption of solar radiation by clouds still continues and has resulted (as we have already seen) in controversial judgments. It is obvious that further theoretical and, first of all, complex field studies are necessary with specific emphasis on 3-D inhomogeneity of cloud cover and cloud optical properties (it should be also reminded that even an old problem of IR continuum absorption by water vapor has not been solved as yet). New efforts in this direction have been started within the ARM (Atmospheric Radiation Measurement) Programme (*Wiscombe*, 1995).

5. Aerosol impact on atmospheric absorption of solar radiation

At the end of the 1940s V. Kastrov from the Central Aerological Observatory (Moscow) started his long-term pyranometric observations of SWR fluxes in the free atmosphere under various conditions over the European part of the former USSR territory (see *Kondratyev*, 1956, 1969). The most important result was the discovery that atmospheric aerosol absorption of solar radiation is close, by its magnitude, to water vapor absorption. Later on balloon and aircraft observations within CAENEX and GAREX Programmes were conducted which confirmed Kastrov's results (*Kondratyev*, 1972; *Kondratyev et al.*, 1976; *Kondratyev* and *Binenko*, 1984). Of special significance were aircraft spectral measurements of SWR fluxes under clear sky and overcast cloudiness conditions with simultaneous measurements of aerosols and clouds properties (aerosol counters and filters were used which allowed to obtain information on not only number concentration and size distribution of aerosol and cloud particles, but also their chemical composition and hence-optical properties).

Aircraft measurements made in the former USSR (European territory, Central Asia, The Arctic, Kamchatka and Chukotka) as well as over the tropical Atlantic confirmed the principal result mentioned above: aerosol absorption of solar radiation is always significant and on the average, is approximately equal to absorption by water vapor. Observations in the presence of overcast (horizontally homogeneous) cloud cover in polluted atmosphere of industrial regions revealed the existence of exceedingly strong SWR absorption by dirty clouds (see also *Chýlek* and *Wong*, 1995; *Stephens*, 1994).

It is quite clear, thus, that in the context of the problem discussed, aerosol impact on atmospheric absorption of solar radiation requires serious attention (*Kondratyev*, 1996). This conclusion has been recently confirmed by *Li* (1997) and *Li et al.* (1997).

6. Conclusions

The basic conclusion is simple and obvious: our knowledge of radiation transfer in the real atmosphere is far from being adequate: there is neither "anomalous" not "excess" absorption of solar radiation. The reality is such that there are several processes which may be responsible for the disagreement between observed and modeled redistribution of absorbed SWR between the atmosphere and the surface, including:

- multiple scattering in clouds with absorbing droplets (they never consist of pure water) which leads to the enhancement of cloud absorption;
- specific features of radiation transfer in a 3-D inhomogeneous medium (broken clouds);
- unknown contribution by water vapor (besides that is known);
- peculiarities of radiation transfer in clouds consisting of a mixture of water droplets and aerosol particles;
- absorbtion of aerosols of various origin.

Last but not least, the reliability of observations should be further assessed. The necessary improvement of radiation parameterization in climate will become possible only on such a basis. Important steps forward are *"A Plan for Research Program on Aerosol Radiative Forcing and Climate Change"* (1996), the CERES Programme (*Wielicki et al.*, 1996) as well as the intercomparisons between numerical modeling results and observations like it has been recently done by *Ellingson* and *Wiscombe* (1996), *Rossow* and *Zhang* (1995), *Salathé* and *Smith* (1996).

References

Abstracts, 1996: *International Radiation Symposium*. The University of Alaska. Fairbanks, August 19-24.

A Plan for Research Program on Aerosol Radiative Forcing and Climate Change, 1996: National Academy Press, Washington, DC.

Arking, A., 1991: The radiative effects of clouds and their impact on climate *Bull. Amer. Meteorol. Soc. 71*, 795-813.

Arking, A., 1996: Absorption of solar energy in the atmosphere: discrepancy between a model and observations, *Science 273*, 779-782.

Arking, A., Chou, M.-D. and *Ridgway, W. L.*, 1996: On estimating the effects of clouds on atmospheric absorption based on flux observations above and below cloud level. *Geophys. Res. Lett.* (in print).

Borisenkov, E. P. and *Kondratyev, K. Ya.*, 1988: *Carbon Dioxide and Climate*. Gidrometeoizdat, Leningrad.

Cess, R.D., Zhang, M.H., Minnis, P., Corsetti, L., Dutton, E.G., Forgan, B.W., Garber, D.P., Gates, W.L., Hack, S.S., Harrison, E.E., Jing, X., Kiehl, J.P., Long, C.N., Morcrette, J.J., Potter, G.L., Ramanathan, V., Subasilar, B., Whitelock, C.K., Young, D.F. and *Zhou, Y.*, 1995: Absorption of solar radiation by clouds: observations versus models. *Science 267*, 496-499.

Cess, R.D. and *Zhang, M.H.*, 1996: Response. *Science 271*, 133-134.

Chou, M.-D., Arking, A., Offerman, J. and *Ridgway, W.L.*, 1995: The effect of clouds on atmospheric absorption of solar radiation. *Geophys. Res. Lett., 22*, 1885-1888.

Chýlek, P. and *Wong, J.*, 1995: Effect of absorbing aerosol on global radiation budget. *Geophys. Res. Lett. 22*, 929-931.

Collins, W.D., Valero, F.P.J., Flatou, P.J., Lubin, D., Grassl, H. and *Pilewskie, P.*, 1996: Radiative effects of convection in the tropical Pacific. *J. Geophys. Res. 101*, 14999-15012.

Crutzen, P.S. and *Ramanathan, V.* (eds.), 1996: *Cloud, Chemistry and Climate.* Springer-Verlag, Berlin.

Ellingson, R.G. and *Wiscombe, W.J.*, 1996: The Spectral Radiance Experiment (SPECTRE): Project description and sample results. *Bull. Amer. Meteorol. Soc. 77*, 1967-1985.

Evans, W.F.J. and *Puckrin E.*, 1996: Near-infrared spectral measurements of liquid water absorption by clouds. *Geophys. Res. Letters 23*, 1941-1944.

Hayasaka, T., Kikuchi, N. and *Tanaka, M.*, 1995: Absorption of solar radiation by stratocumulus clouds: aircraft measurements and theoretical calculations. *J. Appl. Meteorol. 34*, 1042-1055.

Kiehl, J.T. and *Briegleb, B.P.*, 1993: The relative roles of sulfate aerosols and greenhouse gases in climate forcing. *Science 260*, 311-313.

Kiehl, J.T., Hack, J.J. and *Briegleb, B.P.*, 1994: The simulated Earth radiation budget of the National Center for Atmospheric Research community climate model CCM2 and comparisons with the Earth Radiative Budget Experiment (ERBE). *J. Geophys. Res. 99*, 20815-20827.

Kondratyev, K. Ya., 1956: *Actinometry* (in Russian). Gidrometeoizdat, Leningrad.

Kondratyev, K. Ya., 1969: *Radiation in the Atmosphere.* Academic Press, New York.

Kondratyev, K. Ya., 1972: *Complex Atmospheric Energetics Experiment (CAENEX)*, GARP Publ. Ser. 12, WMO, Geneva.

Kondratyev, K. Ya., 1988a: *Earth's Radiation Budget, Aerosols, and Clouds* (in Russian). Progress in Science and Technol., 10, VINITI, Moscow.

Kondratyev, K. Ya., 1988b: *Climate Shocks: Natural and Anthropogenic.* Wiley & Sons, New York.

Kondratyev, K. Ya., 1992: *Global Climate* (in Russian). Nauka Publ., St. Petersburg.

Kondratyev, K. Ya., 1996: Aerosol climate impact in the context of global climate change. *Időjárás 100*, 1-12.

Kondratyev, K. Ya., Barteneva, O.D., Chapursky, L.I., Chernenko, A.P., Grishechkin, V.S., Ivanov, V.A., Korzov, V.L., Lipatov, V.B., Prokofyev, M.A., Tolkachev, M.K., Vasilyev, O.B. and *Zvalev, V.F.*, 1976: Aerosol in the GATE area and its radiative properties. *Atmospheric Sci. Paper 247.* Colorado State Univ., Fort Collins, Co.

Kondratyev, K.Ya., and *Binenko, V.I.*, 1984: *Impact of Clouds on Radiation and Climate* (in Russian). Gidrometeoizdat, Leningrad.

Kondratyev, K.Ya., Binenko, V.L. and *Melnikova, I.N.*, 1996b: *On excessive absorption of solar radiation by clouds in the visible* (in Russian). Doklady Russian Acad. Sci. (in print).

Kondratyev, K. Ya., Moskalenko, N.I. and *Pozdnyakov, D.V.*, 1983: *Atmospheric Aerosols* (in Russian). Gidrometeoizdat, Leningrad.

Li, Z., Bakker, H.W. and *Moreau, L.*, 1995: The variable effects of clouds on atmospheric absorption of solar radiation. *Nature 376*, 486-490.

Li, Z. and *Moreau, L.*, 1996: Alteration of atmospheric solar absorption by clouds: simulation and observations. *J. Appl. Meteorol. 35*, 653-670.

Li, Z., 1997: Influence of absorbing aerosols on the influence of surface solar radiation budget. *J. Climate* (in print).

Li, Z., Moreau, L. and *Arking, A.*, 1997: On solar energy disposition: a perspective from observation and modeling. *Bull. Amer. Meteorol. Soc.* (in print).

Ma, C.-C., Mechoso, C.R., Robertson, A.W. and *Arakawa, A.*, 1996: Peruvian stratus clouds and the tropical Pacific circulation: a coupled ocean-atmosphere GCM study. *J. Climate 9*, 1635-1645.

Marchuk, G.I., Kondratyev, K. Ya., Kozoderov, V.V. and *Khvorostyanov, V.I.*, 1986: *Clouds and Climate.* Gidrometeoizdat, Leningrad.

Pilewskie, P. and *Valero, F.P.J.*, 1995: Direct observations of excess solar absorption by clouds. *Science 267*, 5197, 1626-1629.

Pilewskie, P. and *Valero, F.P.J.*, 1996: Response. *Science 271*, 1134-1136.

Ramanathan, V., Subasilar, B., Zhang, G.J., Conant, W., Cess, R.D., Kiehl, J.D., Grassl, H. and *Shi, L.*, 1995: Warm pool heat budget and shortwave cloud forcing: a missing physics? *Science 267*, 499-503.

Ramanathan, V., Valero, F.P.J. and *Cess, R.D.*, 1996: Excess solar absorption in cloudy atmospheres. *GEWEX News 6*, 6-7.

Rossow, W.B. and *Zhang, Y.-C.*, 1995: Calculation of surface and top atmospheric radiative fluxes from physical quantities based on ISCCP data sets II. *J. Geophys. Res. 100* , 1167-1197.

Ridout, J.A. and *Rosmond, T.E.*, 1996: Global Modeling of cloud radiation effects using ISCCP cloud data. *J. Climate 9*, 1479-1496.

Salathé, E.P. Jr. and *Smith, R.B.*, 1996: Comparison of 6.7 μm radiances computed from aircraft soundings and observed from GOES. *J. Geophys. Res. 101*, 21303-21310.

Stephens, G.L., Paltridge, G.W. and *Platt C.M.R.*, 1978: Radiation profiles in extended water clouds. III: Observations. *J. Atmos. Sci. 35*, 2133-2141.

Stephens, G.L. and *Tsay, S.C.*, 1990: On the cloud absorption anomaly. *Quart. J. Roy. Meteorol. Soc. 116*, 671-704.

Stephens, G.L., 1994: Dirty clouds and global cooling. *Nature 370*, 420.

Stephens, G.L., 1996: How much solar radiation do clouds absorb? *Science, 271*, 1131-1133.

Taylor, J.P., Edwards, J.M., Glew, M.D., Hignett, P. and *Slingo, A.*, 1996: Studies with a flexible new radiation code II: Comparison with aircraft short-wave observations. *Quart. J. Roy. Meteorol. Soc. 122*, 839-361.

Ward, D.M., 1995: Comparison of the surface solar radiation budget derived from satellite data with the simulated by the NCAR CCM2. *J. Climate 8*, 2824-2842.

Wielicki, B.A., Bankstorm, B.R., Harrison E.F., Lee R.B. III, Smith G.L. and *Cooper J.E.*, 1996: Clouds and the Earth's Radiant Energy System (CERES): An Earth Observing System Experiment. *Bull. Amer. Meteorol. Soc. 77*, 853-868.

Wild, M., Ohmura, A., Gilgen, H. and *Roeckner, E.*, 1995: Validation of General Circulation Model radiative fluxes using surface observations. *J. Climate 8*, 1309-1324.

Wiscombe, W.J., 1995: An absorbing mystery. *Nature 376*, 466-467.

Yamanouchi, T. and *Charlock, T.P.*, 1995: Comparison of radiation budget at the TOA and surface in the Antarctic from ERBE and ground surface measurements. *J. Climate 8*, 3109-3120.

IDŐJÁRÁS

Quarterly Journal of the Hungarian Meteorological Service
Vol. 101, No. 2, April–June 1997, pp. 93–103

Meteorological journals — A scientometric approach

S. Zsindely[1] and **G. Major**[2]

[1]*Information Science and Scientometric Research Unit,*
Library of the Hungarian Academy of Sciences,
P.O. Box 1002, 1245-Budapest, Hungary

[2]*Hungarian Meteorological Service,*
P.O. Box 39, 1675-Budapest, Hungary; E-mail: gmajor@met.hu

(Manuscript received 15 January 1997; in final form 22 March 1997)

Abstract—A survey of meteorological journals registered in bibliographical databases is given in this paper. The brief historical review is followed by the publication characteristics: the number of articles published and the impact factors. The difference of journals edited by scientific societies and by profit-oriented publishing houses are shown from the point of view of the prestige, circulation and publication frequency of the journals in question.

Key-words: scientific journal, meteorological journal, bibliographic database, impact factor, demography of journals.

1. Introduction

It was about 300 years ago, when a French nobleman, Denis de Sallo, and nearly at the same time, the Secretary of the Royal Society in London, Henry Oldenburg, lost interest in writing and disseminating between his scholar friends the hundreds of letters related to the newest scientific discoveries. Instead of sending private letters with individual content to each addressee, they wrote only one per topic, which was multiplied by typographical means and the earliest scientific journals, the *Journal des Sçavans* (Paris) and the *Philosophical Transactions* (London) were born (1665): a new era began in the communication system of science (*Ziman*, 1969; *Brookes*, 1980). The scientific journal became the chief carrier, disseminator and preserver of scientific information.

During the years, the number of scientific journals has grown exponentially (*Price*, 1963). In the beginning the content of the journals had a more universal character, but with the development of modern scientific trends, more and more specialized journals appeared.

2. The scientific journals in meteorology

Modern meteorology began when the daily weather maps were developed as a device for weather analysis and forecasting, and the instruments (thermometer, barometer, hygrometer, pluviometer, anemometer) for measuring the most important parameters as well as the telegraph became wide-spread (*Fierro*, 1991).

In spite of the fact that descriptions of meteorological observations can be also found just among the articles published in the abovementioned incipient scientific journals, the first scientific journal serving exclusively the meteorology, the *Ephemerides Societatis Meterologicae Palatinae* appeared in Mannheim in 1781. The *Ephemerides* published meterological data measured by a European network of observing sites. Among these sites was Buda, the capital of the Kingdom of Hungary. The political troubles during and after the French Revolution destroyed this initiative, and the last issue of the *Ephemerides* appeared in 1795 containing the data measured in 1792.

After some attempts for nearly a century, it was only the time of the foundation of the first meteorological observatories when the first viable, regularly published scientific journals appeared in this discipline (*Quarterly Journal of the Royal Meteorological Society*, 1871–; *Annalen der Hydrographie und maritime Meteorologie*, 1873–1944), *Meteorologische Zeitschrift,* (1884–1944, 1948–).

The evolution of the scientific journals of meteorology has shown the same trend as in the case of other scientific journals. As an example let us look at *Időjárás* (the name means: weather). Its first issue appeared in April, 1897. It was a private journal founded by *Dr. Héjas* Endre, a meteorologist of the state meteorological service. His basic purposes were: to increase the meteorological knowledge as well as to help the development of the Hungarian meteorological language. In that time several misbeliefs were frequent about the weather phenomena and even about the climate and its possible modifications. For example it was argued against the regulation of rivers that it would decrease the precipitation. In 1925 the journal was taken over by the Hungarian Meteorological Society and became more scientific. In 1945 it became the official scientific journal of the Hungarian Meteorological Service. Besides the Hungarian ones, papers appeared in English, French, German and Russian as well. Since 1992 the only accepted language is English. The recent policy is to publish original scientific articles in any field of atmospheric sciences from authors of any nationality. Less than half of the papers is written by Hungarian authors, the larger part comes from all the five continents, mainly from Europe, Asia and Africa.

Nowadays scientific journals of this discipline (similarly to other fields of the science) are edited partly by learned societies and partly by profit-oriented publishing houses.

3. Meteorological journals in bibliographical databases

The titles and main data of several journals publishing articles and observed data of meteorological interest for the years 1994-1995 can be found in *Ulrich's International Periodicals Directory* (1994) under the headline "Meteorology". This compilation is, although not exhaustive, but impressive: it includes 466 journals from 58 countries (plus United Nations). Knowing the highly developed meteorological service of Japan, it is not surprising that 161 of the titles there stem from this country.

Besides the name of the periodical, the Directory registers the ISSN Number, the language(s) of the texts, the date of foundation, the editor's name, the address of the publisher, the names of abstract journals indexing the journal in question, the formerly used name(s), if any, amongst others.

Unfortunately, the title of *Időjárás* is missing, but two other Hungarian journals can be found in this chapter of the Directory. These are: *Acta Geographica ac Geologica et Meteorologica Debrecina* (rather geographical in nature, and with irregular publishing sequence) and *Acta Universitatis de Attila József Nominatae. Acta Climatologica*, which focuses on general climatology, bio- and agrometeorology. These periodicals publish those works of university professors or lecturers that are meteorological ones or strongly connected to the different applications of climatological data series.

It is supposed that any given population of periodicals follows, at least in part, the rules of human demography (*Zsindely* and *Schubert*, 1992). For illustrating the "age distribution" of the "still living" meteorological journals, an age-pyramid of the journals registered in *Ulrich's Directory* has been compiled for the years 1994 and 1995 (*Fig. 1*). This diagram depicts separately the journals edited by institutions (societies, institutes, observatories, etc.) and by profit-oriented publishing houses; it includes 284 meteorological journals with regular publication and known year of foundation.

From the figure it can be seen that the oldest, still edited journal containing meteorological information, the *Monthly Notices of the Royal Astronomical Society* (London), was first published in 1827. The profit oriented publication of meteorological journals began mainly after World War II.

The Science Citation Index (SCI) of the Institute of Scientific Information (ISI, Philadelphia, U.S.A.) processes 3430 journals in 160 subfields; the subfield of Meteorology and Atmospheric Sciences is represented by 33 titles in 1995. It is worth mentioning that the list of *Ulrich's Directory* and that of SCI do not overlap perfectly. The selection for the SCI is based, among others, on the average citation rate (impact factor) of the journal to be registered. SCI's journals for meteorology are compiled for the year 1994 in the rank order of their first year of publication in *Table 1*.

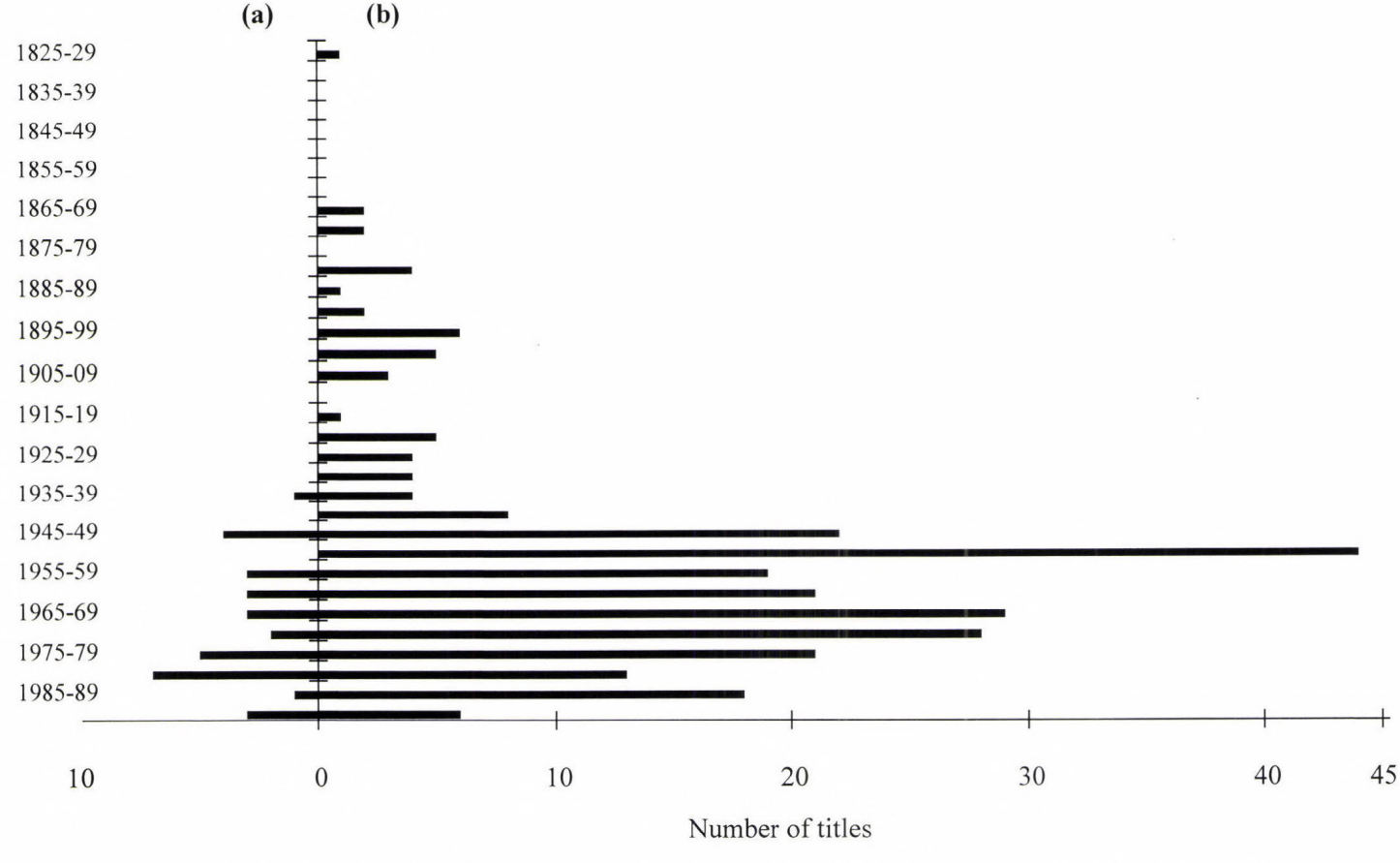

Fig. 1. Age-pyramid of journals registered in *Ulrich's Directory* for the subfield meteorology for 1994 and 1995; (*a*) journals published by publishing houses, (*b*) journals published by scientific societies and institutions.

Table 1. Meteorological journals registered in SCI in 1995

Title	First year of publication	Registration in SCI	Publisher
Q. J. Roy. Meteor. Soc.	1871	1975	Royal Meteor. Soc., Reading, Berkshire
Monthly Weather Review	1872	1975	American Meteorol. Soc., Boston
J. Meteor. Soc. Japan	1882	1982	Meteorological Soc. Japan, Tokyo
J. Geophys. Res. (Atmos.)	1896	1975	American Geophys. Union, Washington
J. Geophys. Res. (Space Ph.)	1896	1975	American Geophys. Union, Washington
Bull. Amer. Meteor. Soc.	1920	1975	American Meteorol. Society, Boston
J. Atmospheric Science	1944	1975	American Meteorol. Society, Boston
Meteor. Atmos. Physics	1949	1975	Springer Verlag, Vienna
Tellus A	1949	1975	Munksgaard Internat. Publ., Copenhagen
Tellus B	1949	1975	Munksgaard Internat. Publ., Copenhagen
Theor. Appl. Climatol.	1949	1987	Springer Verlag, Vienna
J. Atmos. Terr. Physics	1950	1975	Elsevier Science Ltd., Oxford
J. Air Waste Management	1951	1975	Air & Waste Manag. Assoc., Pittsburgh
Australian Meteor. Magazine	1952	1954	Australian Bureau of Meteor., Canberra
Int. J. Biometeorology	1957	1975	Springer Verlag, Berlin
J. Applied Meteorology	1962	1975	American Meteorol. Society, Boston
Atmosphere – Ocean	1963	1987	Canadian Meteorol. Oceanogr. Society
Agricultural Forest Meteor.	1964	1984	Elsevier Science B.V., Amsterdam
Izv. A. N. Fiz. Atmos. Ok.	1965	1980	Izdatelstva Nauka, Moscow
Atmospheric Environment	1967	1975	Elsevier Science Ltd., Oxford
Boundary-Layer Meteorology	1970	1981	Kluwer Scientific Publishers, Utrecht
J. Aerosol Science	1970	1981	ELsevier Science Ltd., Oxford
Climate Change	1977	1977	Kluwer Acad. Publishers, Dodrecht
Dynam. Atmos. Oceans	1977	1977	Elsevier Science B.V. Amsterdam
Advances in Space Research	1981	1993	Elsevier Science Ltd., Oxford
Int. J. Climatology	1981	1982	John Willey Ltd., Journals, Sussex
Annales Geophysicae	1983	1983	Springer Verlag, Heidelberg
J. Atmospheric Chemistry	1983	1984	Kluwer Acad. Publishers, Dodrecht
J. Atmos. Ocean Tech.	1984	1991	American Meteorol. Society, Boston
Climate Dynamics	1986	1992	Springer Verlag, Heidelberg
J. Climate	1986	1986	American Meteorol. Society, Boston
Wheather Forecast	1986	1992	American Meteorol. Society, Boston
Global Biogeochem. Cycl.	1987	1993	American Geophys. Union, Washington

4. The impact factor

From the very beginning of the scientific publication the recognition by the scientific community had been the reward for well done scientific research. This is reflected, inter alia, in the citation of the work in question by fellow researchers in their own publication. The SCI is built on the principle that there is some meaningful relationship between one paper and some other through citations, so a citation index can be constructed. The ISI publishes such an index in each year. On the basis of citation data of articles published in a given journal a so called "impact factor" can be calculated for the journal in question as a tool for evaluation. The impact factor is the measure of the frequency with which the "average cited article" in a journal has been cited by other articles in a particular year. The impact factor of a journal is basically a ratio between citations and citable items published. Thus the 1994 impact factor of a given journal would be calculated by dividing the number of all the SCI source journals' 1994 citations of articles of the given journal published in 1992 and 1993 by the total number of papers it published in 1992 and 1993 (*Garfield*, 1972).

Table 2 shows the rank order of the meteorological journals of ISI by average number of articles. In *Table 3* the annual impact factor for the years 1985–1994 is given. From the latter it can be deduced that the general average value of the impact factor for these meteorological journals is 1.02.

As it can be seen in Table 3, the highest average impact factor (3.989) was reached by *Journal of Geophysical Research*, which is not strictly a meteorological journal. One of the most renowned interdisciplinary journals, *Nature*, which publishes highly cited articles in the whole field of science, announced its impact factor by subfields separately for 1996. These data can be found in *Monthly Nature*, a (since then ceased) collection of the most interesting articles of the weekly *Nature*. It can be seen that the impact factor of *Nature*'s articles in the subfield of earth sciences is 14.01, substantially lower than the value calculated for all of the publications in *Nature* (25.5), but fourteen-times higher than the average impact factor for meteorological journals included in ISI's SCI. In our opinion this difference is not only due to the fact that the greater part of *Nature*'s articles about earth sciences does not deal with meteorology, but deals with more "fashionable" topics, e.g. space research. However, the few meteorological articles published in *Nature* are altogether certainly outstanding.

The values of the impact factor show some changes during the "life" of a given periodical. The changes are more pronounced if they are caused by some "demographical" events (i.e. "change of name", "multiplying by partition", etc). *Tables 4* and *5* give some examples for these phenomena in the "population" of meteorological journals. *Fig. 2* shows the consequences of such changes for the values of the impact factor of the journals in question.

Table 2. Rank order of journals by annual average number of articles (1985–1994) (*Journal Citation Report*)

Rank	Title	Average no. of articles
1	J. of Geophysical Research	961.1
2	J. of Geophysical Research – Solid Planets	431
3	Atmospheric Environment A – General	285
4	Atmospheric Environment	277
5	J. of Geophysical Research – Atmospheres	248.17
6	J. of Geophysical Research – Oceans	242
7	J. of Atmospheric Science	217.5
8	Monthly Weather Review	180.1
9	Izv. Akad. Nauk. Fizika Atmosfery i Okeana	129.22
10	J. of Climate and Applied Meteorology	126.3
11	J. of Air Pollution Control Association	122.6
12	J. of Atmospheric and Terrestrial Physics	121.4
13	J. of Applied Meteorology	121
14	J. of the Air and Waste Management Association	118.4
15	J. of Aerosol Science	105.3
16	J. of Climate	92
17	Boundary-Layer Meteorology	91.5
18	J. Atmos. Ocean Technology	90.25
19	Annales Geophysicae	85
20	Agricultural and Forest Meteorology	80.5
21	Annales Geophysicae B – Terr. Planet. Physics	68
22	J. of Meteorological Society of Japan	62.67
23	Quarterly J. of Royal Meteorological Society	61.2
24	Bull. of the American Meteorological Society	57.8
25	Int. J. of Climatology	55
26	Indian J. of Radio Space	54.78
27	Annales Geophysicae A – Upper Atm. Space Sci.	52
28	J. of Climatology	42.5
29	Theoretical and Applied Climatology	40
30	Atmospheric Environment B – Urban	39.5
31	J. of Atmospheric Chemistry	38.9
32	Climatic Change	38.7
33	Meteorology and Atmospheric Physics	38.67
34	Climate Dynamics	38.33
35	Meteorological Magazine	38.14
36	Tellus B	34
37	Tellus A	33
38	Int. J. of Biometeorology	32.4
39	Atmosphere – Ocean	26.67
40	Australian Meteorological Magazine	25
41	Wheather Forecast	22.5
42	Dynamics of Atmospheres and Oceans	18.5
43	Arch. for Meteorology, Geophys. and Bioclim. A	18
44	Arch. for Meteorology, Geophys. and Bioclim. B	16

Table 3. Rank order of journals by annual average impact factor (1985–1994) (*Journal Citation Report*)

Rank	Title	Average impact factor
1	J. of Geophysical Research	3.989
2	J. of Climate	2.712
3	Climate Dynamics	2.278
4	J. of Atmospheric Science	1.905
5	J. of Atmospheric Chemistry	1.874
6	Tellus B	1.860
7	Quarterly J. of Royal Meteorological Society	1.814
8	Bull. of the American Meteorological Society	1.795
9	Climatic Change	1.615
10	J. of Climatology	1.599
11	Monthly Weather Review	1.544
12	Atmospheric Environment	1.444
13	Atmospheric Environment A - General	1.240
14	Annales Geophysicae	1.200
15	Tellus A	1.191
16	J. of Climate and Applied Meteorology	1.188
17	J. of Geophysical Research - Atmospheres	1.096
18	J. of Atmos. Ocean Technology	1.066
19	Boundary-Layer Meteorology	1.020
20	J. of Atmospheric and Terrestrial Physics	1.006
21	Dynamics of Atmospheres and Oceans	0.895
22	J. of Applied Meteorology	0.888
23	Int. J. of Climatology	0.885
24	J. of Geophysical Research - Solid Planets	0.875
25	Atmosphere – Ocean	0.871
26	Agricultural and Forest Meteorology	0.835
27	J. of Air Pollution Control Association	0.831
28	J. of Geophysical Research - Oceans	0.790
29	J. of Aerosol Science	0.679
30	J. of the Air and Waste Management Association	0.675
31	J. of Meteorological Society of Japan	0.647
32	Atmospheric Environment B - Urban	0.571
33	Wheather Forecast	0.535
34	Meteorology and Atmospheric Physics	0.497
35	Int. J. of Biometeorology	0.337
36	Arch. for Meteorology, Geophys. and Bioclim. B	0.316
37	Theoretical and Applied Climatology	0.293
38	Australian Meteorological Magazine	0.273
39	Arch. for Meteorology, Geophys. and Biocklim. A	0.273
40	Izv. Akad. Nauk. Fizika Atmosfery i Okeana	0.223
41	Meteorological Magazine	0.220
42	Indian J. of Radio Space	0.089
	General average:	1.02

Table 4. Causes of changing names of meteorological journals

Cause	Original title	New title
Internationalization, extended readership	Journal of Climatology	International Journal of Cimatology (1990)
Change in scope	Journal of the Air Pollution Control Association	Journal of the Air and Waste Management Association (1990)
Focusing in scope (bipartition)	Journal of Climate and Applied Meteorology	Journal of Applied Meteorology (1989) Journal of Climate (1989)
Merging	Journal of Geophysical Research, – Atmospheres, – Oceans, – Solid Planets	Journal of Geophysical Research (1991)
Becoming independent	Archives for Meteorology, Geophysics and Bioclimatology, Series A: Meteorol. and Geophys.	Meteorology and Atmospheric Physics (1986)

Table 5. Effects of splitting and reuniting of a journal

Atmospheric Environment (A – General; B – Urban)

	1985	1986	1987	1988	1989	1990	1991	1992	1993	1994
A						300	256	299	285	
Papers published	235	264	274	284	266					339
B						49	26	53	30	
A							1.033	1.358	1.259	1.310
Impact factor	1.465	1.634	1.529	1.340	1.473	1.358	1.312			0.000
B							0.592	0.692	0.389	0.611

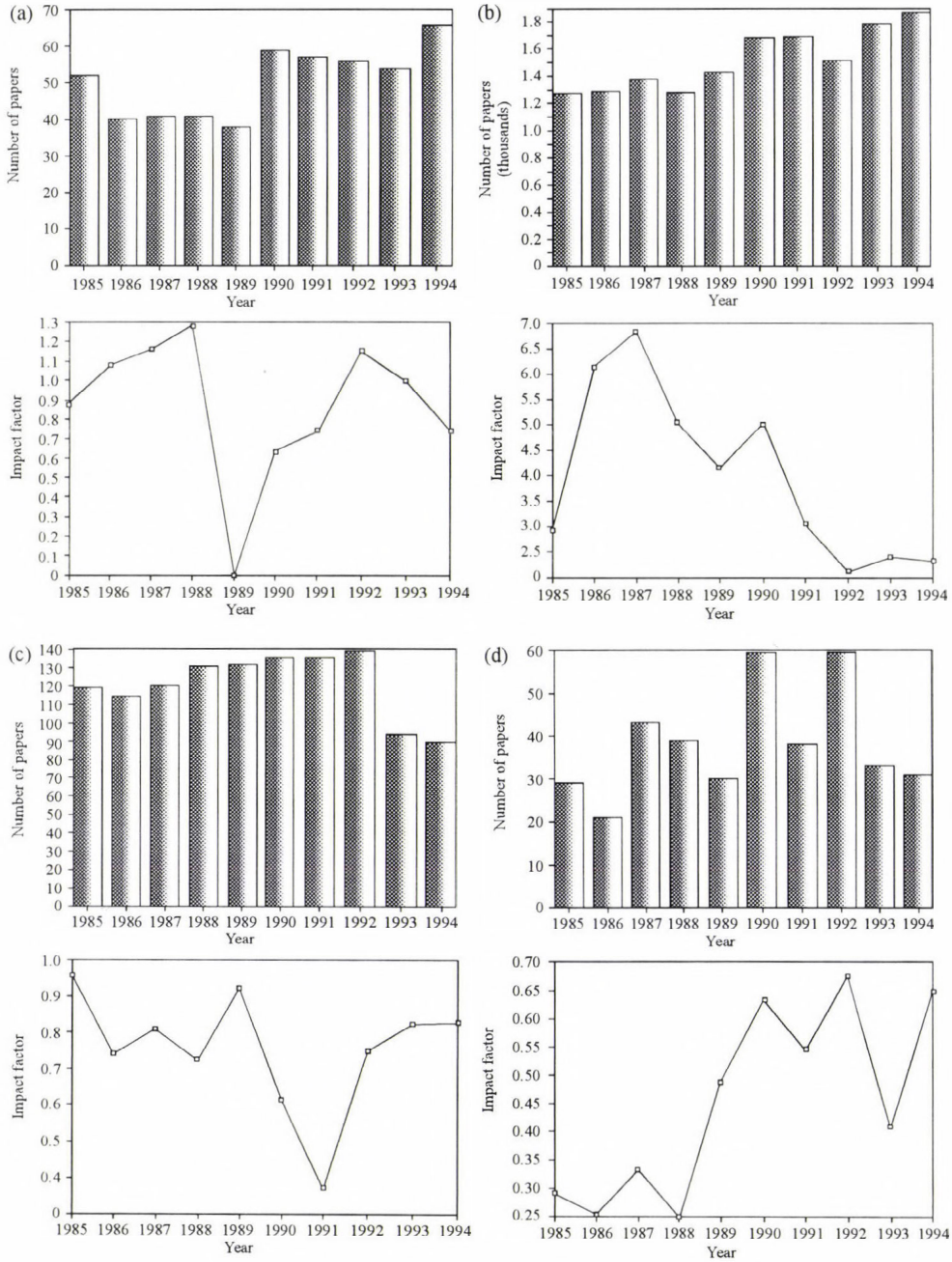

Fig. 2. Changes in the number of papers and impact factors during 10 years (1985–1994) for some meteorological journals: (*a*) Int. Journal of Climatology; (*b*) Journal of Geophysical Research; (*c*) J. of the Air and Waste Management Association; (*d*) Meteorology and Atmospheric Physics.

5. Where to publish?

Now, we can come to the conclusion that a great variety of journals are available for the scientist in meteorology for publication. Especially the journals in SCI's list are worth to mention, from the points of view of prestige, circulation and frequency (*Day*, 1983). There are namely differences between, e.g., a new, attractive journal, published by a commercial publisher without sponsorship of a society; an old, well-known, small journal, published by a famous institute, and a journal, published by a leading scientific society, representing the subfield in question. Perhaps, the latter has the largest circulation, whereas the old, well-known small journal has very limited space, and this is mainly reserved for the members of its publishing institute. Usually, a new, attractive journal, published by a profit-oriented publishing house, is the most specialized periodical in the respective topic, but because of the high subscription price, it has certainly the disadvantage of a low circulation (*Day*, 1983).

In any case, if somebody wants his/her article to be read by as many as possible scientists interested in its topic, the paper has to go to a journal of international prestige. Nowadays, the language of such journals is almost exclusively English. The contents of scientific articles, which appear in obscure periodicals, written in a rarely spoken language, will fail the aim of large scale dissemination of its results and will sink into oblivion.

The quotation: "everybody talks about the weather, but nobody does anything about it" (*Warner*, 1890) is not quite valid today . The meteorologists, even if being unable to do much about the weather, can write about the atmosphere in appropriate scientific journals of international reputation. Perhaps this modest paper will help to find the right one.

Acknowledgement—The authors thank *Prof. T. Braun* for stimulating remarks and discussions.

References

Brookes, B. C., 1980: Aging in scientific literature. *J. Docum. 36*, 164.

Day, Robert A., 1983: *How to Write and Publish a Scientific Paper*. ISI Press, Philadelphia.

Fierro, A., 1991: Histoire de la météorologie. Denoël, Paris.

Garfield, E., 1972: Citation analysis as a tool in journal evaluation. *Science 178*, 471-479.

Journal Citation Report, 1985–1994, Institute for Scientific Information, Philadelphia.

Price, D. J. de Solla, 1963: *Little Science, Big Science*. Columbia Univ. Press., New York, London.

Science Citation Index, 1985-1994, Institute for Scientific Information, Philadelphia.

Ulrich's International Periodicals Directory, 1994-95. 33rd Edition, Vol. 3. The Bowker International Serials Database (ed.: *R.R. Bowker*). New Providence, New Jersey.

Warner, C. D., 1967: Editorial. Hartford, Conn., Courant cont. 1890. In *The Home Book of Quotations* (ed.: *B. Stevenson*). Classical and Modern. 10th Edition, Dodd, Mead & Comp., New York. Often attributed to Mark Twain.

Ziman, M., 1969: Information, communication, knowledge. *Nature 224*, 318.

Zsindely, S. and *Schubert, A.*, 1992: The demography of journals. *New Library World 93* (1102), 17-20.

IDŐJÁRÁS

Quarterly Journal of the Hungarian Meteorological Service
Vol. 101, No. 2, April–June 1997, pp. 105–121

Area averages of ammonia concentrations in high emission areas; measurements and model results

Jan Willem Erisman and **Joris Boermans**

National Institute of Public Health and Environmental Protection, RIVM, P.O. Box 1, 3720 BA Bilthoven, The Netherlands; E-mail: janw@rivm.nl

(Manuscript received 15 October 1996; in final form 22 March 1997)

Abstract—Atmospheric concentrations and deposition of ammonia in the Netherlands and Europe have been described using the long-range transport model TREND (*Asman* and *van Jaarsveld*, 1992). In this paper results are reported of a program aimed at evaluating the TREND model in high ammonia emission density areas. In such areas emissions and concentrations show large horizontal variations. Average concentrations for two areas in the Netherlands were obtained by continuous ammonia measurements at a fixed point. Due to technical problems the time coverage of one of the sites was too low and therefore these data are not taken into account. The representativeness of the Vredepeel fixed point measurements was investigated using mobile measurements, a detailed emission inventory and a short-term/short-range transport model for ammonia (SLAM). The measuring strategy developed for this research provides a good tool for assessing the representativeness of a single point measurement for a larger area surrounding the fixed point. Yearly average concentration during July 1991–July 1992 at Vredepeel was 19.4 μg m^{-3}. The results of the assessment of the representativity of the fixed point showed that the Vredepeel location is representative within 10% in comparison with the surrounding 5 × 5 km area. It is concluded from this study that there was no significant difference between TREND results and the annual average measured concentration for the high emission area at Vredepeel.

Key-words: ammonia, high emission density area, measurements, modeling, representativity.

1. Introduction

Only recently has ammonia been recognized as one of the potential acidifying air pollutants (*van Breemen et al.*, 1982; *Heij* and *Schneider*, 1991, *Sutton et al.*, 1993). Nitrification of deposited ammonia and ammonium by microbial processes in forest soils in the Netherlands has been demonstrated by *van Breemen et al.* (1982). Through this process, acids in gaseous form, in aerosols or in rain droplets initially neutralized by gaseous NH_3 can form two

equivalents of acid when deposited: one can be considered as derived from NH_3 and one from the neutralized acid. Because of incomplete nitrification in the soil or uptake of nitrogen by vegetation the contribution of NH_3 and/or NH_4^+ may be less than one equivalent H^+ per mole NH_3 deposited. This contribution depends on type of soil and vegetation. Furthermore, NH_3 may play an important role in the enrichment of nutrient poor ecosystems (*Heil* and *Diemont*, 1983; *Heij* and *Schneider*, 1991; *Grennfelt* and *Thörnelöf*, 1992). The contribution of NH_3 to the total potential acid deposition in the Netherlands in 1989 was estimated to be 46% (*Erisman*, 1993).

Ammonia is emitted primarily from low level agricultural sources, with varying source strengths (*Buijsman et al.*, 1987; *Erisman*, 1989; *Asman*, 1992). Gaseous NH_3 has a short atmospheric residence time (*Erisman et al.*, 1988). Thus, concentrations (and deposition) will vary substantially over short distances. Measurements at 2 m height, of the horizontal gradient of NH_3 concentrations over a heathland located next to an emission area, showed gradients up to a factor of 20 within 5 km (*Asman et al.*, 1989). Consequently, accurate representative measurement of NH_3 concentrations in the Netherlands, especially in high emission density areas, would require many measuring sites. There are only very few attempts to monitor ammonia concentrations (*Erisman et al.*, 1986; *Allen et al.*, 1988; *Langford et al.*, 1992; *Sutton et al.*, 1993). Large scale monitoring of ammonia concentrations has been limited by a lack of an accurate and reliable measuring method. The number of measurements made in the Netherlands is far too small to obtain an accurate spatial distribution of the concentration. Therefore, the spatial distribution has been estimated from dispersion calculations by a transport model (TREND model, *Asman* and *van Jaarsveld*, 1992), using yearly average meteorological statistics and detailed emission maps. In this way, NH_3 and NH_4^+ concentration estimates on a 5×5 km grid have been obtained over the country. These concentration maps are used together with meteorological measurements, surface characteristics and wet deposition measurements to estimate the total NH_x deposition (*Erisman*, 1993).

From an analysis using all available NH_3 and NH_4^+ concentration measurements in air and in precipitation, it appeared that evaluation of model results in high emission density areas is difficult because of the difficulty of measuring representative area average concentrations (*Asman* and *van Jaarsveld*, 1992; *van Aalst* and *Erisman*, 1991). For this reason a program was started for estimating concentrations of ammonia in high emission areas aimed at further evaluation of the emission–dispersion–concentration–deposition system described in the TREND model (*Boermans* and *Erisman*, 1991, 1993). A measuring strategy based on a phenomenological description of available measurements was developed to account for the complex behavior of NH_3 in the atmosphere. It turned out during the execution of the measuring program that an extra tool was needed for the interpretation of the measurements. This

became the *S*hort-term *L*ocal-scale *A*mmonia transport *M*odel SLAM (*Boermans* and *van Pul*, 1993). SLAM can be used to calculate short-term (hourly) and local-scale (< 15 km) concentrations due to the dispersion of air pollution emitted from a large number of ground-level sources. In this paper the measuring strategy will be explained and the results of the measuring program will be presented.

2. Experimental set-up

2.1 Measuring/modeling strategy

Two regions with high ammonia emission density were selected; one region with predominantly intensive chicken breeding (Lunteren) and one region with predominantly intensive pig breeding (Vredepeel). Cheap and accurate ammonia concentration measuring devices for extensive application were not available. Continuous measurement devices were still under development. A fixed point in each region was therefore selected and equipped with a prototype continuous ammonia measurement instrument (*Wyers et al.*, 1992). Continuous measurements were made during one year at each fixed point. The fixed points were chosen by visual inspection together with detailed emission maps. The sites had to be representative for the region, with no direct influence of nearby sources in relation to emission strength and distribution of wind direction. Representativity of the concentration measured at the fixed point for the average surrounding area of 5 × 5 km (TREND model resolution) was evaluated by mobile measurements at eight sites (see Figs. 1a and 1b). These sites were selected by local inspection together with detailed emission maps. These sites were selected so as to represent parts with high, average and low emission in the grid square.

The mobile measurements were made by using a van in which the same measuring system was installed. Measurements were carried out on 23 days during the year according to a meteorological classification. The meteorological classification was based on a phenomenological study using long-term NH_3 concentration measurements at two sites: Elspeetsche Veld (hourly measurements, *Erisman et al.*, 1993) and Vredepeel (24 hour average measurements, *Erisman et al.*, 1986) (*Boermans* and *Erisman*, 1991). The main results of this study showed a positive correlation between air temperature and NH_3 concentrations. Furthermore, a dependence of wind direction (sources) and stability (mixing) was observed. The classification was based on wind direction, wind speed and temperature and is given in *Table 1*. Meteorological conditions were averaged over the hours the mobile measurements were carried out, to define a meteorological class. The aim was to measure all meteorological classes at least once. Annual averages could then be obtained by weighting the

occurrence of a class during the year. Usually nine measurements were made per day, starting at the fixed point (instrument calibration), then at the remaining eight sites (changing the order each day). If the instrument calibration showed more that 25% deviation, an extra measurement was made at the fixed point at the end of the measuring period.

Table 1. Meteorological classes used for the selection of measuring days in the mobile measuring program (*Boermans* and *Erisman*, 1990)

Wind directions: north, east, south and west, each divided into four classes:

Meteo class	Wind speed $m\ s^{-1}$	Temperature °C
1	≥ 3	> 11
2	≥ 3	≤ 11
3	< 3	> 11
4	< 3	≤ 11

The TREND model was originally developed for estimating concentration and deposition of sulfur compounds and oxidized nitrogen compounds in the Netherlands (*van Jaarsveld*, 1995). Recently the model was extended to treat reduced nitrogen compounds (*Asman* and *van Jaarsveld*, 1992). The more general model concept was validated by comparing model results with measurements of concentrations in air and in precipitation (*van Jaarsveld*, 1989; *Asman* and *van Jaarsveld*, 1992). The model resolution is 5 × 5 km. Within the grid cells the variation in concentration can be very high, especially in high emission density areas. It was desirable to have a tool which could serve as an explanatory model for the hourly measurements at the fixed point and additional measurements within the 5 × 5 km areas. For this purpose the SLAM model was developed (*Boermans* and *van Pul*, 1993). The SLAM model resolution is 100 m, when appropriate emission inventories are available. SLAM is used as an extension to the measurements, because measurements can be simulated and extended for periods where the equipment failed. The results of the SLAM calculations are extensively described in *Boermans* and *van Pul* (1993).

2.2 Measuring method

The NH_3 measurements were performed with an automated thermodenuder system developed at ECN (*Keuken et al.*, 1989; *Wyers et al.*, 1992). The method is based on collection of NH_3 by a V_2O_5-coated annular denuder, desorption and conversion of NH_3 to NO_x at 700°C and measurement of the resulting NO_x concentration by a NO_x-monitor (Ecophysics CLD 700 AL). A data logger controls the system and calculates the sampled NH_3 concentration

from the integrated NO_x signal, the sampling flow rate, the sampling time and a calibration constant. The sampling period was set to 5 minutes within a measuring cycle of 45 minutes. The sampling flow rate was kept at 3.3 ℓ min^{-1}. Two systems were installed in portable cabins at Lunteren and Vredepeel, while one system was installed in a van. Ambient air was sampled through 3 m long tubes (FEP Teflon, 6.35 mm outside diameter), which were renewed every month to prevent adsorption of NH_3 on dirty inlet tubes. Systems were calibrated at the site once every two weeks using a portable calibrator (Environment, model VE3M) provided with an NH_3 permeation tube and a zero-air dilution system. The performance of the thermodenuder system was examined in two field campaigns (*Mennen et al.,* 1992; *Mennen* personal communication) and in a calibration chamber under controlled conditions (*van Putten et al.,* 1992). From the latter, a detection limit of 0.2 $\mu g\ m^{-3}$ was found; precision was better than 0.3 $\mu g\ m^{-3}$ at low concentrations and better than 2% at high concentrations, and the measuring range is 0–300 $\mu g\ m^{-3}$.

2.3 Site description and ammonia emissions

The two locations are Vredepeel (51°32'N; 5°51'E) in the region "de Peel" and Lunteren (52°6'N; 5°38'E) in the region "Gelderse Vallei". In order to generate realistic calculations using TREND and SLAM, detailed emission inventories are needed for both areas. *Erisman* (1989) reports ammonia emissions in the Netherlands on a 5 × 5 km scale for 1988. In this inventory, emissions were assessed per municipality and generated by land use to a 5 × 5 km scale. The inventory is used on a national scale as input for the TREND model. For the two areas more detailed emission inventories were made. The inventory around Vredepeel consists of ammonia sources in an area of 15 × 20 km around the fixed point (*DHV Raadgevend Ingenieursbureau*, 1991). This inventory contains point sources (emissions from stables) and land use specific area sources (application of manure and pasture emissions) and it is an update for 1991 in comparison with the emissions according to *Erisman* (1989). The Lunteren inventory consists of ammonia sources in an area of 15 × 15 km around the fixed point (*Heidemij Adviesbureau*, 1989), this inventory is an update for 1989 in comparison with the emissions according to *Erisman* (1989). *Figs. 1a* and *1b* show point sources of the central 5 × 5 km grid cell of the Vredepeel (a) and Lunteren (b) inventories. In the figures the fixed point (a) and the eight additional sites (1 to 8) are also plotted. Source strength is categorized by annual average emission estimates.

As it can be seen in Fig. 1, the Lunteren area shows many more but smaller point sources in comparison with the Vredepeel area. This difference is caused by a different housing of animals. In Lunteren mainly smaller stables with chickens can be distinguished in comparison with larger stables in the Vredepeel area holding mainly pigs. The Lunteren area is characterized by being rural area

split up by forest from the center to the southeast of the 15 × 15 km area. The Vredepeel area is more homogeneous, showing small forest and a military air base in the south of the 5 × 5 km area and a forest in the west of the 15 × 20 km area. The annual average ammonia emission for the 5 × 5 km grid in Vredepeel was estimated to be 344 t yr^{-1}, and for Lunteren 464 t yr^{-1}. Within the program it was tried to obtain information about agricultural practices, especially about spreading of manure, by sending out an inquiry. Unfortunately only a few questionaires were returned so the results were not used.

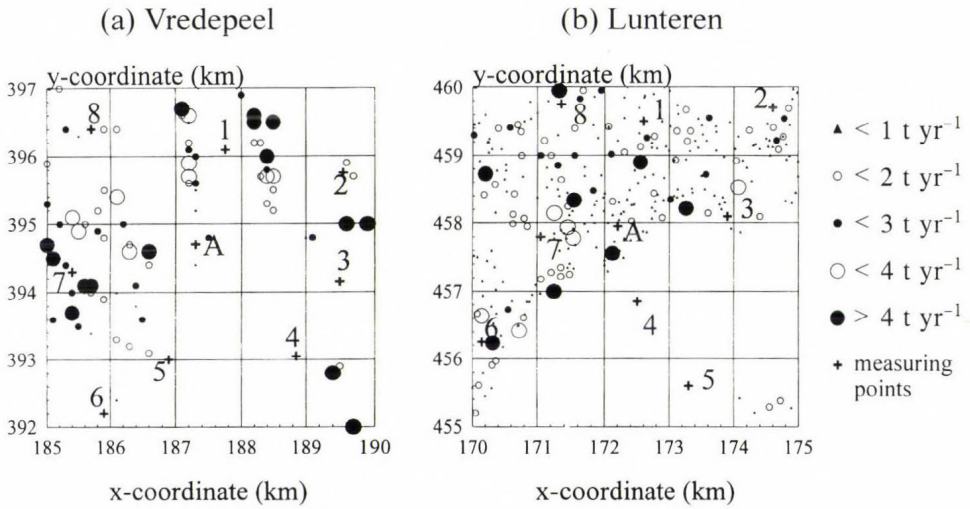

Fig. 1. Emission inventory of point sources in the surrounding 5 × 5 km area arround the location Vredepeel (*a*) and Lunteren (*b*). The measuring sites (A and 1–8) are also plotted. The axes represent coordinates of the Dutch coordinate system.

3. Phenomenology of ammonia at the fixed points

The measurements at the locations Vredepeel and Lunteren were carried out from July 1991 until July 1992. Due to technical problems, mainly bad performance of the data loggers, but also defective ovens, mechanical problems and failure of mains voltage, many measurements failed at the two fixed points, Vredepeel and Lunteren. The Lunteren data show a percentage of cover of only 31%, whereas the Vredepeel data show 69% of coverage during a one year of continuous measurements. Although less operational problems occurred with the mobile measurements, not all 16 meteorological (meteo) classes were covered. Differences between weather forecasts and actual meteorological conditions caused overlaps in meteo classes for the selected measuring days. Operational failures at the fixed points during mobile measurements also resulted in loss of successful days.

Phenomenology of ammonia concentrations show various relationships to meteorological conditions and seasons. *Fig. 2* shows monthly average measured concentrations at the fixed point at Vredepeel (*a*) and at Lunteren (*b*). The percentages of coverage of the monthly measured concentrations are also plotted. Monthly average concentrations show lowest values during the months from July until November. The concentrations show low levels during summer despite of high temperatures (positive relation to emission). This is caused by the growing season and therefore the absence of spreading of manure. The effect on the monthly average concentration of spreading manure in spring is not as clear as expected. Mobile measurements also show that the effect of spreading manure as measured (and visually seen) at one of the eight additional sites in the 5 × 5 km area does not always lead to an increase in concentration at the fixed point depending on the wind direction. In spite of low response to the inquiry to register the spreading of manure in Vredepeel, results also show a lower peak of spreading activities than the expected. Another explanation might be that, despite of the regulations which state that application of manure is not allowed during winter months, spreading activities occur during the whole year. Annual average concentrations are 19.4 $\mu g\ m^{-3}$ (σ = 22 $\mu g\ m^{-3}$) and 32.9 $\mu g\ m^{-3}$ (σ = 55 $\mu g\ m^{-3}$) for Vredepeel and Lunteren, respectively.

Fig. 3 shows measured concentrations in relation to temperature and stability for the whole dataset of Vredepeel. In general, the measured concentrations show a small decrease with increasing temperature. This effect is mainly caused by the high measured concentrations at temperatures below –5°C at stable conditions and the higher concentrations measured within the interval 0–10°C at unstable conditions. Near to neutral conditions the concentrations show no variation with the temperature classes. The effect of stability and wind speed on the measured concentrations is clearly demonstrated. Low wind speed and stable conditions show high concentration levels. These conditions are typical for early morning inversion situations where there is no vertical mixing of pollutants. Due to the high number of ground-level sources, ammonia will accumulate in the thin surface layer during these conditions. This effect can also be seen in the summer and winter average diurnal variation, shown in *Fig. 4*, where high concentration levels occur during nighttime with a maximum of 32 $\mu g\ m^{-3}$ in summer and, a less pronounced maximum of 19 $\mu g\ m^{-3}$ in winter. These daily variations are different from the observations in background areas where smallest concentrations are observed during nighttime and highest during the day (*Langford et al.,* 1992). An example of a time series of continuous measurements of NH_3 concentration during 18–30 October 1991 at Vredepeel, given in *Fig. 5*, clearly illustrates the NH_3 behavior observed here. In this figure variation in temperature is also plotted. This figure also demonstrates that relations between concentrations and temperatures are not simple.

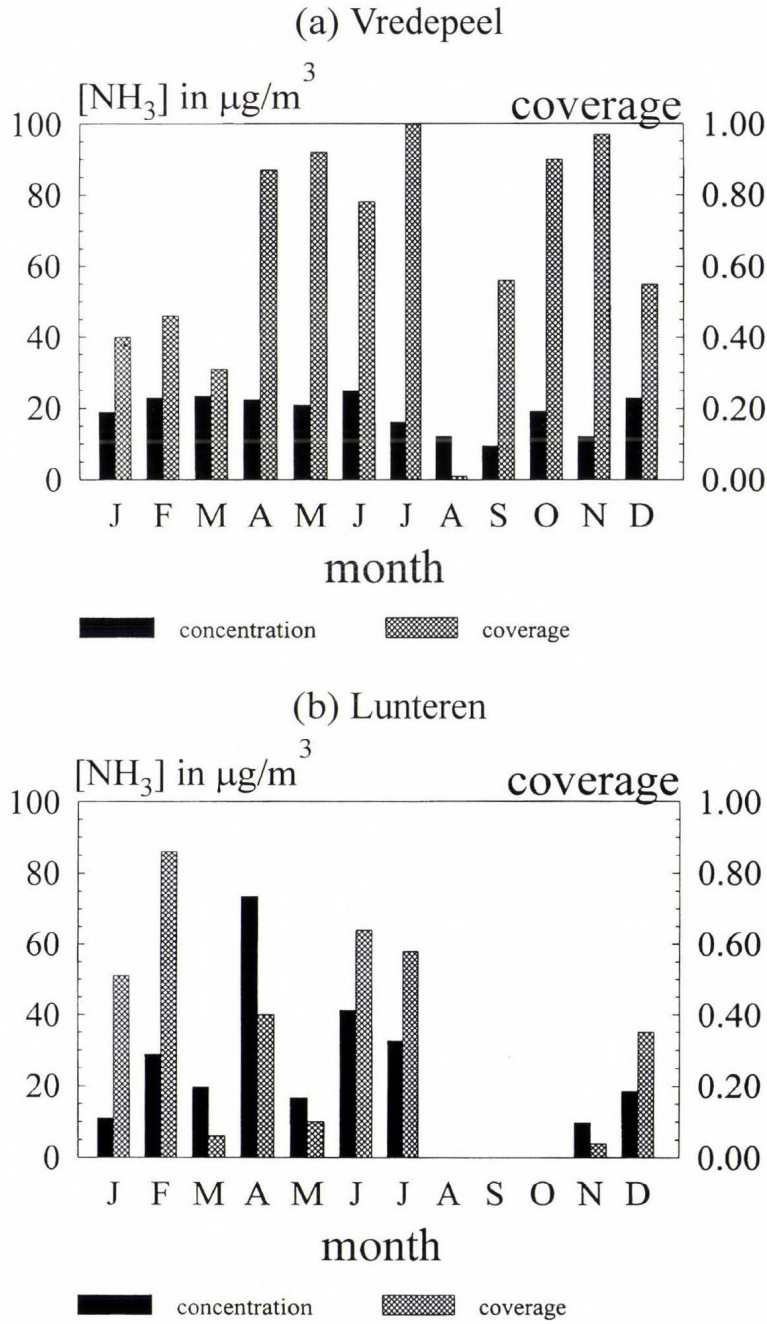

Fig. 2. Monthly average concentrations for Vredepeel (*a*) and for Lunteren (*b*). The percentages of coverage of the monthly measured concentrations are also plotted.

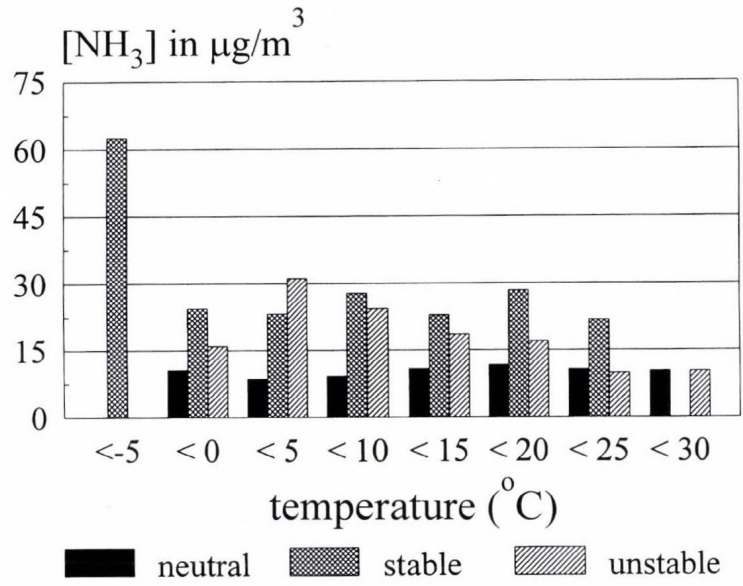

Fig. 3. Measured concentrations of the Vredepeel data related to a temperature and stability classification.

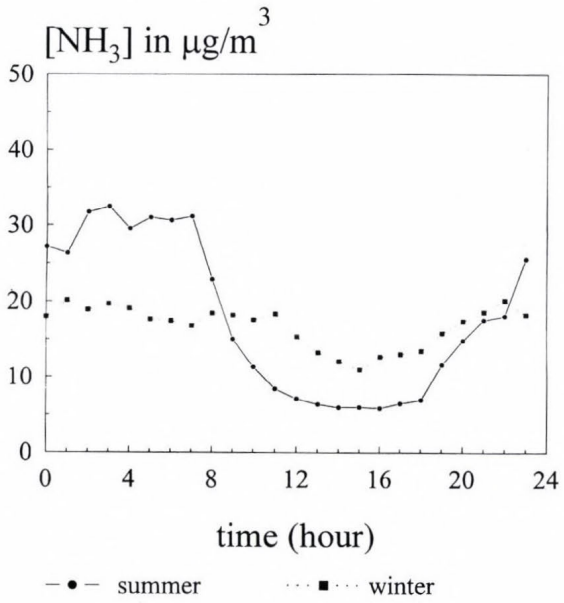

Fig. 4. Annual average diurnal variations of ammonia concentrations at Vredepeel.

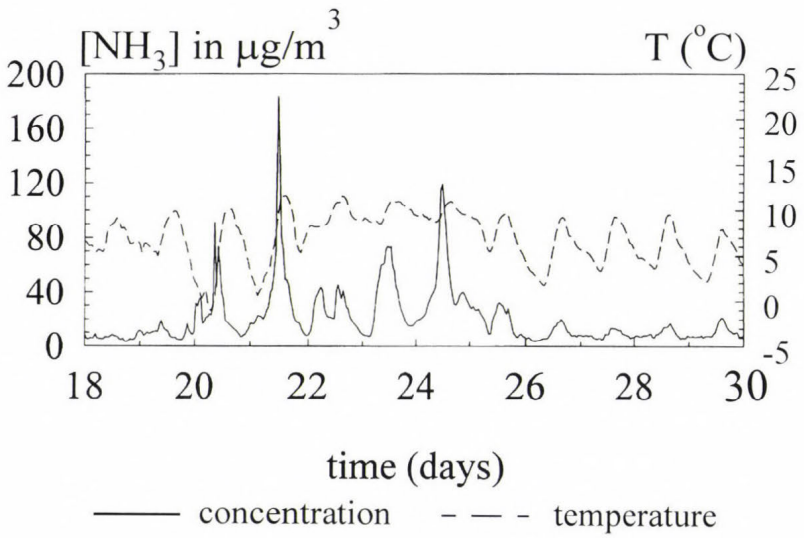

Fig. 5. An example of time series of continuous measurements of NH_3 concentration during 18–30 October 1991 at Vredepeel.

4. Fixed point and mobile measurements

In order to evaluate the representativeness of the fixed points, mobile measurements were made according the measuring strategy developed by *Boermans* and *Erisman* (1991, see Section 2.1). Because of the low coverage of the measurements at Lunteren, this site is not taken into account for model validation purposes. *Fig. 6* shows the fixed point measurements in comparison with the arithmetic averages of the mobile measurements for Vredepeel. Averaged mobile measurements for the Vredepeel area (23 days) show 25% lower concentrations compared to the yearly average fixed point concentration. This underestimation is mainly caused by the high number of meteo classes with wind speed conditions >3 m s^{-1} (19 of a total of 23 days). These conditions show clearly lower concentrations (Section 3). The deviations between the fixed point and the mobile measurements is probably due to the small amount of point sources in the area with high emissions resulting in large concentration gradients (Fig. 1). The average concentration for all mobile measurements at Vredepeel is 15.3 μg m^{-3}, for the fixed point during the same hours this is 14.2 μg m^{-3}. Fixed point results are averaged for all hours of all measuring days and therefore differ slightly in comparison with values presented in Section 3.

In this section a statement has to be made about the spatial representativeness of the fixed points for the 5 × 5 km area around Vredepeel on an annual basis. According to the measuring strategy, a yearly average grid

concentration (5 × 5 km) should have been assessed by averaging the mobile measurement results for all 16 meteo classes multiplied by the occurrence of each class during the year. Even though the fixed point measurements agree well with the mobile measurements, no yearly average grid concentration could be assessed due to the inadequate number of measured meteo classes.

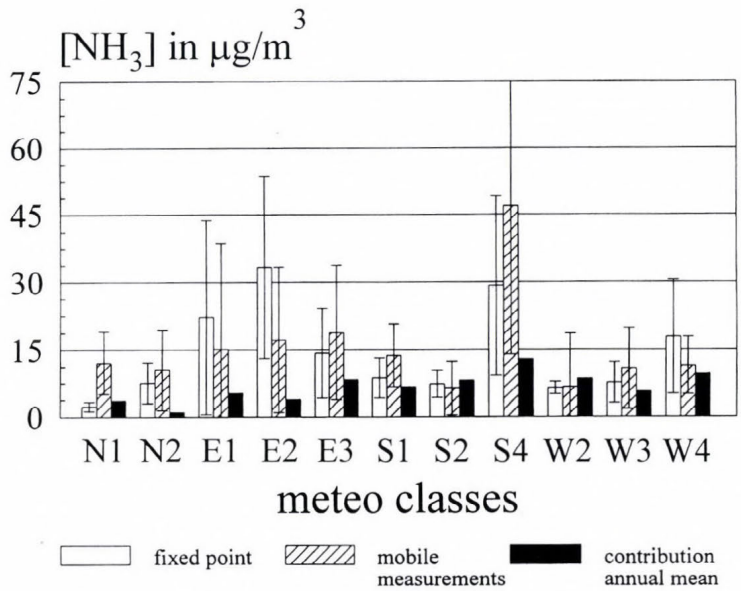

Fig. 6. Fixed point measurements in comparison to the average of mobile measurements in the 5 × 5 km area of Vredepeel for the different meteorological classes. The contribution of the meteo class average concentration to the annual mean concentration, weighted according to the occurrence of the meteo class, is also given.

For Vredepeel the time weighted contribution (%) of the meteorological classes to the annual average concentration based on the fixed point measurements is plotted. The classes for which measurements are available cover 73.6% of the annual (fixed point) concentration. Therefore, measurements have been made during the most important classes. Because no more representativeness measurements could be made, the representativity was investigated further using a model.

At this stage the SLAM model was used to further examine the representativity of the fixed point concentrations relative to the grid averages. The model was tested using measurements presented here (*Boermans* and *van Pul*, 1993). SLAM input consists of all point sources (Fig. 1) and area sources in the studied areas. Model calculations were made to estimate average

concentrations for the fixed points and for the 5 × 5 km grids for all meteo classes (*Boermans* and *Erisman*, 1993). As the model tends to overpredict concentrations at wind speed below 1.5 m s^{-1} (*Boermans* and *van Pul*, 1993), only calculations for wind speed above this value were used. The modeled fixed point concentration at Vredepeel amounted 18.1 $\mu g\ m^{-3}$, versus 19.4 $\mu g\ m^{-3}$ measured, and the calculated grid concentration amounted 17.1 $\mu g\ m^{-3}$. These results show that calculated and measured fixed point concentrations are in reasonable agreement with the calculated grid average concentration (< 10% deviation). As an overall conclusion it can be deduced that the Vredepeel fixed point can be considered representative for the 5 × 5 km grid.

5. Comparison of TREND results with observations

The outcome of the TREND model strongly depends on the emission input. Neither emission nor seasonal/diurnal variations of emission are well known (*Asman* and *Van Jaarsveld*, 1992; *Asman*, 1992). Temporal emission variation plays an important role in the resulting actual hourly (and annual) concentrations. Temporal variation was modeled according to *Asman* (1992). He provides a monthly relationship to agricultural practice and some relationships of emission to wind speed and temperature, characterized by increasing emissions with increasing wind speed and temperature.

TREND calculations were made for three different emission options and two emission files. The results of these calculations are given in *Boermans* and *Erisman* (1993). Here only the results for the best option are given and the variation in input is used to estimate uncertainty in the output. Following options were taken into account: option A is the original model configuration with a diurnal emission variation characterized by an increasing emission during daytime; option B describes constant emissions and option C describes a diurnal emission variation, as well as a seasonal emission variation. Two different emission files were used as input: (1) emissions according to *Erisman* (1989); and (2) a detailed update for the areas Vredepeel (1991) and Lunteren (1989) (see Section 2.3). For each emission file and the three options calculations of annual average ammonia concentrations for the period from July 1991 until July 1992 were made by averaging monthly calculated ammonia concentrations. Calculations were made using monthly assessed national and local meteorological statistics. TREND calculation using different emission variations show different results. These results show again the importance of knowledge on emissions. Constant emissions show higher calculated yearly average concentration levels compared to a diurnal and/or seasonal emission variation. From the calculations it appeared that option C with the detailed emissions and the local meteorological statistics could be considered as the best and most realistic option. *Fig. 7* shows the monthly average measured and modeled

concentrations for Vredepeel according to option C. The error bars represent variation in the model outcome as a result of input variation (option A and B, emissions according to *Erisman* (1989) and national meteorological statistics). This variation might be regarded as uncertainty in model results.

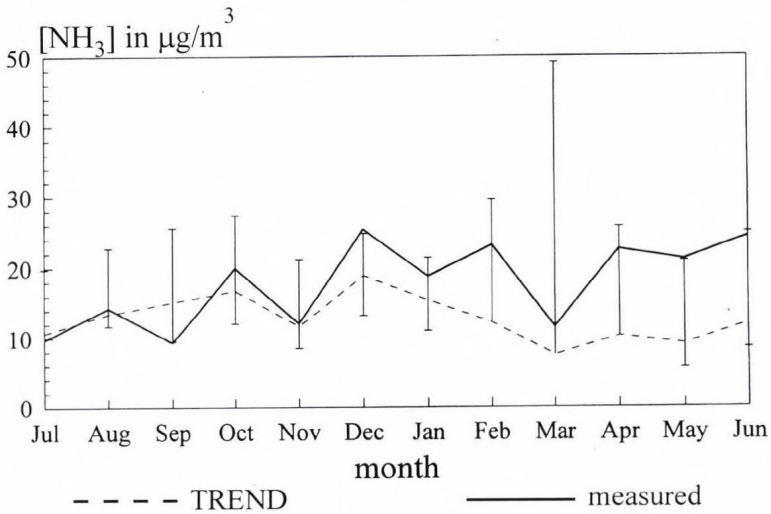

Fig. 7. Comparison of the Vredepeel measured fixed point concentration with the monthly calculated TREND concentrations.

Fig. 7 shows that the variation in monthly average modeled and measured concentrations is similar, but measured concentrations tend to be somewhat higher in spring and in winter. It must be stressed that the representativity of the fixed point is studied on an annual basis. Monthly averaged measurements at the fixed point might not be representative for the grid concentration, depending on meteorological conditions and emissions during the month. However, measured and modeled values at Vredepeel are not considered to be significantly different when the uncertainty in both values is taken into account. The uncertainty in annual average measured concentrations was estimated to be 20–25% (*Boermans* and *Erisman*, 1993).

For the Vredepeel area TREND calculations using local meteorological conditions and using 1991 updated emissions show reasonable agreement with the yearly average measured concentration, 16.2 and 19.4 $\mu g\ m^{-3}$, respectively. For the Lunteren area TREND calculations shows ca. 30% lower concentrations in comparison with the average measured fixed point concentration (only 30% cover), 20.5 and 32.9 $\mu g\ m^{-3}$, respectively. These results are in line with the indications obtained from the mobile measurements and SLAM calculations. A final statement however on the representativeness of the fixed point has not been made.

Up to this level comparison studies were made only looking at concentrations. A deposition estimate has been made based on hourly measured ammonia concentrations. Hourly flux of ammonia for the 5 × 5 km area has been calculated by the summation of the hourly measured ammonia concentration and the hourly estimated deposition velocity. The deposition velocity is estimated using the resistance analogy with measured meteorological parameters and a grid average roughness length value as input (*Hicks et al.*, 1987; *Erisman*, 1993). Hourly fluxes were calculated using the RIVM Laboratory of Air Research surface flux routine (*Erisman*, 1993). Yearly average ammonium deposition was generated only for the Vredepeel area. According to this method the yearly deposition of ammonium is 3510 mol ha^{-1} yr^{-1}. TREND calculations, using a surface resistance of 30 s m^{-1}, show an yearly average deposition of 3050 mol ha^{-1} yr^{-1}, which agrees reasonably well with the deposition estimate based on air concentration measurements and modeled deposition velocities.

6. Synthesis and conclusions

In this paper ambient ammonia concentration measurements are used to evaluate TREND model results. The results of this research show that fixed point measurements might be used to evaluate long-range transport models. Provided representativeness for a larger area is investigated. This is especially relevant in NH_3 source areas where large horizontal concentration gradients are expected. The measuring strategy used for the evaluation provides a good tool for estimating the representativeness measurements at a single-point location for a larger area surrounding the fixed point. An extra tool to evaluate representativeness is the SLAM model with a detailed emission map (*Boermans* and *van Pul*, 1993). The largest uncertainty in comparing model results with measurements is due to uncertainty in emission estimates and temporal variations in emissions. Treating temporal variation in emission as a function of application of manure and agricultural practice and applying a fixed statistical diurnal variation characterized by a higher emission during daytime than during nighttime (*Asman*, 1992) provided the best agreement between model and measurements. The uncertainty in the yearly average concentrations measured at the two fixed points studied is estimated at 20–25%. Evaluation of representativeness of those fixed point measurements using mobile measurements show that the fixed point concentrations at Vredepeel agree within ca. 10% with grid average concentrations. For Lunteren no statement was made for the representativeness of the fixed point for the 5 × 5 km area.

Different emission files, temporal emission variations and national and local meteorological conditions were evaluated using the TREND model to estimate uncertainty in model results. The final conclusion of this research is that there

was no significant difference between TREND results and yearly average measured concentrations at a high ammonia emission area (Vredepeel). It is recommended that measured concentrations at point locations should be evaluated on representativeness for a surrounding 5 × 5 km area and local meteorological data and best guess on emissions should be used as input for model (e.g. TREND) calculations. A comparison of TREND results with measurements made prior to this research showed that there were no systematic differences between model estimates and measurements in background areas and in moderate ammonia concentration areas (*Asman* and *van Jaarsveld*, 1992). The uncertainty in 5 × 5 km TREND results is estimated to vary from ca. 20% for background and low emission areas up to ca. 30% for high emission areas.

To evaluate the emission–transport–concentration–deposition system of NH_3 in the future, a monitoring network of about eight locations has been established in the Netherlands where hourly average NH_3 concentrations are measured. Three locations are located in high NH_3 emission density areas with different animals (pigs, chickens and cows) dominating in stables. Furthermore, two locations are located in remote areas, not directly influenced by local sources, and three locations in background areas. Evaluation of representativeness by mobile measurements is done annually in the areas showing a high emission density, once every three years in the remote areas and once every 5 to 10 years in the background areas surrounding the fixed monitoring sites. This is expected to be sufficient for annual evaluation of TREND model results used for mapping concentration and deposition of NH_3 in the Netherlands. As an important part of this evaluation it should be mentioned that the use of local updated emissions on ammonia and local assessed meteorology is necessary. Furthermore, the network should provide an evaluation of the success of abatement strategies by signaling achieved reduction in emissions.

Acknowledgements—This research was carried out with substantial assistance of colleagues at the Netherlands Energy Centre (ECN). We acknowledge the work of *Paul Wyers, Han Möls* and *others*. We also thank *Marcel Mennen, Henk Boelhouwer, Jaap Schippers, Bernard van Elzakker, Edith van Putten* and *Erik Zwart* of the Laboratory of Air Research at RIVM for their contribution to this project. We would like to thank *Hans van Jaarsveld* for his comments on the manuscript and for the assistance with the TREND model.

References

Aalst, R.M. van and *Erisman, J.W.*, 1991: Atmospheric input. In *Acidification Research in the Netherlands* (eds.: *G.J. Heij* and *T. Schneider*). Studies in Environmental Science 46, Elsevier, Amsterdam.

Allen, A.G., Harrison, R.M. and *Wake, M.T.*, 1988: A meso-scale study of the behaviour of atmospheric ammonia and ammonium. *Atmospheric Environment 22*, 1347-1353.

Asman, W.H.A., 1992: Ammonia emissions in Europe: Updated emissions and emission variations. Laboratory of Air Research, National Institute of Public Health and Environmental Protection RIVM: *Report*, No. 228471008. Bilthoven, The Netherlands.

Asman, W.A.H., Pinksterboer, E.F., Maas, H.F.M., Erisman, J.W. and *Horst, T.W.*, 1989: Gradients of the ammonia concentration in a nature reserve: model results and measurements. *Atmospheric Environment 23*, 2259-2265.

Asman, W.H.A. and *Jaarsveld, J.A. van* 1992: A variable-resolution transport model applied for NHx for Europe. *Atmospheric* Environment *26A*, 445-464.

Boermans, G.M.F. and *Erisman, J.W.*, 1991: Development of a measurement strategy for the investigation of the representativeness of measuring points for the ammonia concentration; phenomenology of ammonia. Laboratory of Air Research, National Institute of Public Health and Environmental Protection RIVM: *Report*, No. 222105001. Bilthoven, The Netherlands.

Boermans, G.M.F. and *Erisman, J.W.*, 1993: Final report on the *Additional Programme on Ammonia*. Laboratory of Air Research, National Institute of Public Health and Environmental Protection RIVM: *Report*, No. 222105002. Bilthoven, The Netherlands.

Boermans, G.M.F. and *Pul, W.A.J. van*, 1993: SLAM, a transport model for short-term and short distance applied for simulation of the dispersion of ammonia. National Institute of Public Health and Environmental Protection RIVM: *Report*, No. 222105003. Bilthoven, The Netherlands.

Breemen, N. van, Burrough, P.A., Velthorst, E.J., Dobben, H.F. van, Wit, T. de, Ridder, T.B. and *Reinders, H.F.R.*, 1982: Soil acidification from atmospheric ammonium sulphate in forest canopy throughfall. *Nature 299*, 548-550.

Buijsman, E., Maas, J.F.M. and *Asman, W.A.H.*, 1987: Anthropogenic NH_3 emissions in Europe. *Atmospheric Environment 21*, 1009-1022.

DHV Raadgevend Ingenieursbureau BV, 1991: Ammonia emission inventory in the surroundings of the measuring site of Vredepeel. *Dossier* D1907-81-001, DHV, Amersfoort, The Netherlands.

Erisman, J.W., Vermetten, A.W.M., Asman, W.A.H., Mulder, W., Slanina, J. and *Waijers-IJpelaan, A.*, 1986: Ammoniak en ammonium concentraties in de Nederlandse buitenlucht Concentrations of ammonia and ammonium over the Netherlands: Report R86-3, IMOU, State University of Utrecht, The Netherlands.

Erisman, J.W., Vermetten, A.W.M., Asman, W.A.H., Slanina, J. and *Waijers-IJpelaan, A.*, 1988: Vertical distribution of gases and aerosols: the behaviour of ammonia and related copmponents in the lower atmosphere. *Atmospheric Environment 22*, 1153-1160.

Erisman, J.W., 1989: Ammonia emissions in the Netherlands in 1987 and 1988. *Report*, No. 228471006. National Institute of Public Health and Environmental Protection. Bilthoven, The Netherlands.

Erisman, J.W., 1992: Atmospheric deposition of acidifying compounds in the Netherlands. Ph.D. Thesis. University of Utrecht, The Netherlands.

Erisman, J.W., 1993: Acid deposition onto nature areas in the Netherlands; Part I. Methods and results. *Water Soil Air Pollut. 71*, 51-80.

Erisman, J.W., Elzakker, B.G. van, Mennen, M. G., Hogenkamp, J., Zwart, E., Beld, L. van den, Römer, F.G., Bobbink, R., Heil, G., Raessen, M., Duyzer, J.H., Verhage, H., Wyers, G.P., Otjes, R.P. and *Möls, J.J.*, 1993b: The Elspeetsche Veld experiment on surface exchange of trace gases: summary of results. *Atmospheric Environment 28*, 487-496.

Grennfelt, P. and *Thörnelöf, E.*, 1992: Critical loads for nitrogen. *Report*, No. Nord 1992:41, Nordic Council of Ministers, Copenhagen, Denmark.

Heidemij Adviesbureau, 1989: Local ammonia dispersion in the research area sorrounding Ede. Research as part of the ammonia execution program. Heidemij, Arnhem, The Netherlands.

Heij, G.J. and *Schneider, T.*, 1991: Acidification research in the Netherlands. *Studies in Environmental Science 46*. Elsevier, Amsterdam.

Heil, G.W. and *Diemont, W.H.*, 1983: Raised nutrient levels change heathlands into grasslands. *Vegetatio 53*, 113-120.

Hicks, B.B., Baldocchi, D.D., Meyers, T.P., Hosker, Jr. R.P. and *Matt, D.R.*, 1987: A preliminary multiple resistance routine for deriving dry deposition velocities from measured quantities. *Water Air Soil Pollut. 36*, 311-330.

Jaarsveld, J.A. van, 1989: A model approach for assessing transport and deposition of acidifying compounds on different spatial scales. In *Changing Composition of the Troposphere*. Special Environment Report No. 17, WMO No. 724, 197-204. Geneva, Switzerland.

Jaarsveld, J.A. van, 1995: Modelling the long-term atmospheric behaviour of pollutants on various spatial scales. *Ph.D. thesis*, University of Utrecht, The Netherlands.

Keuken, M.P., Wayers-IJpelaan, A., Mols, J.J., Otjes, R.P. and *Slanina, J.*, 1989: The determination of ammonia in ambient air by an automated thermodenuder system. *Atmospheric Environment, 23,* 2177-2185.

Langford, A.O., Fehsenfeld, F.C., Zachariassen, J. and *Schimel, D.S.*, 1992: Gaseous ammoni fluxes and background concentrations in terrestrial ecosystems of the United States. *Global Biogeochem. Cycl. 6*, 459-483.

Mennen, M.G., Elzakker, B.G. van, Wyers, G.P., Otjes, R.P., Verhage, A.J.L., Wouters, L.W., Heffels, C.J.G., Römer F., Beld, L. van den, Tetteroo, J.E.H. and *Hoogervorst, A.*, 1992: A field intercomparison with five automatic ammonia monitors. *Report*, No. 223107002. National Institute of Public Health and Environmental Protection. Bilthoven, The Netherlands.

Putten, E.M. van, Mennen, M.G., Uiterwijk, J.W. and *Regts, T.A.*, 1992: Performance study of three automatic ammonia monitors under controlled conditions. *Report*, No. 223107003, National Institute of Public Health and Environmental Protection. Bilthoven, The Netherlands.

Sutton, M.A., Pitcairn, C.E.R. and *Fowler, D.*, 1993: The exchange of ammonia between the atmosphere and plant communities. *Advances in Ecol. Res. 24*, 301-393.

Wyers, G.P., Vermeulen, A.T. and *Slanina, J.*, 1992: Measurement of the dry deposition of NH_3 on a forest. *Envir. Pollut. 75*, 25-28.

IDŐJÁRÁS

Quarterly Journal of the Hungarian Meteorological Service
Vol. 101, No. 2, April–June 1997, pp. 123–142

Graupel production and agent residence time within the seeding zone of a Cb cloud

Mladjen Ćurić and **Dejan Janc**

Institute of Meteorology, University of Belgrade,
11000 Belgrade, P.O. Box 550, Yugoslavia; E-mail: curic@rudjer.ff.bg.ac.yu

(Manuscript received 1 July 1996; in final form 25 February 1997)

Abstract—A one-dimensional kinematic model with detailed microphysics is applied to investigate the graupel production in the seeding zone defined between the isotherm levels of -8°C and -12°C. We calculate the final graupel production and the agent residence time, two important parameters determining the success of an Hail Suppression Operational Project. The agents are injected at the level of -8°C. Their interaction with the cloud environment is simulated by a microphysical model with the Khrgian-Mazin (KM) size distribution of drops. The seeding agents are considered by using the maximum agent mixing ratios and corresponding agent particle masses and radii, because their chemical composition are the same. It is shown:

- Final graupel production is heavily dependent on vertical velocity at the bottom boundary of the seeding zone, while the agent residence time is independent of an agent type. The model results suggest that the PP-6 agent is the most efficient in producing graupel within the seeding zone;
- The rate of rain accreting to cloud ice formed by deposition nucleation is the most important mechanism for graupel formation although its magnitude is the smallest or nearly smallest compared to other mechanisms. This is due entirely to the numerous active deposition nuclei which convert into the cloud ice immediately.

Key-words: graupel production, seeding agents, hail suppression, seeding zone, numerical model of seedings.

1. Introduction

A Hail Suppression Project has been in operation in Serbia for more than twenty years. The main aim of hail suppression is a decrease of damages caused by the hail. The operational project for hail suppression follows the Soviet method given by *Sulakvelidze* (1967). Later, the concept and the effectiveness of the hail suppression in Serbia were described in more details by *Radinović* (1989) and *Mesinger* and *Mesinger* (1992). The silver iodide is injected in the

zone between isotherm levels of -8°C and -12°C, where the most probable formations of natural hail embryos are (*Fukuta*,1980). After seeding is performed, silver iodide produces artificial graupel particles. The final graupel production and the agent residence time in the seeding zone are the most important factors determining the success of hail suppression, according to the hypothesis of competing embryos (*Sulakvelidze*, 1967).

Great progress in the investigation of agent reaction with cloud environment in theory and experiment has been made in the last twenty years. The pioneer work in this field was the model of contact nucleation mechanisms of AgI with highly parameterized dynamics given by *Alkezweeny* (1971). Further, *Young* (1974a-c) introduced a model with uncoupled microphysics and dynamics using the continuous bin technique to examine the seeding influence. Recently, *Young* (1993) constructed the kinematic model with detailed microphysics. Most numerical models simulate the seeding operation with the Eulerian treatment using the bulk-water parameterization scheme. Some 2-D convective cloud model simulations investigate the seeding influence on precipitation enhancement as those published by *Hsie et al.* (1980), *Orville* and *Chen* (1982), *Orville et al.* (1984) or *Kopp* (1988). The application of 3-D cloud models and mesoscale models to the weather modification problems is now more and more frequent (*Levy* and *Cotton*, 1984; *Farley et al.*, 1994; *Holroyd et al.*, 1995). The more recent work by *Farley* (1987) and *Farley et al.* (1996) use a 20-category ice particle hail model to investigate the seeding effects, while the other microphysical fields are treated by the bulk-parameterization scheme. Some more complex models (for example, *Reisen et al.*, 1996) treat the complete microphysics by stochastic concept. Numerical models make it possible to simulate some of the agent nucleation mechanisms which may be measured only with difficulty with the available techniques.

The primary aim of our manuscript is to evaluate roughly the capability of the seeding agents (in use in hail suppression in Serbia) to produce the graupel within the seeding zone after agent injection at the level of -8°C for a great variety of atmospheric conditions and chosen parameters of drop size distribution. We especially focus on total graupel number concentration produced by seeding agent following the hail suppression methodology in Serbia. Under this concept, the seeding is terminated when the graupel concentration is 100 m^{-3} within the seeding zone. Therefore, we think that the bulk-water parameterization scheme is applicable in this case. A one-dimensional (1-D) kinematic model is used. The silver iodide interaction with cloud environment is simulated by help of a microphysical model. In contrast to the model version of *Ćurić* and *Janc* (1990), the one we used in this paper assumes the Khrgian-Mazin size distribution function for liquid water fraction and also include phoretic processes. The bulk microphysics is treated using the results of *Hsie et al.* (1980) and *Lin et al.* (1983). Vertical motion of graupel particles is considered by the kinematic concept.

2. Model

2.1 Microphysical model equations

The interaction of AgI particles with the cloud environment is simulated by a microphysical model version without immersion freezing with implemented Khrgian-Mazin size distribution function (hereafter called KM) for the entire drop spectrum. In an earlier version of the model we have used the monodisperse size distribution for cloud droplets and the *Marshall-Palmer* (1948) one for raindrops (*Ćurić* and *Janc*, 1990). This conventional approach produces an unnatural gap in the size range of the drop spectrum. Therefore the drop spectrum is now approximated by the unique KM size distribution function. The lower boundary for the raindrop spectrum is taken to be R_{min} = 50 μm, in agreement with *Hsie et al.* (1980). Graupeln in the model are distributed according to the exponential size distribution.

Following the model scheme the cloud ice is produced by both contact (Brownian and inertial collection rates due to cloud droplets; phoretic processes) and deposition nucleation mechanisms. The accretion of cloud ice by raindrops is the sink term for cloud ice. The graupel is produced via the Brownian and inertial collection rates due to raindrops and accretion of generated cloud ice by raindrops. The cloud water is depleted by the Brownian and inertial collection rates as well as the accretion of cloud droplets by graupeln. The sink term for raindrops is the source term for graupel particles. The microphysical model involves only those processes which lead to cloud ice/graupel formation in an early glaciation period (just after the agent injection in the seeding zone) in agreement with *Ćurić* and *Janc* (1990). As noted, the presence of raindrops is necessary for graupel formation in accordance with *Hsie et al.* (1980) or *Lin et al.* (1983). These papers indicate that the interaction of ice crystals with raindrops is important for graupel (hail) formation in the simulation of continental clouds. Recently, *Reisen et al.* (1996) also emphasized the importance of raindrop proportion for graupel formation in both maritime and continental clouds.

The KM size distribution of drops (*Pruppacher* and *Klett*, 1978; *Ćurić* and *Vuković*, 1991) may be written as

$$f(R) = AR^2 \exp(-BR), \tag{1}$$

where

$$A = 1.46 \frac{\rho Q}{\rho_w R_M^6}, \quad \text{and} \quad B = \frac{3}{R_M}. \tag{2}$$

Here Q is the liquid water mixing ratio, R_M is the mean radius of drop spectrum, ρ and ρ_w are the air and liquid water densities, while R is the drop radius. The cloud droplet (N_c) and raindrop number concentrations (N_r) are respectively

$$N_c = \frac{2A\alpha_1}{B^3}; \quad N_r = \frac{2A\beta_1}{B^3}, \tag{3}$$

where

$$\alpha_1 = \frac{\Gamma(3; BR_{\min})}{2}; \quad \beta_1 = 1 - \alpha_1. \tag{4}$$

The microphysical production terms with implemented KM size distribution are given in Appendix A.

2.2 Kinematic model equations

A 1-D kinematic model is employed to investigate the seeding agent behavior in the seeding zone. We suppose that the agent cloud center with associated maximum agent mixing ratio moves upwards and leads to the change of the vertical velocity due to buoyancy and loading effects. The equation of motion for a seeded air parcel may be written in the form:

$$\frac{dw}{dt} = g\frac{dT}{T} - g\frac{M_i N_{ci,d}}{\rho}, \tag{5}$$

where the first term on the right-hand side of Eq. (5) represents the buoyancy effects caused by phase transitions after the agent injection in the seeding zone, while the second one represents the loading by deposition on the ice forming nuclei (AgI), which only increases its effect comparing with the non seeding case. The freezing of the water drops and the accretion mechanisms do not change the total hydrometeor mixing ratio (drops and ice particles). The temperature change dT is determined by the first law of thermodynamics given in Appendix B. The loading term depends on the number concentration of cloud ice generated by deposition nucleation ($N_{ci,d}$) and distributed according to the monodisperse size distribution. A single cloud ice crystal mass is supposed to be $M_i = 4.2 \times 10^{-13}$ kg according to *Lin et al.* (1983).

The number concentration of contact or deposition nuclei is calculated using corresponding efficiency curves proposed by *Cooper* (1974), *Hsie et al.* (1980) and *Kopp* (1988). In principle, it is possible to find the activation curves for each agent. But, due to the lack of experimental data, we use the same efficiency curve for each agent. The continuity equation for the maximum agent mixing ratio (X_s) for a 1-D

case is given by

$$\frac{dX_s}{dt} = -\mu X_s + S_{bfc} + S_{ic} + S_{br} + S_{ir} + S_d, \tag{6}$$

where the first term on the right-hand side represents the turbulent diffusion of silver iodide in the seeding zone. It is assumed that the entrainment coefficient (μ) depends on the vertical velocity in accordance with *Wisner et al.* (1972) in the following manner

$$\mu = Kw, \tag{7}$$

where $K = 5 \times 10^{-4}$ m^{-1}.

The terms on the right-hand side with subscripts *bfc, ic, br, ir* and *d* describe the Brownian collection rates due to cloud droplets and phoretic effects,the inertial collection rate due to cloud droplets, the Brownian and inertial collection rates due to raindrops and deposition nucleation, respectively. The silver iodide mixing ratio is expressed in kg kg^{-1} while the terms on the right-hand side of Eq. (6) are expressed in kg kg^{-1} s^{-1}. The sink terms of the silver iodide mixing ratio for contact and deposition nucleation mechanisms may be written as

$$S_y = -J_y \frac{X_s}{N_{cn}}; \qquad S_d = -\frac{N_d(\Delta T)X_s}{N_d(20^0)\Delta t}, \tag{8}$$

where the subscript y may be *bfc, ic, br* and *ir*, respectively. The terms J_y are given in Appendix A. $N_d(\,)$ represents the number of activated deposition nuclei at given supercooling while Δt is the time increment.

In our model the time increment is $\Delta t = 1$ s, while for substantial derivations the Lagrangian time forward scheme is used. Then the discrete form of corresponding time changes is:

$$\frac{dY}{dt} \rightarrow \frac{Y^{n+1} - Y^n}{\Delta t}, \tag{9}$$

where $n + 1$ and n designate successive time steps. The numerical techniques used prevent the appearance of the negative seeding agent mixing ratio values.

3. Experiments

3.1 Agent characteristics

Four agent types are used in the Hail Suppression Operational Project in Serbia. The available experimental data for the agents used are given in *Table 1*. Some characteristics of the TG-10 agent are published by *Huter et al.* (1988). All agents have the same chemical composition but they differ from each other in geometry and in a particle mass. The size distribution of the SAKO-6 agent particles is of a log-normal type with weak scattering around its modal radius ($R_s = 0.03$ μm). Over 80% of the agent particles are found around the modal value of the size distribution function. The size distributions for the other agents coincide well with that of the SAKO-6. Therefore, the monodisperse size distribution for the seeding agent particles seems to be justified. The maximum seeding agent mixing ratios and the agent particle mass are determined following the results of *Hsie et al.* (1980).

Table 1. The characteristics of agents used in the Hail Suppression Operational Project

Agent type	TG-10	TG-5	SAKO-6	PP-6
Pyrotechnic mixture mass (g)	400	400	400	400
AgI content (%)	15	15	25	20
Activity (-10°C) (particles per gram)	1.2×10^{12}	1.2×10^{12}	1.7×10^{12}	3×10^{12}
Particle mass (m_s) ($\times 10^{-16}$ kg)	8.3	8.3	5.9	3.3
AgI mixing ratio (X_s) ($\times 10^{-9}$ kg kg^{-1})	0.08	0.19	0.31	0.20

3.2 Initial and boundary conditions

Within the seeding zone, the initial temperature lapse rate is 7 K/km, while the pressure at $t = -10$°C is $p = 550$ hPa representing the mean climatological values for the April–October period with active hail suppression in Serbia. The seeding zone depth in our calculations is $d = 571$ m.

The initial simulated vertical velocity profile is taken from a model simulation of a hail cloud performed by *Ćurić* and *Janc* (1989) in the form:

$$w_0(z) = w_0 + k_w z, \tag{10}$$

where w_0 is the vertical velocity at the bottom boundary, while $k_w = 0.008$ s^{-1}. Eq. (10) represents in-cloud vertical velocity for unseeded case and it is held

fixed in time. It also includes the loading of total hydrometeor content (drops and ice particles).

Both cloud and rain water mixing ratios are set to be fixed with height in agreement with calculated profiles (*Ćurić* and *Janc*, 1989) within the seeding zone. Total liquid water mixing ratio is supposed to be $Q = 5 \times 10^{-3}$ kg kg^{-1} in all experiments. This implies that the mean cloud drop radius is also fixed with height in agreement with Eqs. (1) and (2). Two values of the mean drop spectrum radius are used: $R_M = 10$ and 20 μm, respectively.

At the bottom boundary temperature and pressure are respectively –8 °C and 570 hPa. Vertical velocity (w_0) at the bottom boundary of the seeding zone takes values of 5, 10, 15 and 20 m s^{-1}. At the top boundary the temperature is –12 °C, while the pressure is determined by the static equation. The vertical velocity is calculated by Eqs. (5) and (10).

3.3 Results

In order to investigate the capability of seeding agents to produce the additional cloud ice and then graupel within the seeding zone under certain atmospheric conditions, we perform numerical experiments taking into account the characteristics of seeding agents which are used in hail suppression in Serbia (Table 1). We especially focus on analyses of different mechanisms leading to graupel formation.

Fig. 1 shows the number concentration of cloud ice formed via contact nucleation ($N_{ci,cn}$, m^{-3}) versus time within the seeding zone for different cloud atmospheres and $w_0 = 5$ m s^{-1}. According to the proposed efficiency curve for contact nuclei which shows an exponential dependence on supercooling, it is reasonable that the number concentration of cloud ice grows with time for each agent. The cloud ice production is the greatest for PP-6 agent (greatest value of X_s, Table 1) because the active number of contact nuclei is proportional to X_s (*Hsie et al.*, 1980). Number concentrations of cloud ice are much smaller for $R_M = 20$ μm (Fig. 1b) than for $R_M = 10$ μm (Fig. 1a). This is entirely due to more KM distributed raindrops for $R_M = 20$ μm, which in turn, produce more efficient collisions with cloud ice to form graupeln.

In contrast to cloud ice produced by contact nucleation, with that formed by deposition one provides much higher number concentrations (*Fig. 2*; an order of magnitude 10^3 m^{-3} for PP-6 agent) due to different nature of these mechanisms. Cloud ice is formed instantaneously from activated deposition nuclei (*Lamb et al.*, 1981; *Ćurić* and *Janc*, 1990), as opposed to that formed via less efficient contact nucleation mechanisms. Consequently, the cloud ice number concentrations are only slightly smaller for $R_M = 20$ μm (Fig. 2b) than for $R_M = 10$ μm (Fig. 2a).

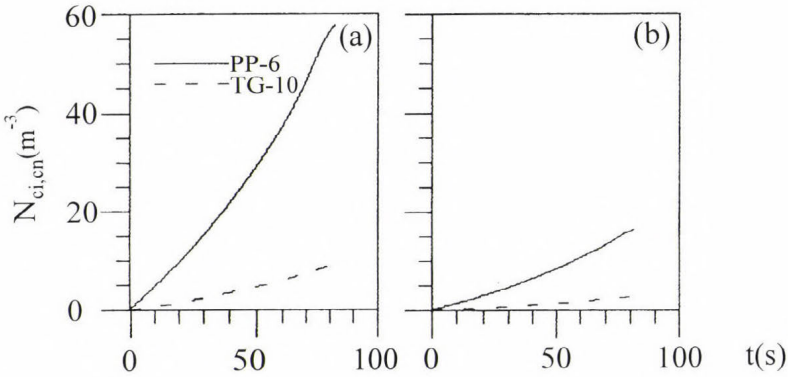

Fig. 1. Cloud ice number concentration generated via contact nucleation, ($N_{ci,cn}$, m^{-3}), versus time for TG-10 and PP-6 agents. Figures labeled *a* and *b* refer to R_M = 10 μm and R_M = 20 μm, respectively. Calculations are performed for w_0 = 5 m s^{-1}.

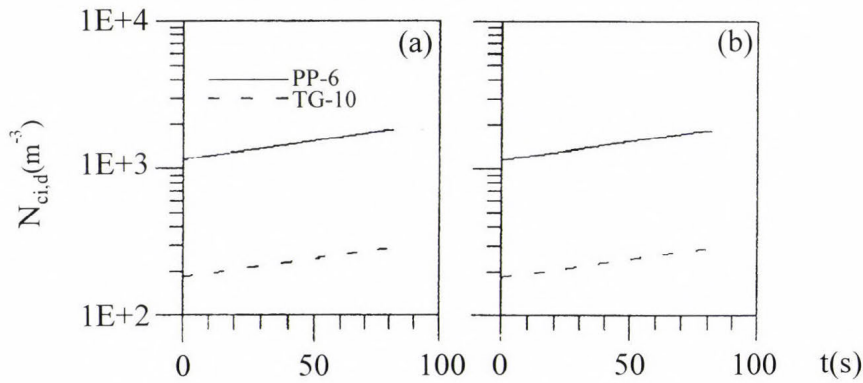

Fig. 2. As in Fig. 1, but for number concentration of cloud ice generated via deposition nucleation ($N_{ci,d}$, m^{-3}).

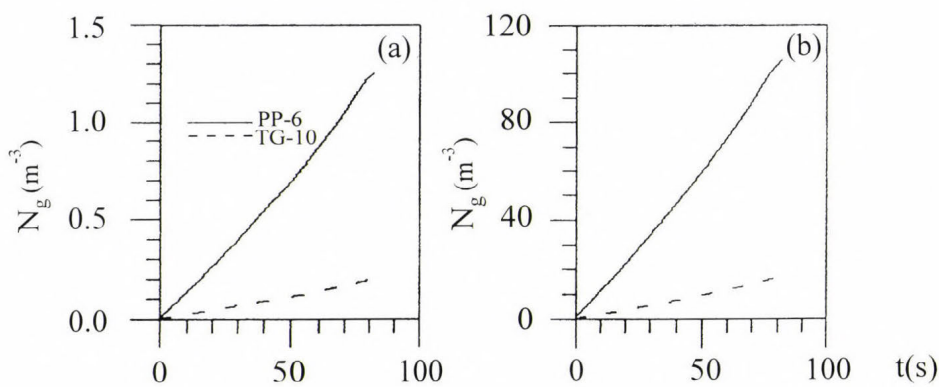

Fig. 3. As in Fig. 1 but for graupel number concentration (N_g, m^{-3}).

Fig. 3 clearly shows that the graupel number concentration grows with time as a consequence of the simultaneous cloud ice production within the seeding zone. Corresponding graupel production depends heavily on raindrop number concentration due to the rain/cloud ice collisions. Therefore graupel number concentration is several times greater for $R_M = 20$ μm (Fig. 3b) than for the smaller value of the mean cloud drop spectrum radius (Fig. 3a).

The number of active contact (or deposition) nuclei shows the rapid growth with increased supercooling (maximum at $\Delta T = 20°C$ for contact nuclei and corresponding maximum for deposition ones at still lower temperature). On the other hand, the turbulent diffusion of the agent particles (Eq. 6) cannot reduce significantly the number of active nuclei within the short time interval ($t \sim 100$ s). Therefore, the number concentrations of both contact and deposition active nuclei grow with time for each agent (*Fig. 4*).

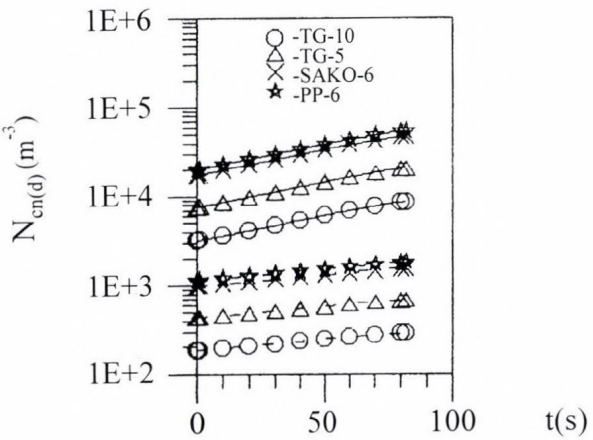

Fig. 4. Number concentrations of active contact nuclei (N_{cn}, m^{-3}; solid lines) and deposition ones (N_d, m^{-3}; dash lines) within the seeding zone for different agents and $w_0 = 5$ m s^{-1}.

Time evolution of each particular mechanism within the seeding zone for PP-6 agent and two cloud environments is presented in *Fig. 5*. It should be noted that each particular mechanism grows with time (Figs. 5a and 5b) because the number concentrations of active contact and deposition nuclei increase with time (Fig. 4) and simultaneously, cloud ice and graupel number concentrations increase. For $R_M = 10$ μm (Fig. 5a), the graupel growth rate with respect to cloud water (J_{gc}) takes the greatest value, and successively the Brownian and inertial collection rates due to cloud droplets (J_{bc} and J_{ic}), the rates of rain accreting cloud ice formed by contact and deposition nucleations (J_{rcn} and J_{rd}) and the Brownian and inertial collection rates due to raindrops (J_{br} and J_{ir}).

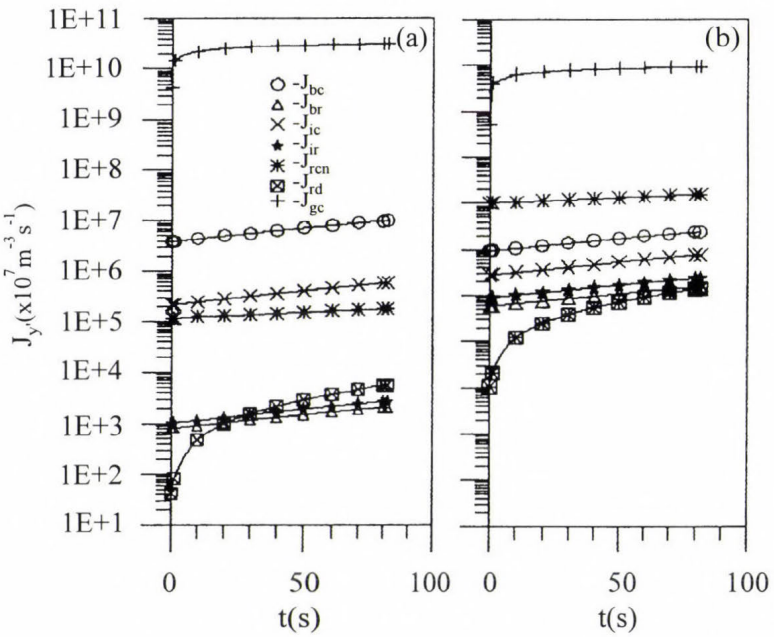

Fig. 5. Time evolution of different mechanisms, ($J_{y'}$, 10^7 m^{-3} s^{-1}) for PP-6 agent within the seeding zone for w_0 = 5 m s^{-1}. The subscript *y'* may be *bc* (Brownian collection rate due to cloud droplets), *br* (Brownian collection rate due to raindrops), *ic* (inertial collection rate due to cloud droplets), *ir* (inertial collection rate due to raindrops), *rcn* (collection rate of raindrops with respect to cloud ice generated via contact nucleation), *rd* (collection rate of raindrops with respect to cloud ice generated via deposition nucleation and *gc* (graupel growth with respect to cloud water). Figures labeled *a* and *b* refer to R_M = 10 μm and R_M = 20 μm, respectively.

In contrast to cloud environment with R_M = 10 μm, that one with R_M = 20 μm consists of more large drops and less small ones, which in turn, leads to an increase in magnitude of all mechanisms with raindrops and a corresponding decrease of those with cloud droplets (except inertial collection rate; *Fig. 6b*). Now, the term J_{rcn} surpasses terms J_{bc} and J_{ic}, while those denoted by J_{br} and J_{ir} surpass the term J_{rd}. Since the behavior of different mechanisms with time for the other agents is alike that for PP-6 agent, they are not represented graphically (number concentration of active contact or deposition nuclei shows a linear dependence of X_s).

In order to answer the question which mechanism contributes most to cloud ice, graupel formation and depletion of cloud water, we have done additional analysis whose results are represented over the coefficient

$$k_{ty'} = \frac{\dfrac{dN_{ty'}}{dt}}{\dfrac{dN_t}{dt}}, \tag{11}$$

where the subscript t refers to cloud ice formed by contact nucleation (*icn*), graupel (*g*) and cloud water (*c*), while *y'* refers to the Brownian and inertial collection rates due to cloud droplets and raindrops (*bc, ic, br, ir*), rates of rain accreting cloud ice formed by contact and deposition nucleation (*rcn, rd*) and graupel growth rate with respect to cloud water (*gc*). The quantity of a type $N_{ty'}$ or N_t refers to corresponding number concentration.

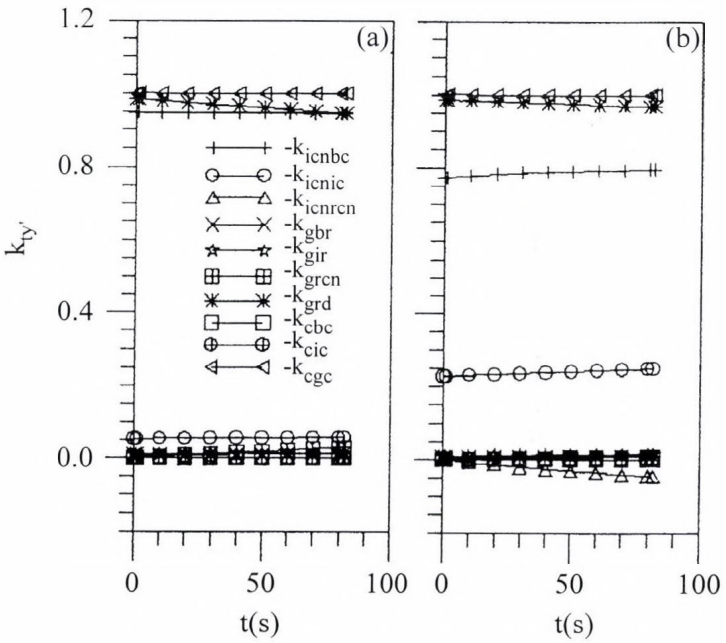

Fig. 6. Coefficient $k_{ty'}$ versus time for different mechanisms which contribute to cloud ice formed via contact nucleation (t = *icn*), graupel production (t = *g*) and depletion of cloud water (t = *c*). Figures labeled *a* and *b* refer to R_M = 10 μm and R_M = 20 μm, respectively. Calculations are performed for w_0 = 5 m s^{-1}.

The coefficient (11) versus time for w_0 = 5 m s^{-1} and two mean drop spectrum radii is represented in Fig. 6. It should be noted that the Brownian collection rate due to cloud droplets contributes most to cloud ice, the main sink

term for cloud water is the graupel accretional growth, while the collisions of raindrops and cloud ice of deposition nucleation origin is the main source for graupel. The role of the other mechanisms can be ignored ($k_{ty'}$ close to zero) except somewhat the inertial collection rate due to cloud droplets as a source term for cloud ice ($k_{ty'}$ is 0.05 for $R_M = 10$ μm, see Fig. 6a; $k_{ty'}$ varies between 0.23 and 0.25 for $R_M = 20$ μm, see Fig. 6b). Also, the role of the Brownian collection rate due to cloud droplets in cloud ice formation decreases for $R_M = 20$ μm due to smaller number concentration of small droplets in such a drop spectrum (Fig. 6b). As noted, the magnitude of the collision rate between rain and cloud ice formed by deposition nucleation is nearly the smallest compared to the other mechanisms (Figs. 5a and b), but its role in graupel production is the most important. It is in agreement with the nature of deposition nucleation where the numerous deposition active nuclei convert water vapor into cloud ice immediately (see Fig. 2).

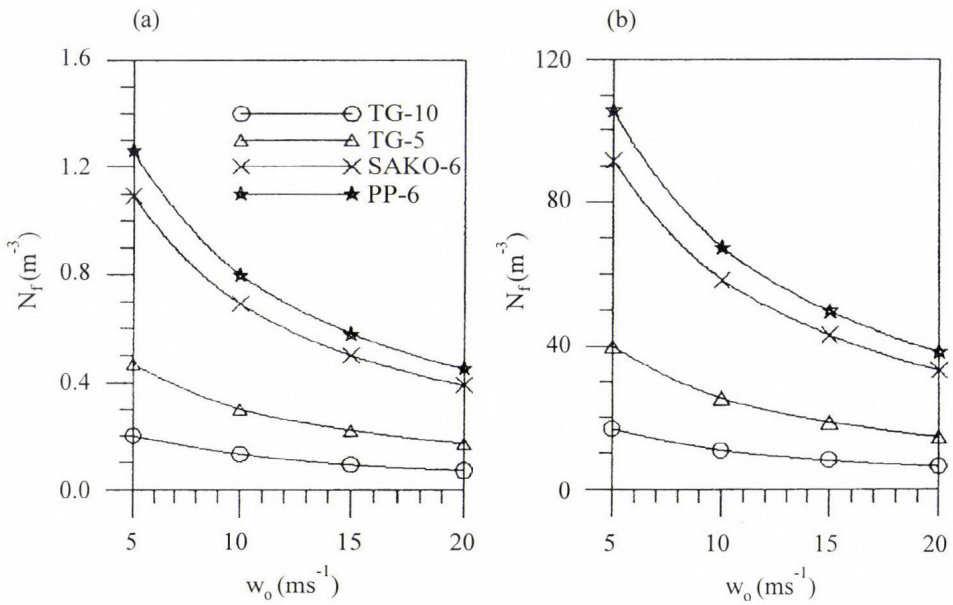

Fig. 7. Final graupel production, N_f (m^{-3}), vs vertical velocity at the bottom boundary, w_0 ($m\ s^{-1}$), for different agents. Figures labeled *a* and *b* refer to $R_M = 10$ μm and $R_M = 20$ μm, respectively.

Finally, we show the parameters which are important from the point of view of hail suppression methodology as it is applied in Serbia. They are: the graupel number concentration at the top boundary of the seeding zone called the final

graupel production (N_f) and the time need for the seeded air parcel to ascend throughout the seeding zone called the agent residence time (t_R). The final graupel production (produced from a single rocket per m^{-3}) versus vertical velocity at the bottom boundary of the seeding zone is presented in *Fig. 7.* Our findings give us the opportunity to conclude that the final graupel production shows an exponential dependence on corresponding vertical velocity. The PP-6 agent is the most efficient in graupel production. It produces the graupel number concentrations of 1.26 m^{-3} and 105.7 m^{-3} within its residence time of 82 s for $w_0 = 5$ m s^{-1}.

The agent residence time for different vertical velocities at the bottom boundary is shown in *Table 2.* As noted, it is independent of an agent type because the buoyancy effects and the loading term in Eq. (5) can be ignored. The effect of phase transitions on vertical velocity is not important due to the small amounts of the agents and the short agent residence time. Calculated residence times agree well with results of *Slinn* (1971).

Table 2. The agent residence time (t_R) for different vertical velocities at the bottom boundary of the seeding zone (w_0)

w_0 (m s^{-1})	5	10	15	20
t_R (s)	82	48	34	26

The considered graupel production refers only to that associated with the maximum seeding agent mixing ratio. Our calculations show that the representative value of the spread parameter due to the agent dispersion is 50 m within the agent residence time according to the procedure proposed by *WMO* (1980). Concentration of the agent particles decreases rapidly (most often exponentially, *Hsie et al.*, 1980) outside the agent cloud center. On such a way, most of the graupel production per unit volume is taken into account.

4. Conclusions

1-D kinematic model with detailed microphysics is used to find out the graupel production within the seeding zone after agent injection at its bottom boundary following the concept of the hail suppression in Serbia. The behavior of four seeding agents is investigated. They all have the same chemical composition but they differ from each other in geometry. For conditions close to those occurring during the seeding operation we conclude:

- The PP-6 agent gives the largest, and TG-10 the smallest graupel production within the seeding zone. The final graupel production is an

exponential function of the vertical velocity at the bottom boundary of the seeding zone, while the agent residence time is independent of an agent type. The better performance of the PP-6 agent directly depends on the ratio of its maximum mixing ratio and mean particle size;

- Among mechanisms which are responsible for graupel production, the Brownian collection due to cloudy droplets is the greatest in magnitude for the cloud atmosphere with the lack of raindrops, while the rate of rain accreting cloud ice formed via contact nucleation is the greatest for an environment with larger drops. However, the rate of rain accreting cloud ice of deposition nucleation origin is the most important for graupel production due to numerous active deposition nuclei which convert water vapor into cloud ice immediately.

Acknowledgements—The research was supported by the Hydrometeorological Service of Serbia under the contract "The Research in Hail Suppression". Two anonymous reviewers have made many suggestions in the reviewing process that increased the completeness and clarity of the paper. These contributions are appreciated.

References

Alkezweeny, A.J., 1971: A contact nucleation model for seeded clouds. *J. Appl. Meteor. 10*, 732-738.

Cooper, W.A., 1974: A possible mechanism for contact nucleation. *J. Atmos. Sci. 31*, 1832-1837.

Cotton, W.R., Stephens, M.A., Nehrkorn, T. and *Tripoli, G.J.*, 1982: The Colorado State University three-dimensional cloud/mesoscale model-1982. Part II: An ice phase parameterization. *J. Rech. Atmos. 16*, 295-320.

Cotton, W.R., Tripoli, G.J., Rauber, R.M. and *Mulvhill, E.A.*, 1986: Numerical simulation of the effects of varying ice crystal nucleation rates and aggregation processes on orographic snowfall. *J. Climate Appl. Meteor. 114*, 718-733.

Ćurić, M. and *Janc, D.*, 1989: Dynamic entrainment rate influence on products of a one-dimensional cumulonimbus model. *Atmos. Res. 24*, 305-323.

Ćurić, M. and *Janc, D.*, 1990: Numerical study of the cloud seeding effects. *Meteorol. Atmos. Phys. 42*, 145-164.

Ćurić, M. and *Vuković, Z.*, 1991: The influence of thunderstorm thunderstorm-generated acoustic waves on coagulation. Part I: Mathematical formulation. *Z. Meteorol. 41*, 164-169.

Farley, R.D., 1987: Numerical modeling of hailstorms and hailstone growth. Part III: Simulation of an Alberta hailstorm-natural and seeded cases. *J. Climate Appl. Meteor. 26*, 789-812.

Farley, R.D., Nguyen, P. and *Orville, H.D.*, 1994: Numerical simulation of cloud seeding using a three-dimensional cloud model. *J. Wea. Mod. 26*, 113-124.

Farley, R.D., Chen, H., Orville, H.D. and *Hjelmleft, H.R.*, 1996: The numerical simulation of the effects of cloud seeding on hailstorms. *Preprints 13th Conf. on Planned and Inadvertent Weather Modification*. Atlanta. GA. Amer. Meteor. Soc., 23-30.

Fuchs, N.A., 1964: *The Mechanics of Aerosols*. Pergamon Press, Oxford.

Fukuta, N.,1980: Advances in Cloud Physics. (Textbook). University of Utah.

Holroyd, E.W., Heimbach, J.A. and *Super, A.*, 1995: Observations and model simulation of AgI seeding within the winter storm over Utah's Wasatch Plateau. *J. Wea. Modif. 27*, 36-56.

Hsie, E-Y., Farley, R.D. and *Orville, H.D.*, 1980: Numerical simulation of ice-phase convective cloud seeding. *J. Appl. Meteor. 19*, 950-977.

Huter, M., Prelesnik, B., Ćurić, M., Mitić, D. and *Herak, R.*, 1988: X-ray diffraction analysis of aerosols obtained burning of the AgI based pyrotechnics. In *Atmospheric Aerosols and Nucleation* (eds.: *P.E. Wagner* and *G. Vali*). Springer, Berlin, Heidelberg. (Lecture Notes in Physics, 309).

Kopp, F.J., 1988: A simulation of Alberta cumulus. *J. Appl. Meteor. 27*, 626-641.

Lamb, D., Hallett, J. and *Sax, R.I.*, 1981: Mechanistic limitations to the release of latent heat during the natural and artificial glaciation of deep convective clouds. *Quart. J. Roy. Meteor. Soc. 107*, 935-954.

Levy, G. and *Cotton, W.R.*, 1984: A numerical investigation of mechanisms linking glaciation of the ice-phase to the boundary layer. *J. Climate Appl. Meteor. 23*, 1505-1519.

Lin, Y-L., Farley, R.D. and *Orville, H.D.*, 1983: Bulk parameterization of the snow field in a cloud model. *J. Climate Appl. Meteor. 22*, 1065-1092.

Liu, J.Y. and *Orville, H.D.*, 1969: Numerical modeling of precipitation and cloud shadow effects on mountain-induced cumuli. *J. Atmos. Sci. 26*, 1283-1298.

Marshall, J.S. and *Palmer, W. McK.*, 1948: The distribution of raindrops with size. *J. Meteor. 5*, 165-166.

Mesinger, F. and *Mesinger, N.*, 1992: Has hail suppression in Eastern Yugoslavia led to a reduction in the frequency of hail? *J. Appl. Meteor. 34*, 104-111.

Murakami, M., 1990: Numerical modeling of dynamical and microphysical evolution of an isolated convective cloud - the 1981 July 1981 CCOPE cloud -. *J. Meteor. Soc. Japan 68*, 107-128.

Orville, H.D. and *Chen, J.-M.*, 1982: Effects of cloud seeding, latent heat of fusion,and condensate loading on cloud dynamics and precipitation evolution: A numerical study. *J. Atmos. Sci. 39*, 2807-2827.

Orville, H.D., Farley, R.D. and *Hirsch, J.H.*, 1984: Some suprising results from simulated seeding of stratiform-type clouds.*J. Climate Appl. Meteor.* 12, 517-521.

Pruppacher, H.R. and *Klett, J.D.*, 1978: *Microphysics of Clouds and Precipitation*. D. Reidel, Dordrecht.

Radinović, Dj., 1989: Effectiveness of hail control in Serbia. *J. Wea. Mod. 21*, 75-84.

Reisin, T., Levin, Z. and *Tzivion, S.*, 1966: Rain production in convective clouds as simulated in an axisymmetric model with detailed microphysics. Part I: Description of the model. *J. Atmos. Sci. 53*, 497-519.

Slinn, W.G.N., 1971: Time constants for cloud seeding and tracer experiments. *J. Atmos. Sci. 27*, 299-307.

Sulakvelidze, G.K., 1967: *Showers and Hail* (in Russian). Gidrometeoizdat, Leningrad.

Young, K.C., 1974a: The role of contact nucleation in ice-phase initiation in clouds. *J. Atmos. Sci. 31*, 768-776.

Young, K.C., 1974b: A numerical simulation of wintertime,orographic precipitation:Part I. Description of model microphysics and numerical techniques. *J. Atmos. Sci. 31*, 1735-1748.

Young, K.C., 1974c:A numerical simulation of wintertime, orographic precipitation: Part II, Comparison of natural and AgI-seeded conditions. *J. Atmos. Sci. 31*, 1749-1767.

Young, K.C., 1993: *Microphysical Processes in Clouds*. Oxford University Press, Oxford.

Wisner, C.E., Orville, H.D. and *Myers, C.G.*, 1972: A numerical model of a hail-bearing cloud. *J. Atmos. Sci. 29*, 1160-1181.

WMO, 1980: *Dispersion of Cloud Seeding Reagents*. Precipitation Enhancement Project. Rep. No. 14, Weather Modification Programme. WMO, Geneva.

APPENDIX A

Microphysical production terms

The rate of change in number concentration (m^{-3} s^{-1}) of cloud ice produced by the Brownian collection rate due to cloud droplets and phoretic processes (diffusiophoresis and thermophoretic contact nucleations) is in agreement with *Cotton et al.* (1986)

$$J_{bfc} = 4\pi D_s N_{cn} F \int_0^{R_{min}} Rf(R)\,dR = \frac{24\pi D_s AFN_{cn}\alpha_2}{B^4}, \tag{A1}$$

where

$$\alpha_2 = \frac{\Gamma(4; BR_{\min})}{6}; \quad F = 1 + \frac{F_2}{D_s}\left(f_T - \frac{R_V T}{L_V}\right); \quad F_2 = \frac{G(T,p)SL_v}{p} \tag{A2}$$

and

$$f_T = \frac{0.4\left[1 + 1.45K_N + 0.4\,K_N \exp(-1/K_N)\,(K_N + 2.5\,K_N K_A)\right]}{(1 + 3K_N)(2K + 5K_A K_N + K_A)}. \tag{A3}$$

The quantities in Eqs. (A1) to (A3) are: D_s is the diffusivity of the silver-iodide, S is the saturation ratio over water, L_V is the latent heat of vaporization, R_V is the specific gas constant for water vapor, p is the in-cloud pressure, T is the in-cloud temperature, K is the thermal conductivity of the air, K_A is the thermal conductivity of the silver-iodide taken to be 5.39×10^{-9} J m^{-1} s^{-1} K^{-1}, e_S is the saturated water vapor pressure at temperature T, K_N is the Knudsen number, N_{cn} is the number concentration of contact nuclei, and $G(T,p)$ is the thermodynamic function as defined by *Cotton et al.* (1982).

The rate of change in number concentration of graupel particles formed by Brownian collection rate due to raindrops is calculated similarly to that for cloud droplets, i.e.:

$$J_{br} = 4\pi D_s N_{cn} \int_{R_{\min}}^{\infty} Rf(R)\,dR = \frac{24\,\pi D_s N_{cn} A(1 - \alpha_2)}{B^4}. \tag{A4}$$

The inertial collection rates due to cloud droplets and raindrops and the accretion terms require the knowledge of terminal velocities of drops and graupel particles. We use the expressions for terminal velocities of cloud droplets (U_c), raindrops (U_r) and graupel particles (U_g) proposed by *Murakami* (1990), *Liu* and *Orville* (1969) and *Lin et al.* (1983), respectively as follows

$$U_c = cR^d \frac{\rho_0}{\rho}; \quad U_r = aR^b \left(\frac{\rho_0}{\rho}\right)^{0.5}; \quad U_g = kR_g^{0.5}; \quad k = \left(\frac{8\rho_g}{3\rho C_d}\right)^{0.5}, \tag{A5}$$

where $c = 1.2 \times 10^8$ m^{-1} s^{-1}, $d = 2$, $a = 1465$ m$^{0.2}$ s^{-1}, $b = 0.8$, ρ_0 is the reference air density (set to 1.2 kg m^{-3}), ρ_g is the graupel density with a value appropriate for hard ice, C_d is the drag coefficient (set to 0.6) and R_g is the graupel radius.

The rate of change in number concentration of cloud ice formed by the inertial collection due to cloud droplets is in agreement with *Hsie et al.* (1980)

$$J_{ic} = \pi E_{ac} N_{cn} \int_0^{R_{\min}} U_c R^2 f(R)\, dR = \frac{720\, \pi\, c E_{ac} A N_{cn} \rho_0 \alpha_3}{\rho B^7}, \tag{A6}$$

where

$$\alpha_3 = \frac{\Gamma(7; BR_{\min})}{720} \tag{A7}$$

and E_{ac} is the collection efficiency of cloud droplets for the seeding agent particles, set to 10^{-4} (*Pruppacher* and *Klett*, 1978).

The rate of change in number concentration of graupeln produced by the inertial collection rate due to raindrops may be derived similarly to Eq. (A6) as:

$$J_{ir} = \pi E_{ar} N_{cn} \int_{R_{\min}}^{\infty} U_r R^2 f(R)\, dR = \frac{\pi a E_{ar} A N_{cn} \Gamma(5.8)(1 - \alpha_4)}{B^{5.8}} \left(\frac{\rho_0}{\rho}\right)^{0.5}, \tag{A8}$$

where

$$\alpha_4 = \frac{\Gamma(5.8; BR_{\min})}{\Gamma(5.8)} \tag{A9}$$

and E_{ar} is the collection efficiency of raindrops for the seeding agent particles set to 0.5×10^{-4} (*Fuchs*, 1964).

The rate of change in number concentration of graupeln by collisions between raindrops and cloud ice formed by contact or deposition nucleations may be derived by applying the stochastic collection equation with "sweep-out" concept in the form:

$$J_{rx} = \int_{R_{\min}}^{\infty} \pi R^2 E_{rx} U_r N_{ci,x} f(R)\, dR = \frac{\pi a E_{rx} N_{ci,x} A \Gamma(5.8)(1 - \alpha_4)}{B^{5.8}} \left(\frac{\rho_0}{\rho}\right)^{0.5}, \tag{A10}$$

where E_{rx} is the collection efficiency of raindrops for cloud ice taken to be 0.1 in accordance with *Lamb et al.* (1981), while $N_{ci,x}$ is the number concentration of cloud ice formed by contact ($x = cn$) or deposition ($x = d$) nucleations.

The rate of change in number concentration of graupeln due to the accretion of cloud water by graupeln is determined by the integration of the stochastic collection equation under the assumption that the graupel terminal velocity always exceeds that of cloud droplets as follows

$$J_{gc} = \pi E_{gc} \int_0^{R_{\min}} \int_0^{\infty} (R + R_g)^2 \, | U_c - U_g | N_g f(R) dR \, dR_g$$

$$= \pi E_{gc} N_{0g} A \sum_{i=1}^{3} C_i \left[\frac{k\Gamma(6 - i; BR_{\min})\Gamma(i + 0.5)}{B^{6-i}(2\lambda_g)^{i+0.5}} - \frac{c\Gamma(8 - i; BR_{\min})\Gamma(i)}{B^{8-i}(2\lambda_g)^{i}} \right], \quad \text{(A11)}$$

where $C_1 = C_3 = 1$, $C_2 = 2$; E_{gc} is the collection efficiency of graupel for cloud water taken to be 0.5 in accordance with *Lamb et al.* (1981); N_{0g} is the intercept value in graupel size distribution; N_g is the graupel number concentration and λ_g is the slope parameter of graupel size distribution. The graupel growth via gravitational coagulation is equal to zero for cloud droplets less than 10 μm in diameter (*Pruppacher* and *Klett*, 1978). The parameter N_{0g} in graupel size distribution is calculated by the help of number concentration and mixing ratio of graupel particles as well as their prognostic equations in the following manner.

Number concentration and mixing ratio of the graupel particles can be calculated as

$$N_g = \int_0^{\infty} N_{0g} \exp(-\lambda_g D_g) \, dD = \frac{N_{0g}}{\lambda_g}, \quad \text{(A12)}$$

$$Q_g = \int_0^{\infty} \frac{\pi}{6} \frac{\rho_w}{\rho} D_g^3 N_{0g} \exp(-\lambda_g D_g) dD_g = \frac{\rho_w}{\rho} \pi \frac{N_{0g}}{\lambda_g^4}, \quad \text{(A13)}$$

where D_g is the graupel diameter.

The prognostic equation for graupel number concentration is in accordance with *Ćurić* and *Janc* (1990)

$$\frac{dN_g}{dt} = J_{bfc} + J_{ic} + J_{br} + J_{ir} + J_{rcn} + J_{rd}, \quad \text{(A14)}$$

where the terms on the right-hand side of (A14) are (A1), (A6), (A4), (A8) and (A10), respectively. The prognostic equation for graupel mixing ratio is

$$\frac{dQ_g}{dt} = S_{bfc} + S_{ic} + S_{br} + S_{ir} + S_{rcn} + S_{rd}, \tag{A15}$$

where the first four terms on the right-hand side of Eq. (A15) are calculated by Eq. (8) and the last two by

$$S_{rcn} = J_{rcn}\frac{M_i}{\rho}; \quad S_{rd} = J_{rd}\frac{M_i}{\rho}. \tag{A16}$$

By the help of Eqs. (A13) to (A16), we can find corresponding parameters of the graupel size distribution at each time step.

APPENDIX B

The first law of thermodynamics

Latent heat of fusion or sublimation is released during the formation of cloud ice and graupel or during their growth. In an early phase both ice crystals or graupel particles and supercooled cloud droplets and raindrops may exist. The sublimation growth of crystals operates together with evaporation of the supercooled drops. Therefore, in terms of sublimation growth of ice crystals we use the latent heat of fusion instead of latent heat of sublimation (*Lamb et al.*, 1981).

The adopted rates of heat released due to the contact nucleation of cloud droplets (Q_{cnc}), accretion of cloud droplets by graupel particles (Q_{gc}) and freezing of raindrops (Q_r) for the implemented *KM* size distribution are respectively

$$\frac{dQ_{cnc}}{dt} = L_f\left(\frac{3840\pi^2 D_s N_{cn} FA\rho_w\alpha_3}{B^7} + \frac{4838\pi^2 c E_{ac} N_{cn} A\rho_w\rho_0\alpha_5}{\rho B^{10}}\right), \tag{B1}$$

where

$$\alpha_5 = \frac{\Gamma(10; BR_{\min})}{\Gamma(10)}, \tag{B2}$$

$$\frac{dQ_{gc}}{dt} = L_f\left\{\frac{4}{3}\pi^2 E_{gc} N_{0g}\rho_w A\sum_{i=1}^{3} C_i\left[\frac{k\Gamma(9-i; BR_{\min})\Gamma(i+0.5)}{B^{9-i}(2\lambda_g)^{i+0.5}} - \frac{c\Gamma(11-i; BR_{\min})\Gamma(i)}{B^{11-i}(2\lambda_g)^i}\right]\right\}, \tag{B3}$$

$$\frac{dQ_r}{dt} = L_f \left[\frac{3840\pi^2 D_s N_{cn} A(1-\alpha_3)}{B^7} + \frac{4\pi^2 a \rho_w A \Gamma(8.8)(1-\alpha_6)}{3B^{8.8}} \left(\frac{\rho_0}{\rho} \right)^{0.5} \right.$$

$$\left. \times \left(E_{ar} N_{cn} + E_{rcn} N_{ci,cn} + E_{rd} N_{ci,d} \right) \right], \tag{B4}$$

where

$$\alpha_6 = \frac{\Gamma(8.8; BR_{\min})}{\Gamma(8.8)}. \tag{B5}$$

In Eqs. (B1), (B3) and (B4) L_f is the latent heat of fusion. In the case of sublimation growth of cloud ice the corresponding heat released for frozen cloud droplets (Q_{cn}) and crystals produced by deposition nucleation (Q_d) may be written in the form (*Lamb et al.*, 1981)

$$\frac{dQ_{cn}}{dt} = L_f N_{cn} \left(4\pi \overline{R_c} D \Delta\rho \right), \tag{B6}$$

$$\frac{dQ_d}{dt} = L_f N_d \left(4\pi C_{id} D \Delta\rho \right), \tag{B7}$$

where $\Delta\rho$ is the difference between saturated water vapor density with respect to water and ice, and C_{id} the electrostatic capacity for ice crystals generated by deposition nucleation set to be 35 μm. The mean cloud droplet spectrum radius is calculated as

$$\overline{R_c} = \frac{3\alpha_2}{B\alpha_1}. \tag{B8}$$

The total rate of released heat may be obtained by summation of Eqs. (B1), (B3), (B4), (B6) and (B7).

IDŐJÁRÁS

Quarterly Journal of the Hungarian Meteorological Service
Vol. 101, No. 2, April–June 1997, pp. 143–153

Ambient air quality status assessment in industrial belts — A case study of Hazira Kawas region

Swaroop R. Mudaliar, C. S. Sunil Kumar, Pawan Kumar, S. D. Badrinath and **C. V. Chalapati Rao**

National Environmental Engineering Research Institute, Nagpur–20, India; E-mail: root%neeri@ren.nic.in

(Manuscript received 14 February 1994; in final form 10 October 1994)

Abstract—The area of Hazira (India) has several industrial establishment. For investigation of the heavy pollution a well designed air quality monitoring network of 18 stations has been installed. The measurement program includes the determination of suspended particulate matter, sulfur dioxide, nitrogen dioxide, aldehyde, ammonia and some meteorological elements. The results obtained in May of 1991 are presented.

To predict the impact of the emitted pollution a steady state Gaussian plume dispersion model has been used. The predicted ground level concentration of nitrogen oxides, found to be a significant parameter, was computed as 37 $\mu g\ m^{-3}$, 37 $\mu g\ m^{-3}$ and 41 $\mu g\ m^{-3}$ in the NE direction during 10–18 hrs, 18–02 hrs and 02–10 hrs, respectively. The distances at which the maximum concentrations are likely to occur were predicted to be 0.5 km, 6 km and 6 km, respectively from the sources.

Key-words: nitrogen oxides, suspended particulate matter, sulfur dioxide, aldehydes, ammonia, modeling.

1. Introduction

The trend towards urbanization and greater industrialization has led, among other things, to the concentration of population in residential areas and heavier use of city highways. These in turn, have resulted in more severe and widespread contamination of our atmosphere. The atmosphere contains such a great variety of elements of different concentrations in time and space that its exact composition will always be somewhat indeterminate. Analytical methods can be used for measuring special forms and low levels of concentration of many elements which pollute the ambient air. The present paper describes the application of various tools and techniques used during the studies carried out in Hazira-Kawas region, India.

1.1 Study area

The study area is located at Hazira in western India which is situated 18 km North-West of Surat city in Gujarat State. The site is located west of Surat city and north of the Arabian sea (*Fig. 1*).

The major industries located in this region include:

- Oil and Natural Gas Commission (ONGC)'s gas processing complex,
- Essar's Sponge Iron Project,
- GAIL — gas receiving and compression station,
- National Thermal Power Corporation (NTPC)'s gas based power plant,
- Plant of the Petro Polyols Ltd.,
- Narmada Cement Company,
- Petrochemical Complex of Reliance Industries Ltd.

The siting of so many industries in a small area has increased the level of pollution. The proximity of the densely populated Surat city to this area has made the issue of pollution more acute.

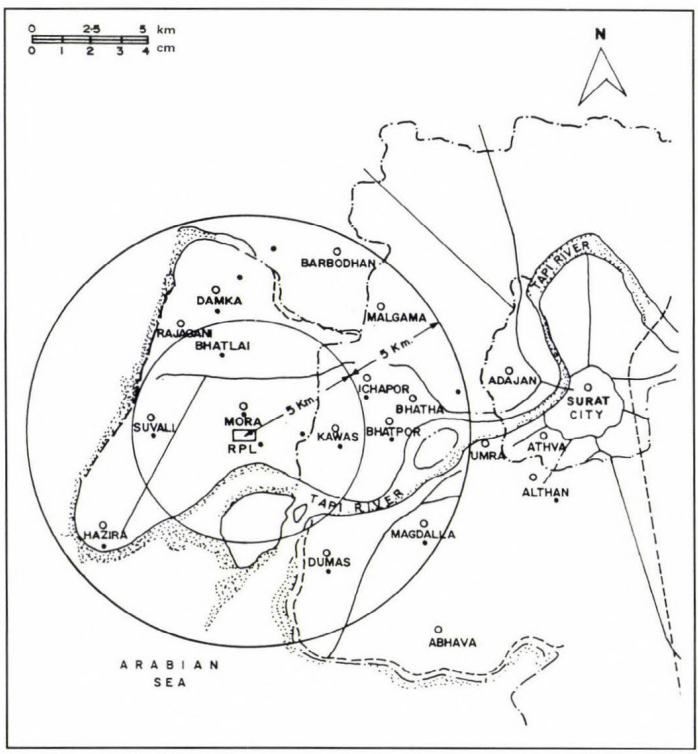

Fig. 1. Ambient air quality monitoring stations.

2. *Materials and methods*

2.1 Measurements

Ambient Air Quality was assessed through a network of 18 ambient air quality stations (*Indian Standards*, 1979) during summer season i.e. in May, 1991. Suspended particulate matter (SPM), sulfur dioxide, nitrogen oxides, ammonia and aldehydes were monitored during the study period. High volume samplers were used for collection of aerosol samples for SPM while sampling of gaseous pollutants were carried out by means of impingers of 35 ml capacity. Into the impingers the air was drawn at an impingement rate of 1 ℓ m^{-1}.

The following analytical methods were used for measuring the concentrations of various gases:

Sulfur dioxide	—	West and Gaeke method (see: *Indian Standards*, 1969)
Nitrogen dioxide	—	Jacob and Hochhiesser method (see: *Indian Standards*, 1974)
Aldehyde	—	Methyl benzothiazolone hydrozone hydrochloride method (see *Katz*, 1977)
Ammonia	—	Nesslerisation method (see *Katz*, 1977).

The various meteorological parameters e.g. wind speed, wind direction and temperature were recorded using a computerised weather monitoring unit. These data were recorded at every 10 minutes and further averaged for each hour during the whole study period. Hourly wind data were, later on, processed for wind-rose diagrams.

2.2 The model

In the study region, twenty-seven elevated point sources were identified in the proposed industrial complex out of which 21 stacks were considered as significant elevated continuous point sources for mathematical modeling (*Fig. 2* and *Table 1*).

Neither line nor area sources were considered because of the insignificant contribution of pollutants from these sources.

Hence, a short-term multiple point source Gaussian Plume Dispersion Model has been identified as the suitable model for prediction of impacts on air environment. The values of the dispersion were determined from Pasquill-Gifford dispersion curves suggested by *Turner* (1970). The hourly wind speed, solar insolation and total cloudiness during day time; and wind speed and total cloudiness during night time were used to determine the hourly atmospheric stability (*Turner,* 1970; *Pasquill*, 1974).

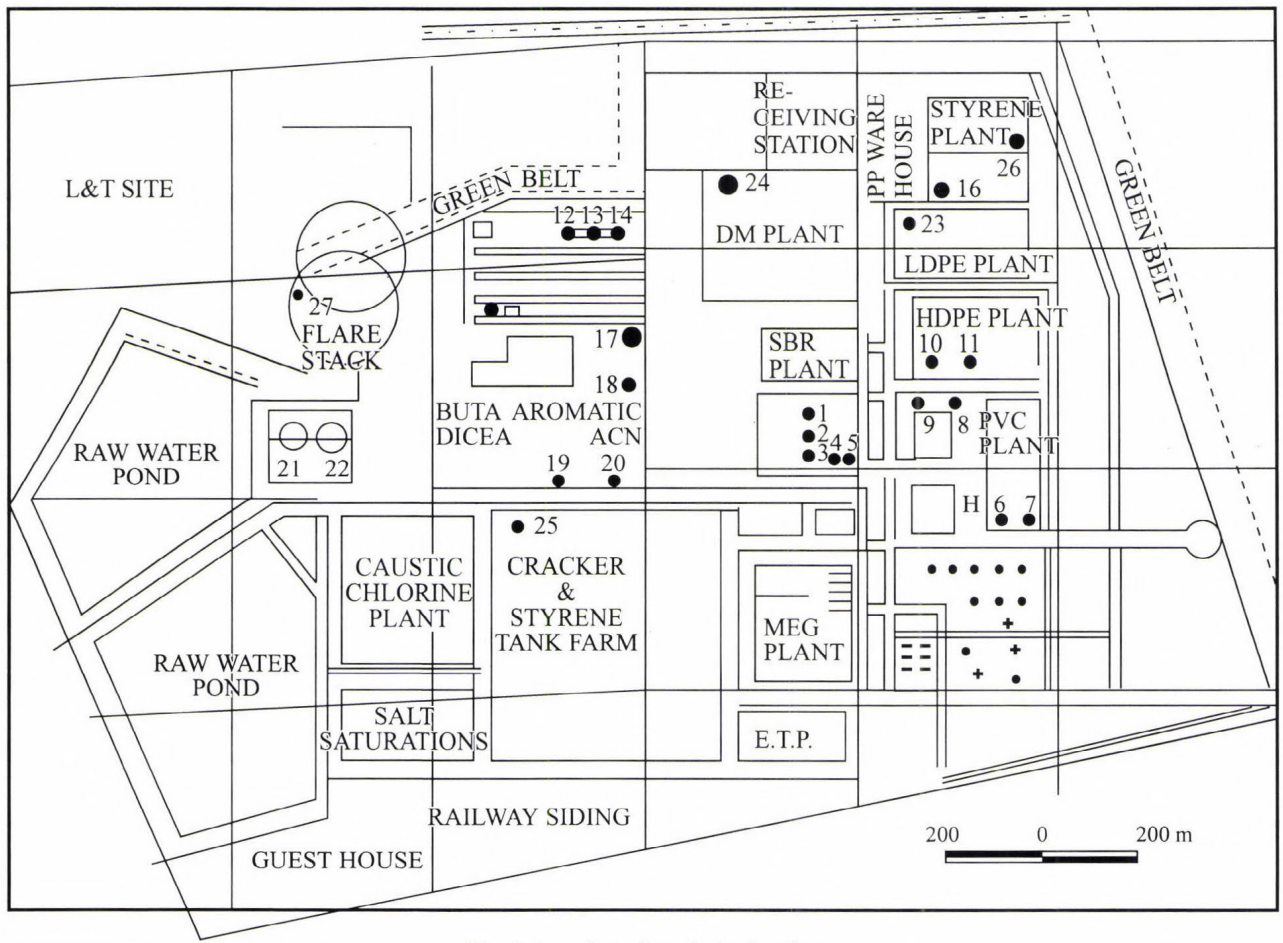

Fig. 2. Location of stacks in the plant.

Table 1. Expected emissions from different stacks

Stack No.	Stack description	NO_x emission rate 10^{-3} kg/sec
1.	Boiler-I	18.75190
2.	Boiler-II	18.75190
3.	Boiler-III	18.75190
4.	By-pass-I	9.78685
5.	By-pass-II	9.78685
6.	PVC dryer-I	0.777
7.	PVC dryer-II	0.777
8.	EDC cracking furnace-I	0.1263
9.	EDC cracking furnace-II	0.1263
10.	Incinerator	0.5277
11.	Hot oil heater	3.653
12.	Cracker furnace-I	4.311
13.	Cracker furnace-II	3.61100
14.	Cracker furnace-III	3.61100
15.	Cracker furnace-IV	3.61100
16.	Styrene reactor furnace	0.72200
17.	ACN reactor	0.34400
18.	HCN incinerator	0.08610
19.	Power plant	14.8500
20.	Power plant	12.66000
21.	Flare stack-I	4.8
22.	Flare stack-II	4.8
23.	LLDPE plant	Negligible
24.	Polypropylene plant	Negligible
25.	Polystyrene plant	Negligible
26.	Chlorine cumbercent	Negligible
27.	Flare stack	4.8

Note:
- Out of first five stacks, only three are used at a time.
- Normally gas is used as fuel.
- Flare stack emissions are normally from pilot burning.
- SO_2 from gas burning is negligible. The fuel gas supplied by ONGC is sweet gas.
- 23–26 are only vents for pneumatic conveying system. So except SPM & C12 (in the case of caustic/chlorine) other pollutants are not present.

2.3 Source data

The atmospheric emission rates from different stacks were computed based on emission factors for natural gas combustion and mass balance of raw materials and products involved in different processes.

The computed emission rates for nitrogen oxides are based on the theoretical estimates made for normal operating conditions which include all the forms of oxides of nitrogen e.g. NO, NO_2, but NO_2 forms a major portion of these oxides.

3. Results

The observed concentrations of various pollutants at all the sampling stations were processed for different statistical parameters like arithmetic mean, arithmetic standard deviation, geometric mean, geometric standard deviation, and various percentile values. The baseline levels of SPM, sulfur dioxide, nitrogen oxides, aldehyde and ammonia are expressed in $\mu g\ m^{-3}$ (*Tables 2* to *6*).

The arithmetic mean of 8 hourly SPM values at all these stations, ranged between 121 and 304 $\mu g\ m^{-3}$ whereas 95th percentile values of concentrations varied between 178 and 535 $\mu g\ m^{-3}$.

The higher SPM concentrations observed at Athwalines and Surat can be attributed to local and transportation activities.

At Reliance Petrochemicals Ltd. (RPL) site the SPM concentrations were found to be high due to construction activities and vehicular traffic through kuchha roads. At all other sites the 95th percentile values of suspended particulate matter concentrations were well within the limits stipulated by Central Pollution Control Board—India, National Ambient Air Quality Standards (NAAQS).

Lower concentrations of gaseous pollutants i.e. sulfur dioxide and nitrogen dioxide were observed during the period of study. The arithmetic mean of sulfur dioxide and nitrogen dioxide were found to be in the range of 3.0–17.8 and 3.0–7.9 $\mu g\ m^{-3}$, whereas the 95th percentile values were observed to be in the range of 3–28 $\mu g\ m^{-3}$ and 3–17 $\mu g\ m^{-3}$, respectively.

The 95th percentile values of ammonia and aldehydes varied in the range of 42–98 $\mu g\ m^{-3}$ and 13–30 $\mu g\ m^{-3}$, respectively, whereas average concentrations of ammonia and aldehydes ranged respectively between 24.2–5 $\mu g\ m^{-3}$ and 7.85–20.9 $\mu g\ m^{-3}$, thereby indicating very less concentrations in ambient air.

Aldehydes which have also been detected during ambient air quality monitoring could prove to be toxic, these are formed during the incomplete combustion and by interaction of nitrogen dioxide and hydrocarbons under influence of sunlight.

Sulfur dioxide levels were observed to be low as natural gas is used as basic raw material and fuel in the industries and hence sulfur dioxide contribution from industries is very low.

At the time of the study, KRIBHCO, ONGC and ESSAR plants were the major industries already in operation and the RPL plant was under construction.

Table 2. Ambient air quality status for suspended particulate matter (summer season; May 1991)

8 hrs avg. Unit : $\mu g\ m^{-3}$

Stat. No.	Sampling locations	Min. obs.	Percentile 10%	25%	50%	80%	95%	Max. obs.	Arithmetic Mean	S.D.	Geometric Mean	S.D.
1.	Ichchapore	59	59	111	156	192	278	316	166.2	70.16	151.1	1.58
2.	Kawas	126	126	178	223	336	454	476	265.5	108.64	243.7	1.52
3.	RPL site	74	84	130	220	310	533	549	237.9	137.43	201.8	1.79
4.	Mora	39	52	96	123	160	178	191	125.7	40.98	117.2	1.49
5.	Malgama	87	94	119	154	248	463	688	219.1	143.14	187.4	1.69
6.	Barbodhan	85	105	167	194	268	333	383	188.7	94.2	140.4	1.37
7.	Dumas	74	91	183	283	329	398	455	221.1	119.55	173.4	1.43
8.	Bhatpore	122	128	177	234	368	469	600	271.3	126.31	245.9	1.55
9.	Althan	65	68	88	159	357	435	509	215.2	137.58	174.3	1.94
10.	Adajan	127	129	180	233	304	384	403	207.6	112.74	191.9	1.39
11.	Bhata	142	148	178	256	400	475	523	292.2	120.49	267.8	1.52
12.	Suvali	150	152	167	183	269	299	300	215.1	52.67	208.9	1.27
13.	Bhatlai	48	65	164	195	344	471	545	249.3	132.66	212.7	1.83
14.	Damka	154	165	195	229	324	483	496	279.1	104.89	261.8	1.43
15.	Surat	185	187	244	290	312	535	581	303.5	99.9	289.5	1.34
16.	Umra	105	111	135	220	282	349	450	226.6	90.1	208.8	1.51
17.	Magdulla	116	124	145	191	286	354	456	212.4	103.73	178.5	1.47
18.	Hazira	47	50	75	90	157	248	303	121.3	69.59	105.7	1.67

Table 3. Ambient air quality status for sulfur dioxide (summer season; May 1991)

8 hrs avg. Unit : $\mu g\ m^{-3}$

Stat. No.	Sampling locations	Min. obs.	Percentile 10%	25%	50%	80%	95%	Max. obs.	Arithmetic Mean	S.D.	Geometric Mean	S.D.
1.	Ichchapore	3	3	3	3	3	4	6	3.7	1.1	3.0	1.3
2.	Kawas	3	3	3	3	3	3	3	3.0	0.0	3.0	1.0
3.	RPL site	3	3	3	3	3	5	7	3.4	1.11	3.2	1.27
4.	Mora	3	3	3	3	3	5	6	3.3	0.84	3.2	1.22
5.	Malgama	3	3	3	3	3	4	8	3.2	1.18	3.1	1.26
6.	Barbodhan	3	3	3	3	3	3	3	3.0	0.0	3.0	1.00
7.	Dumas	3	3	3	3	5	7	8	3.9	1.62	3.6	1.41
8.	Bhatpore	3	3	3	4	6	9	10	5.0	2.17	4.5	1.52
9.	Althan	3	3	3	3	3	6	10	3.5	1.68	3.3	1.36
10.	Adajan	3	3	3	3	0	6	7	3.5	1.19	3.4	1.31
11.	Bhata	3	3	3	3	5	6	8	3.7	1.31	3.5	1.33
12.	Suvali	3	3	3	3	3	5	9	3.6	1.46	3.4	1.33
13.	Bhatlai	3	3	3	3	4	7	9	3.8	1.25	3.5	1.39
14.	Damka	3	3	3	3	3	3	3	3.0	0.0	3.0	1.0
15.	Surat	3	3	12	20	24	28	28	17.8	7.74	15.2	1.92
16.	Umra	3	3	3	3	3	3	3	3.0	0.0	3.0	1.0
17.	Magdulla	3	3	3	3	4	7	9	3.7	1.57	3.4	1.36
18.	Hazira	3	3	3	3	3	3	3	3.0	0.0	3.0	1.0

Table 4. Ambient air quality status for nitrogen oxides (summer season; May 1991)

8 hrs avg. Unit : $\mu g\ m^{-3}$

Stat. No.	Sampling locations	Min. obs.	Percentile 10%	25%	50%	80%	95%	Max. obs.	Arithmetic Mean	S.D.	Geometric Mean	S.D.
1.	Ichchapore	3	3	3	3	3	3	3	3.0	0.0	3.0	1.0
2.	Kawas	3	3	3	3	3	9	12	4.29	2.52	3.84	1.52
3.	RPL site	3	3	3	3	3	3	3	3.0	0.0	3.0	1.0
4.	Mora	3	3	3	3	3	3	3	3.0	0.0	3.0	1.0
5.	Malgama	3	3	3	3	3	3	3	3.0	0.0	3.0	1.0
6.	Barbodhan	3	3	3	3	3	3	3	3.0	0.0	3.0	1.0
7.	Dumas	3	3	3	3	5	4	3	3.0	0.0	3.0	1.0
8.	Bhatpore	3	3	3	4	6	4	5	3.27	0.58	3.23	1.16
9.	Althan	3	3	3	3	3	6	8	3.47	1.24	3.33	1.29
10.	Adajan	3	3	3	4	7	11	11	5.38	2.89	4.73	1.64
11.	Bhata	3	3	3	3	5	6	7	3.83	1.34	3.65	1.35
12.	Suvali	3	3	3	3	3	3	3	3.0	0.0	3.0	1.0
13.	Bhatlai	3	3	3	3	4	3	3	3.0	0.0	3.0	1.0
14.	Damka	3	3	3	3	3	3	3	3.0	0.0	3.0	1.0
15.	Surat	3	3	5	6	7	17	2.5	7.89	5.37	6.63	1.76
16.	Umra	3	3	3	3	3	3	3	3.0	0.0	3.0	1.0
17.	Magdulla	3	3	3	3	4	3	3	3.0	0.0	3.0	1.0
18.	Hazira	3	3	3	3	3	3	3	3.0	0.0	3.0	1.0

Table 5. Ambient air quality status for ammonia (summer season; May 1991)

8 hrs avg. Unit : $\mu g\ m^{-3}$

Stat. No.	Sampling locations	Min. obs.	Percentile 10%	25%	50%	80%	95%	Max. obs.	Arithmetic Mean	S.D.	Geometric Mean	S.D.
1.	Ichchapore	15	14	20	40	71	142	180	59.2	48.81	44.40	2.11
2.	Kawas	3	3	6	15	49	160	236	44.5	66.52	17.90	3.87
3.	RPL site	3	3	3	20	54	67	81	29.9	66.40	15.20	3.76
4.	Mora	3	3	3	3	3	6	7	3.6	1.32	3.50	1.34
5.	Malgama	34	36	44	48	100	127	158	73.3	35.35	65.70	1.59
6.	Barbodhan	11	10	12	33	74	132	179	54.0	50.28	35.93	2.51
7.	Dumas	11	12	14	24	30	74	106	30.6	20.72	24.61	1.84
8.	Bhatpore	13	13	18	30	49	63	63	35.5	17.39	31.10	1.69
9.	Althan	3	3	3	11	78	91	105	33.0	36.11	15.13	3.77
10.	Adajan	3	3	3	41	74	95	103	44.7	35.93	21.24	4.49
11.	Bhata	4	4	7	15	26	41	44	20.0	12.92	15.01	2.16
12.	Suvali	3	3	3	3	13	31	46	10.6	12.68	6.40	2.51
13.	Bhatlai	3	3	3	3	20	35	46	12.9	13.28	7.70	2.75
14.	Damka	3	4	7	19	32	64	77	25.9	21.10	17.90	2.53
15.	Surat	11	11	25	41	50	54	57	36.6	14.18	32.90	1.66
16.	Umra	3	3	4	16	32	40	44	18.8	13.87	13.10	2.55
17.	Magdulla	3	3	6	12	38	77	140	26.4	34.37	14.01	3.01
18.	Hazira	3	3	3	3	8	12	12	5.8	3.46	4.90	1.76

Table 6. Ambient air quality status for aldehyde (summer season; May 1991)

8 hrs avg. Unit : $\mu g\ m^{-3}$

Stat. No.	Sampling locations	Min. obs.	Percentile					Max. obs.	Arithmetic		Geometric	
			10%	25%	50%	80%	95%		Mean	S.D.	Mean	S.D.
1.	Ichchapore	3	3	4	5	8	11	12	5.9	3.02	5.2	1.61
2.	Kawas	3	4	5	6	10	12	14	6.8	2.96	6.3	1.51
3.	RPL site	3	3	3	3	14	39	44	11.5	13.41	6.7	2.66
4.	Mora	3	3	3	4	6	7	9	4.3	1.71	4.0	1.41
5.	Malgama	3	3	3	6	9	19	21	7.1	5.30	5.7	1.87
6.	Barbodhan	3	3	3	4	6	14	18	6.0	4.49	4.9	1.77
7.	Dumas	3	4	7	9	11	13	14	9.0	3.12	8.1	1.52
8.	Bhatpore	4	4	4	7	9	11	112	7.1	2.68	1.6	1.49
9.	Althan	3	4	6	8	9	15	28	8.6	5.49	7.6	1.59
10.	Adajan	3	3	3	5	7	8	110	5.0	2.14	4.6	1.51
11.	Bhata	3	3	3	3	4	8	27	4.8	5.44	3.0	1.67
12.	Suvali	3	3	3	3	3	3	3	3.0	0.0	5.0	1.00
13.	Bhatlai	3	3	3	3	9	22	33	7.5	8.61	5.4	2.17
14.	Damka	3	3	4	5	7	13	20	6.2	4.07	5.4	1.66
15.	Surat	3	3	3	5	9	11	17	6.3	3.56	4.3	1.67
16.	Umra	3	3	3	4	5	8	9	4.6	1.84	3.0	1.43
17.	Magdulla	3	3	3	3	3	3	3	3.0	0.00	3.2	1.00
18.	Hazira	3	3	3	3	3	5	8	3.4	1.25	3.0	1.28

3.1 Micrometeorology

The 24 hour wind-rose at RPL shows the maximum occurrence of wind from WSW and SW directions. The predominant wind speed was observed to be in the range of 11–15 km/h.

Synoptic scale wind was observed to be dominant over diurnal sea and land breezes thereby nullifying their effect.

Therefore, insignificant diurnal variation in wind pattern was observed during the study period. During the survey period predominant wind directions were observed to be WSW and SW (diurnal).

3.2 Modeling results

To delineate the zone of high nitrogen oxides concentration (impact zone) isopleths were plotted. *Fig. 3* presents the isopleths of predicted nitrogen oxides during different time periods.

During summer season, predominant wind blew from the S-W quadrant. During day time, the maximum predicted nitrogen oxides concentration of 37 $\mu g\ m^{-3}$ (10–18 hrs) occurs at a distance of 1 km in NE direction. The occurrence of higher concentration near to the sources may be due to the prevailing unstable atmospheric conditions and higher mixing heights during day

time. During night time (18–02 hrs), maximum predicted nitrogen oxides concentration of 37 $\mu g\ m^{-3}$ occurs at 9–10 km far in NE direction, whereas during 02–10 hrs, it was found to be 41 $\mu g\ m^{-3}$ at 10 km distance in NE direction. The predicted concentration at far off distance from sources may be attributed to the combination of high stacks and stable atmospheric conditions. It can be concluded from the figures that the impact zone is limited to the NE sector during summer season. However, the post-project air quality status i.e. the super-imposition of predicted air quality over baseline air quality is within the recommended ambient air quality status.

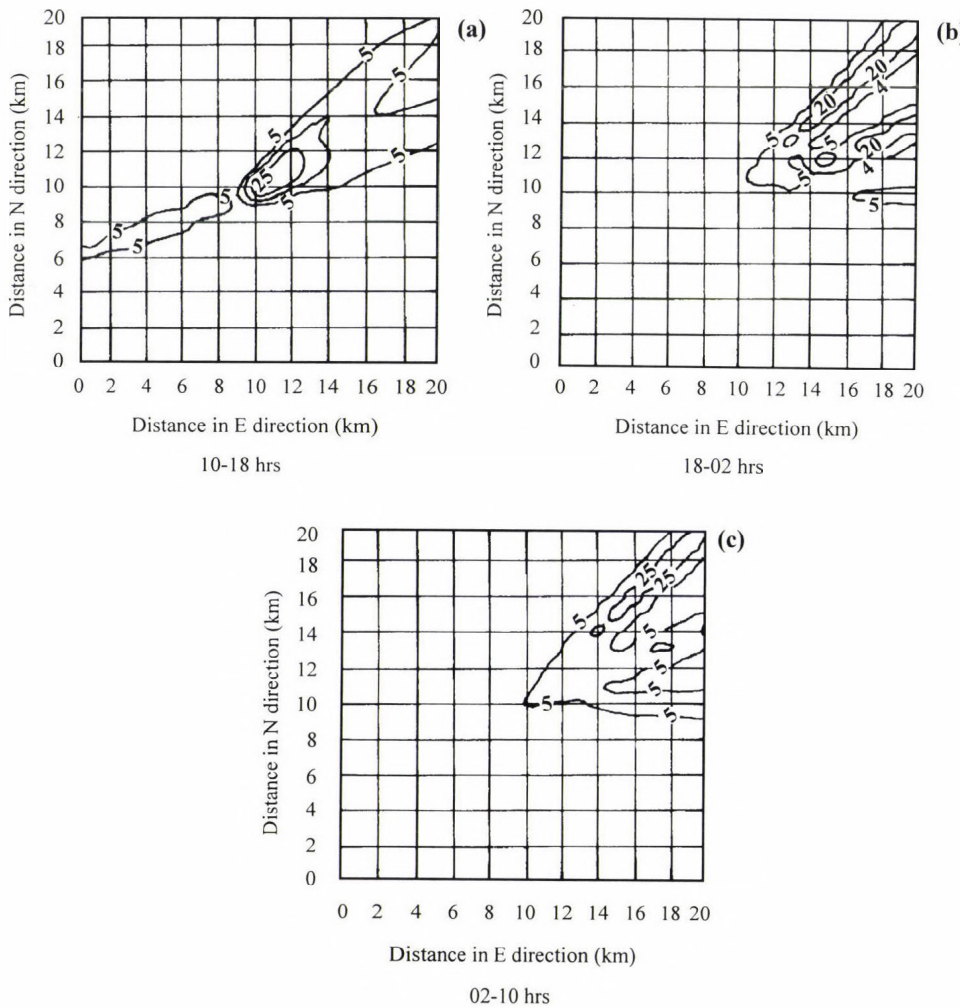

Fig. 3. Isopleths showing predicted NO_x concentration.

4. Recommendations

In order to avoid further degradation and maintain the ambient air quality status in Hazira region at least at the current levels in short run and improve the same the long run, following recommendations are made.

- The industrial area houses many industries as mentioned above (ESSAR, KRIBHCO, ONGC, GAIL); hence it is necessary to monitor the ambient air quality, stack emissions and meteorology on a regular basis through a well designed network.
- For reduction of nitrogen oxides, carbon monoxide, hydrocarbon emissions from various industries, the following measures are proposed:
  - proper burner maintenance,
  - good atomisation of liquid fuels,
  - optimum excess air levels,
  - staged combustion fuel gas recirculation.
- For reduction of hydrocarbons from storage tanks as fugitive emissions the following measures should be taken:
  - provision of floating roof or pressure storage for light hydrocarbons,
  - replacement of gland packing of pumps by mechanical seals,
  - proper maintenance of valves and other leakage prone areas.
- For reduction of particulates from the various industries, cyclones, scrubbers, or electrosatic precipitators or a combination of these can be used depending upon the type and size of the particulates.
- Greenbelt development should be undertaken to facilitate attenuation of pollutants from diverse industrial activities in the region. A minimum of 50–100 m greenbelt has been suggested around the proposed plant based on the attenuation of pollutants in the study area.

Acknowledgements—Authors wish to thank *Prof. P. Khanna*, Director of NEERI, for the kind approval to present the paper.

References

Indian Standards, 1969: *Methods for Measurements of Air Pollution — Sulfur dioxide*. 5182, Part II.

Indian Standards, 1974: *Suspended Particulate Matter*. 5182, Part IV.

Katz, M. (ed.), 1977: *Methods of Air Sampling and Analysis*. 2nd edition. American Public Health Association, Washington.

Pasquille, F., 1974: *Atmospheric Diffusion*. Wiley, New York.

Turner, D.B., 1970: *Workbook of Atmospheric Dispersion Estimates*. AP-26, Office of Air Programmes, USEPA, RTP, NC.

BOOK REVIEW

Richard J. Doviak, Dusan S. Zrnic: **Doppler Radar and Weather Observations.** Second edition. Academic Press Inc., 1993, San Diego, 11 chapters with problems to be solved, 5 appendices, 562 numbered pages, hundreds of figures, including many color plates, around 800 numbered formulae and equations, over 500 references.

This is a revised version of the book published under the same title in 1984. The many changes that have resulted in radar networking, development and implementation of new techniques in the USA explain this revision: changing the aged incoherent radars for Doppler-radars (NEXRAD with WSR-88D), implementation of Terminal Doppler Weather Radars (TDWR) at major airports, establishment of a demonstration network of wind profilers and radio acoustic sounding systems for vertical temperature distribution. This work is based on the authors' lectures on radar meteorology at the University of Oklahoma and their lecturing in different short courses, and on the comments received. The new material consists of an expanded Chapter 1, which now contains a short history of radar, sections on polarimetric measurements and data processing, an updated section on radio acoustic sounding systems and a section on wind profilers. Furthermore, Chapters 9-11 have been expanded and updated to include new figures of phenomena observed with the WSR-88D.

Chapter 1 provides historical background. Hungarian readers may find — with certain national pride — their country among those where efforts were made for radar developments already in the 1930s. *Chapter 2* introduces the essential properties of radio waves and describes the effects the atmosphere has on the path of the radar pulse and its echo. *Chapter 3* starts to develop weather radar theory, tracing the transmitted pulse to a single hydrometeor and considering the coherent or Doppler radar (equation can directly be applied to the commonly used incoherent weather radar). *Chapter 4* extends the radar principles to a conglomerate of hydrometeors that produces a continuous stream of echoes with random fluctuations of amplitude and phase, thus the weather radar equation is developed for the echo power in terms of radar and meteorological parameters. In *Chapter 5* the discrete Fourier transform is considered and applied to weather signals so as to make a connection between the Doppler spectrum and shear and turbulence of the flow. *Chapter 6* presents proven methods of weather signal processing with emphasis on obtaining the first three spectral moments and a section on methods to obtain simultaneously spectral moments and polarimetric measurements. *Chapter 7* examines limitations in pulsed Doppler radar observations of weather, presents various

techniques to mitigate them, and briefly considers how radar hardware affects measurement accuracy. *Chapter 8* deals with precipitation measurements by radar, describing the physics behind. Single- and multiple-parameter techniques and polarization diversity and its utility for quantitative precipitation measurements and discrimination between different types of hydrometeors are comprehensively discussed. Color plates ease evaluation of the various techniques. Following a brief introduction to storm structure the huge *Chapter 9* considers radar observations of winds, storms and related phenomena (tornadoes, density currents, convergence bands, downbursts and microbursts, lightning, etc.) in an illustrative manner. It discusses single- and multiple Doppler data analyses and interpretation of severe weather events with examples of wind fields, obtained from Doppler radar data analyses on storms and photographs of several significant phenomena associated with storms. The purpose of *Chapter 10* is to introduce the basic concepts of turbulence and to establish a firm connection between physical (statistical) properties of the atmosphere and Doppler-derived measurements. Relationships between turbulence and the mean Doppler velocity and the spectrum width are presented in this chapter. *Chapter 11* considers theories to explain radar echoes from clear-air refractive index irregularities. Relations between irregularity characteristics and Doppler-shifted signals are amply illustrated with specific examples and are used to explain actual observations. It also discusses vertical profiling of winds with specialized radars and measurements of temperature with radio acoustic sounding systems.

After reading through and studying the book one can confirm that the authors' intention, i.e. this book is meant to be a reference for users and developers of Doppler systems has been attained. Attaching a problem at the end of each chapter makes this edition more suitable for graduate courses on radar meteorology. To a meteorologist practicing at the borderland between meteorology and radar technique sometimes the language of the book (special words, terms, phrases) may sound slightly unusual, without causing confusion, however. Just very few and easily identifiable misprints occur in the enormous quantity of equations and formulae. This book shows great promise to be well received by the small but firm community of specialists that grew up in our country during the last decades.

Kapovits Albert

NEWS

VIIth Seminar on Surface and Meteorological Observations from Space

Budapest (Hungary), March 13–14, 1997

The seminar was organized by the Section of Earth Sciences and Department of Natural Sciences of the Hungarian Academy of Sciences and by the Hungarian Astronautical Society, with the sponsorship of the Hungarian Space Office and GRID-Budapest, the Budapest center of the Global Resource Information Database network.

The seminar began with the opening remarks by *Dr. I. Almár*, president of the Hungarian Astronautical Society, who reminded the participants that this series of seminars dates back to 1974, when the predecessor of the Hungarian Astronautical Society formed a working committee named *Earth Photography*. Since then Hungarian specialists in meteorology, cartography, geodesy, hydrology, geology, agriculture and Earth informatics (or *geomatics*) gather regularly to report on the recent national and international developments in their specific area. This occasion was not an exception; the presentations covered a number of topics of the above fields.

In addition to the six oral sessions, a poster session, including software presentations, was also held; this, considering the principal importance of the visualisation of satellite imagery in surface investigations, proved to be highly useful and efficient.

The presentations concentrated on various scientific, economic and educational aspects of the processing of satellite data with the final aim of obtaining geophysical information on the Earth's surface. Several talks discussed the retrieval of meteorological parameters needed for the accurate removal of atmospheric effects from the satellite signal, such as atmospheric profiling by GPS (Global Positioning System) and TOVS (TIROS-N Operational Vertical Sounder) systems, cloud detection and the retrieval of cloud properties. Other papers presented methods to derive surface physical parameters (land surface temperature, albedo etc.) or specific indexes characterizing the surface (vegetation "greenness" indexes etc.). A large number of presentations reported then on the application of the above information in vegetation cover identification, yield estimation, soil classification, geological investigations and water quality monitoring. As still there is no general consensus regarding some of these economically important topics, these sessions offered the possibility for a fruitful exchange of ideas.

The discussions also covered a wide range of satellite systems and instruments, from LANDSAT satellites that have been providing high spatial and spectral resolution imagery for a quarter of a century, through the operational meteorological satellites METEOSAT and NOAA, to the recently developed synthetic aperture radar (SAR) technology and many more. Almost all presentations placed their results in the context of international projects. An entire presentation was devoted to the participation of the Hungarian remote sensing community in the activities of various international organizations. Two speakers presented image processing software of leading commercial enterprises.

The organizers acknowledged the performance of the best young presenters. Among the awardees was *É. Borbás* (Hungarian Meteorological Service, Satellite Research Laboratory) for the presentation of her paper "GNSS applications in meteorology".

The seminar was concluded by a round-table discussion "The role of Earth Photograpy in the solution of the problems of the 90s". Here first *Dr. Gy. Tófalvi*, head of the Hungarian Space Office informed the community on the current financial situation of space research in Hungary. Then leaders of various research communities made their contributions, regarding financial, economic and scientific aspects. One of the main conclusions of the discussion was the need for further, more efficient collaboration between the institutions to ensure the continuation of the traditionally high quality application of satellite data for surface and atmospheric investigations in Hungary.

The presented papers have been published in the seminar proceedings.

I. Csiszár

ATMOSPHERIC ENVIRONMENT

an international journal

To promote the distribution of Atmospheric Environment *Időjárás* publishes regularly the *contents* of this important journal. For further information the interested reader is asked to contact *Prof. P. Brimblecombe,* School for Environmental Sciences, University of East Anglia, Norwich NR4 7TJ, U.K.; E-mail: atmos_env@uea.ac.uk

Volume 31 Number 8 1997

Volume 31 Number 9 1997

NOTES TO CONTRIBUTORS

The purpose of *Időjárás* is to publish papers in the field of theoretical and applied meteorology. These may be reports on new results of scientific investigations, critical review articles summarizing current problems in certain subject, or shorter contributions dealing with a specific question. Authors may be of any nationality but papers are published only in English.

Papers will be subjected to constructive criticism by unidentified referees.

* * *

The manuscript should meet the following formal requirements:

Title should contain the title of the paper, the names(s) of the author(s) with indication of the name and address of employment.

The title should be followed by an *abstract* containing the aim, method and conclusions of the scientific investigation. After the abstract, the *key-words* of the content of the paper must be given.

Three copies of the manuscript, typed with double space, should be sent to the Editor-in-Chief: *P.O. Box 39, H-1675 Budapest,* Hungary.

References: The text citation should contain the name(s) of the author(s) in Italic letter or underlined and the year of publication. In case of one author: *Miller* (1989), or if the name of the author cannot be fitted into the text: *(Miller,* 1989); in the case of two authors: *Gamov* and *Cleveland* (1973); if there are more than two authors: *Smith et al.* (1990). When referring to several papers published in the same year by the same author, the year of publication should be followed by letters a,b etc. At the end of the paper the list of references should be arranged alphabetically. For an article: the name(s) of author(s) in Italics or underlined, year, title of article, name of journal, volume number (the latter two in Italics or underlined) and pages. E.g. *Nathan, K. K.,* 1986: A note on the relationship between photosynthetically active radiation and cloud amount. *Időjárás 90,* 10-13. For a book: the name(s) of author(s), year, title of the book (all in Italics or underlined with except of the year), publisher and place of publication. E.g. *Junge, C. E.,* 1963: *Air Chemistry and Radioactivity.* Academic Press, New York and London.

Figures should be prepared entirely in black India ink upon transparent paper or copied by a good quality copier. A series of figures should be attached to each copy of the manuscript. The legends of figures should be given on a separate sheet. Photographs of good quality may be provided in black and white.

Tables should be marked by Arabic numbers and provided on separate sheets together with relevant captions. In one table the column number is maximum 13 if possible. One column should not contain more than five characters.

Mathematical formulas and *symbols:* non-Latin letters and hand-written marks should be explained by making marginal notes in pencil.

The final text should be submitted both in manuscript form and on *diskette.* Use standard 3.5" or 5.25" DOS formatted diskettes for this purpose. The following word processors are supported: WordPerfect 5.1, WordPerfect for Windows 5.1, Microsoft Word 5.5, Microsoft Word 6.0. In all other cases the preferred text format is ASCII.

* * *

Authors receive 30 *reprints* free of charge. Additional reprints may be ordered at the authors' expense when sending back the proofs to the Editorial Office.

Published by the Hungarian Meteorological Service

Budapest, Hungary

INDEX: 26 361

HU ISSN 0324-6329

IDŐJÁRÁS

QUARTERLY JOURNAL
OF THE HUNGARIAN METEOROLOGICAL SERVICE

CONTENTS

****

http://www.met.hu/firat/ido-e.html

VOL. 101 * NO. 3 * JULY–SEPTEMBER 1997

IDŐJÁRÁS

Quarterly Journal of the Hungarian Meteorological Service

Editorial Office: P.O. Box 39, H-1675 Budapest, Hungary or
Gilice tér 39, H-1181 Budapest, Hungary
E-mail: gmajor@met.hu or *antal@met.hu*
Fax: (36-1) 290-7387

Subscription by

mail: IDŐJÁRÁS, P.O. Box 39, H-1675 Budapest, Hungary;
E-mail: gmajor@met.hu or *antal@met.hu*; *Fax: (36-1) 290-7387*

IDŐJÁRÁS

Quarterly Journal of the Hungarian Meteorological Service
Vol. 101, No. 3, July–September 1997, pp. 161–171

Variations and trends of land surface air temperature, 1891–1992

Zsuzsanna Iványi

Department of Meteorology, Eötvös Loránd University,
Ludovika tér 2, H-1083 Budapest, Hungary; E-mail: ivanyi@ludens.elte.hu

(Manuscript received 15 October 1996; in final form 3 January 1997)

Abstract—Long-term land surface air temperature series have been used for investigation of their variation and trends. Seasonal distribution was also considered. Besides global and hemispherical averages, sub-regions — corresponding more or less to the continents — were considered for not only long-term, but also shorter periods. For the long period significant warming trend was found for the global and hemispherical scales and also for the continents except Africa. Warming rates for some continents exceed in each season the global and hemispherical trends. Variation of trend with time revealed that no significant trend exist for the sub-periods except the last one: 1970–1992. Maximum of warming rates was found in months D-J-F on global and hemispherical scales. In these months North Asia shows extreme warming rate in the last sub-period. Relations between the warming rates for the various scales are different. Global and northern hemispherical trends correlate well, however very weak connections were found between the continents of the Northern Hemisphere.

Key-words: global warming, temperature trend, seasonal and geographical distribution.

1. Introduction

Surface air temperature variations show very different pictures on the various scales. The earlier theoretical and empirical investigations were mostly focused on global and hemispherical scales, but it has soon turned out that not only the value of the trend, but also the sign is different on regional scales. Trends of surface air temperature have widely been reported by several papers in the past using various data base with different length and spatial resolution (e.g. see *Jones et al.*, 1982; *Ghil* and *Vantard*, 1991; *Nitta* and *Yoshimura*, 1993; *Jones*, 1988 and 1994). The common finding of these studies was that the trend of the surface air temperature changed during the past 100 year. For global temperature averages a warming period was found from 1880 to 1940, then a cooling

period was observed. The duration of the cooling period is different according to the different authors. The end of this period varies between 1960 and 1970. After 1970 a warming period started again. These statements had been confirmed by the last report of *IPCC* (1996). The results mentioned above are valid for the global averages, however hemispherical, continental and regional averages show different characteristics.

Nitta and *Yoshimura* (1993) studied the trends and interdecadal variations of the global, hemispherical and continental land surface air temperature during the last 100 year period using the most available up-to-date temperature data series till 1990. A warming rate of about 0.54°C/100 years was found on global scale. However, the temperature had interdecadal variation, with the largest warming rate after 1970 up to now. Confirming former results cooling trend was found between 1940 and 1970 not only on global scale, but also in the sub-regions, but the rate was very different.

It seemed to be worthwhile to carry out a detailed investigation, to see how the surface air temperature trends changed during the past approximately 100 years on global, hemispherical and continental scale in the different seasons. The seasonal variation of the temperature trends has already been studied by some authors. *Angell* (1988) made a temperature analysis for the surface and for three upper layers using data between 1958 and 1977 for three zones of the globe. A difference was found between the temperature trends and between the seasons and it was advised to extend the analysis using the longest record available. *Jones et al.* (1982) and *Kelly et al.* (1982) studied surface air temperature trends between 1881 and 1980 for the Northern Hemisphere. All seasons showed similar long-term trends, but there were noticeable differences on time-scales of 10 years or less. Both the magnitude of the long-term trends and the year to year variability were the greatest in winter. It is confirmed by the report of *IPCC* (1996) showing that recent warming is most noticeable in winter and spring over the mid-latitude continents of the Northern Hemisphere.

For the characterization of the geographical distribution *Hansen* and *Lebedeff* (1987) used also long temperature series (1880–1985) to analyze the variation of trends. Global, hemispherical, regional (16 boxes) averages were calculated. The seasonal variation was also included, but main emphasis was taken for the yearly averages and their geographical distributions. They found that earlier warming was focused at high latitudes of the Northern Hemisphere, while recent warming is more global. *Trenberth* (1990) investigated the geographic spatial structure of the interdecadal temperature variations associated with changes in the atmospheric circulation. He found that there exist some links, but this does not rule out other external mechanism.

It is not a question that the global, hemispherical and continental surface temperature averages, furthermore their variations are very much different, i.e. the nature or character of the surface air temperature trends on various scales is still not clear. In this paper seasonal temperature trends gained for global

and hemispherical averages, furthermore for the northern and southern part of the continents are introduced and compared. The question to be answered is, what kind of relation exists between the temperature trends in the different regions of the globe. A special emphasis is put on the period following 1970, since, as it was indicated by *Nitta* and Yoshimura (1993), the highest warming trend was found in the period of 1970–1990. It is worth to recite *Jones*'s result (1988), who stated that during the period of 1967–1986 the warming was the strongest in the mid-latitudes in the Northern Hemisphere between 30° and 60°, with the exception of Europe.

2. Data base

This study is based on the same data base used by *Nitta* and *Yoshimura* (1993), except that the latest available data were also considered. The above mentioned temperature data set was provided by the Japan Meteorological Agency and includes monthly mean land air temperatures for 1881–1992. The procedure of averaging is described by *Nitta* and *Yoshimura* (1993). Briefly summarizing the procedure the main steps were as follows:

(i) Reference period was chosen to be 1951–1980.

(ii) Deviations from the monthly mean temperature average defined above had been calculated for each of the individual stations, then anomalies had been determined for each grid using a distance-dependent weighting factor measured from the center of the grid.

(iii) Mean temperature anomalies had been determined for the following 8 sub-regions: Europe, North Asia, North America, North Africa, South Asia, South Africa, Oceania, South America. Hemispherical and global averages had also been calculated.

Data used for the analyses include only land surface air temperatures. In spite of the fact that the effect of oceans is extremely important in the dynamics of the atmosphere and in the process of global warming, only land surface air temperature time series was used for these analyses in order to provide long data-series without uncertainties and avoiding difficulties due to the great number of missing data. The sporadic available temperature data over oceans and their unreliability might have caused some errors. One more thing should be stressed: Trends presented in this study might slightly overestimate the real values, since heat-island effect was not eliminated from the data. However *Hansen* and *Lebedeff* (1987) have shown that neglecting temperature data referring to big cities does not cause much change in the value of warming. The difference between the two cases is less than 10%. However, one should keep in mind that in specific areas urbanization effects may be significant (*IPCC*, 1996).

3. Data analysis

The huge amount of data had been classified according to the seasons for each subregion, the two hemispheres and the globe, as well. Since many data were missing in the period between 1881 and 1890, final analyses were executed for the period of 1891–1992. Linear regression was applied, though it requires perfect independence with time between the elements, which is not absolutely true for the temperature. Results gained by the statistical analysis can be considered as approximate indicators for the probably expectable variations of the temperature on various scales over land surfaces. Trends for the total period without considering seasons can be found in *Nitta* and *Yoshimura*'s paper (1993). On the basis of our researches seasonal trends are presented for the various scales for the whole period and for a short one lasting from 1970 to 1992. Temperature trends contained by the following tables are related to the whole- and sub-period. In the tables asterisks denote where significant trend was found. In these cases the values of temperature change show the probable warming trend with a confidence level higher than 95%.

For the whole period a significant warming trend exists for each season in most of the cases. Non-significant cases are not marked. In months of S-O-N the number of significant cases is low, which can not be explained for the time being. For significant trends it can be seen from *Table 1* that there are differences in the values of warming trends for the continents. North Asia shows the highest rate of warming, which occurred in winter (D-J-F) and spring (M-A-M). Northern Hemisphere and Europe have also high values of positive trend in the same seasons, which are higher then the annual warming rates. In the Southern Hemisphere the seasonal differences are not so marked. Altogether in D-J-F North Asia had the highest rate of temperature change, then South Africa, South America and Europe. In spring (M-A-M) North Asia is the first in the order, then comes South America, South Africa and Europe. In summer (J-J-A) an extreme warming rate was found in North America, furthermore in South America and South Africa values are higher than the global and hemispherical averages. In the months of S-O-N South America experienced the highest warming rate.

Seasonal temperature deviations from the reference period for the Northern Hemisphere is depicted in *Fig. 1* for the whole period. In the figures the circles show the length of the sub-periods. *Fig. 2*, *Fig. 3* and *Fig. 4* are the same, but for the Southern Hemisphere, North Asia and Europe, respectively. The reason for choosing North Asia is that extremely high warming rates occurred. In the Northern Hemisphere the highest rate of temperature increase was experienced in D-J-F and M-A-M. In the other two seasons the rate of change is about less than half of that (Fig 1.). In the Southern Hemisphere the rate of temperature increase varies between 0.52°C/100 yr and 0.36°C/100 yr, so the differences between the seasons are not high (*Fig. 2*). In North Asia the rate of warming

is very extreme in D-J-F and M-A-M, but similar to the global and hemispherical averages in the other two seasons (Fig. 3). In Europe the highest warming rate was found in winter and spring, but no significant warming was found in summer (Fig. 4).

Table 1. Seasonal temperature trends in °C/100 yr for the whole period (1891–1992)

Region/months	D-J-F	M-A-M	J-J-A	S-O-N
Global	*0.61	*0.59	*0.31	*0.32
Northern Hemisphere	*0.65	*0.63	*0.28	*0.29
Southern Hemisphere	*0.50	*0.52	*0.38	*0.37
Europe	*0.63	*0.67	0.17	*0.36
North Asia	*1.50	*1.20	*0.27	0.36
North America	0.23	*0.56	*0.71	0.13
North Africa	*0.28	*0.51	0.05	0.06
South Asia	*0.30	*0.35	*0.29	0.27
South Africa	*0.72	*0.68	*0.49	0.18
Oceania	0.01	*0.33	*0.27	0.17
South America	*0.69	*0.68	*0.52	*0.82

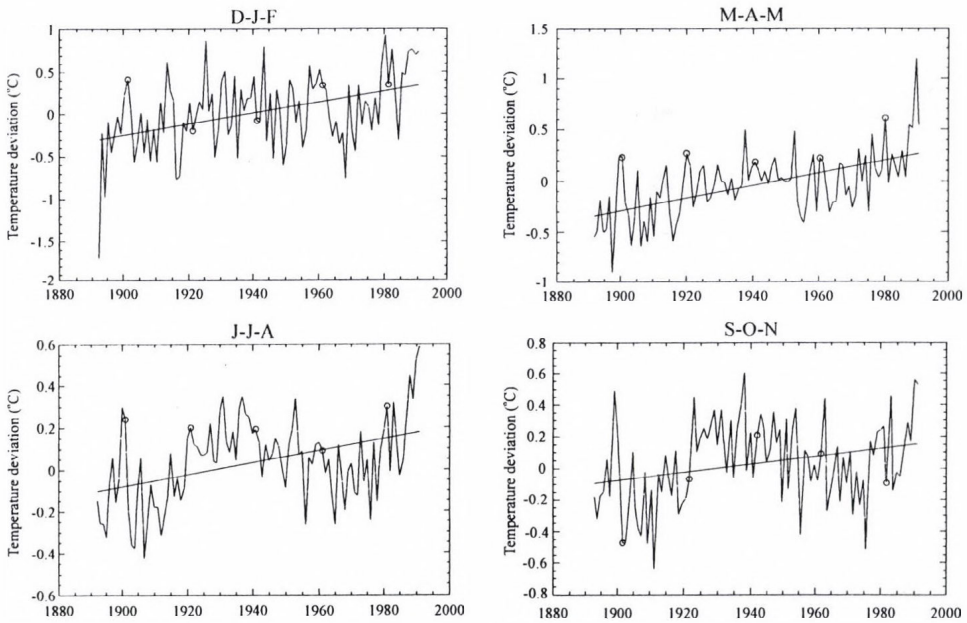

Fig. 1. Seasonal temperature deviations (°C) from the reference period (1951–1980) averages for the Northern Hemisphere.

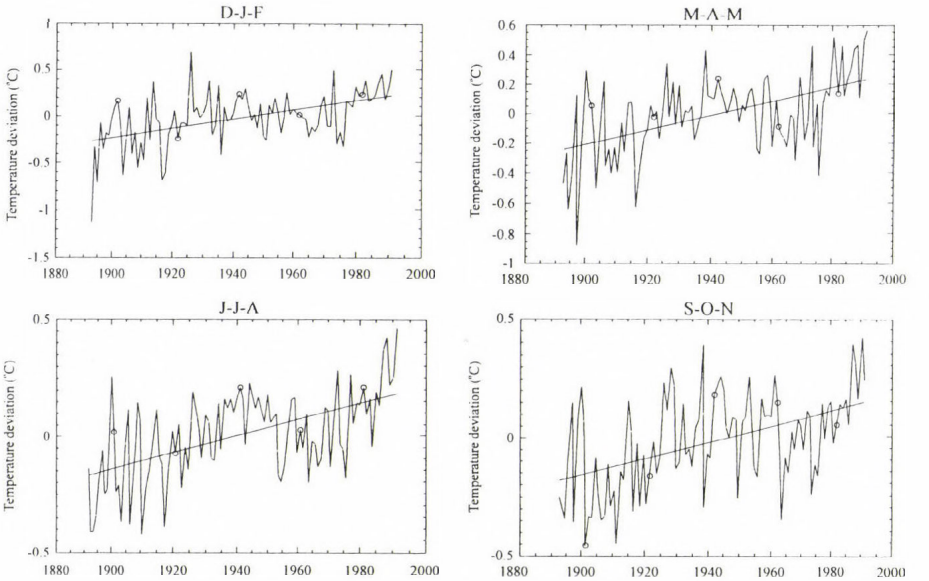

Fig. 2. Seasonal temperature deviations (°C) from the reference period (1951–1980) averages for the Southern Hemisphere.

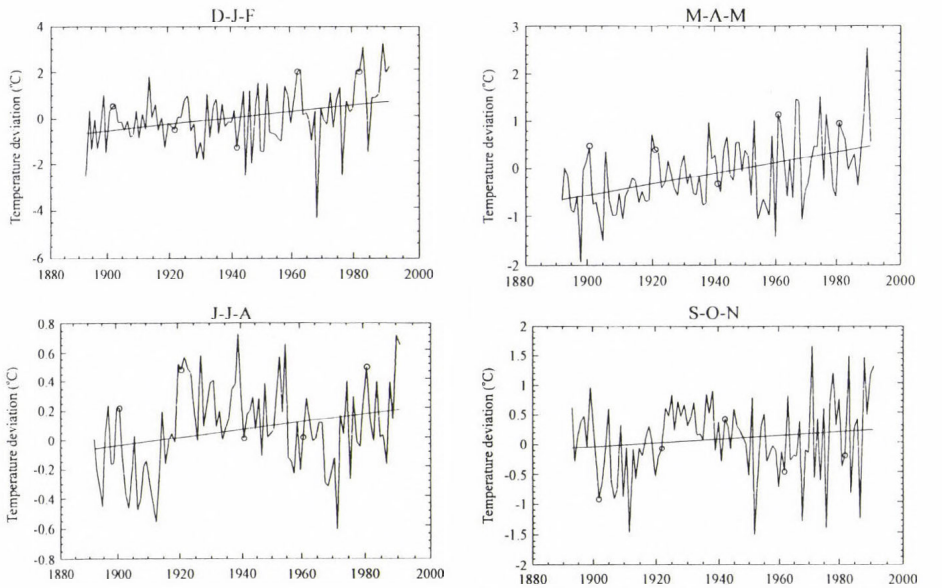

Fig. 3. Seasonal temperature deviations (°C) from the reference period (1951–1980) averages for North Asia.

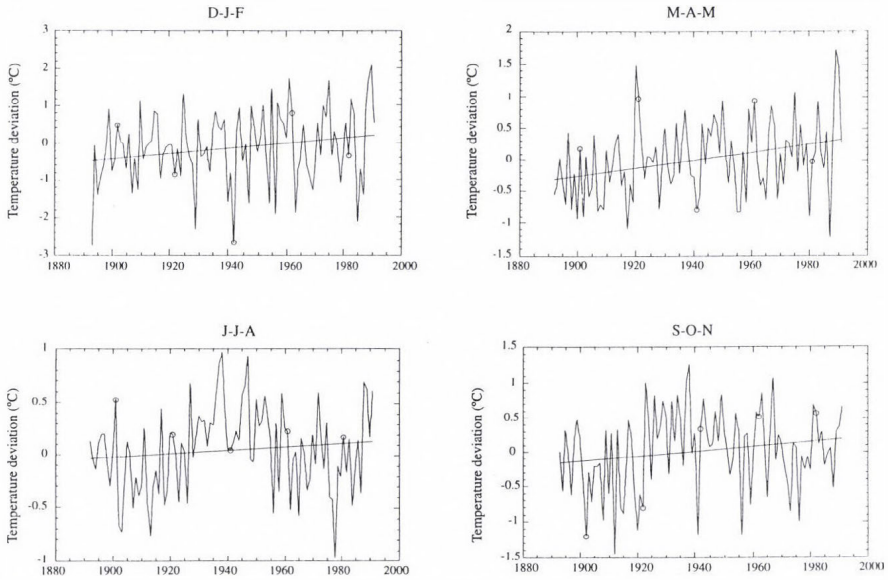

Fig. 4. Seasonal temperature deviations (°C) from the reference period (1951–1980) averages for Europe.

In the figures the differences can be seen clearly, i.e. there were warming and cooling periods in the past 100 years. For this reason trends were calculated for shorter sub-periods in order to show, how trends vary with time. The length of sub-periods was chosen to be 21 year starting from 1890, 1900 etc., so overlapping periods were considered. Very different warming and cooling rates were experienced and it can also be stated that warming rates are usually higher than those found for the total period. In the sub-periods significant trends were not found in as many cases as it was for the long period. This statement is valid for each season. *Table 2* presents calculated values of temperature change for each sub-periods for D-J-F. No significant trend exists for these short periods except the last one (1970–1992). Significant trends are marked by asterisks. North Asia has extreme value again 1.0°C/10 yr, while in other significant cases values of temperature increase vary between 0.20–0.39°C/10 yr, which are very high. South Asia and South Africa have values of 0.35°C/10 yr and 0.32°C/10 yr, respectively. These values highly exceed the warming rate received for the whole period. It has to be mentioned that in Europe no significant warming trend was found in any of the sub-periods. One more interesting thing is that in North America no significant warming rate was received even for the whole period.

Seasonal temperature trends for the last sub-period (1970–1992) are presented in *Table 3*. It is interesting that among significant cases the highest

Table 2. Temperature trends in °C/10 yr for the subperiods in D-J-F months

Region/subperiods	1890-1910	1900-1920	1910-1930	1920-1940	1930-1950	1940-1960	1950-1970	1960-1980	1970-1990	whole per.
Global	0.15	-0.09	0.11	0.03	0.08	-0.01	-0.03	-0.03	*0.34	*0.06
Northern Hemisphere	0.18	-0.08	0.09	0.04	-0.11	0.01	-0.04	-0.07	*0.39	*0.07
Southern Hemisphere	0.10	-0.09	0.17	-0.01	-0.02	-0.05	0.01	0.05	*0.21	*0.05
Europe	0.38	0.19	0.40	0.11	-0.13	0.34	-0.42	-0.08	0.15	*0.06
North Asia	0.31	0.04	-0.34	0.04	0.05	0.12	-0.15	-0.34	*1.00	*0.15
North America	0.41	-0.50	0.44	-0.14	-0.53	-0.02	-0.03	-0.19	0.57	0.02
North Africa	-0.20	0.03	0.17	-0.09	0.02	0.01	0.14	0.05	0.02	*0.03
South Asia	0.09	-0.11	0.01	0.06	-0.01	0.01	0.06	0.08	*0.35	*0.03
South Africa	-0.18	0.11	0.38	-0.02	0.02	-0.16	-0.01	-0.11	*0.32	*0.07
Oceania	-0.01	-0.08	-0.08	-0.01	0.14	0.07	0.06	0.17	0.09	0.01
South America	0.22	-0.04	0.02	0.14	-0.01	0.02	0.04	-0.07	*0.20	*0.07

Table 3. Seasonal temperature trends in °C/10 yr for the period of 1970-1992

Region/months	D-J-F	M-A-M	J-J-A	S-O-N
Global	*0.34	*0.31	*0.22	*0.19
Northern Hemisphere	*0.39	*0.33	*0.25	*0.21
Southern Hemisphere	*0.21	*0.25	*0.16	*0.16
Europe	0.15	0.24	0.14	0.23
North Asia	*1.00	0.39	*0.27	*0.29
North America	0.57	*0.40	*0.25	0.07
North Africa	0.02	*0.27	*0.33	*0.33
South Asia	*0.35	*0.29	*0.23	*0.27
South Africa	*0.32	*0.30	*0.28	*0.21
Oceania	0.09	*0.26	0.01	*0.22
South America	*0.24	*0.29	*0.13	*0.14

warming rate did not occur in winter months in every regions, e.g. in the Southern Hemisphere and South America the maximum occurs in M-A-M, not in J-J-A, which mean winter in the Southern Hemisphere. In spite of the fact that for the Northern Hemisphere significant trend exists for each seasons, it is not the same for each continent situating in the Northern Hemisphere. What can be stated is that in North America high values of temperature change occurred in the examined period in M-A-M and J-J-A, but not in the other months. In North Africa temperature increased a lot in each season except D-J-F, which was not significant. In the southern continents in most of the cases significant warming trends were found except for Oceania. However the seasonal differences are not high due to its geographical position. Comparing the two hemispherical results, it can be seen that the warming rate is higher in the north in each case.

A correlation coefficient had been determined between the rates of global, hemispherical and regional warming rates for the annual and seasonal averages. The results received for the annual averages and for the months D-J-F are summarized in *Table 4* and *Table 5*, where the comparison mostly focuses on the Northern Hemisphere, though Southern Hemisphere itself is also indicated. It can well be seen that the strongest relation exists between the global and hemispherical scales for both the annual and winter averages. Differences can be found between the correlation coefficients received for the northern continents. For the annual values North America correlates well with the global and hemispherical results. The next was found to be North Asia, then comes Europe: the correlation coefficient is only 0.559 between the Northern Hemisphere and Europe. However, the relation between Europe and North Asia seems to be stronger than that one between Europe and North America.

Table 4. Correlation coefficients between the warming rates of the sub-regions

	Global	N. Hemisph.	S. Hemisph.	Europe	N. Asia	N. America
Global	1.000	0.989	0.771	0.504	0.611	0.728
N. Hemisphere	0.989	1.000	0.673	0.559	0.651	0.734
S. Hemispere	0.771	0.673	1.000	0.122	0.298	0.499
Europe	0.504	0.559	0.122	1.000	0.476	0.154
North Asia	0.611	0.651	0.298	0.476	1.000	0.207
North America	0.728	0.734	0.499	0.154	0.207	1.000

Table 5. Correlation coefficients between the warming rates of the sub-regions for month D-J-F

	Global	N. Hemisph.	S. Hemisph.	Europe	N. Asia	N. America
Global	1.000	0.991	0.885	0.466	0.691	0.599
N. Hemisphere	0.991	1.000	0.814	0.511	0.738	0.592
S. Hemispere	0.885	0.814	1.000	0.250	0.426	0.553
Europe	0.466	0.511	0.250	1.000	0.486	0.036
North Asia	0.691	0.738	0.426	0.486	1.000	0.090
North America	0.599	0.592	0.533	0.036	0.090	1.000

4. Conclusions

Final statement can be summarized as follows:

(i) The global and hemispherical seasonal warming rates are exceeded by continental averages in each season. For the total period investigated, the following sub-regions show higher warming rates than the global and hemispherical averages: North Asia, South Africa and South America in D-J-F; North Asia, South Africa and South America in M-A-M; North America, South America and South Africa in J-J-A; South America in S-O-N.

(ii) The variation of trend with time has shown that cooling and warming periods occurred in each continent during the past 100 years. However, no significant trend was found in the sub-periods except the last one: 1970–1992. In months of D-J-F trends for the last sub-period show extremely high warming rate not only on global and hemispherical scales, but also in some regions. The seasonal variation of trend in the last sub-period shows maximum: in D-J-F on global and hemispherical scales, furthermore in North Asia, South Asia and South Africa; in M-A-M in North America; in J-J-A in North Africa; in S-O-N in North Africa.

(iii) The relations between warming trends for the various scales are very much different. Global and northern hemispherical trends correlate well, however the relations between the warming rates for the Northern Hemisphere and some continents (North America, North Asia) are not so remarkable. Very weak connection was found between the warming trends of the Northern Hemisphere and Europe. The same statement can be made for the correlation coefficients between Europe, North America and North Asia.

Finally it can be stated that the variability of the temperature change has a remarkable geographical and seasonal distribution. A very high and significant warming rate was found in the period of 1970–1992, however the relation between the warming trends for the various scales can not be explained. It means that the reason, i.e. the ratio of natural and anthropogenic factors influencing the variation of temperature, is still not clear.

Acknowledgements—The work has been supported by the Centre for Climate System Research, University of Tokyo during the author's visit in the Centre. The author wishes to extend her thanks for the support to the Centre, to *Prof. T. Matsuno*. Thanks are also extended to *Dr. Nitta*, *Dr. Nakajima* and *Dr. Baik* for their assistance.

References

Angell, J.K., 1988: Variations and trends in tropospheric and stratospheric global temperatures, 1958-87. *Journal of Climate 1*, 1296-1313.

Ghil, M. and *Vantard, R.*, 1991: Interdecadal oscillations and the warming trend in global temperature time series. *Nature 350*, 324-327.

Hansen, J. and *Lebedeff, S.*, 1987: Global trends of measured surface air temperature. *J. Geophys. Res. 92*, 13,345-13,371.

IPCC, 1996: *Climate Change 1995. The Science of Climate Change*. Contribution of Working Group I to the Second Assesment Report of the IPCC. Eds.: *J.T. Houghton, L.G. Meira Filho, B.A. Callender, N. Harris, A. Kattenberg* and *K. Maskell*. Cambridge University Press, Cambridge, U.K.

Jones, P.D., Wigley, T.M.L. and *Kelly, P.M.*, 1982: Variations in surface air temperatures: Part 1. Northern Hemisphere, 1881-1980. *Monthly Weather Review 2*, 59-70.

Jones, P.D., 1988: Hemispheric surface air temperature variations: recent trends and an update to 1987. *Journal of Climate 1*, 654-660.

Jones, P.D., 1994: Hemispheric surface air temperature variations; a reanalysis and update to 1993. *Journal of Climate 7*, 1794-1802.

Kelly, P.M., Jones, P.D., Sear, C.B., Cherry, B.S.G. and *Tavakol, R.K.*, 1982: Variations in surface air temperatures: Part 2. Arctic regions, 1881-1980. *Monthly Weather Review 2*, 71-83.

Nitta, T. and *Yoshimura, Y.*, 1993: Trends and interannual and interdecadal variations of global land surface air temperature. *J. Meteorol. Soc. Japan 3*, 367-375.

Trenberth, K.E., 1990: Recent observed interdecadal climate changes in the Northern Hemisphere. *Bull. Amer. Meteorol. Soc. 71*, 988-993.

IDŐJÁRÁS

Quarterly Journal of the Hungarian Meteorological Service
Vol. 101, No. 3, July–September 1997, pp. 173–179

Finite Markov model of long-term variations of precipitation

B. G. Vager[1] and **N. K. Serkov**[2]

[1]*Department of Calculating Mathematics,*
St. Petersburg State University of Architecture and Civil Engineering,
198005, 2nd Krasnoarmeiskaya, 4, St. Petersburg, Russia,
E-mail: BVager@compmath.abu.spb.ru

[2]*State Hydrological Institute,*
199053, 2nd liniya, V.O., 23, St. Petersburg, Russia

(Manuscript received 20 March 1996; in final form 3 January 1997)

Abstract—The finite Markov chain as a simple, robust and adequate model of long-term variations of hydrometeorological elements is suggested. The main mathematical foundations are given. Proposed techniques are illustrated with an example of annual precipitation series. The results of numerical experiments are in good agreement with observed data.

Key-words: Markov chain, factorization of state-continuous stochastic process, long-term variations, precipitation, wet (dry, normal) periods.

1. Introduction

At present mathematical methods and computers are widely used in all applied sciences including hydrometeorology. Therefore, the choice of an adequate and convenient mathematical technique is a problem of importance.

In this paper, we deal with the finite Markov chains which are convenient and effective tools for several concrete cases. The main construction in the theory of Markov chains is the transition matrix $\mathbf{P} = (p_{ij})$ whose elements are the conditional probabilities of process transitions from one state to another at the next moments. (Also, complex Markov chains may be considered. In this case a probability of current state j is suggested to be depending on k preceeding states $i_1, i_2, \ldots, i_k$, where $k > 1$.) There are many statistical criteria to decide if the given random sequence is a Markov chain or not (see, e.g. *Vager* and *Serkov*, 1995).

Reasonable classification of hydrometeorological processes, states and data for estimating transition probabilities are necessary to construct the finite Markov model. In an early stage of finite Markov chain applications the quality aspects of hydrometeorological phenomena such as synoptic positions, types of atmospheric circulation, wet and dry days etc. (*Sarymsakov et al.*, 1947; *Gabriel* and *Neumann*, 1962; *Weiss*, 1964) were analyzed.

On the other hand, finite Markov chain $C_m(t)$ with m states $\{1,2,\ldots,m\}$ can be obtained as a result of factorization of state-continuous stochastic process $X(t)$:

$$C_m(t) = i \quad \text{if} \quad a_{i-1} < X(t) \le a_i \quad (i = 1,\ldots m; \quad t = 0,1,\ldots), \tag{1}$$

where $a_0, a_1,\ldots, a_m$ are defined by the investigator:

$$-\infty = a_0 < a_1 \ldots < a_m = \infty.$$

This approach was used by *Babkin* and *Serkov* (1974). Authors suggested to consider the annual river runoff as a finite Markov chain. The values a_i can be chosen depending on the aim of the investigation. It should be considered that the number of states can not be too large. This number is limited by data available to estimate the transition probabilities.

Finite Markov chains have some advantages in comparison with other stochastic models (*Jeffers*, 1981):

(1) They are easy to construct based on experimental data.
(2) Profound knowledge of internal mechanisms of process under consideration is not required. Moreover, the analyses of models may reveal those aspects where such knowledge is important.
(3) The results of modeling may be easily presented in graphical form.
(4) The expense of computer time is not too much.

It may be added that "roughness" of finite models leads to statistical persistence (robustness) (*Huber*, 1981) of obtained estimators. It is especially important in case of short time series.

The main limitations are the sufficient volume of initial information required for statistical significant estimation of transition probabilities and independence of functional mechanisms of process in question.

The above mentioned items are considered in a monograph (*Serkov* and *Vager*, 1995) in more details.

Specific mathematical aspects of the Markov chain theory are considered in special mathematical literature (see e.g. *Romanovskiy*, 1949; *Feller*, 1957; *Aivazyan*, 1975; *Billingsley*, 1961) but not in this paper. Our aim was to illustrate how a relatively simple mathematical tool gives important climatological information.

Most of the valuable algorithms are coded in FORTRAN-77 in a program package for personal computers.

2. *Mathematical foundations*

For solving agrometeorological and other economical problems it is important to estimate the statistical properties of dry and wet periods.

A year is considered wet if the annual precipitation exceeds a given critical value, dry if it is less than another critical value and normal in between. It corresponds to the case $m = 3$ in Eq. (1).

The transition matrix is (p_{ij}) $(i,j = 1,2,3)$, where indices "1", "2" and "3" means dry, normal and wet states, respectively.

The matrix (non-stochastic) of corresponding standard deviations is denoted by (s_{ij}) $(i,j = 1,2,3)$, as

$$s_{ij} = [p_{ij}(1 - p_{ij})/n_i]^{1/2}, \tag{2}$$

where n_i is the number of state "i" (*Romanovskiy*, 1949).

Dry (wet, normal) period of length n is a sequence of n dry (wet, normal) years defined by non-wet (-dry, -normal) years at both sides. It is easy to show (see e.g. *Feller*, 1957) that the probability of the dry period having the length of n is equal to

$$Pn(1) = p_{11}^{n-1}(1 - p_{11}), \tag{3}$$

where $p_{11} = Pr\{1 \mid 1\}$ is the corresponding conditional probability. The mean length $n_m(1)$ of the dry period is equal to

$$n_m(1) = (1 - p_{11})^{-1}. \tag{4}$$

Similar formulae hold for normal and wet periods.

3. *An example*

The time series of annual precipitation amounts at the meteorological station of Cola (Murmansk region, Russia) during the years 1897–1981 was chosen for a numerical experiment (*Fig. 1*).

The mean of value EX is equal to 431 mm, standard deviation s = 94 mm. The critical values a_1 and a_2 in Eq. (1) were chosen as a_1 = EX - 0.5 s = 394 mm, a_2 = EX + 0.5 s = 478 mm.

Transition probabilities were estimated by the maximum likelihood method (*Romanovskiy*, 1949) resulting in the formula

$$p_{ij} = n_{ij}/n_i, \tag{5}$$

where n_{ij} is the number of transitions from "i" to "j", n_i is the sum of n_{ij}. The transition matrix obtained is

$$\begin{matrix} 0.40 & 0.32 & 0.28 \\ 0.33 & 0.43 & 0.24 \\ 0.09 & 0.59 & 0.32 \end{matrix}$$

and corresponding standard deviations (2) are

$$\begin{matrix} 0.10 & 0.09 & 0.09 \\ 0.08 & 0.08 & 0.07 \\ 0.06 & 0.10 & 0.10 \end{matrix}$$

It is evident that the values p_{ij} twice and more times larger than their standard deviations s_{ij}.

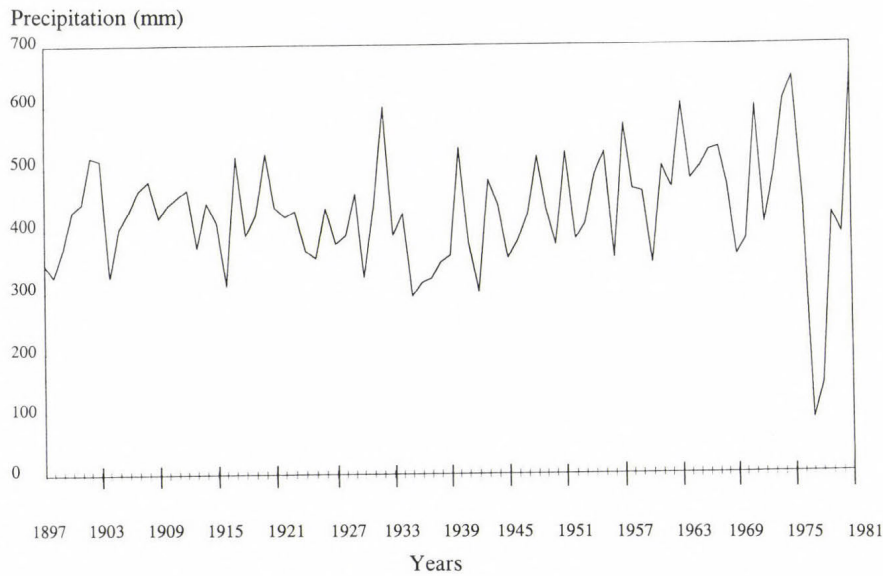

Fig. 1. The time series of annual precipitation at meteorological station Cola between 1897–1981.

The probability distribution of lengths of dry, normal and wet periods calculated with Eqs. (3) and (4) are presented in *Table 1*. (The datum in numerator is corresponding to formulae (3) and (4), and the one in denominator is corresponding to the empirical estimator.)

There is a good fit of the model to experimental values.

Table 1. The probability distribution of lengths of periods

i	1	2	3
p_{ii}	0.40	0.43	0.32
$P_1(i)$	0.60 — 0.60	0.57 — 0.48	0.68 — 0.80
$P_2(i)$	0.24 — 0.27	0.24 — 0.33	0.22 — 0.07
$P_3(i)$	0.10 — 0.07	0.11 — 0.14	0.07 — 0.07
$P_4(i)$	0.04 — 0.00	0.05 — 0.05	0.02 — 0.00
$P_5(i)$	0.02 — 0.07	0.02 — 0.00	0.01 — 0.07
$n_m(i)$	1.67 — 1.70	1.75 — 1.76	1.47 — 1.50

4. Concluding remarks

The long-range fluctuations of such hydrometeorological elements as runoff, precipitation, evaporation, air temperature and others were investigated in many papers reviewed by *Vager* and *Serkov* (1995). Among these investigations, the works of scientists of the State Hydrological Institute (St. Petersburg, Russia) are to mentioned especially (*Babkin* and *Serkov*, 1974; *Babkin et al.*, 1984; *Vuglinskiy et al.*, 1986; *Voskresenskiy et al.*, 1977; *Plitkin*, 1987; *Rumyantzev* and *Bovikin*, 1985 and others). The general conclusion is that results of these papers are in good accordance with prior ideas about long-range fluctuations of hydrometeorological elements.

The comparison of two models describing groups of years with low and high runoff was carried out by Serkov (see *Vager* and *Serkov*, 1995). These models were the two-states Markov chain and continuous-states *Ratkovich* (1976) models. It was shown that finite Markov chain parameters may be estimated more objective and statistically reliable. Moreover the former model leads to results which are corresponding better to available data.

Serkov (1991) developed existing method for statistical treatment of hydrological time series when zero values are in presence in order to take into

account the dynamic of a process in question. The author worked out a mixed Markov model combining the gamma-distribution and a constant equal to zero. So, the problem pointed out by *Kartvelishvili* and *Korganova* (1972) has been solved.

There are many ecological problems solved by the use of finite Markov chain techniques, i.e. weather forecasts, evaluation of atmosphere and runoff pollution, water supply, estimation of probability characteristics of low runoff periods etc. (see, e.g. *Romanof* and *Elekesh*, 1977; *Romanof* and *Tumanov*, 1993; *Serkov*, 1989 and others).

Kashyap and *Rao* (1976) note that more rough, more aggregative, more simple stochastic models may be in better accordance with experimental data in case of complex physical processes than too sophisticated models.

References

Ayvazyan, S.N., 1975: Statistical analyses of Markov chains (in Russian). Moscow.

Babkin, V.I. and *Serkov, N.K.*, 1974: Modeling of hydrological characteristics using Markov chains (in Russian). *Meteorology and Hydrology,* No. 7, 55-59.

Babkin, V.I., Vuglinskiy, V.S. and *Yudina, V.K.*, 1984: The regularities of long-range fluctuations of input and level at the Lake Baikal (in Russian). In *Hydrology of the Lake Baikal and other Reservoirs*. Novosibirsk, 110-118.

Billingsley, P., 1961: *Statistical Inference for Markov Processes*. Univ. Chicago Press, Chicago.

Feller, W., 1957: *Introduction to Probability Theory and its Applications*. 2d edition, New York. Wiley & Sons, London, Chapman & Hall.

Gabriel, K.P. and *Neumann, J.*, 1962: Markov chain model for daily rainfall occurrence at Tel-Aviv. *Quart. J. Royal Metal. Soc. 88*, No. 375, 90-95.

Huber, P.J., 1981: *Robust Statistics* (in Russian). Mir, Moscow.

Jeffers, J.N.R., 1981: *An Introduction to System Analysis: with Ecological Applications* (in Russian). Mir, Moscow.

Kartvelishvili, N.A. and *Korganova, N.S.*, 1972: Modern problems of stochastic hydrology (in Russian). *Water Resources 3*, 147-160.

Kashyap, R.L. and *Rao, A.R.*, 1976: *Dynamic Stochastic Models from Empirical Data*. Academic Press, New York.

Plitkin, G.A., 1986: Investigation of some regularities of forming and long-range river runoff resources fluctuations (in Russian). *Geography and Natural Resources 4*, 56-67.

Ratkovich, D.Ya., 1976: Long-term fluctuations of river runoff (in Russian). Gidrometeoizdat, Leningrad.

Romanov, N. and *Elecesh, N.*, 1977: On statistical dependence and robustness of some meteorological conditions having influence on an air pollution (in Russian). In *Meteorological aspects of atmospheric pollution,* Part 2, Leningrad, 80-85.

Romanov, N. and *Tumanov, S.*, 1993: Adapted Gaussian plume model characteristics and space-time structure of the estimated SO_2-concentration field due to elevated sources. *Időjárás 97*, 99-111.

Romanovskiy, V.I., 1949: *Discrete Markov Chains* (in Russian). Gostekhizdat, Moscow.

Rumyantzev, V.A. and *Bovikin, I.V.*, 1985: *Space-time Regularity in Runoff Fluctuations of Eurasian Rivers*. Nauka, Leningrad.

Sarymsakov, T.A., Dgordgio, V.A. and *Bugaev, V.A.*, 1947: On the weather formation at Central Asia (in Russian). *Reports of the USSR Acad. of Sci. 58*, 1949-1952.

Serkov, N.K., 1989: Finite Markov models (applications in hydroecology and the package of applied programs). *Theses of Coordinational Conference on Mathematical Modeling in Hydroecology*. Leningrad.

Serkov, N.K., 1991: Mixture Markov model of long-term fluctuations of periodically interrupted minimal river runoff (in Russian). *Transactions of the State Hydrological Institute, 355*, 72-76.

Vager, B.G. and *Serkov, N.K.*, 1995: *Finite Markov Chains in Meteorology and Hydrology* (in Russian). SPbGASU, St. Petersburg.

Voskresenskiy, K.P., Ivanova, I.B., Denisov, A.P. and *Savchenko, O.G.*, 1977: Water resources of the Trans-Caucasus (in Russian). *Transactions of the State Hydrological Institute*, 241, 88-98.

Vuglinskyi, V.S., Babkin, V.I., Gronskaja, T.N. and *Titova, T.E.*, 1986: On long-range characteristics computation of input to the main USSR HES reservoirs (in Russian). *Meteorology and Hydrology 8*, 89-93.

Weiss, L.L., 1964: Sequences of wet and dry days described by a Markov chain model. *Monthly Weather Rev. 92*, 169-176.

IDŐJÁRÁS

Quarterly Journal of the Hungarian Meteorological Service
Vol. 101, No. 3, July–September 1997, pp. 181–197

Acid rain in a squall line system in the Taiwan area: A numerical experiment

Ching-Sen Chen, Chuan-Yao Lin, Zen-Sing Deng and **Jing-Shiou Chen**

Institute of Atmospheric Physics, National Central University, Chung-Li, Taiwan, R. O. C.; E-mail: tchencs@storm.atm.ncu.edu.tw

(Manuscript received 12 April 1996; in final form 3 February 1997)

Abstract—In Taiwan acid rain has become one of the major environmental issues. The Environment Protection Administration of the Republic of China has set up ten stations around Taiwan island since April 1990. The average pH values from 1990 to 1994 indicated that a pH value of less than 5.0 was found in northern Taiwan where Taipei city and some industrial areas were located. As well, a station was set up in the mountainous area of central Taiwan away from both city and industrial areas, since April 1994. The mean pH value in April and May was 4.84. A cloud model with a terrain following coordinate system was used to simulate a squall line system which occurred in the Taiwan area. The model squall line passed through a polluted area where SO_2 and particulate dry sulfate were released. pH value was calculated following *Hegg et al.* (1984) and *Rutledge et al.* (1986) where the squall line system interacted with SO_2 and particulate dry sulfate. Simulation results indicated that the distribution of acid precipitation associated with the squall line system was influenced by the internal flow structure of the squall line system and the SO_2 and initial particulate sulfate profiles specified. Acid precipitation could be transported up to 100 km downstream following the precipitation system.

Key-words: acid rain, squall line, numerical study.

1. Introduction

The problem of acid rain has become one of major public concerns. Many research work has indicated that acid precipitation is widespread in Europe, in the northern United States and in southern China (*Likens* and *Bormann*, 1974; *Galloway et al.*, 1982; *Zhao et al.*, 1988). In Taiwan acid precipitation has emerged as a subject of increasing public attention since the living standard has increased so quickly. Some studies have indicated that precipitation with a pH value of less than 5 is very common on the western side of Taiwan island (*Sun* and *Wu*, 1980; *Lu et al.*, 1985). In order to obtain a better understanding of the

characteristics of acid rain in the Taiwan area, the *EPA* (Environment Protection Administration of the Republic of China) has, since April, 1990, set up ten stations (*Fig. 1*) around Taiwan island. Precipitation samples were collected automatically if precipitation occurred.

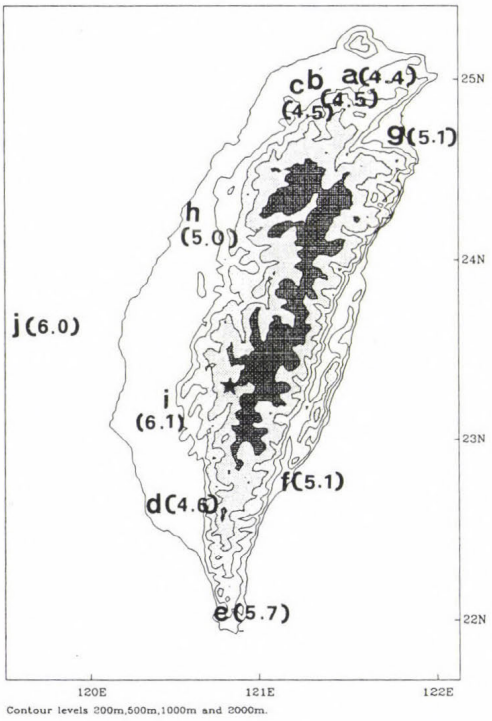

Fig. 1. The average pH value (inside the parenthesis) from April 1990 to March 1994 at ten stations (a through j) around Taiwan island. ★ denotes the mountain station set up in 1994.

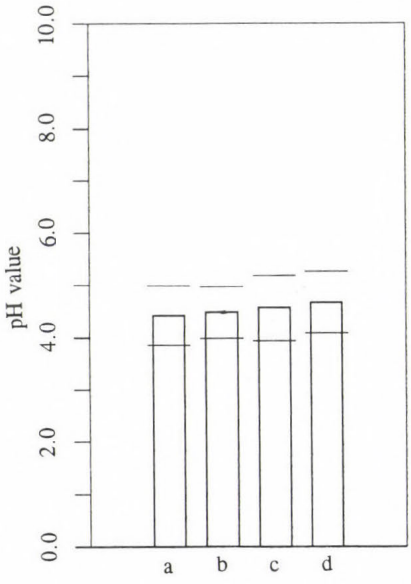

Fig. 2. The average pH value and standard deviation at stations: (a) Taipei, (b) Kuesan, (c) Chungli, (d) Kaohsiung.

The average pH value from April 1990 to March 1994 is shown in Fig. 1. pH values of less than 5.0 existed in northern Taiwan (Taipei, Kuesan and Chungli) and southern Taiwan (Kaohsiung). pH values of less than 4.0 in northern Taiwan were not unusual (*Fig. 2*). Taipei is the largest city in Taiwan and Kuesan, Chungli and Kaohsiung are the industrial cities. The pH values at the other six stations were larger than 5.0. The molar ratio of the $[SO_4^{2-}/NO_3^-]$ varied from 1.75 to 3.5 at those four sites. Thus sulfate was a major component of the acidity of precipitation in the Taiwan area. In order to find the pH value

in mountainous areas a station was set up, after April, 1994, in the Central Mountain Range about 100 km away from cities or industrial areas. The mean pH value in April and May was 4.84. A lower pH value can be found in eastern United State (pH value less than 4.2; *National Research Council*, 1983) and southern China (pH value about 4.0 in 1982/1984, Zhao et al., 1988). Thus the low pH value of acid precipitation in Taiwan is comparable to the values of these countries.

Taiwan is located near to southern Mainland China. As Mainland China is one of the major sources of SO_2 in Asia (*Akimoto* and *Narita*, 1994), the effect of SO_2 from Mainland China on acid rain in the Taiwan area cannot be ignored. However, Taiwan is also a source of SO_2 (*Akimoto* and *Narita*, 1994). Thus, the acid rain in Taiwan is certainly influenced by local sources. Therefore the first step to understand the characteristics of acid rain was to investigate how the locally released SO_2 influenced the pH value in a precipitation system. Another objective in this study was to see whether acid precipitation could occur about 100 km downwind of the polluted area. The precipitation system chosen in this study was a squall line system observed in northern Taiwan during the Taiwan Area Mesoscale Experiment (TAMEX) in 1987 (*Kuo* and *Chen*, 1990). Squall line systems usually occurred in the Taiwan area in spring every year (*Deng* and *Chen*, 1980). The squall line system that occurred in 1987 was well investigated by some studies (*Wang et al.*, 1990; *Lin et al.*, 1990; *Chen*, 1991). It was orientated in a north-south direction and propagated generally eastward from the Taiwan strait toward the island. Over the Taiwan strait, a front to rear inflow prevailed at all levels on the front side of the convective regions, while a shallow rear to front flow entered from the back of the squall line. New cells formed along the gust front in front of the squall line system and propagated into the squall line, thus prolonging the life time of the squall line. Its detailed structure was analyzed by *Wang et al.* (1990) and simulated by *Chen* (1991). Finally it became weaker in the mountain areas. In Wang et al., an area with radar reflectivity higher than 20 dBZ was found below 5 km, which corresponded to the melting level estimated from environmental sounding (*Fig. 3*). The maximum reflectivity was about 45 dBZ. In Chen's study, the basic dynamic of the squall line system did not differ substantially whether the ice phase microphysics was included or excluded. Thus we would not include ice phase microphysics in the current study of the first approximation. Here we try to use a dynamic model, including terrain, to simulate this squall line system numerically. Then we want to study the pH value in this squall line system when it passes through the polluted area in a numerical model. SO_2 and particulate sulfate were specified as the pollutants in the model. The interaction of SO_2 and particulate sulfate with cloud and rain obtained from a dynamic model produced sulfate and then the pH value could be calculated. Through this study we hope that we can attain a better understanding of the characteristics of pH values in a squall line system in the Taiwan area.

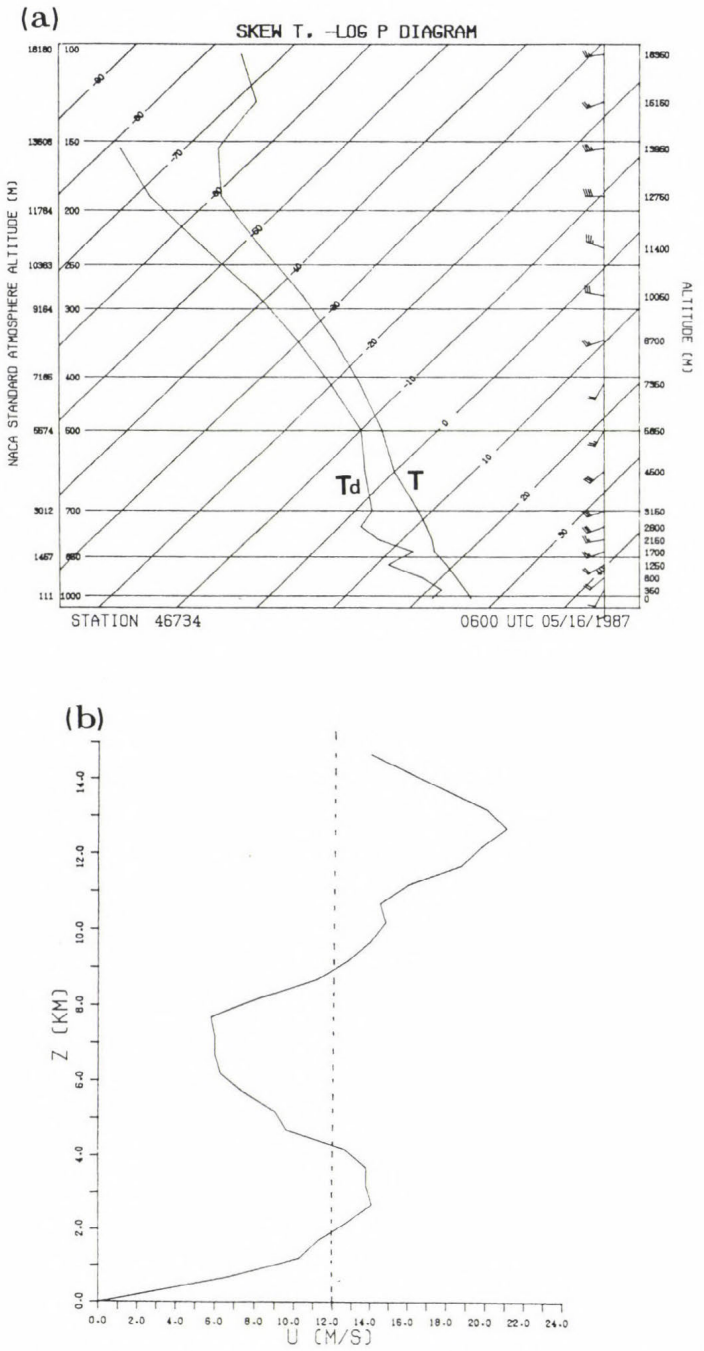

Fig. 3. (*a*): The initial temperature (T), moisture (T_d) and (*b*): wind profiles used in the model.

2. *Numerical simulation*

2.1 A brief description of the numerical model

A two-dimensional terrain-following coordinate cloud model was used to investigate orographic effects on the characteristics of a precipitation system moving from the plain toward the mountain. This model has been described in all the details by *Durran* and *Klemp* (1982). It was a two-dimensional version of *Klemp-Wilhelmson*'s (1978) cloud model with a terrain-following coordinate system introduced. In addition, a wave-absorbing layer was added to the top of the domain. Our study retained the same cloud and rainwater variables as in the Klemp-Wilhelmson model.

The base of the domain ($Z = 0$) and the surface pressure were assumed to be 0 m and 1000 hPa, respectively. The grid size in the x direction was constant and was taken to be 1.0 km, while in the z direction it was stretched vertically to allow for finer resolution in the lower atmosphere. There were 451 and 30 grid points in the horizontal and vertical directions, respectively. The time step was 4 seconds.

The model domain was 450 × 18.9 km. An 8.3 km thick sponge layer was assumed at the top of the model. The horizontal velocity, vertical velocity, non-dimensional pressure perturbation, potential temperature, and subgrid-scale mixing coefficient and the mixing ratio of water vapor, cloud water, and rainwater in the vertical direction were determined at levels whose locations are shown in *Table 1*. A more detailed description of the dynamic model structure is presented in the Appendix. The initial temperature, moisture conditions and the initial wind profile for the simulation are shown in Fig. 3. Their locations in the vertical direction for the terrain-following coordinate system were calculated by

$$\eta = \frac{Z_t (Z - Z_s)}{Z_t - Z_s},$$

where Z_t was the top of the domain (18.9 km). The terrain features (Z_s) used in the model are shown at the bottom of *Fig. 4*. The highest peak was 1.5 km in height at $x = 260$ km. Initially the observed east-west wind component was assigned everywhere in the model above the mountain top. Below the mountain peak, the wind gradually increased over 1.5 h from zero to the observed value of the sounding. Meanwhile, all the prognostic variables were integrated forward except for cloud and rain. Then we let the model adjust itself by integrating forward without considering any microphysical processes for another hour. The model time was reset to zero. At this time, low-level cooling was applied in a region 40 km away from the left boundary. This cooling area was 10 km wide and 3.8 km deep. The cooling rate was 0.01 K sec^{-1} and lasted for 10 minutes. All the parameters were taken from *Chen* (1991) in order to initi-

Table 1. The location of variables in the vertical direction. Vertical velocity is located at the ZRW position and all other variables are located at the ZRT position

Level	P (hPa)	ZRT(m)	ZRW (m)
30	71	18485	18031
29	83	17582	17138
28	96	16698	16263
27	112	15834	15409
26	129	14989	14573
25	148	14163	13758
24	169	13357	12961
23	192	12570	12184
22	216	11803	11426
21	242	11055	10688
20	269	10326	9969
19	298	9617	9270
18	329	8928	8590
17	360	8257	7929
16	393	7606	7288
15	428	6975	6666
14	463	6363	6064
13	500	5770	5481
12	538	5197	4918
11	577	4643	4374
10	616	4109	3849
9	656	3594	3344
8	697	3098	2858
7	738	2622	2391
6	779	2165	1944
5	821	1728	1516
4	861	1310	1108
3	902	911	719
2	942	532	350
1	981	173	0

alize the simulated squall line systems in the model. Then, a series of cells formed and moved eastward toward the mountainous area. The characteristics of the formation of series of cells were observed by *Wang et al.* (1990). Fig. 4 shows the maximum radar reflectivity in a vertical column varying with time. The radar reflectivity was derived from the mixing ratio of rain according to the model of *Fovell* and *Ogura* (1988). Over the plane area, the characteristics of radar reflectivity were similar to that in *Chen*'s results (1991). The precipitation over the top of the mountain was due to the lifting effect from the mountain on the moist air. At 120 min. the front edge of the squall line system was near to 140 km. Then we assumed there was a region of SO_2 located some distance

ahead of the squall line system (*Fig. 5*). The profiles for SO_2 were similar to *Hegg et al.* (1984) as follows:

$$q_{SO_2}(x,z,t=0) = q_{SO_2}(x_0,0)\, e^{-R/R_0} e^{-z/H} - q_{th},$$

where $q_{SO_2}(x,z,t=0)$ was the initial mixing ratio of SO_2 in the model, $q_{SO_2}(x_0,0)$ was the mixing ratio of SO_2 on the surface at $x = x_0$ km, H was the scale height, R_0 was the specified horizontal distance and R was the distance from (x_0) to any point in the model, horizontally. The q_{SO_2} was set to zero if it was negative. q_{th} was the threshold for q_{SO_2} being held in a specified area. Beyond this specified area, no pollution existed initially. Here we assumed that q_{th} was 10 μg kg^{-3}. Besides, R_0 and H were assumed to be 5 km. SO_2 was released in the model instantaneously. Then the interaction of the cloud and rain with q_{SO_2} was mainly taken from *Hegg et al.* (1984) and *Rutledge et al.* (1986). The interaction of solid precipitation particles with SO_2 in *Hegg et al.* and *Rutledge et al.* was not considered here, due to the secondary role of ice phase microphysics on the dynamic structure of the squall line system. The concentration of H_2O_2 and O_3 were also adapted from *Hegg et al.* as the profiles for H_2O_2 and O_3 were not available in Taiwan. The profiles for particulate sulfate were assumed to be similar to that of SO_2.

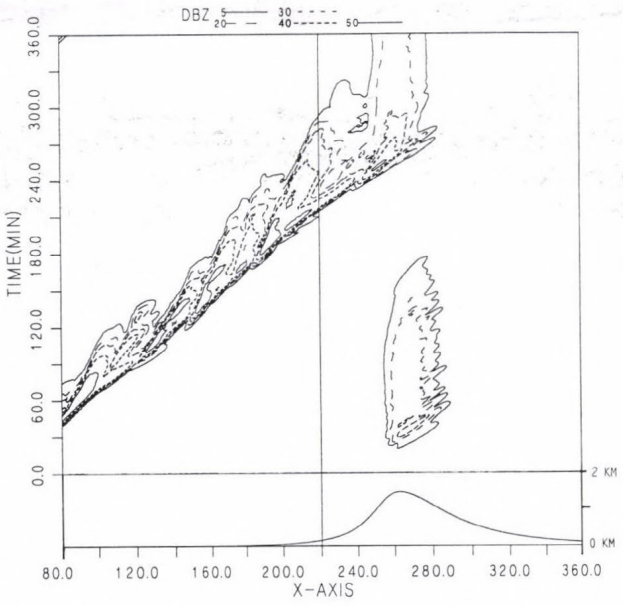

Fig. 4. The maximum radar reflectivity in a vertical column derived from the model results. The contours are 5, 20, 30, 40 and 50 dBZ. The terrain features used in the model are shown at the bottom of the figure.

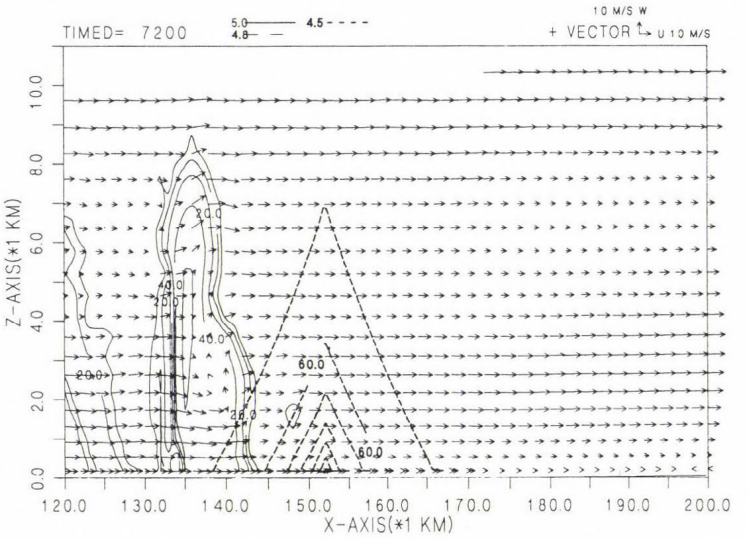

Fig. 5. The vertical cross section of radar reflectivity (solid line, contour intervals, 10 dBZ) and the mixing ratio of SO_2 (contour intervals, 50 μg kg^{-3}) at 120 min. of model time. The wind vectors relative to the ground are superimposed on the figure.

2.2 Simulation results

Seven initial q_{SO_2} profiles were considered. In experiment A, we assumed that the air was highly polluted. x_0 was assumed to be 151 km. It was about 8 km ahead of the front edge of the squall line at 120 min. (Fig. 5). q_{SO_2} was 393 μg kg^{-3} ($\approx$ 150 ppb) and no particulate sulfate was initially specified. In Taiwan the maximum daily average of SO_2 could reach this value in the industrial area (*EPA*, 1991). The 150 ppb value also appeared in Guiyang city in Mainland China (*Zhao et al.*, 1988). However 75 ppb of SO_2 (maximum daily average) could be found in the metropolitan area in Taiwan (*EPA*, 1991). The monthly mean sulfate was 8 (15) (μg kg^{-3}) for the metropolitan (industrial) area (*EPA*, 1991).

Since the formation of the new cell was in front of the squall line, the movement of the squall line system (14 m s^{-1} in the plain area) was faster than the environmental wind below 9 km in height, shown in Fig. 3. (*Wang et al.*, 1990, *Chen*, 1991). The whole squall line system could catch SO_2 originally, ahead of the squall line. The interaction of cloud and rain with SO_2 ahead of the squall line occurred first in a new cell at x near to 165 km at 150 min. (*Fig. 6a*). A region of rain water with a pH value of less than 5.0 extended upward. This was because part of the SO_2 in the low level was transported upward in the updraft area. Part of the SO_2 flew into the squall line system from the

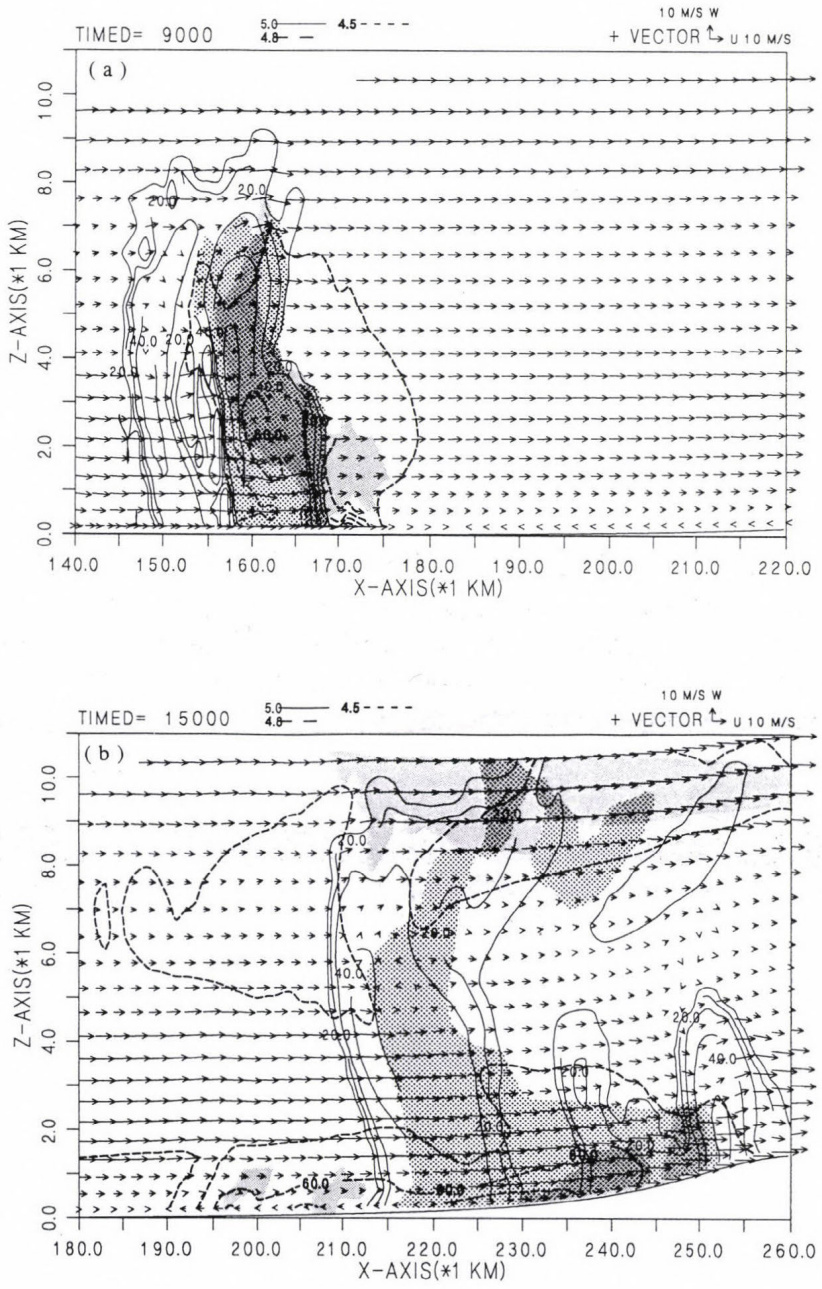

Fig. 6. The vertical cross section of radar reflectivity and mixing ratio of SO_2 like in Fig. 5. The shaded and dotted area represent the area with a pH value of less than 5.0 in both cloud and rain water, respectively. (*a*) 150 min. (*b*) 250 min.

forward side due to an inflow from the front relative to the squall line system (*Wang et al.*, 1990; *Chen*, 1991). This could help the formation of acid precipitation in the upper level. At this time some SO_2 was still located ahead of the squall line system. The acid rain area was about 10 km wide. The pH value in the cloud water had a similar pattern (Fig. 6a) but extended upward and backward from a low level near to the front side of the squall line following the airflow. As the squall line system moved toward the mountain slope at 220 min., most of the SO_2 was inside the precipitation area at the low level (figure not shown here). Some SO_2 was transported upward and backward from the squall line system. This was due to low level air flowing into the squall line from the front and going upward and backward relative to the squall line (*Wang et al.*, 1990; *Chen*, 1991). Thus part of the SO_2 was present on the backside of the squall line system in the upper level. Therefore acid precipitation with a pH value of less than 5 existed in the whole squall line system. The downdraft associated with the high reflectivity area could help the SO_2 to move downward toward the low level and spread toward the front and back sides. The area with a pH value of less than 5 in the cloud water could be found at the upper level as well as at the low level due to the existence of cloud and SO_2 in these two areas (figure not shown here). At 250 minutes of the simulation, the squall line system over the mountain slope became weaker. This was because the new cell in front of the squall line system did not grow strong enough to prolong the squall line system, while the old cell dissipated. Most of the SO_2 was traveling with the squall line system concentrated at the low levels (*Fig. 6b*). Low level SO_2 could not be transported upward easily due to the weak updraft. Therefore SO_2 moved with the airflow along the mountain slope and the horizontal area of acid rain increased. This acid rain region could extend toward the mountain when the squall line system moved over the mountain.

Fig. 7 indicates the variation of the minimum pH in rain water in a vertical column over time, for experiment A. A region with a pH less than 4.6 could extend from $x = 150$ km (where the initial q_{SO_2} was located) toward the mountain top. While areas with a pH less than 4.4 could extend 70 km from the plain toward the mountain slope. Before 180 min. the area with a lower pH value was located in the central part of the precipitation system where a high concentration of SO_2 and intensive rain were located (Fig. 6a). After 180 min. the area with a lower pH value was located on the front edge of the precipitation system, as intensive rain was found there (Fig. 6b). In experiment B, x_0 was changed to 161 km from experiment A more than 10 km distant from the squall line. It was designed to see how the separation distance between the pollution source and the precipitation system affected the property of the acid rain. Since the maximum q_{SO_2} initially specified was further away from the precipitation system, the pH value was slightly higher than in experiment A, but the pattern was similar (figure not shown). An area with a pH value of less than

4.6 could extend 60 km toward the mountainous slope areas, and a 4.7 pH value area could move further inland toward the mountain top. In experiment C, H was decreased to 2.5 km from experiment A. This meant that more SO_2 was concentrated near to the surface. The minimum pH in the vertical column was similar to the values of experiment A (figure not shown). In experiment D, the initial q_{SO_2} was reduced to 75 ppb with no sulfate specified initially. The pattern was similar to that in experiment A (Fig. 7) but the minimum pH value was higher in experiment D. An area with a pH value less than 4.7 could extend from $x = 150$ km near to the plain toward the mountain top. In experiment E, the initial SO_2 was assumed to be a quarter of the 393 μg kg^{-3} (or 38 ppb) but with no sulfate initially. The simulation results (figure not shown here) indicate that a pH value of less than 4.7 (4.8) could extend 40 km (70 km) downstream from $x = 150$ km. A pH value of less than 4.9 could be found in the sloped area half way to the top of the mountain.

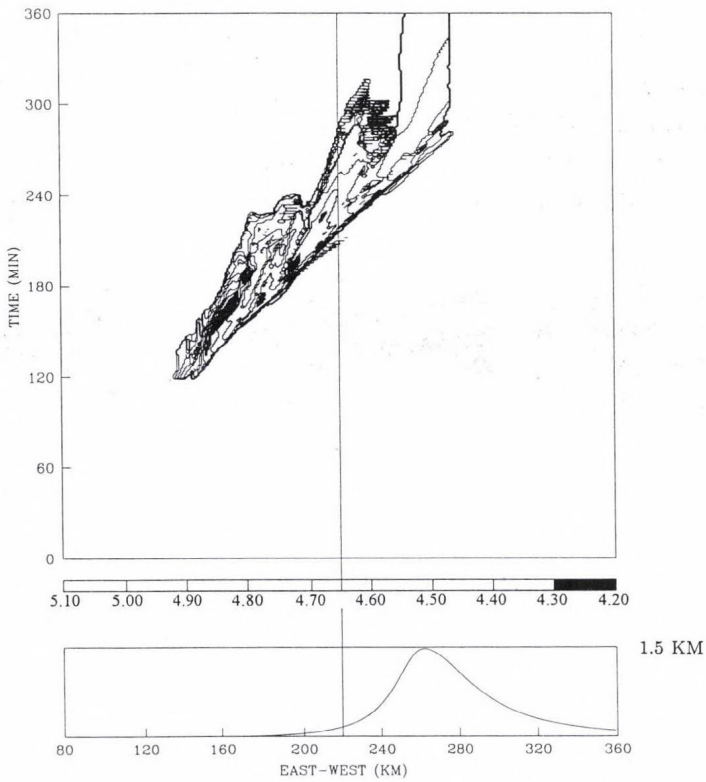

Fig. 7. The minimum pH value in a vertical column varying with time for experiment A. The various pH values are denoted by the different colors with the darker representing the lower pH value. The terrain features used in the model is shown at the bottom of the figure.

The experiment F is similar to experiment E but with additional particulate sulfate initially, with the maximum value of 10 μg kg^{-3}. The sulfate profile was the same as for SO_2. The minimum pH value in rainwater in a vertical column (*Fig. 8*) was similar to that in experiment E, but the pH value could be less than 4.6 near $x = 150$ km where the sulfate was released and near $x = 200$ km. No significant difference was found further away. The last experiment (experiment G) was designed to investigate the characteristics of acid precipitation when the model squall line encountered the "background" distribution of SO_2 and particulate sulfate. The distribution of background SO_2 and particulate sulfate were similar to that in *Hegg et al.* (1984) but the maximum value (near to the surface) of SO_2 and particulate sulfate were 20 μg kg^{-3} and 6 μg kg^{-3}, respectively. *Fig. 9* shows the minimum pH value in a vertical column over time, for experiment G. The minimum value for this case was similar to that in the previous one. But the area covered by pH value less than 5.0 was smaller in experiment G. This difference was attributed to the transportation of higher concentration of SO_2 to the back side of the squall line system in the previous case.

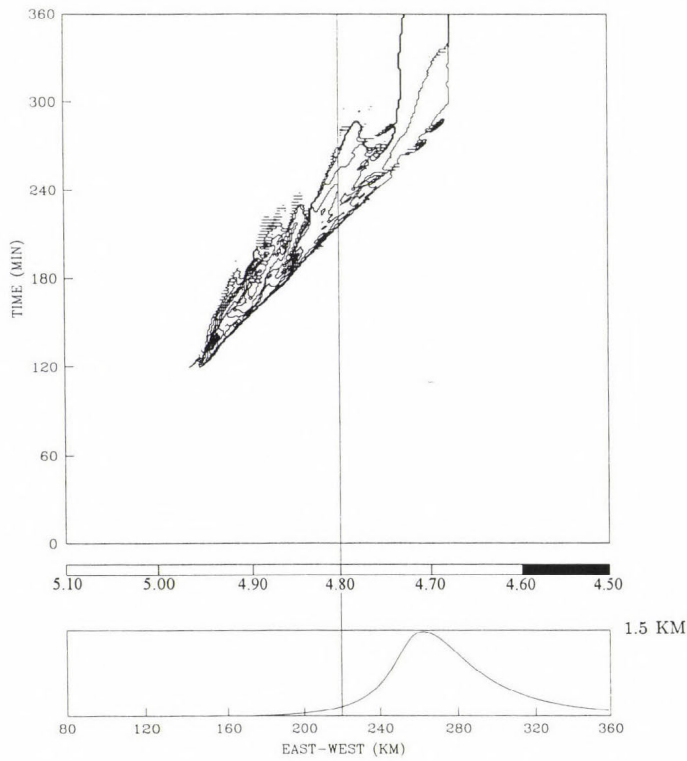

Fig. 8. Similar to Fig. 7 but for experiment F.

These seven experiments indicated that the pH value inside the squall line system was influenced by the internal flow structure and the distribution of both SO_2 and particulate sulfate. The lowest pH value in rain was strongly affected by the maximum of SO_2 concentration, particulate dry sulfate. Acid precipitation could be transported downstream over 100 km away from the pollutant area following the precipitation system. Thus acid rain occurring in mountainous areas in Taiwan was not unusual.

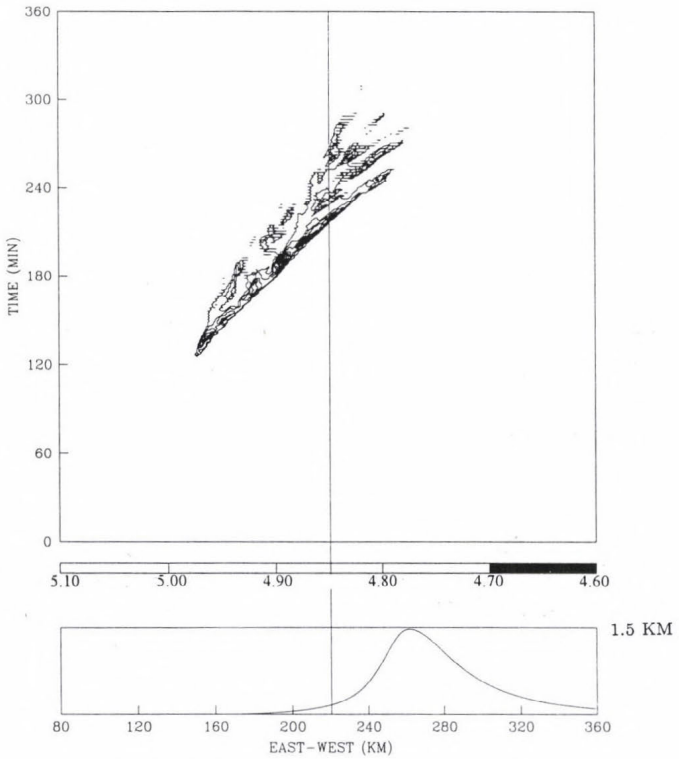

Fig. 9. Similar to Fig. 7 but for experiment G.

3. Conclusion

From ten stations around Taiwan island, we found that pH values of less than 5.0, averaged from four years of data (April 1990 to March 1994), existed at four stations. These four stations were either in Taipei, the largest city in Taiwan, or in industrial areas. A numerical model was employed to investigate the acid rain in a squall line system when it was assumed to pass through a

polluted area. Six different initial SO_2 and particulate sulfate profiles were assumed. These were determined by the maximum concentration of SO_2 or dry sulfate, the scale height of the SO_2 and sulfate, and the relative position of SO_2 and sulfate to the squall line system. The characteristics of acid rain inside the squall line system were influenced by the internal flow structure and the initial profiles of SO_2 and particulate sulfate. The decrease of the concentration of SO_2 by one-half and one quarter, the minimum pH value increased from 4.2 to 4.4 and 4.6, respectively. The initial particulate dry sulfate decreased the pH value near the source region. Acid precipitation could be transported 100 km downstream following the precipitation system.

In the future we will study the characteristics of acid rain in different precipitation systems in different seasons. The air flow inside the precipitation systems especially needs to be explored, either by observation or by simulation. Understanding the flow structure could help us to know the transportation effects of pollution on acid rain. Besides, the improvement of the dynamic and chemical model is also a very important task. For example, we need to consider nitrogen compounds in our chemical model to evaluate their effects on acid rain. To upgrade the observation data related to the acid rain is another challenge at the same time.

Acknowledgements—The reviewers' comments and suggestions were highly appreciated. This work was supported by the Environment Protection Administration of the Republic of China, under Grants EPA-83-E3F1-09-04. The computer resources were supplied by the Institute of Atmospheric Physics, National Central University, Chung-Li, Taiwan, R. O. C.

References

Akimoto, K. and *Narita, H.*, 1994: Distribution of SO_2, NO_x and CO_2 emissions from fuel combustion and industrial activities in Asia with $1° \times 1°$ resolution. *Atmospheric Environment 28*, 213-225.

Chen, C.-S., 1991: A numerical study of a squall line over the Taiwan strait during TAMEX IOP\#2. *Mon. Wea. Rev. 119*, 2677-2698.

Deng, Z.-S. and *Chen, C.-S.*, 1990: An analysis on the environment of squall line in Taiwan area. *Atmospheric Sciences 18*, 149-158 (in Chinese).

Durran, D.R. and *Klemp, J.B.*, 1982: The effects of moisture on trapped mountain lee waves. *J. Atmos. Sci. 39*, 2490-2506.

EPA (Environment Protection Administration of the Republic of China), 1991: The Annual Assessment Report of the Air Pollution Control in Taiwan area for 1991 (in Chinese).

Fovell, R.G. and *Ogura, Y.*, 1988: Numerical simulation of a midlatitude squall line in two dimensions. *J. Atmos. Sci. 45*, 3846-3879.

Galloway, J.N., Likens, G.E., Keene, W.C. and *Miller, J.M.*, 1982:The composition of precipitation in remote areas of the world. *J. Geophy. Res. 87*, 8771-8786.

Hegg, D.A., Rutledge, S.A. and *Hobbs, P.V.*, 1984: A numerical model for sulfur chemistry in warm-frontal rainbands. *J. Geophy. Res. 89*, No. D5, 7133-7147.

Klemp, J.B. and *Wihelmson, R.B.*, 1978: The simulation of three-dimensional convective storm dynamics. *J. Atmos. Sci. 35*, 1070-1096.

Kuo, Y.H. and *Chen, G.T.J.*, 1990: The Taiwan area mesoscale experiment (TAMEX): An overview. *Bull. Amer. Meteor. Soc. 71*, 488-503.

Likens, G.E. and *Bormann, F.H.*, 1974: Acid rain: A serious regional environmental problem. *Sciences 184*, 1176-1179.

Lin, Y.-J., Chen Wang, T.-C., Pusken, R.W., Shen, H. and *Deng, Z.-S.*, 1990: Characteristics of a subtropical squall line determined from TAMEX dual-Doppler data. PART II: Dynamic and thermodynamic structures and momentum budget. *J. Atmos. Sci. 47*, 2382-2399.

Lu, S.-C., Chen, F.-L. and *Miu, T.-C.*, 1985: The effect of air pollution on the pH value of rainwater over Taiwan area. *Atmospheric Sciences 2*, 69-72 (in Chinese).

National Research Council, 1983: *Acid Deposition Atmospheric Processes in Eastern North America: A Review of Current Scientific Understanding*. National Academy Press.

Rutledge, S.A., Hegg, D.A. and *Hobbs, P.V.*, 1986: A Numerial model for sulfur and nitrogen scavenging in narrow cold-front rainbands. 1. Model description and discussion of microphysical fields. *J. Geophy. Res. 91*, No. D13, 14385-14402.

Sun, Y.-C. and *Wu, R.-Y.*, 1980: The acid rain in the Taiwan area. *Scientific Development 8*, 428-434. Published by National Science Council, Rep. of China (in Chinese).

Wang, C.T.-C., Lin, Y.-J., Pasken, R.W. and *Shen, H.*, 1990: Characteristics of a subtropical squall line determined from TAMEX dual-Doppler data. Part I: Kinematic structure. *J. Atmos. Sci. 47*, 2357-2381.

Zhao, D., Xiong, J., Xu, Y. and *Chan, W.H.*, 1988: Acid rain in southwestern China. *Atmospheric Environment 22*, 349-358.

Appendix
Dynamic equations for the model

The model equations are cast in terrain-following coordinates (x,ζ) with

$$\xi = \frac{Z_t(Z - Z_S)}{Z_t - Z_S}, \tag{1}$$

where $Z_s = Z_s(x)$ is the height of the terrain above $Z = 0$ and Z_t is the height of the top of the model. The three tensor transformation terms used to describe the equations in the (x, ζ) coordinate system are

$$H^* = G^{\frac{1}{2}} = \frac{\partial \xi}{\partial z} = \frac{Z_t}{Z_t - Z_S}. \tag{2a}$$

$$G^{13} = \frac{\partial \xi}{\partial x} \frac{(\xi - Z_t)}{(Z_t - Z_S)} \tag{2b}$$

Using the above expressions, the momentum equations can be written as

$$\frac{\partial u}{\partial t} + C_p \bar{\theta}_v \left[\frac{\partial \pi}{\partial x} + G^{13} \left(\frac{\partial \pi}{\partial \xi} \right) \right] = A\tilde{D}X + \tilde{D}_u K_m, \tag{3a}$$

$$\frac{\partial w}{\partial t} + C_p \bar{\theta}_v \left[H^* \left(\frac{\partial \pi}{\partial \xi} \right) \right] = A\tilde{D}Z + q \left[\frac{\theta}{\bar{\theta}} - 1 + 0.64 \, (q_v - \overline{q_v}) \right] + \tilde{D}_w K_m, \quad (3b)$$

where

$$\theta_v = \theta (1 + 0.61 \, q_v), \quad (4a)$$

$$A\tilde{D}X = -u \left[\frac{\partial u}{\partial x} + G^{13} \left(\frac{\partial u}{\partial \xi} \right) \right] + wH^* \left(\frac{\partial u}{\partial \xi} \right), \quad (4b)$$

$$A\tilde{D}Z = -u \left[\frac{\partial w}{\partial x} + G^{13} \left(\frac{\partial w}{\partial \xi} \right) \right] + wH^* \left(\frac{\partial w}{\partial \xi} \right), \quad (4c)$$

$$\begin{aligned} \tilde{D}_u = {} & \frac{\partial}{\partial x} \left[2 \left(\frac{\partial u}{\partial x} + G^{13} \left(\frac{\partial u}{\partial \xi} \right) \right) - \frac{2}{3} \left(\frac{\partial u}{\partial x} + G^{13} \frac{\partial u}{\partial \xi} + H^* \frac{\partial w}{\partial \xi} \right) \right] \\ & + G^{13} \frac{\partial}{\partial x} \left[2 \left(\frac{\partial u}{\partial x} + G^{13} \left(\frac{\partial u}{\partial \xi} \right) \right) - \frac{2}{3} \left(\frac{\partial u}{\partial x} + G^{13} \frac{\partial u}{\partial \xi} + H^* \frac{\partial w}{\partial \xi} \right) \right] \\ & + H^* \frac{\partial}{\partial \xi} \left(H^* \frac{\partial u}{\partial \xi} + \frac{\partial w}{\partial} x + G^{13} \frac{\partial w}{\partial \xi} \right), \end{aligned} \quad (5a)$$

$$\begin{aligned} \tilde{D}_w = {} & \frac{\partial}{\partial x} \left(H^* \frac{\partial u}{\partial \xi} + \frac{\partial w}{\partial x} + G^{13} \frac{\partial w}{\partial \xi} \right) + G^{13} \frac{\partial}{\partial \xi} \left(H^* \frac{\partial u}{\partial \xi} + \frac{\partial w}{\partial x} + G^{13} \frac{\partial w}{\partial \xi} \right) \\ & + H^* \frac{\partial}{\partial \xi} \left[2 H^* \frac{\partial w}{\partial \xi} - \frac{2}{3} \left(\frac{\partial u}{\partial x} + G^{13} \frac{\partial u}{\partial \xi} + H^* \frac{\partial w}{\partial \xi} \right) \right], \end{aligned} \quad (5b)$$

θ is the potential temperature, q_v, q_c, and q_r are the mixing ratio of water vapor, cloud water and rain water, respectively, and θ_v is the virtual potential temperature. Bars over individual variables refer to the initial undisturbed state.

In Eqs. (3a) and (3b) the eddy mixing coefficient K_m is estimated according to *Lilly* (1962). The first law of thermodynamics is taken to be

$$\begin{aligned} \frac{\partial \theta}{\partial t} = {} & - \left[\left(u \frac{\partial \theta}{\partial x} + u G^{13} \frac{\partial \theta}{\partial \xi} \right) + H^* \left(w \frac{\partial \theta}{\partial \xi} \right) \right] + \left(\frac{\partial}{\partial x} + G^{13} \frac{\partial}{\partial \xi} \right) \left[K_h \left(\frac{\partial \theta}{\partial \xi} + G^{13} \frac{\partial \theta}{\partial \xi} \right) \right] \\ & + H^* K_h \left(\frac{\partial}{\partial z} \frac{\partial \theta}{\partial \xi} \right), \end{aligned} \quad (6)$$

where K_h is the eddy diffusivity of heat. The value of K_h is assumed to be three times of K_m in this study. The pressure equation model takes the form

$$\frac{\partial \Pi}{\partial t} + \frac{\overline{C}^2}{C_p \overline{\theta}_v}\left[\frac{\partial u}{\partial x} + G^{13}\left(\frac{\partial u}{\partial \xi}\right) + \frac{H}{\overline{\rho}}\frac{\overline{\partial \rho w}}{\partial \xi}\right] = 0 \tag{7}$$

and Exner function Π is the non-dimensional pressure in the form $\left(\frac{P}{P_0}\right)^{\frac{R_d}{C_p}}$. Here P_0 is the base state pressure at ground level and R_d is the gas constant for dry air. C is the speed of sound.

The mixing ratio of water vapor, q_v, mixing ratio of cloud water, q_c, and the mixing ratio of rain water, q_r, are considered in the model. The equations for q_v, q_c, q_r are

$$\frac{\partial q_v}{\partial t} = -\left[\left(u\frac{\partial q_v}{\partial x} + uG^{13}\frac{\partial q_v}{\partial \xi}\right) + H^*\left(w\frac{\partial q_v}{\partial \xi}\right)\right] + \left(\frac{\partial}{\partial x} + G^{13}\frac{\partial}{\partial \xi}\right)\left[K_h\left(\frac{\partial q_v}{\partial x} + G^{13}\frac{\partial q_v}{\partial \xi}\right)\right.$$

$$\left. + H^*\frac{\partial}{\partial \xi}\left(K_h H\frac{\partial q_v}{\partial \xi}\right)\right], \tag{8}$$

$$\frac{\partial q_c}{\partial t} = -\left[\left(u\frac{\partial q_c}{\partial x} + uG^{13}\frac{\partial q_c}{\partial \xi}\right) + H^*\left(w\frac{\partial q_c}{\partial \xi}\right)\right] + \left(\frac{\partial}{\partial x} + G^{13}\frac{\partial}{\partial \xi}\right)\left[K_h\left(\frac{\partial q_c}{\partial x} + G^{13}\frac{\partial q_c}{\partial \xi}\right)\right]$$

$$+ H^*\frac{\partial}{\partial \xi}\left(K_h H\frac{\partial q_c}{\partial \xi}\right), \tag{9}$$

$$\frac{\partial q_r}{\partial t} = -\left[\left(u\frac{\partial q_r}{\partial x} + uG^{13}\frac{\partial q_r}{\partial \xi}\right) + H^*\left(w\frac{\partial q_r}{\partial \xi}\right)\right] + \left(\frac{\partial}{\partial x} + G^{13}\frac{\partial}{\partial \xi}\right)\left[K_h\left(\frac{\partial q_r}{\partial x} + G^{13}\frac{\partial q_r}{\partial \xi}\right)\right]$$

$$+ H^*\frac{\partial}{\partial \xi}\left(K_h H\frac{\partial q_r}{\partial \xi}\right). \tag{10}$$

IDŐJÁRÁS

Quarterly Journal of the Hungarian Meteorological Service
Vol. 101, No. 3, July–September 1997, pp. 199–213

A case study on generation, conversion and dissipation of kinetic energy during the Bay of Bengal depression of 4-8 July 1979

R. K. Singh[1] and **U. S. Singh**[2]

[1]*Agrometeorology Section,*
G.B. Pant University of Agriculture and Technology, Hill Campus,
Ranichauri-249 199, Tehri-Garhwal, India

[2]*Department of Geophysics, Banaras Hindu University,*
Varanasi-221005, India

(Manuscript received 8 February 1995; in final form 19 July 1996)

Abstract—The vertical motion was obtained through the solution of the omega equation at 200, 400, 600 and 800 hPa surfaces over the Indian region for a depression over the head of the Bay of Bengal using MONEX-1979 data at 1.875 deg. lat/long grid resolution. Using velocity components as input, generation, conversion and dissipation of zonal and eddy kinetic energy have been computed at different isobaric surfaces. The zonal kinetic energy shows decreasing trend with altitude, with a minimum at 400 hPa and a maximum at 200 hPa which may be associated with the jet stream. The downward transfer of eddy kinetic energy from the upper to the middle troposphere seems to be a vital source of kinetic energy in the middle troposphere. Effects of the depression were observed to increase the eddy kinetic energy in the lower troposphere. The dissipation of kinetic energy throughout the atmosphere with a minimum at about the 400 hPa surface has been observed.

Key-words: kinetic energy, synoptic feature, monsoon depression.

1. Introduction

The southwest monsoon is generated due to the uneven heating of land and ocean during the summer. Usually 5 to 8 disturbances develop over the Bay of Bengal and the Arabian Sea at a frequency of 2 to 3 per month during the SW monsoon. Lows, depressions or deep depressions all are cyclones with moderate winds, they only differ in their wind intensity within the distance of 250 km from the center. Depressions follow northerly or northwesterly paths and play a very important role in bringing copious rain along its track over the Indian region. They are often associated with synoptic features of horizontal

convergence and upward vertical motion in the lower troposphere followed by horizontal divergence in the upper troposphere near to and in advance of the depression center. At the rear of the center, the horizontal divergence and the vertical motion become reversed. Movement and deviation of the depression mainly depend upon the generation, conversion and dissipation of zonal and eddy kinetic energy in the atmosphere. Hence, the study of generation, conversion and dissipation of kinetic energy during the depression period is of vital importance over the Indian region. In the past, several investigations have been made on the energy budget of the atmosphere over the Indian region including *Rao* and *Rajamani* (1968), *Keshavamurty* and *Awade* (1970), *Rao* and *Rajamani* (1970, 1972), *Rao et al.* (1978), *Singh et al.* (1980), *Desai* (1986), *Rajamani* and *Kulkarni* (1986) and *Masters* and *Kung* (1986). *Anjaneyulu* (1971) estimated the kinetic energy over the Indian monsoon trough zone and found that the Indian monsoon trough zone is an exporter of kinetic energy in the upper troposphere. *Mandal et al.* (1981) studied the kinetic energy budget of a cyclone over the Arabian Sea in June 1979. *Saha* and *Saha* (1988) discussed the thermal budget of this depression.

In this paper, an attempt has been made to study the generation, conversion and dissipation of zonal and eddy kinetic energy at different isobaric surfaces in the atmosphere to present the analysis of the energetics of a depression of 4–8 July formed over the Bay of Bengal during MONEX 1979, at a grid resolution of 1.875° lat/long which has never been attempted in the past over the Indian region.

2. Weather and associated synoptic feature

Out of the several charts for contour analyses of the observed height and wind fields from the 100 hPa through the 1000 hPa surfaces, it has been considered adequate to present the charts for the observed contour heights (*Fig. 1*) at 100 hPa, 500 hPa, and 900 hPa surfaces on the 5 to 8 July 1979 at 12.00 UTC only for better understanding, because these charts are helpful to illustrate the position of the low and its trend during the occurrence of the disturbance. It has been observed that a region of low pressure with associated cyclonic circulation extending to the middle troposphere entered the northeastern part of the Bay across the Arakan Coast on 4 July. It was stationary without appreciable development until the 6 July, and then concentrated into a depression in the morning on 7 July with its center at 03.00 UTC near to 19.5°N, 89.5°E about 400 km east-southeast of Paradip (20°N, 87°E). Moving westwards it crossed the northern part of the Orissa Coast near Paradip in the afternoon of 8 July. The track of monsoon depression are shown in *Fig. 2*. Moving west-northwestwards, the depression weakened into a low over northwest Madhya Pradesh by the 10 July and merged with seasonal trough on 11 July. The

system was probably a deep depression till the morning of 8 July. Upper N/NE winds of 30–40 kt up to 0.9 km above sea level was reported on 8 July in the morning at Bhubaneswar. From the dropsonde reports of the research aircrafts of MONEX, which flew over the depression field on 7 July, it is seen that the depression sloped southwestwards by about 3 degrees of latitude between the surface and 500 hPa. The monsoon was generally weak over Assam and its adjacent states and over West Bengal during the week. It was active to vigorous over Orissa on 7 and 8 July and in Madhya Pradesh on 8 and 9. Moderate heat wave conditions prevailed over many parts of Uttar Pradesh and Bihar on 7 and 8 July.

The interesting point about this sequence of events was (a) an initial northward movement followed by (b) a rapid westward movement of the depression. There was a considerable difference in the position of the cyclonic velocity maximum on 4 July between 700 and 900 hPa. But later, this tended to even up.

3. Data and area of computation

As part of the FGGE level-IIIb data base, special grid point data sets for 12.00 UTC at 1.875 deg. lat/long grid resolution were obtained from the European Centre for Medium Range Weather Forecasts (ECMWF) for the Indian region at 100 hPa, 300 hPa, 500 hPa, 700 hPa, 850 hPa and 1000 hPa surfaces for the period 4–8 July 1979. The area of computation extends from 9.4 to 30°N and 69.4 to 101.3°E. There are 18 grid points in the zonal direction and 12 grid points in the meridional direction.

A cubic interpolation technique was applied to interpolate the grid point data to the 900 hPa surface using the wind data for the 100 hPa, 300 hPa, 500 hPa, 700 hPa, 850 hPa and 1000 hPa surfaces, thus resulting in input fields at the 100 hPa, 300 hPa, 500 hPa, 700 hPa and 900 hPa surfaces, which were used to compute the vertical velocity at the 200 hPa, 400 hPa, 600 hPa and 800 hPa surfaces, respectively.

4. Method of computation

The ECMWF analyses of u, v fields have been used to solve the nonlinear reverse balance equation (*Singh* and *Singh*, 1990) including the Jacobian and beta terms for the calculation of the geopotential and solenoidal wind fields U_ψ and V_ψ at the 100 hPa, 300 hPa, 500 hPa, 700 hPa and 900 hPa surfaces. These were considered as input fields for solving the omega equation at the 200 hPa, 400 hPa, 600 hPa and 800 hPa surfaces (*Singh* and *Singh*, 1992a).

The basic equations were used in deriving the formulae for various forms of energy and their transformation based on *Lorenz*'s (1955) formulation. The rate of change of zonal and eddy kinetic energy may be expressed as

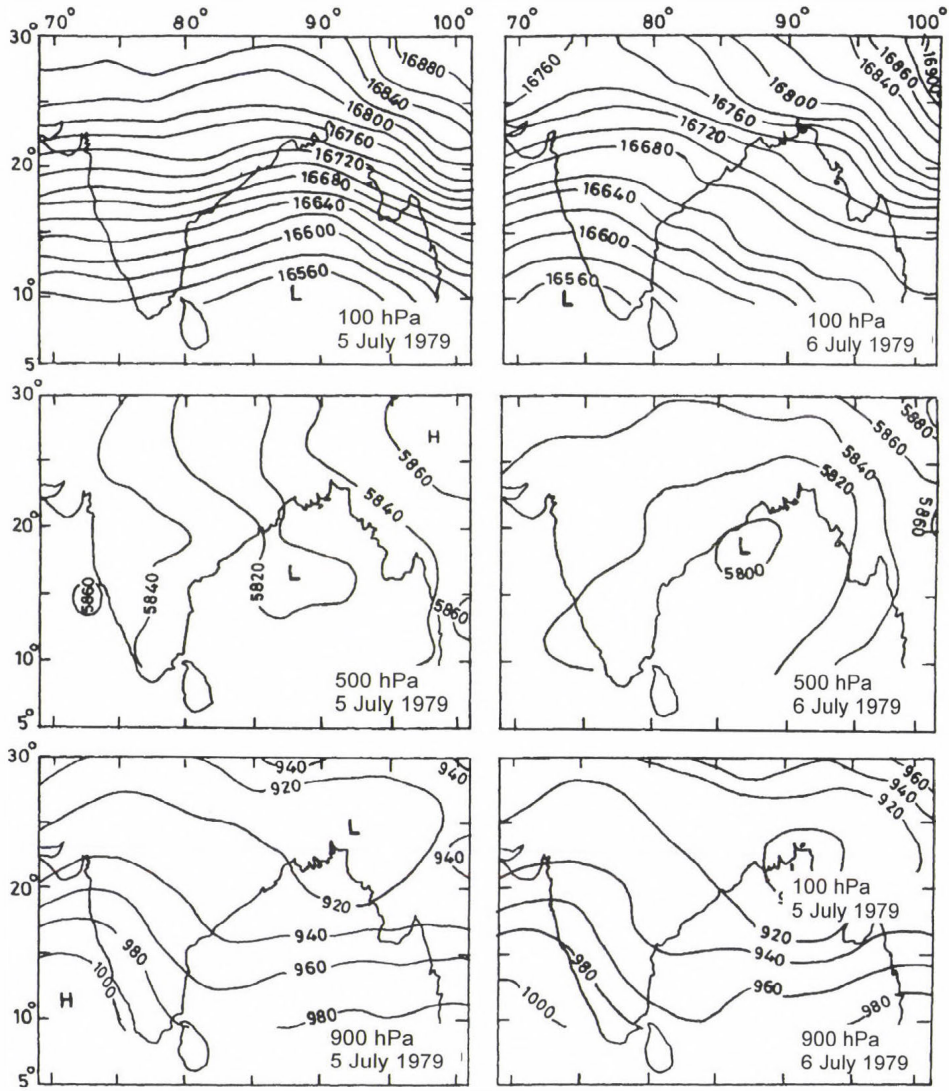

Fig. 1a. Observed contours in GPM at different isobaric surfaces on 5 and 6 July, 1979 (12.00 UTC).

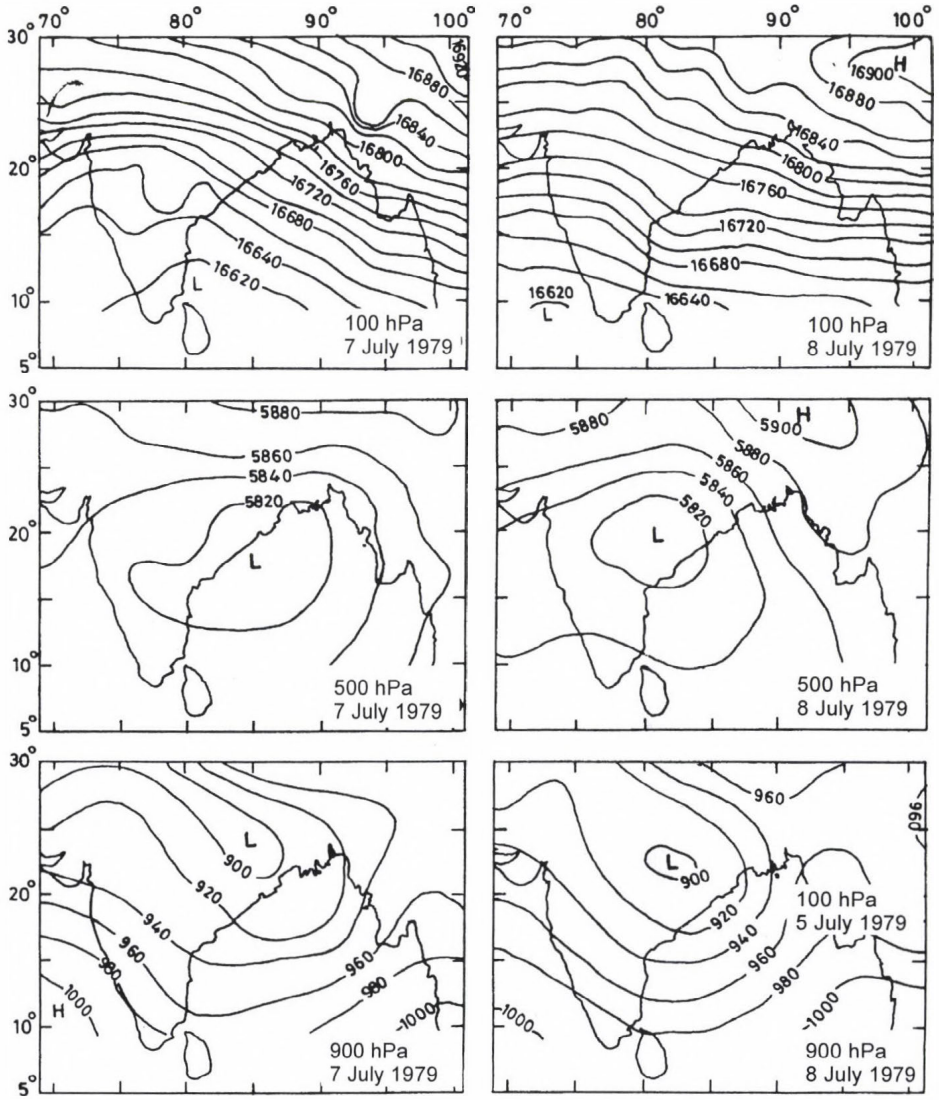

Fig. 1b. Observed contours in GPM at different isobaric surfaces on 7 and 8 July, 1979 (12.00 UTC).

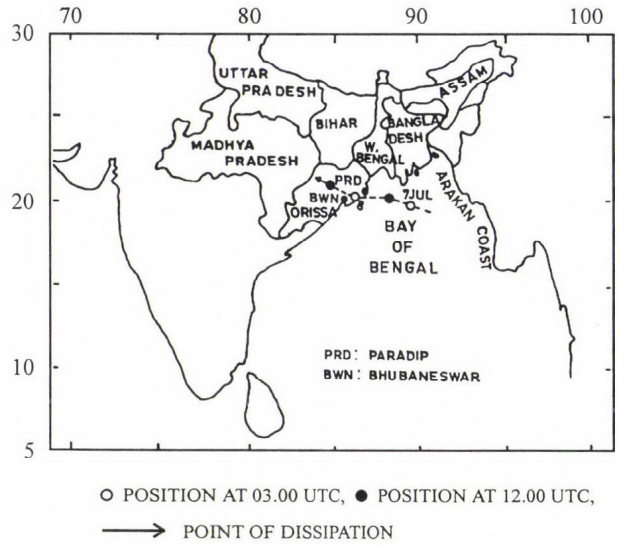

Fig. 2. Track of the Bay of Bengal depression of 4–8 July 1979.

$$\frac{\delta K_Z}{\delta t} = C_Z - C_k - D_Z, \tag{1}$$

$$\frac{\delta K_E}{\delta t} = C_E + C_K - D_E. \tag{2}$$

The various energy terms are defined as:

$$K_Z = \frac{1}{2} \int_M ([U]^2 + [V]^2)\, dM, \tag{3}$$

$$K_E = \frac{1}{2} \int_M ([U^{*2}] + [V^{*2}])\, dM, \tag{4}$$

$$C_Z = - \int_M [\omega]'' [\alpha]''\, dM, \tag{5}$$

$$C_E = \int_M [\omega^* \alpha^*]\, dM, \tag{6}$$

$$C_K = -\int_M [U^* V^*] \cos\phi \frac{\delta}{a\delta\phi}([U]\cos^{-1}\phi)\,dM - \int_M [V^{*2}]\frac{\delta[V]}{a\delta\phi}\,dM$$

$$+ \int_M [U^{*2}][V]\frac{\tan\phi}{a}\,dM - \int_M [U^*\omega^*]\frac{\delta}{\delta P}[U]\,dM - \int_M [U^*\omega^*]\frac{\delta}{\delta P}[V]\,dM, \quad (7)$$

$$D_Z = \int_M ([U][F_\lambda] + [V][F_\phi])\,dM, \quad (8)$$

$$D_E = \int_M ([U^* F_\lambda^*] + [V^* F_\phi^*])\,dM. \quad (9)$$

where F_ϕ and F_λ are the longitudinal and latitudinal components of the frictional force expressed as (*Oliger et al.*, 1970)

$$F_\lambda = \frac{\delta T_\lambda}{\delta Z} + F_{\lambda H}, \qquad F_\phi = \frac{\delta T_\phi}{\delta Z} + F_{\phi H}, \quad (10)$$

where T_λ and T_ϕ are the longitudinal and latitudinal components of the Reynold's stress. They are expressed as

$$T_\lambda = \rho K_{MV}\frac{\delta U}{\delta Z}, \qquad T_\phi = \rho K_{MV}\frac{\delta V}{\delta Z}, \quad (11)$$

where K_{MV} is the vertical kinematic eddy viscosity. The formulation of the horizontal eddy viscosity terms $F_{\lambda H}$ and $F_{\phi H}$ was obtained from *Smagorinsky* (1963).

Energy integrals are denoted as follows:

$$[X] = \frac{1}{(\lambda_1 - \lambda_2)}\int_{\lambda_1}^{\lambda_2} X\,d\lambda \qquad : \text{zonal mean},$$

$$\bar{X} = \frac{1}{A}\int_{\lambda_1}^{\lambda_2}\int_{\phi_1}^{\phi_2} X\,d\lambda\,d\phi \qquad : \text{areal mean},$$

$$X = [X] + X^* = X'' + \bar{X},$$

$$[X]'' = [X] - \bar{X},$$

where A is the area considered, X is any arbitrary function, [ ] represents the zonal mean, (-) the areal mean, * represents the deviation from the zonal mean, and [ ]" the perturbation in the zonal mean field upon its areal mean.

5. *Advection of energy terms*

Since we have performed the computations over a limited region it is necessary, as pointed out by *Smith* (1969), to compute the advection of energy terms. *Rao* and *Rajamani* (1972) and *Pandey et al.* (1989) computed the fluxes at the boundary and noted that even for a depression, the horizontal advection of available potential energy and kinetic energy may be safely neglected. We have also computed the fluxes at the boundary which were observed to be insignificant.

6. *Discussion of results*

Fig. 3 shows the vertical distribution of zonal (K_Z) and eddy (K_E) kinetic energy on 5, 6 and 7 July 1979, 12.00 UTC at the 200 hPa, 400 hPa, 600 hPa and 800 hPa surfaces, respectively. The vertical profile for the zonal kinetic energy indicates that it decreases from the 800 hPa to the 400 hPa surface where it becomes minimum. The westerlies of the lower troposphere weaken with height and changes to easterlies above 400 hPa (usually in the mid troposphere) where the winds and as such the kinetic energy have minimum values. Above 400 hPa the kinetic energy increases gradually up to the 200 hPa surface. In general, the zonal kinetic energy is larger than the eddy kinetic energy at each level in the vertical with a minimum at about 400 hPa. *Kida* (1977), *Pagnotti* and *Bosart* (1984), *Rajamani* and *Kulkarni* (1986) noted that the zonal kinetic energy is larger than the eddy kinetic energy. The sharp increase of the zonal kinetic energy above 400 hPa is due to the combined effects of sub-tropical westerly and tropical easterly jets. The eddy kinetic energy above 400 hPa is smaller than the zonal kinetic energy as the perturbations in the upper troposphere are extremely small. In the lower and middle troposphere we noted a gradual decrease in the zonal as well as in the eddy kinetic energy from 800 hPa to 400 hPa. This is because of the gradual decrease in the south-westerly current (monsoon current) along with the embedded depression in the lower troposphere/on the surface. *Kung* (1966) found maximum generation of kinetic energy by pressure forces to be strongest near the jet stream level. A secondary maximum exists in the planetary boundary layer, where larger temperature contrasts and strong ageostrophic components of motion are found. As the westerly decreases with height and becomes easterly around an anticyclonic circulation situated in the upper troposphere over the Indian peninsula during the period of the study, the lowest value of the zonal kinetic energy seems to occur due to this reason. The eddy kinetic energy distribution in the lower troposphere showed a marginal increase from 5 to 7 July as the depression intensified on 7 July.

Fig. 4 shows the vertical distribution of the zonal (C_Z) and the eddy (C_E) conversion of available potential energy to kinetic energy on 5, 6 and 7 July 1979, 12.00 UTC at the 200 hPa, 400 hPa, 600 hPa and 800 hPa surfaces,

respectively. We note that there was a conversion from zonal available potential energy to zonal kinetic energy above 400 hPa on 5 July and a conversion from zonal kinetic energy to zonal available potential energy below 400 hPa. This changed on 5 and 7 July from A_Z to K_Z below 400 hPa and K_Z to A_Z above 400 hPa. Thus, during the active phase of the depression, the conversion was from K_Z to A_Z on 5 July, then it was changed and the energy was converted from A_Z to K_Z on 6 and 7 July in the lower and middle troposphere. Thus, the effects of the depression on the active days (6th and 7th) were noted to introduce a conversion of energy from $K_E \rightarrow A_E \rightarrow A_Z \rightarrow K_Z$ in the lower and middle troposphere.

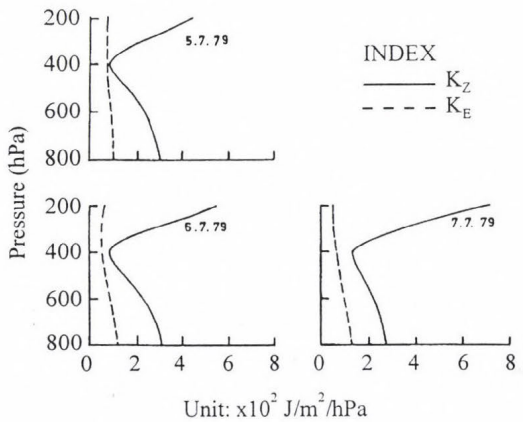

Fig. 3. Vertical distribution of zonal and eddy kinetic energy from 5 to 7 July 1979 (12.00 UTC).

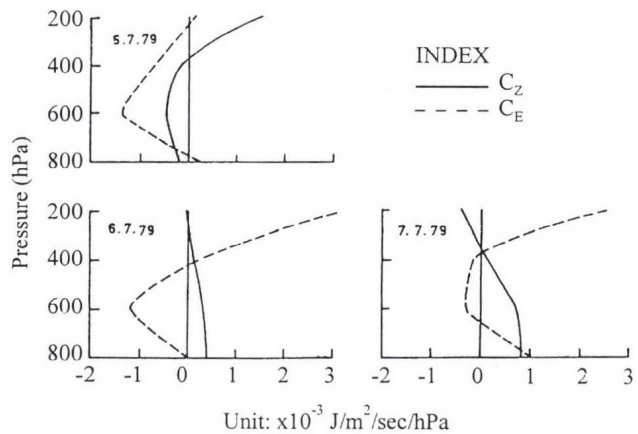

Fig. 4. Vertical distribution of C_Z and C_E from 5 to 7 July 1979 (12.00 UTC).

The conversion from eddy kinetic energy to eddy available potential energy on 5 July had a maximum at 600 hPa and from 800 to 200 hPa the eddy kinetic energy was acting as a source of eddy available potential energy. On the following days, i.e. on 6 and 7 July, the region of negative conversion in the middle troposphere was decreased above 400 hPa and below 600 hPa it changed to a positive value indicating that the eddy kinetic energy drew its energy from the eddy available potential energy as the depression became active on 7 July.

In the middle troposphere there was a conversion of eddy available potential energy to zonal available potential energy (*Singh* and *Singh*, 1992b; Fig. 4 a-c). This loss of eddy available potential energy was maintained by the eddy kinetic energy which was acting as a source for its conversion from eddy kinetic energy to eddy available potential energy around 600 hPa. Thus, in the middle troposphere we note that the mean flow drew its potential energy from A_E, and A_E drew its energy from K_E. *Kung* (1966) noted that there must be a downward transfer of kinetic energy from the upper to the middle troposphere. Through this result it seems there must have been a transfer of eddy kinetic energy from the lower as well as the upper troposphere to the mid-troposphere.

Fig. 5 shows the vertical distribution of each component of C_K, namely C_{K1} through C_{K5}, along with the sum of these components on 5, 6 and 7 July 1979, 12.00 UTC at the 200 hPa, 400 hPa, 600 hPa and 800 hPa surfaces, respectively. It was observed that the contribution of C_{K3} was insignificant at each level in the vertical during the life cycle of the depression. Positive values of the conversion from zonal to eddy kinetic energy in C_{K1} were observed in the layer between 450 hPa and 200 hPa on 5 July which indicated that the transfer of momentum due to eddies happened along the gradient of the meridional wind whereas below 450 hPa it was against the gradient with a peak at 600 hPa extending up to the 750 hPa surface. The horizontal transfer of momentum was gradually penetrating downward in the middle and upper troposphere along the gradient of the meridional wind on 6 and 7 July with the depth of penetration up to 700 hPa on 7 July with a maximum around 400 hPa. *Masters* and *Kung* (1986) observed large generation of K_E due to a cross isobaric flow in the upper troposphere. The contribution of C_{K2} was also significant and mostly negative from 5 to 7 July, except on the 7th between 350 hPa and 600 hPa, where it showed a positive value, indicating that, in general, the meridional transfer of mean meridional momentum was against the gradient of meridional wind throughout the atmosphere, except on the active phase of the depression what was observed on 7 July in the middle troposphere. The contribution of C_{K4} illustrates the vertical transfer of zonal momentum which was mostly upward between 800 hPa and 200 hPa with minima in the middle troposphere showing a downward transfer on the 7 July around 600 hPa. This seemed to be due to the strong sinking motion at 600 hPa on 7 July between 90°E to 100°E longitude and 10°N to 30°N latitude (*Singh* and *Singh*, 1992a).

The contribution of C_{K5} is dependent upon the vertical transfer of the mean meridional momentum which shows that on 5 July it was throughout upward with a maximum at 600 hPa, which continued on 6 July with a change over to upward in the lower and upper troposphere. On 7 July it was dominated by an upward transfer of the mean meridional momentum from 800 hPa to 400 hPa. The combined effects of the transfer of momentum showed that on 5 July, between 800 hPa and 400 hPa, the meridional transfer of momentum due to eddies was against the gradient of the meridional wind. The eddy kinetic energy acted as a source of zonal kinetic energy below 400 hPa resulting in a barotropically stable atmosphere. This continued on 6 July also, whereas on 7 July from 800 hPa to 600 hPa the eddy kinetic energy was acting as a source of zonal kinetic energy indicating that this atmospheric layer was barotropically stable, while between 650 hPa and 200 hPa the zonal kinetic energy was acting as a source of eddy kinetic energy resulting in barotropic instability in the middle and upper troposphere. Thus, we conclude that in the lower and middle troposphere which was barotropically stable, the eddy kinetic energy was acting as a source of K_Z, whereas in the upper troposphere above 400 hPa, where K_Z acted as a source of K_E, barotropically unstable conditions prevailed gradually strengthening the barotropic instability in the middle and upper troposphere. Besides that, the effects of the depression were observed to increase the conversion from K_E to K_Z from 5 to 7 July in the lower troposphere. *Masters* and *Kung* (1986) also noted that the upper troposphere acts as an important energy source by the significant downward transport of kinetic energy to mid-troposphere.

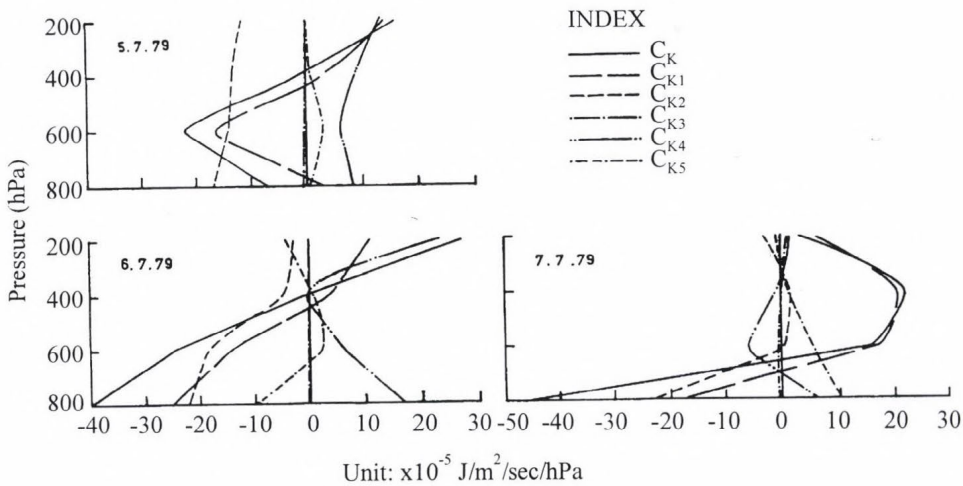

Fig. 5. Vertical distribution of C_K with its components from 5 to 7 July 1979 (12.00 UTC).

Fig. 6 shows the vertical distribution of zonal (D_Z) and eddy (D_E) dissipation of the kinetic energy on 5, 6 and 7 July 1979, 12.00 UTC at the 200 hPa, 400 hPa, 600 hPa and 800 hPa surfaces, respectively. It can be seen that the maximum dissipation of the eddy kinetic energy is at 800 hPa on 5 July with a gradual decrease in its magnitude up to 400 hPa, which further shows gradual increase in zonal and eddy dissipation of kinetic energy in the upper troposphere. Each day we observed a larger eddy dissipation as compared to the zonal dissipation in the lower and middle troposphere, whereas in the upper troposphere the zonal dissipation of kinetic energy exceeded the eddy dissipation of kinetic energy during the active phase of the depression, i.e. 7 July. In the lower troposphere, the larger number of eddies as well as the zonal dissipation of kinetic energy seemed to be due to the vertical diffusion of the momentum, whereas in the upper troposphere the horizontal diffusion was responsible for the gradual increase in the zonal and eddy dissipation of the kinetic energy.

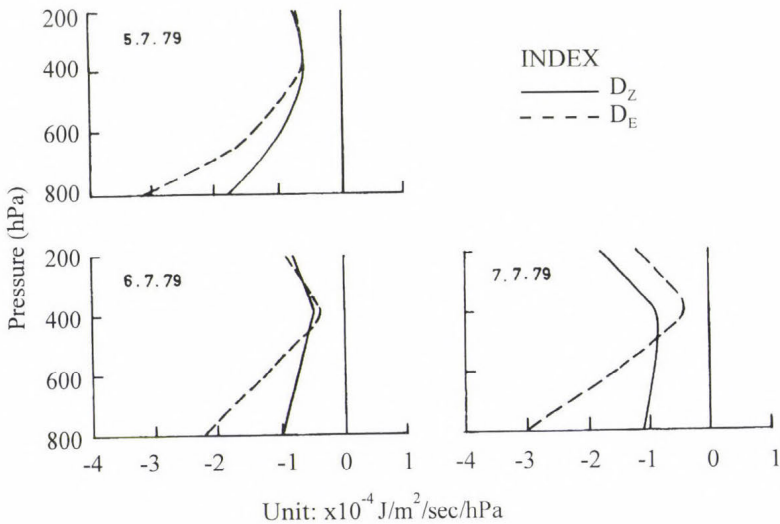

Fig. 6. Vertical distribution of D_Z and D_E from 5 to 7 July 1979 (12.00 UTC).

7. Summary

From our study it may be concluded that:

(1) The zonal kinetic energy decreases with height in the vertical during the life cycle of the depression, resulting in a minimum at 400 hPa. Then it increases with a maximum at 200 hPa, which seems to be associated with the jet stream. Above 400 hPa the eddy available potential energy

acts as a source of the eddy kinetic energy, whereas in the middle troposphere, the eddy kinetic energy is transferred to eddy available potential energy. Hence, the downward transfer of kinetic energy from upper to middle troposphere appears to be an important mechanism to supply the eddy kinetic energy in the middle troposphere. Besides that, a decrease in the loss of eddy kinetic energy or an increase in the gain of eddy kinetic energy results in the lower troposphere due to the effects of the depression as the conversion tends to become positive or reduce the magnitude of a negative C_E. This results in the zonal conversion from potential energy to kinetic energy associated with the meridional overturning, the warm air is associated with the rising motion and the cold air with the sinking motion.

(2) The depression generally introduces a conversion of eddy available potential energy to eddy kinetic energy, which results in an increase in the amount of conversion from A_E to K_E or in a change of the existing direction of conversion from K_E to A_E into A_E to K_E in the lower troposphere, whereas in the upper troposphere this positive conversion is due to effects of the anticyclonic circulation above 400 hPa, resulting in a strong subsidence and hence cooling. In the zonal form of energy conversion, the depression introduces a conversion from K_Z to A_Z during the active phase of the depression in the lower and middle troposphere.

(3) The zonal and eddy dissipation of kinetic energy takes place due to the frictional forces throughout the atmosphere. In the lower troposphere, larger dissipation of the zonal and eddy kinetic energy was noted which may be due to the vertical diffusion of momentum and the subgrid scale mixing. However, in the upper troposphere, the larger dissipation of kinetic energy must be due to the horizontal diffusion of momentum. The minimum dissipation of zonal as well as eddy kinetic energy was observed at the 400 hPa surface where zonal and eddy kinetic energy was being minimum.

(4) A gradual strengthening of barotropic instability in the middle and upper troposphere and a barotropic stability in the lower troposphere was observed during the life cycle of the depression.

Acknowledgements—The authors express their appreciation to *R. N. Maurya* for his help during the preparation of the manuscript, and to *Shri P. K. Chaterjee* for neatly typing the manuscript.

References

Anjaneyulu, T.S.S., 1971: Estimates of kinetic energy over the Indian monsoon trough zone. *Q. J. R. Meteor. Soc. 97*, 103-109.

Desai, D.S., 1986: Study of energetics of strong and break monsoon. *Mausam 37*, 365-367.

Keshavamurty, R.N. and *Awade, S.T.*, 1970: On the maintenance of the mean monsoon trough over North India. *Mon. Wea. Rev. 98*, 315-319.

Kida, H., 1977: A numerical investigation of the atmospheric general circulation and stratospheric-tropospheric mass exchange: I. Long term integration of a simplified general circulation model. *J. Meteor. Soc. Japan 55*, 52-70.

Kung, E.C., 1966: Kinetic energy generation and dissipation in the large scale atmospheric circulation. *Mon. Wea. Rev. 94*, 67-82.

Lorenz, E.N., 1955: Available potential energy and the maintenance of the general circulation. *Tellus 7*, 157-167.

Mandal, G.S., Rao, R.V.R.K. and *Gupta, S.C.*, 1981: Characteristics of an Arabian Sea cyclone. *Mausam 32*, 139-144.

Masters, S.E. and *Kung, E.C.*, 1986: An energetics analysis of cyclonic development in the Asian winter monsoon. *J. Meteor. Soc. Japan 64*, 35-51.

Oliger, J.E., Wellck, R.E., Kasahara, A. and *Washington, W.M.*, 1970: Description of NCAR global circulation model. *NCAR Technical Notes-56 + STR*. National Center for Atmospheric Research, Boulder, Colorado, 94.

Pagnotti, V. and *Bosart, L.*, 1984: Comparative diagnostic case study of east coast secondary cyclogenesis under weak versus strong synoptic scale forcing. *Mon. Wea. Rev. 112*, 5-30.

Pandey, S.N., Chattopadhyay, J. and *Singh, U.S.*, 1989: Studies of energy during strong and weak monsoon situations over India. *Mausam 40*, 417-420.

Rajamani, S. and *Kulkarni, J.R.*, 1986: On some energy aspects of the monsoon depression during its life cycle. *Mausam 37*, 9-16.

Rao, K.V. and *Rajamani, S.*, 1968: Diagnostic study of a monsoon depression by geostrophic baroclinic model. *Sci. Rep.* No. 54. India Met. Dep., 1-26.

Rao, K.V. and *Rajamani, S.*, 1970: Diagnostic study of a monsoon depression by geostrophic model. *Indian J. Meteor. Geophys. 21*, 187-194.

Rao, K.V. and *Rajamani, S.*, 1972: Study of heat sources and sinks and the generation of available potential energy in the Indian region during the southwest monsoon season. *Mon. Wea. Rev. 100*, 383-388.

Rao, K.V., Rao, G.S.P. and *Rajamani, S.*, 1978: Diagnostic study of a monsoon depression. *Indian J. Meteor. Geophys. 29*, 260-272.

Saha, K.R. and *Saha, S.*, 1988: Thermal budget of a monsoon depression in the Bay of Bengal during FGGE-MONEX-1979. *Mon. Wea. Rev. 116*, 342-354.

Singh, U.S. and *Singh, R.K.*, 1990: Solution of the balance equation over the Indian monsoon region. *Proc. Indian Nat. Sci. Acad. 56A*, 55-62.

Singh, U.S. and *Singh, R.K.*, 1992a: Vertical motion and diabatic heating over the Indian monsoon region during the Bay of Bengal depression of 5-8 July, 1979. *Pure Appl. Geophys. 138*, 115-133.

Singh, U.S. and *Singh, R.K.*, 1992b: Study of available potential energy of a depression pattern in the region of Bay of Bengal. *Időjárás 96*, 93-105.

Singh, S.S., Kulkarni, A.A. and *Bandyopadhyaya, A.*, 1980: The kinetic energy budget of monsoon circulation over the Indian region during ISMEX-1973. *Pure Appl. Geophys. 119*, 16-23.

Smagorinsky, J., 1963: General circulation experiments with the primitive equations: I. The basic experiment. *Mon. Wea. Rev. 91*, 99-164.

Smith, P.J., 1969: On the contribution of a limited region to the global energy budget. *Tellus 21*, 202-207.

List of symbols

a	—	radius of earth
C_K	—	transformation from zonal to eddy kinetic energy
C_Z , C_E	—	zonal and eddy conversion of available potential energy to kinetic energy
D_Z , D_E	—	zonal and eddy dissipation of kinetic energy
dM	—	mass increment
dP	—	pressure increment
dt	—	time increment
F_λ , F_ϕ	—	frictional forces per unit mass along the zonal and meridional direction.
K_Z , K_E	—	zonal and eddy kinetic energy
M	—	mass of the atmosphere
U, V	—	zonal and meridional component of wind
ω	—	vertical velocity
α	—	specific volume
λ, ϕ	—	longitude, latitide.

IDŐJÁRÁS

Quarterly Journal of the Hungarian Meteorological Service
Vol. 101, No. 3, July–September 1997, pp. 215–231

Solar radiation characteristics at Qena/Egypt

Sayed M. El-Shazly[1], **A. M. Abdelmageed** and **M. El-Noubi Adam**

Department of Physics, Faculty of Science,
South Valley University, Qena/Upper Egypt, E-mail: svalleyu@frcu.eun.eg

(Manuscript received 1 December 1995; in final form 24 June 1996)

Abstract—Measurements of the hourly global solar radiation (G) and its diffuse component (D) on a horizontal surface have been carried out in Qena/Upper Egypt in the period from June 1992 to May 1993. The corresponding diffuse fraction (D/G) is calculated. Diurnal variations of the results have been studied. Also the daily total values and their monthly and seasonal averages as well as their frequency distributions were computed and examined. The seasonal and climatic effects on the fluctuation of the results are discussed. These effects were particularly large during spring and winter months owing to the high fluctuation of the atmospheric conditions with respect to cloud amounts, water content, and concentration of aerosol dust particles. The influence of clouds has small effect on the results. The relative reduction of global solar radiation by cloud over the whole period is around 4.5% due to the low degree of cloudiness in the study region. The relation between the diffuse fraction and clearness index (G/G_0) shows that most of the points lie in the region of the high availability of the incoming solar radiation.

Key-words: global radiation, diffuse radiation, diffuse fraction, monthly and seasonal variations, effect of clouds, clearness index, radiation climate.

1. Introduction

Over the past years, a decided need for additional solar radiation data has arised due to the increased use of solar energy systems. The detailed knowledge of these data is of fundamental importance to the successful development of projects for the practical utilization of solar energy by agriculturists, hydrologists, architects and engineers, particularly in the region where sunshine is available in abundance (*Atwater* and *Ball*, 1981; *Moriarity*, 1991; *Kuye* and *Jagtap*, 1992; *Neuwirth*, 1980).

[1]Corresponding author

Qena is a city of abundant solar radiation along most of the months of the year. Accordingly, it would appear to be well suited to the use of solar energy in different application owing to the interest, which this form of clean energy presents to solve the energy demand problem. In this concern we attempt in this study to provide solar radiation information for designers of solar energy utilization systems under the climatic conditions of Qena/Egypt, which may also serve as a useful reference for system designers and users in other regions with similar climatic conditions.

2. General climate of Qena/Egypt

Qena is located in the south part of Egypt at latitude 26°10'N, longitude 32°43' E and elevation 78 m above sea level. Climatically, Qena lies within the subtropical region characterized by hot, dry and calm weather with low cloudiness (80% of the days of the year are cloudless) and nearly no precipitation. Trend values of average temperature and relative humidity range from 14.5°C in January to 34°C in July and from 21% in May and June to 48% in December, respectively. Significant percentage of winds is calm (52%). The prevailing winds are W, NW, SW and N, with percentages of occurrence of 15.9%, 11.83%, 11.7% and 4.52%, respectively. The majorority of winds range from 2 to 3.1 m s^{-1} and the least occurrence of speed intervals ranges from 8.8 to 10.8 m s^{-1}.

3. Experiments

Measurements of hourly global (G) and diffuse (D) solar radiation were made from sunrise to sunset from June 1992 to May 1993, using two Kipp and Zonen pyranometers (Model CM 6B). One of them is used to measure the global radiation and the other is fitted with a shadow band of radius of 610 mm and width of 60 mm, constructed following Kipp and Zonen rules, to measure the diffuse component. The pyranometer specifications meet the majority of the requirements set for class 1 radiation sensors by the World Meteorological Organization (*WMO*, 1983). The setting of the shadow band was checked twice a day making sure of the centering of the sun shade on the receiver head of the pyranometer all day around. Every few days the band position is adjusted according to the actual declination of the sun. Irradiances (G and D) in W m^{-2} were measured and integrated over 60 minutes period using a two-channel-integrator (Kipp and Zonen Model CC12). The instruments were used for the first time in this study and calibrated by the manufacturers themselves. The pyranometer has a directionality error <20 W m^{-2} at 100 W m^{-2} and a non linearity error $<1.5\%$, while the inaccuracy of the solar integrator lies within

0.2% + 1 digit. The measured values of D were multi-plied by a correction factor f (1 to 1.14), calculated daily to compensate the part of the diffuse sky radiation, which is obstructed by the shadow band. This value is determined by *Latimer* and *Mac Dowall*, 1971 as:

$$f = 1/(1 - F/D), \tag{1}$$

in which — assuming the isotropic distribution of sky radiance —

$$F/D = 2\omega / \pi r \cos^3 \delta \, (\sin\phi \, \sin\delta \, H_0 + \cos\phi \, \cos\delta \, \sin H_0), \tag{2}$$

where ω is the width of the band, r is its radius, δ is the solar declination, ϕ is the latitude of the station and H_0 is the hour angle of the sun at sunset.

The extinction by water vapor is given by *Iqbal* (1983):

$$a_W = 2.4959 \, U_1 \left[(1.0 + 79.034 \, U_1)^{0.6828} + 6.385 \, U_1\right]^{-1}, \tag{3}$$

where

$$U_1 = W m_r, \tag{4}$$

in which W is the perceptible water thickness in cm and m_r is the relative air mass. *Leckner* (1978) presented the following formula for calculating W:

$$W = 0.493 \, (\phi_r / T) \exp (26.23 - 5416/T), \tag{5}$$

where ϕ_r is the relative humidity in fraction of one and T is the ambient temperature in Kelvin.

The relative air mass m_r is given by *Kasten* (1966):

$$m_r = \left[\cos Z + 0.15 \, (93.885 - Z)^{-1.253}\right]^{-1}, \tag{6}$$

where Z is the zenith angle in degrees.

The extinction by aerosols is obtained from

$$a_A = 1 - T_A, \tag{7}$$

where T_A is the transmissivity after the extinction by aerosols:

$$T_A = \exp (-\tau_A m_r), \tag{8}$$

in which τ_A is the aerosol optical depth estimated with the aid of Rayleigh (T_R) and ozone (T_{oz}) transmissivities and water vapor absorption (a_W) (*Al-Jamal et al.*, 1987) as:

$$\tau_A = (-1/m_r) \ln [(I/I_0) / (T_{oz} \, T_R - a_W)], \tag{9}$$

I is the direct beam radiation (W m^{-2}) and I_0 is the corresponding extraterrestrial one (W m^{-2}) calculated using the following equations:

$$G = I \sin h + D, \tag{10}$$

where h is the solar elevation angle,

$$I_0 = 1367 \left(1 + 0.033 \cos(360 d_n/365)\right), \tag{11}$$

where d_n is the Julian day number.

4. Results and discussion

The different solar radiation components are functions of several variables (*Atwater* and *Ball*, 1981; *Kudish et al.*, 1983) such as the solar elevation angle, the nature and extent of cloudiness (cloud amount), the atmospheric scattering by air molecules (Rayleigh scattering), and aerosol (Mie scattering) as well as the absorption by atmospheric gases (H_2O, O_2, CO_2, O_3 in specific wavelength bands) and aerosol.

4.1 Characteristics of global solar radiation (G) on a horizontal surface

4.1.1 All sky conditions measurements (G_a)

(a) Hourly variation of global solar radiation (G_{ah})

Table 1 gives the average values of the hourly global solar radiation in Wh m^{-2} received on a horizontal surface through a day at different months in the measurement period (Local Apparent Time is used). From this table one can see clearly that the rise and fall of the hourly global solar radiation throughout the day is generally symmetrical with respect to the solar noon for all days the year around.

(b) Variation of daily totals of global solar radiation (G_{ad}).

Fig. 1 illustrates the variation of the daily totals of global solar radiation through the whole measurement period from June 1992 to May 1993. In this figure, the value of G_{ad} varies from 8713 Wh m^{-2} (at the day number 159: June 8) to 1564 Wh m^{-2} (at the day number 7: January 7) with remarkable variation from day to day. This "vibration" is due to the fluctuation of the atmospheric conditions with respect to water content, dust and amount and type of clouds, which change from hour to hour and day to day. According to the astronomical

Table 1. Results of mean values of hourly and daily global solar radiation (Wh m^{-2}) at all (G_a) and cloudless (G_c) sky conditions (June 1992–May 1993; Qena/Egypt)

LAT		Sr-5	5-6	6-7	7-8	8-9	9-10	10-11	11-12	12-13	13-14	14-15	15-16	16-17	17-18	18-SS	Daily totals
Jun 1992	G_a	2	86	282	514	718	882	997	1042	1018	928	776	578	351	136	11	8323
	G_c	2	87	285	518	720	885	1000	1043	1020	930	778	580	352	137	11	8358
Jul	G_a	1	79	279	503	704	868	983	103	101	926	766	564	343	1266	9	8210
	G_c	1	79	279	503	704	868	983	103	101	927	769	568	346	127	9	8220
Aug	G_a		45	229	455	662	820	952	100	978	880	719	511	281	79	3	7586
	G_c		45	229	455	664	821	954	100	981	878	718	510	279	79	3	7605
Sep	G_a		16	166	406	616	779	900	951	924	823	646	432	206	31		6873
	G_c		16	166	397	616	779	900	951	924	824	646	432	208	31		6896
Oct	G_a		2	89	301	508	686	801	843	819	712	544	330	122	6		5764
	G_c		2	90	303	509	687	804	846	825	720	554	335	123	6		5829
Nov	G_a			35	194	379	558	673	717	682	594	437	251	66	1		4588
	G_c			34	189	390	553	666	718	695	602	448	258	67	1		4662
Dec	G_a			9	124	306	458	574	651	627	558	431	258	79	3		4077
	G_c			9	119	301	467	589	655	650	578	438	257	73	3		4180
Jan 1993	G_a			1	58	233	414	556	647	665	627	497	348	163	27		4236
	G_c			0.8	61	248	445	596	690	719	682	574	402	197	32		4635
Feb	G_a			3	97	308	505	669	776	814	770	643	480	277	78	1	5419
	G_c			3	99	312	505	670	791	822	789	658	492	285	78	1	5635
Mar	G_a		1	25	179	400	613	784	884	914	859	740	556	331	112	4	6414
	G_c		1	27	194	415	632	795	890	924	872	736	539	317	107	4	6532
Apr	G_a		8	108	316	509	725	878	952	970	862	743	556	347	131	8	7111
	G_c		8	109	339	562	752	911	968	100	930	790	581	374	141	8	7561
May	G_a		32	200	428	618	774	904	987	974	832	708	539	327	186	11	7472
	G_c		33	203	438	639	792	955	1034	1046	977	826	625	384	153	12	8121
Summer	G_a	2	56	240	466	668	827	948	100	975	881	720	515	292	91	8	7670
	G_c	10	56	242	469	677	837	960	101	988	893	730	525	300	91	8	7824
Autumn	G_a		3	60	240	434	609	724	771	743	652	492	296	99	8		5110
	G_c		3	60	241	442	614	730	779	757	663	505	303	103	8		5324
Winter	G_a			5	90	286	471	622	725	746	698	573	413	215	52	2	4824
	G_c			5	92	295	490	650	751	788	753	620	452	243	54	2	5236
Spring	G_a	2	38	174	395	593	776	914	984	984	875	746	561	344	134	9	7551
	G_c	2	39	177	413	626	802	947	100	101	939	795	591	367	141	9	7976
Year	G_a	2	42	133	302	499	675	806	873	864	779	634	446	237	78	7	6289
	G_c	9	41	137	309	517	694	828	890	886	810	661	462	246	77	7	6590

cycle of the earth, the sites situated outside the tropics in the northern hemisphere have the maximum and minimum global solar radiation at the June solstice (June 20/21) and the December solstice (December 20/21), respectively (*Morris et al.*, 1982). The observed shift is due to the high amount of clouds observed at the June solstice (5 octas) in comparison to the clear sky in June 8, and the dense and dark clouds, which covered the sky from sunrise to sunset at January 7 (8 octas).

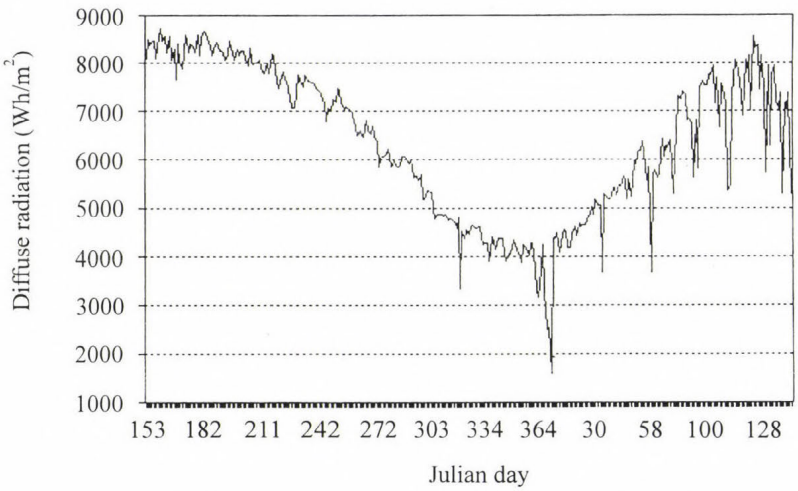

Fig. 1. Variation of daily totals of global solar radiation (June 1992–May 1993) in Qena/Egypt.

(i) Variation of monthly average of daily totals of global solar radiation (G_{ad})

The variation of the monthly average of G_{ad} are also included in Table 1. The average value of daily totals of G_{ad} ranges from 8323 Wh m^{-2} in June to 4077 Wh m^{-2} in December. The standard deviation has relatively high values at May $\pm$869), January ($\pm$829), and April ($\pm$749), compared with the small values at July ($\pm$194) and June ($\pm$246). This is due to the strong fluctuation of atmospheric dust particles and clouds in these three months (May, January, and April).

(ii) Variation of seasonal averages of G_{ad}

Table 1 gives the seasonal averages of G_{ad} as well as its average over the whole measurement period. From this table one can see that the average G_{ad} over the year is 6289 Wh m^{-2} with a seasonal variation from 4824 Wh m^{-2} in winter to 7670 Wh m^{-2} in summer. This relatively temperate variation is typical of the

climate of North Africa and also reflects the low degree of cloudiness in the study region (1 octa on the average through the measurement period). The standard deviation of the results, has high values in winter (±1023) and spring (±864) and a small value in summer (±529) indicates the higher stability of the atmosphere in the summer months.

(iii) Percentage frequency distribution of G_{ad}

The percentage frequency distributions of G_{ad} are given in *Table 2* for each month, season and the whole period, respectively. From this table, it can be seen that about 95.6% of the days in the year have values of G_{ad} within the range from 4–9 kWh m^{-2}. In summer 92.6% and in spring 80.6% of the measurements were observed in the range of 7–9 kWh m^{-2}, while in autumn 96.1% and in winter 86.5% were observed in the range of 4–7 kWh m^{-2}. In June, July and August, almost all days receive G_{ad} in the range of 7–9 kWh m^{-2} and 88.9% of these days get between 8 and 9 kWh m^{-2} in June and July. The above distribution of the solar radiation is characteristic for the climate of subtropical regions and indicates the richness of the study region in solar energy.

Table 2. Percentage of frequency distribution of daily totals of global solar radiation through the measurement period in Qena/Egypt

Range (kWh m^{-2})		1–2	2–3	3–4	4–5	5–6	6–7	7–8	8–9
June	1992	0.0	0.0	0.0	0.0	0.0	0.0	11.1	88.9
July		0.0	0.0	0.0	0.0	0.0	0.0	11.1	88.9
August		0.0	0.0	0.0	0.0	0.0	0.0	92.6	7.4
September		0.0	0.0	0.0	0.0	0.0	56.0	44.0	0.0
October		0.0	0.0	0.0	3.7	66.7	29.6	0.0	0.0
November		0.0	0.0	4.0	96.0	0.0	0.0	0.0	0.0
December		0.0	0.0	23.1	76.9	0.0	0.0	0.0	0.0
January	1993	3.8	7.7	3.8	76.9	7.7	0.0	0.0	0.0
February		0.0	0.0	7.7	0.0	76.9	15.4	0.0	0.0
March		0.0	0.0	0.0	0.0	31.3	43.8	25.0	0.0
April		0.0	0.0	0.0	0.0	14.8	22.2	59.3	3.7
May		0.0	0.0	0.0	0.0	10.5	5.3	52.6	31.6
Summer		0.0	0.0	0.0	0.0	0.0	7.4	49.4	43.2
Autumn		0.0	0.0	3.9	51.3	23.7	21.1	0.0	0.0
Winter		1.4	2.7	9.5	35.1	36.5	14.9	0.0	0.0
Spring		0.0	0.0	0.0	0.0	9.0	10.4	47.8	32.8
Year		0.3	0.7	3.4	21.8	17.1	13.4	24.2	19.1

4.1.2 Comparison between average global solar radiation (G_a) and global radiation at cloudless skies (G_c)

To illustrate the influence of clouds on the incoming global solar radiation, the behavior of global solar radiation in case of cloudless sky conditions (G_c) is discussed and compared with those measured in all sky conditions (G_a). The results of measurements of G_c are summarized in Table 1.

(a) Comparison between the hourly global solar radiation in all (G_{ah}) and cloudless (G_{ch}) sky conditions

According to Table 1, the comparison between the average values of G_{ch} and G_{ah} in the whole measurement period shows that:

(i) The course of G_{ch} is similar to that of G_{ah} with somewhat higher values of G_{ch}, because of the missing attenuation by clouds.

(ii) The average cloud effect seems to be small in Qena over the whole measurement period because the low effect in some months decreases the high one in other months. Also the study region is characterized by high thin clouds, which have only small effect in depleting the global solar radiation.

(b) Comparison between the daily totals of global solar radiation in all (G_{ad}) and cloudless (G_{cd}) sky conditions

As we already found in section (4.1.2.a) for (G_{ch}), the behavior of G_{cd} shows the same general pattern as G_{ad} for both monthly and seasonal averages, but with higher values. The relative percentage of exceeding G_{cd} by G_{ad} was found to be maximum in January (9%), May (8%) and winter (7.9%), while it is minimum in July (0.1%) and summer (2%). In the whole period the average value is (4.6%). This may be explained in terms of the elimination of cloud effect, which was maximum in January (1.79 octas), May (2.68 octas) and winter (1.61 octas) while it was minimum in July, September (0.08 octa) and summer (0.11 octa). As shown in Table 1 the average values of G_{cd} vary from 8358 Wh m^{-2} in June to 4180 Wh m^{-2} in December and from 7976 Wh m^{-2} in spring to 5236 Wh m^{-2} in winter with average value over the whole measurement period equals to 6590 Wh m^{-2}.

4.2 Characteristics of diffuse solar radiation (D)
4.2.1 All sky conditions measurements (D_a)

(a) Hourly variation of diffuse solar radiation (D_{ah})

Table 3 gives the results of hourly variation of diffuse solar radiation in Wh m^{-2} through the measurement period. The measured mean values of D_{ah} are maxi-

Table 3. Results of mean values of hourly and daily diffuse solar radiation (Wh m^{-2}) at all (D_a) and cloudless (D_c) sky conditions (June 1992–May 1993; Qena/Egypt)

LAT		Sr-5	5-6	6-7	7-8	8-9	9-10	10-11	11-12	12-13	13-14	14-15	15-16	16-17	17-18	18-SS	Daily totals
Jun 1992	D_a	2	56	126	172	202	219	227	237	235	224	206	183	147	83	10	2327
	D_c	2	56	123	168	197	213	219	230	229	219	201	178	145	82	10	2271
Jul	D_a	1	45	103	142	166	181	191	194	194	183	174	153	119	66	7	1920
	D_c	1	46	104	142	166	181	190	193	190	180	171	151	118	67	8	1908
Aug	D_a		28	96	141	154	170	178	180	181	172	166	138	103	44	2	1752
	D_c		26	96	141	148	163	171	173	171	163	152	135	100	42	2	1683
Sep	D_a		14	85	143	180	202	212	217	213	201	185	154	104	31		1943
	D_c		13	84	141	174	195	204	212	206	194	178	147	99	24		1871
Oct	D_a		2	49	105	133	160	168	173	167	161	141	111	61	5		1435
	D_c		2	50	104	134	157	164	168	162	155	136	108	60	5		1404
Nov	D_a			24	84	123	148	165	159	155	149	138	105	46			1297
	D_c			24	83	122	146	160	152	151	142	121	101	45	1		1247
Dec	D_a			7	58	104	133	141	154	150	137	119	99	49	2		1155
	D_c			8	58	104	125	133	142	128	120	104	91	45	2		1059
Jan 1993	D_a			1	38	88	129	150	160	172	170	142	118	74	17		1260
	D_c				35	78	110	130	135	143	136	124	104	71	21		1089
Feb	D_a			2	45	99	134	159	166	164	161	144	120	96	39	1	1330
	D_c			2	46	95	128	147	146	141	139	135	110	87	39	1	1216
Mar	D_a			17	83	139	168	190	199	207	203	196	179	133	62	3	1780
	D_c			19	91	150	180	197	198	206	200	186	169	132	68	4	1800
Apr	D_a		5	63	131	172	185	212	224	213	215	200	175	126	62	5	1988
	D_c		6	70	144	172	165	179	197	182	184	178	165	125	71	6	1843
May	D_a		27	108	139	176	265	280	281	275	245	231	187	133	73	10	2430
	D_c		27	118	148	166	184	201	220	229	206	197	155	116	73	8	2046
Summer	D_a	2	34	101	145	168	184	193	197	195	185	176	160	112	52	7	1899
	D_c	1	32	98	142	164	180	188	192	188	178	166	144	108	48	7	1838
Autumn	D_a		3	35	93	130	153	165	168	162	154	135	109	56	8		1371
	D_c		3	38	95	132	154	164	166	160	152	132	109	58	8		1371
Winter	D_a			4	48	103	141	102	170	179	174	155	128	89	29	2	1385
	D_c			4	45	93	124	143	148	145	141	132	110	82	32	1	1200
Spring	D_a	2	31	96	157	194	214	253	251	247	236	221	193	144	77	8	2323
	D_c	2	37	104	157	186	196	206	222	218	208	194	173	137	78	8	2126
Year	D_a	2	28	64	108	146	170	188	192	191	183	168	141	97	43	6	1726
	D_c	2	29	70	112	144	164	175	180	176	169	155	133	94	44	6	1652

mum in the hours around midday (11–13 LAT). Its average value over the whole measurement period is equal to 192 Wh m^{-2}, ranging from 237 Wh m^{-2} in June to 150 Wh m^{-2} in December. At early morning (Sunrise till 7 LAT) and late afternoon (17 LAT till Sunset), the recorded values are minimum, with average value during the whole period ranges from 2 to 64 Wh m^{-2}.

(b) Variation of monthly and seasonal averages of daily totals of diffuse solar radiation (D_{ad})

The variation of D_{ad} through the measurement period is graphically represented in *Fig. 2*. The value of D_{ad} fluctuates strongly from day to day according to the corresponding change of the atmospheric conditions (water content, amount of cloud, aerosol particles, etc). It ranges from 4360 Wh m^{-2} at the day number 129 (May 8) to 734 Wh m^{-2} at the day number 345 (Dec 10). The variation of monthly and seasonal averages of D_{ad} is given also in Table 3.

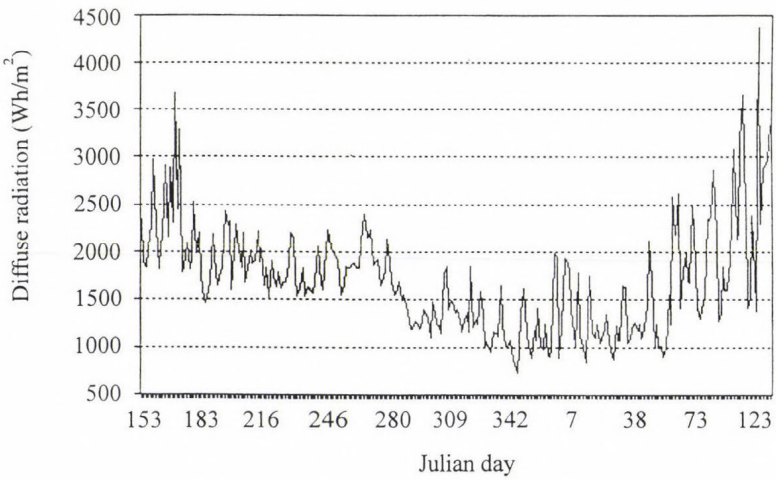

Fig. 2. Variation of daily totals of diffuse solar radiation (June 1992–May 1993) in Qena/Egypt.

(c) Percentage frequency distributions of D_{ad}

The percentage frequency distributions of D_{ad} in the different months, seasons and the whole measurement period are summarized in *Table 4*. The table shows that the percentage frequency of D_{ad} received on a horizontal surface in the study region in the range >4 kWh m^{-2} is very low compared to that of the corresponding global solar radiation (G_{ad}) (see Table 2). About 93.2% of the days in the year have the values of D_{ad} within the low range 0.5–2.5 kWh m^{-2}.

Table 4. Percentage of frequency distribution of daily totals of diffuse solar radiation through the measurement period in Qena/Egypt

Range (Pk Wh/m^{-2})		0.5-1	1-1.5	1.5-2	2-2.5	2.5-3	3-3.5	3.5-4	4-4.5
June	1992	0.0	0.0	34.6	42.3	15.4	3.8	3.8	0.0
July		0.0	8.3	54.2	37.5	0.0	0.0	0.0	0.0
August		0.0	0.0	85.2	14.8	0.0	0.0	0.0	0.0
September		0.0	0.0	64.0	36.0	0.0	0.0	0.0	0.0
October		0.0	69.2	26.9	3.8	0.0	0.0	0.0	0.0
November		12.5	75.0	12.5	0.0	0.0	0.0	0.0	0.0
December		38.5	46.2	15.4	0.0	0.0	0.0	0.0	0.0
January	1993	20.0	60.0	20.0	0.0	0.0	0.0	0.0	0.0
February		17.4	56.5	17.4	4.3	4.3	0.0	0.0	0.0
March		0.0	30.8	38.5	15.4	15.4	0.0	0.0	0.0
April		0.0	14.3	23.8	42.9	4.8	9.5	4.8	0.0
May		0.0	12.5	12.5	12.5	37.5	12.5	0.0	12.5
Summer		0.0	2.6	66.7	28.2	1.3	0.0	1.3	0.0
Autumn		10.8	60.8	24.3	4.1	0.0	0.0	0.0	0.0
Winter		20.9	47.8	22.4	4.5	4.5	0.0	0.0	0.0
Spring		0.0	14.0	20.0	38.0	14.0	8.0	4.0	2.0
Year		8.2	32.1	35.4	17.5	4.1	1.5	0.7	0.4

4.2.2 Comparison between diffuse solar radiation in all (D_a) and cloudless (D_c) sky conditions

The results of diffuse solar radiation measurements in cloudless sky conditions (D_c) are summarized in Table 3. A comparison study has been done between the diffuse solar radiation measured in both all sky (D_a) and cloudless (D_c) sky conditions for investigating to what extent the clouds affect the values of diffuse solar radiation. The following conclusions may be deduced from this table:

(i) The same behaviors are generally observed for the variations of hourly and daily totals (monthly and seasonal averages) of diffuse solar radiation in all sky (D_{ah}, D_{ad}) and cloudless sky conditions (D_{ch}, D_{cd}). However the measured values of D_{ch} and D_{cd} were smaller than those of D_{ah} and D_{ad}, reflecting the influence of clouds in increasing the diffuse solar radiation.

(ii) The average value of D_{ch} over the whole measurement period is maximum at midday hours (11–13 LAT). It has the value 180 Wh m^{-2} ranging from 230 Wh m^{-2} in June to 128 Wh m^{-2} in December, while it is minimum in the early morning (Sunrise-7 LAT) and late afternoon (17 LAT-Sunset) being in some months in the order of the instrument offset.

(iii) The monthly and seasonal average values of D_{cd} were maximum in May (2046 Wh m^{-2}) and spring (2126 Wh m^{-2}), while it is minimum in December (1059 Wh m^{-2}) and winter (1200 Wh m^{-2}). Its average value over the year is 1652 Wh m^{-2}.

(iv) Over the whole period the influence of clouds is not large because the low effect in some months reduce the high one in other months.

4.3 Characteristics of diffuse fraction (k) of global solar radiation

The diffuse fraction is defined as the ratio between the diffuse solar radiation and the global solar radiation, both received on a horizontal surface. Its diurnal and seasonal variations are represented and discussed in the following sections.

4.3.1 All sky conditions measurements (k_a)

(a) Hourly variation of diffuse fraction (k_{ah})

Table 5 summarizes the results of hourly variation of diffuse fraction from sunrise to sunset through the period from June 1992 to May 1993. From this table we can see that k_{ah} decreases from sunrise till midday and then increases again in the direction of sunset.

(b) Variation of daily averages of diffuse fraction of global solar radiation (k_{ad})

The variation of k_{ad} is shown in *Fig. 3*. Its value fluctuates obviously from day to day corresponding to the fluctuation of G_{ad} and D_{ad} discussed in sections 4.1.b and 4.2.b. It ranges from 0.14 (at the day number 56 (Feb 25)) to 0.9 (at the day number 7 (Jan 7)) and is characterized by remarkable fluctuations in the days numbered from 326 to 172, in which k_{ad} value tends to be higher than in the other days of the measurement period. This is evident considering the instability of the atmosphere in these days with respect to water content, dust and clouds, which have also somewhat higher values in these days, as mentioned above. The average values of k_{ad} for each month and season in the measurement period are also given in Table 5. The maximum values of average k_{ad} were observed in May (0.39) as well as in winter and spring (0.31), while the minimum ones were recorded in July & August (0.23) and summer (0.25).

(c) Relation between daily average of diffuse fraction (k_{ad}) and clearness index (k_{td})

The clearness index is defined as the ratio of global solar radiation at the earth's surface (G_a) to extraterrestrial solar radiation (G_0) received on a horizontal surface. The relation between k_{ad} and k_{td} is represented graphically in the scatter plot in *Fig. 4* for all the daily measurements in all sky conditions. The figure shows that:

Table 5. Results of mean values of hourly and daily diffuse fraction at all (K_a) and cloudless (K_c) sky conditions (June 1992–May 1993; in Qena/Egypt)

LAT		Sr-5	5-6	6-7	7-8	8-9	9-10	10-11	11-12	12-13	13-14	14-15	15-16	16-17	17-18	18-SS	Daily total
Jun 1992	K_a	0.78	0.65	0.46	0.34	0.28	0.25	0.23	0.23	0.24	0.24	0.27	0.32	0.43	0.62	0.92	0.28
	K_c	0.78	0.64	0.43	0.32	0.27	0.24	0.22	0.22	0.23	0.24	0.26	0.31	0.42	0.62	0.91	0.27
Jul	K_a	0.79	0.58	0.37	0.28	0.24	0.21	0.19	0.19	0.19	0.20	0.23	0.27	0.35	0.54	0.87	0.23
	K_c	0.79	0.58	0.37	0.28	0.24	0.21	0.19	0.19	0.19	0.19	0.22	0.27	0.35	0.53	0.87	0.23
Aug	K_a		0.61	0.42	0.31	0.23	0.21	0.19	0.18	0.19	0.20	0.23	0.27	0.37	0.57		0.23
	K_c		0.60	0.42	0.31	0.22	0.20	0.18	0.17	0.18	0.19	0.21	0.27	0.37	0.57		0.22
Sep	K_a		0.87	0.54	0.37	0.30	0.26	0.23	0.23	0.23	0.25	0.29	0.36	0.51	0.81		0.28
	K_c		0.87	0.52	0.36	0.29	0.25	0.23	0.22	0.22	0.24	0.28	0.34	0.48	0.81		0.27
Oct	K_a		0.76	0.53	0.35	0.27	0.23	0.21	0.20	0.20	0.22	0.26	0.34	0.50	0.82		0.25
	K_c		0.76	0.54	0.34	0.26	0.23	0.20	0.20	0.20	0.25	0.25	0.33	0.49	0.81		0.24
Nov	K_a			0.71	0.44	0.34	0.27	0.25	0.22	0.24	0.26	0.32	0.42	0.69	0.76		0.29
	K_c			0.70	0.42	0.31	0.26	0.24	0.21	0.22	0.23	0.27	0.39	0.64			0.27
Dec	K_a			0.77	0.48	0.35	0.29	0.25	0.24	0.20	0.26	0.29	0.40	0.64	0.80		0.29
	K_c			0.75	0.45	0.34	0.26	0.23	0.22	0.20	0.21	0.24	0.36	0.61			0.25
Jan 1993	K_a			0.76	0.66	0.42	0.34	0.31	0.28	0.30	0.31	0.35	0.41	0.53	0.69		0.34
	K_c				0.59	0.32	0.25	0.22	0.20	0.20	0.20	0.22	0.26	0.35	0.62		0.23
Feb	K_a			0.68	0.48	0.33	0.28	0.25	0.22	0.21	0.22	0.27	0.28	0.37	0.53	0.78	0.26
	K_c			0.67	0.45	0.30	0.26	0.22	0.18	0.17	0.17	0.20	0.22	0.31	0.49	0.78	0.22
Mar	K_a			0.78	0.53	0.39	0.30	0.26	0.23	0.24	0.26	0.29	0.34	0.43	0.58	0.86	0.29
	K_c			0.79	0.54	0.39	0.30	0.26	0.23	0.23	0.24	0.26	0.31	0.40	0.57	0.86	0.28
Apr	K_a			0.68	0.43	0.52	0.28	0.27	0.27	0.24	0.30	0.33	0.38	0.47	0.60	0.78	0.32
	K_c			0.65	0.43	0.31	0.22	0.20	0.20	0.18	0.20	0.23	0.30	0.37	0.53	0.72	0.25
May	K_a		0.86	0.61	0.39	0.33	0.31	0.35	0.32	0.34	0.48	0.50	0.49	0.58	0.68	0.86	0.39
	K_c		0.86	0.60	0.31	0.21	0.16	0.16	0.15	0.14	0.14	0.18	0.22	0.32	0.56	0.91	0.29
Summer	K_a	0.79	0.65	0.43	0.31	0.25	0.22	0.20	0.20	0.20	0.21	0.24	0.29	0.39	0.60	0.88	0.25
	K_c	0.77	0.63	0.41	0.30	0.24	0.21	0.19	0.19	0.19	0.20	0.23	0.28	0.38	0.59	0.87	0.23
Autumn	K_a		0.82	0.64	0.40	0.31	0.25	0.23	0.22	0.22	0.24	0.28	0.38	0.59	0.83		0.27
	K_c		0.82	0.61	0.39	0.30	0.25	0.22	0.21	0.21	0.23	0.26	0.36	0.56	0.83		0.27
Winter	K_a			0.75	0.57	0.39	0.33	0.28	0.25	0.27	0.28	0.32	0.37	0.49	0.64	0.83	0.31
	K_c			0.73	0.52	0.33	0.26	0.23	0.20	0.19	0.20	0.22	0.25	0.36	0.58	0.82	0.24
Spring	K_a	0.77	0.76	0.59	0.39	0.39	0.27	0.26	0.26	0.25	0.30	0.33	0.37	0.46	0.62	0.88	0.31
	K_c	0.80	0.75	0.55	0.35	0.29	0.23	0.21	0.21	0.21	0.22	0.24	0.30	0.40	0.59	0.83	0.27
Year	K_a	0.78	0.71	0.58	0.42	0.33	0.27	0.24	0.23	0.23	0.25	0.29	0.35	0.49	0.66	0.87	0.28
	K_c	0.79	0.70	0.54	0.38	0.28	0.24	0.21	0.20	0.20	0.21	0.24	0.30	0.43	0.64	0.85	0.25

(i) Most values of diffuse fraction condense at the right lower part of the plot (low k_{ad} and high k_{td}) giving further evidence to the high availability of incoming solar radiation in most of the year in Qena.

(ii) At any value of clearness index k_{td}, there are many values of diffuse fraction k_{ad}, which means that k_{ad} depends on other parameters in addition to k_{td}. The most important parameter is the sun elevation, which plays an active part in this consideration. This conclusion seems to be more clear in view of the not very high correlation found between k_{ad} and k_{td} (correlation coefficient = - 0.68).

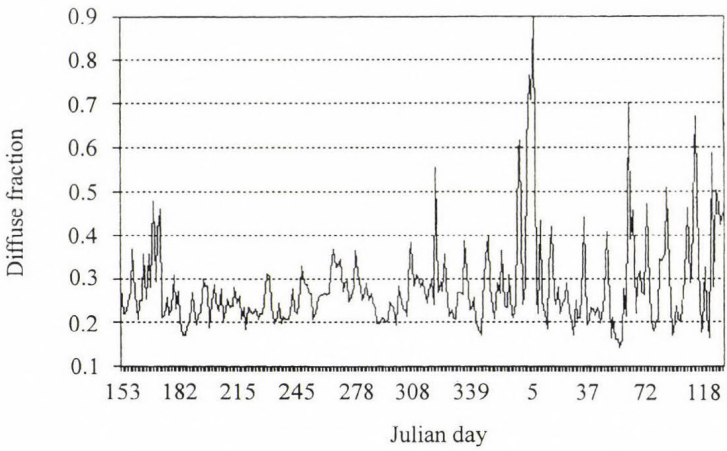

Fig. 3. Variation of daily diffuse fraction (June 1992–May 1993) in Qena/Egypt.

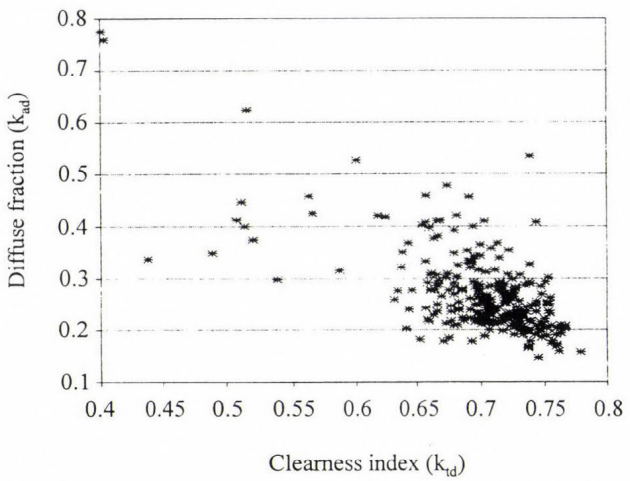

Fig. 4. Relation between daily values of diffuse fraction and clearness index.

4.3.2 Comparison between the diffuse fraction in all (k_a) and cloudless (k_c) sky conditions

Table 5 summarizes the results of k_c through the measurement period. The maximum values of average k_c were observed in March and May (0.28) and spring (0.27), while the minimum ones were recorded in August (0.22), summer (0.23). Considering that the main affecting parameters on k_c are the water vapor and suspended dust particles, the above mentioned variation seems to be explainable in view of the dusty khamaseen wind blowing in the spring months in the study region and leading to high concentrations of aerosols.

4.4 Effect of atmosphere

4.4.1 Effect of cloud

Fig. 5 represents the monthly variation of the G/G_0 and average cloud amount in octas from June 1992 to May 1993. The effect of clouds appears in the higher values of G/G_0 at cloudless days compared to their values at all days measurements. As it is clear in this figure this effect is negligible in the months from June to November and obvious from December to May according to the average amount of clouds observed in these months. It varies from 0.08 octas at July and September to 2.68 octas in May. Most of the clouds were fairly transparent Cirrus (transmissivity $\approx$0.6 to 0.75), except in December to February and some days in April and May, in which As and St types (transmissivity $\approx$0.43 to 0.60) were observed.

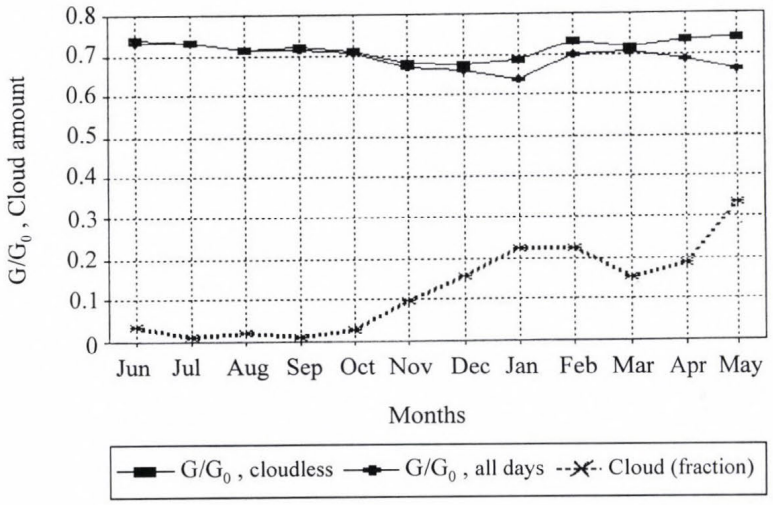

Fig. 5. Effect of clouds on clearness index (G/G_0) in Qena/Egypt.

4.4.2 *Effect of aerosol and water vapor*

Fig. 6 shows the variation of the G/G_0 with the extinction of the incoming solar radiation caused by aerosol a_A and water vapor a_W at cloudless days through the measurement period. This figure shows clearly a high contribution of aerosol dust particles (0.254–0.342) in the reduction of G/G_0 in comparison with that of water vapor (0.118–0.144). This is in a good agreement with the nature of the study region, because Qena is not an industrial district and characterized by a high content of dust particles dispersed from near eastern desert and various human activities (*El-Shazly*, 1989).

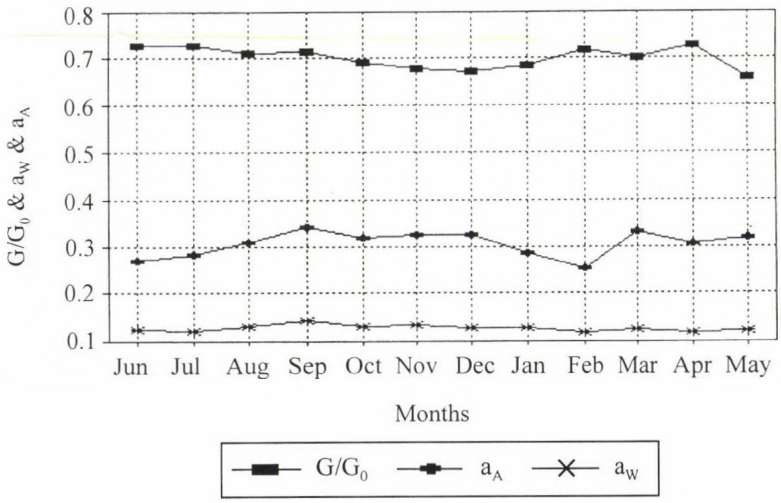

Fig. 6. Effect of aerosols and water vapor on clearness index at cloudless days in Qena/Egypt.

5. Conclusion

(i) The study region receives a considerable quantity of solar energy. 95.6% of the days through the year have values of global solar radiation in the high range of 4–9 kWh m^{-2}, while 96.7% of the days have diffuse solar radiation in the low range from 0.5 to 2.5 kWh m^{-2}.

(ii) The reduction of global solar radiation by clouds represents a small percentage (4.6%), which refers to the low degree of cloudiness in the study region (1 octa in average over the year).

(iii) The relation between the diffuse fraction k_{ad} and clearness index as well the low diffuse fraction indicate the high availability of incoming solar radiation in most of the year.

(iv) Considerable fluctuations of the different solar radiation components were observed in March, April, May and January owing to the high fluctuation of the atmospheric conditions in these months.

(v) The average value of daily total of global solar radiation measured in Qena is comparable with that recorded by Meteorological Authority of A.R. Egypt, 1992 at different locations in Egypt (see *Table 6*).

Table 6. Comparison between the yearly average of daily totals of global solar radiation (G) arriving at horizontal surface in all sky conditions at different locations in Egypt

Location	Qena	Matruh	Tahrir	Cairo	Kharag	Aswan
G(Wh m^{-2})	6289	5525	5294	6394	6416	6416

All these above conclusions indicate that the incoming solar energy at Qena is a significant source of renewable clean energy, which is sufficient to supply people with the necessary energy and encourages us to use it for developing this region, the subject which should be considered in the future.

References

Al-Jamal, K., Ayyash, S., Rasas, M., Al-Aruri, S. and *Shaban, N.*, 1987: Atmospheric turbidity in Kuwait. *Atmospheric Environment 21*, 1855-1859.

Atwater, M.A. and *Ball, J.T.*, 1981 : Effect of clouds on insolation models. *Solar Energy 27*, 37-44.

El-Shazly, S.M., 1989: Studies of the number concentrations and size distribution of the suspended dust particles in the atmosphere of Qena/Egypt. *Water, Air and Soil Pollution* 45, 121-132.

Iqbal, M., 1983: *An Introduction to Solar Radiation*. Academic Press, New York.

Kasten, F., 1966: A new table and approximate formula for relative nnnn optical air mass. *Arch. Meteor. Geophys. Bioklimatol.* Ser. 14, 206-223.

Kudish, A.T., Wolf, D. and *Machlay, Y.*, 1983: Solar radiation for Beer Sheva Israel. *Solar Energy 30*, 33-37.

Kuye, A. and *Jagtap, S.S.*, 1992: Analysis of solar radiation data for port harcourt, Nigeria. *Solar Energy 49*, 139-145.

Latimer, J.R. and *Mac Dowall, J.*, 1971: Radiation measurement, International field year for the great lakes. *Technical Manual Series*, No. 2.

Leckner, B., 1978: The spectral distribution of solar radiation at the earth's surface. Elements of the model. *Solar Energy 20*, 143-150.

Moriarity, W.W., 1991: Estimation of diffuse from measured global solar radiation. *Solar Energy 47*, No. 2, 75-82.

Morris, N., James, G.E. and *William, D.B.*, 1982: *Understanding our Atmospheric Environment*. W.H. Freeman Company, San Francisco.

Neuwirth, F., 1980: The estimation of global and sky radiation in Austria. *Solar Energy 24*, 421-426.

World Meteorological Organization (WMO), 1983: Guide to Meteorological Instruments and Method of Observation. Geneva, Switzerland.

NEWS

Academy Prize for hydrologists

The Hungarian Academy of Sciences (Budapest) awarded a joint prize on the CLX. General Assembly in May 1997 to *Ödön Starosolszky* Civ. Eng., member of the editorial board of IDŐJÁRÁS and to *Károly Szesztay* Civ. Eng., the wellknown Hungarian hydrologist for the development of the principles of the environmental hydrology and hydraulics, for the establishment of the environmentally sound water management and for the promotion of application of scientific results on international scale. During the awarding ceremony considerable emphasis was given to the comprehensive report "The impact of climate change on hydrological and water-quality parameters" submitted by the team leader, Ö. Starosolszky in 1994 to the Hungarian National Science Foundation.

Dr. Ö. Starosolszky is a member of the editorial board of IDŐJÁRÁS since 1986 and wellknown not only among hydrologists, but among meteorologists as well. He is particularly appreciated due to his activity in the World Meteorological Organization. Among others, he was co-author and editor of the following WMO publications: Hydrology of Disasters (1989), Hydrological Aspects of athe Accidental Water Pollution (1993), the National Capabilities for the Assessment of Water Resources (1996). He was co-director of two NATO meetings "Flood Defence" Advance Study Institute (1994) and "Controversies between Water Resources Development and the Environment" Advance Research Workshop (1996), and editor of the relevant publications. He contributed to IAHR seminars on ecohydraulics (Utrecht, 1991, and Trondheim, 1994).

As president of the Commission for Hydrology of WMO (1984–93) and vice-president of IAHIR he acted, as chairman or general reporter on several international meetings. He was member of WG-II of the Intergovernmental Panel on Climate Change, lead author for the theme of Hydrology (1995). He participated in a PECO project of the European Union for climate change impact on the European water resources. In the last six years he was chairman of the Committee on Water Science of the Hungarian Academy of Sciences.

The name of *Dr. K. Szesztay* sounds very well in the meteorological community. He wrote several studies in the last four decades on the heat and water budget of the Carpathian-Basin, and about the evaporation of free water surface. On the other hand, he is an internationally wellknown expert of the Hungarian water management, who participated in the organisation of the UN

Water Conference (Mar del Plata, 1977). He had great merits in the formulation of the conference report. He served more than 6 years in New York at the UN headquarters, as senior expert. He was the president of the international Association for Hydrological Sciences (IAHS). During his career he devoted several years to the scientific base of the hydrological forecasts, the water demand of the vegetation, the long-term planning of water resources, including the third Water Resources Master-Plan of Hungary. In the last years his major interest was paid to the identification of the environmental aspects in the water management. The award was also justified by his book on the "Finite Tolerance of our Planet" (Akadémiai Kiadó, 1992, Budapest), where he analyzed the technical development and the change of the global environment with regard to the tolerance of the Earth. He went beyond the basic problems of the water management, since he attempted to quantify the general problem of the water economy. His latest outstanding work is his comprehensive review on the effect of climate change on the water quality.

The Editorial Board wishes both awarded experts further success and fruitful collaboration with the meteorologists.

E. Antal

ATMOSPHERIC ENVIRONMENT

an international journal

To promote the distribution of Atmospheric Environment *Időjárás* publishes regularly the *contents* of this important journal. For further information the interested reader is asked to contact *Prof. P. Brimblecombe,* School for Environmental Sciences, University of East Anglia, Norwich NR4 7TJ, U.K.; E-mail: atmos_env@uea.ac.uk

Volume 31 Number 10 1997

Volume 31 Number 11 1997

Volume 31 Number 12 1997

Aeronox: Atmospheric impact of NO_x emissions From aircraft

Volume 31 Number 13 1997

NOTES TO CONTRIBUTORS

The purpose of *Időjárás* is to publish papers in the field of theoretical and applied meteorology. These may be reports on new results of scientific investigations, critical review articles summarizing current problems in certain subject, or shorter contributions dealing with a specific question. Authors may be of any nationality but papers are published only in English.

Papers will be subjected to constructive criticism by unidentified referees.

* * *

The manuscript should meet the following formal requirements:

Title should contain the title of the paper, the names(s) of the author(s) with indication of the name and address of employment.

The title should be followed by an *abstract* containing the aim, method and conclusions of the scientific investigation. After the abstract, the *key-words* of the content of the paper must be given.

Three copies of the manuscript, typed with double space, should be sent to the Editor-in-Chief: *P.O. Box 39, H-1675 Budapest,* Hungary.

References: The text citation should contain the name(s) of the author(s) in Italic letter or underlined and the year of publication. In case of one author: *Miller* (1989), or if the name of the author cannot be fitted into the text: *(Miller,* 1989); in the case of two authors: *Gamov* and *Cleveland* (1973); if there are more than two authors: *Smith et al.* (1990). When referring to several papers published in the same year by the same author, the year of publication should be followed by letters a,b etc. At the end of the paper the list of references should be arranged alphabetically. For an article: the name(s) of author(s) in Italics or underlined, year, title of article, name of journal, volume number (the latter two in Italics or underlined) and pages. E.g. *Nathan, K. K.,* 1986: A note on the relationship between photosynthetically active radiation and cloud amount. *Időjárás 90,* 10-13. For a book: the name(s) of author(s), year, title of the book (all in Italics or underlined with except of the year), publisher and place of publication. E.g. *Junge, C. E.,* 1963: *Air Chemistry and Radioactivity.* Academic Press, New York and London.

Figures should be prepared entirely in black India ink upon transparent paper or copied by a good quality copier. A series of figures should be attached to each copy of the manuscript. The legends of figures should be given on a separate sheet. Photographs of good quality may be provided in black and white.

Tables should be marked by Arabic numbers and provided on separate sheets together with relevant captions. In one table the column number is maximum 13 if possible. One column should not contain more than five characters.

Mathematical formulas and *symbols:* non-Latin letters and hand-written marks should be explained by making marginal notes in pencil.

The final text should be submitted both in manuscript form and on *diskette.* Use standard 3.5" or 5.25" DOS formatted diskettes for this purpose. The following word processors are supported: WordPerfect 5.1, WordPerfect for Windows 5.1, Microsoft Word 5.5, Microsoft Word 6.0. In all other cases the preferred text format is ASCII.

* * *

Authors receive 30 *reprints* free of charge. Additional reprints may be ordered at the authors' expense when sending back the proofs to the Editorial Office.

Published by the Hungarian Meteorological Service

Budapest, Hungary

INDEX: 26 361

HU ISSN 0324-6329

IDŐJÁRÁS

QUARTERLY JOURNAL
OF THE HUNGARIAN METEOROLOGICAL SERVICE

CONTENTS

****

http://www.met.hu/firat/ido-e.html

VOL. 101 * NO. 4 * OCTOBER–DECEMBER 1997

IDŐJÁRÁS

Quarterly Journal of the Hungarian Meteorological Service

Editorial Office: P.O. Box 39, H-1675 Budapest, Hungary or
Gilice tér 39, H-1181 Budapest, Hungary
E-mail: gmajor@met.hu or *antal@met.hu*
Fax: (36-1) 290-7387

Subscription by

mail: IDŐJÁRÁS, P.O. Box 39, H-1675 Budapest, Hungary;
E-mail: gmajor@met.hu or *antal@met.hu*; *Fax: (36-1) 290-7387*

IDŐJÁRÁS

Quarterly Journal of the Hungarian Meteorological Service
Vol. 101, No. 4, October–December 1997, pp. 239–260

Application of two methods for N_2O emission estimates to Bulgaria and the Netherlands

Carolien Kroeze[1] and **Stanislav Bogdanov**[2]

[1]*Wageningen Institute for Environment and Climate Research*
Wageningen Agricultural University,
P.O. Box 9101, 6700 HB Wageningen, The Netherlands;
E-mail: carolien.kroeze@wimek.cmkw.wau.nl

[2]*National Institute of Meteorology and Hydrology*
66 Tsarigradsko chaussee 1784, Sofia, Bulgaria
E-mail: stas@ozon.rthsf.meteo.bg

(Manuscript received 2 January 1997; final form 14 July 1997)

Abstract—Nitrous oxide (N_2O) is one of the greenhouse gases in the earth's atmosphere. This study focuses on two methodologies for estimating N_2O emissions at the national scale: a method developed in the Netherlands (NEO method), and the IPCC Guidelines for National Greenhouse Gas Inventories (IPCC method). The purpose of this study is: (i) to apply both the IPCC and NEO methods to Bulgaria and the Netherlands, (ii) to investigate differences between the NEO and IPCC methods and (iii) to compare emissions from Bulgaria to emissions from the Netherlands.

There are a number of differences between the NEO and IPCC methods. First, the NEO method includes more sources of N_2O than the IPCC method. Second, some emissions are estimated in different ways. Due to these differences the IPCC method results in higher total emissions than the NEO method: for both countries IPCC emissions are about 20% higher than those of the NEO method (mid-point estimates). These differences result from a net effect; for some sources the IPCC method exceeds the NEO method (in particular for agriculture) and for others the IPCC estimates are lower. The sources not included in the IPCC method are natural emissions, enhanced background emissions from mineral soils, N_2O induced by NO_x deposition, chemical industries other than nitric and adipic acid production, atmospheric formation of N_2O, use in anaesthesia, enhanced emissions due to global warming and aquatic emissions due to non-agricultural nitrogen inputs.

NEO and IPCC estimates for N_2O emissions from Bulgaria are 24 and 29 Gg N y^{-1}, respectively, and from the Netherlands 37 and 45 Gg N y^{-1} (mid-point estimates). Thus annual anthropogenic N_2O emissions from the Netherlands are about 15 Gg N_2O-N higher than those from Bulgaria. Dutch emissions exceed Bulgarian in particular for the following sources: agriculture, traffic and nitric acid production. These differences are caused by differences in human activities mainly.

Key-words: nitrous oxide, N_2O, Bulgaria, The Netherlands, greenhouse gas inventory.

1. Introduction

Nitrous oxide (N_2O) is one of the gases contributing to the enhanced greenhouse effect (*Houghton et al.,* 1995). The atmospheric concentrations of N_2O have been increasing (*Prinn et al.,* 1990), because of human activities. Food production, energy use, industry and production of waste result in emissions of N_2O. Worldwide emissions are nowadays 50% higher than in pre-industrial times (*Bouwman et al.,* 1995). Agriculture is one of the most important sources of N_2O. Global inventories indicate that about two-thirds of the anthropogenic nitrous oxide emissions are related to human food production (e.g. *Bouwman et al.,* 1995; *Nevison et al.,* 1996).

Bulgaria and the Netherlands, like all other parties to the United Nations Framework Convention on Climate Change (UNFCCC), agreed to report their national greenhouse gas emissions. Most countries estimate their N_2O emissions following the IPCC Guidelines for National Greenhouse Gas Inventories (*IPCC/OECD,* 1995, 1997). These guidelines provide default methodologies for estimating greenhouse gas emissions on a national scale. Although IPCC Guidelines are available, countries are free to use their own, country-specific methods. For Bulgaria an inventory of N_2O emissions exists, which was made following the 1995 IPCC Guidelines for Greenhouse Gas Inventories, using default emission factors (*Bogdanov,* 1995, 1996).

The Netherlands is one of the few countries that reported N_2O emissions using an alternative method (*Van Amstel et al.,* 1994; *VROM,* 1994). The Dutch method is based on a review of experimental studies in and outside the Netherlands (referenced in *Kroeze,* 1994, 1995). Other than in the Netherlands, no experimental studies on N_2O emissions have been performed for Bulgaria. This implies that a Bulgarian inventory should be based on data from other regions of the world. In the present study we will investigate to what extent the Dutch method, or NEO method, is applicable to Bulgaria and to what extent it differs from the IPCC Guidelines (IPCC method). This would not only result in an improved insight into Bulgarian emissions, but it would also contribute to the evaluation of inventory methods in general. The purpose of this study is: (i) to apply both the IPCC and NEO methods to Bulgaria and the Netherlands, (ii) to investigate differences between the NEO and IPCC methods and (iii) to compare emissions from Bulgaria to emissions from the Netherlands.

2. Methods for estimating national N_2O emissions

In this study two methods for estimating N_2O emissions are compared: the IPCC Guidelines for national Greenhouse Gas Inventories (*IPCC/OECD,* 1995, 1997) and a Dutch methodology developed for the Dutch National Environmental Outlooks (NEO) by the National Institute for Public Health and Environmental Protection (*Kroeze,* 1994, 1995).

3. *IPCC Guidelines for National Greenhouse Gas Inventories (IPCC method; Box 1)*

The IPCC method was developed such that it is applicable to any country of the world. It should assist countries in reporting their emissions as required for parties to the United Framework Convention on Climate Change. In the IPCC method emissions are estimated by applying a given (default) emission factor to activity data. The input data needed are usually available from existing databases such as those provided by the Food and Agricultural Organization (FAO). The following sources of N_2O are considered in the IPCC Guidelines: agriculture, waste, energy, and industry (*IPCC/OECD,* 1995, 1997). The most important sources are described below (see also *Box 1*).

In 1995 the first version of the IPCC Guidelines was published (*IPCC/-OECD,* 1995). An evaluation resulted in Phase II Guidelines (*IPCC/OECD,* 1997), which differs from the existing guidelines for N_2O emissions from agriculture and waste (sewage) (*Mosier et al.,* in press). In the present study we will use this updated version of the IPCC Guidelines.

3.1 Agriculture

Agriculture is one of the most important sources of N_2O and gives rise to short-term and long-term emissions of N_2O. The updated (Phase II) IPCC method aims at considering the full nitrogen cycle. Three sources of N_2O related to the N cycle are distinguished in the IPCC method (*Mosier et al.,* in press):

(i) direct emissions from agricultural soils, taking place as a result of fertilization of soils,
(ii) emissions from animal production and
(iii) N_2O produced after the nitrogen leaves the agricultural field (indirect emissions).

The direct emissions from agricultural fields take place shortly after nitrogen additions to soils (*Mosier,* 1994). In the IPCC Guidelines direct emissions are estimated as 1.25 (0.25–2.25)% of the nitrogen input from fertilizers, biological nitrogen fixation or crop residues, in line with the work by *Bouwman* (1996). The N input is from synthetic and organic fertilizers, nitrogen in crop residues and from nitrogen fixing plants. Another source of direct soil emissions of N_2O are cultivated histosols. These are assumed to emit 5 kg N_2O-N per hectare in regions with temperate or boreal climates and 10 kg N_2O-N per hectare in the tropics.

Animals are the second agricultural sources of N_2O considered in the IPCC Guidelines (*Oenema,* 1995). Animals not only cause N_2O emissions when manure is used as fertilizer, but also when manure is stored in stables or during grazing of animals (e.g. *Bouwman et al.,* 1995; *Velthof* and *Oenema,* 1994a).

Box 1. Summary of IPCC method for estimating N_2O emissions (kg N y^{-1}); see for a detailed description *IPCC/OECD* (1995, 1997) and *Mosier et al.* (in press)

Agriculture

direct soil emissions = EF1 · N-INPUT + EF2 · AREAHIS
animal related emissions = sum ($EF3_t$ · $N\text{-}AWMS_t$)
indirect emissions = EF4 · (NO_x + NH_3) + EF5 · NLEACH

Waste

emissions from waste incineration = EF6 · MSW
emissions from sewage treatment = EF7 · NSEWAGE

Energy

emissions from stationary combustion = EF8 · FUEL
emission from mobile combustion = EF9 · KM

Industry

emissions from adipic acid production = EF10 · AA
emissions from nitric acid production = EF11 · NA, where

EF1	= 0.0125 (0.0025–0.0225) kg N_2O-N/kg N/y
EF2	= 5 or 10 kg N_2O-N per hectare of histosol per year
EF3	= emission factor in kg N_2O-N/kg N/y = 0.001 (<0.002) for anaerobic lagoon and liquid systems; 0.02 (0.005–0.03) for solid storage, dry lot, pasture range and paddock; 0.005 for other systems
EF4	= 0.01 (0.002–0.02) kg N_2O-N/kg N/y
EF5	= 0.025 (0.002–0.12) kg N_2O-N/kg N/y
EF6	= 0.019 (0.006–0.127) kg N_2O-N/kg MSW incinerated
EF7	= 0.01 (0.002–0.12) kg N_2O-N/kg N/y
EF8	= 0.064 (0–0.7), 0.382 (0–1.782) and 0.891 (0–6.343) g N_2O-N/GJ, for gas, oil and coal, respectively
EF9	= emission factors for several types of vehicles (see *IPCC/OECD*, 1995)
EF10	= 0.191 kg N_2O-N/kg adipic acid
EF11	= 17 (7–27) g N_2O-N/kg nitric acid
N-INPUT	= N input to soils from fertilizers (excluding NH_3 emissions), crop residue and N fixation (kg N y^{-1}) = Fsn + Faw + Fbn + Fcr
Fsn	= synthetic fertilizer use (kg N y^{-1}) excluding 10% that is emitted as NH_3 and NO_x
Faw	= manure N used as fertilizer = manure N produced · (1 – (fraction produced in meadows + fraction lost as NH_3 + fraction used for fuel)); manure production in meadows is from *IPCC/-OECD* (1997), 20% of manure-N is lost as NH_3 and 0% used as fuel in Bulgaria and the Netherlands
Fbn	= biological N fixation (kg N y^{-1}) = 3% of the dry matter legume production = 3% of twice the production of pulses and soybean as reported by FAO
Fcr	= N in crop residues left on the field (kg N y^{-1}); calculated as 55% of the total N in crop biomass (assuming 45% is removed as crop) = 45% of 3% and 1.6% of the dry matter production of legumes and other crops, respectively = 45% of 3% and 1.6% of twice the production of pulses/soybean and other crops in FAO data, respectively
AREAHIS	= area of cultivated histosols in the country (ha)
N-AWMS	= manure N produced in different types (t) of Animal Waste Management Systems (AWMS) (kg N y^{-1}) estimated from default values for N excretion per animal and fraction of N produced per type of AWMS from *IPCC/OECD* (1997)
NO_x + NH3	= NO_x and NH_3 emitted in the country (kg N y^{-1})
NLEACH	= N leaching (kg N y^{-1}) = 30% of N-INPUT
NSEWAGE	= human sewage N production (kg N y^{-1}) = 16% of annual protein intake in kg
MSW	= municipal solid waste incineration (kg y^{-1})
FUEL	= stationary combustion of gas, coal and oil (GJ y^{-1})
KM	= vehicle-kilometers (km y^{-1}) or fuel use (GJ y^{-1}) per vehicle type
NA	= nitric acid production (kg y^{-1})
AA	= adipic acid production (kg y^{-1})
t	= type of AWMS

The related N_2O emissions are estimated as a percentage of the amount of nitrogen produced by animals in different animal waste management systems (Box 1). The starting point for the calculations is the nitrogen excretion by different six animal types (dairy cattle, non-dairy cattle, poultry, sheep, swine and other) in six different animal waste managing systems, AWMSs (anaerobic lagoon, liquid systems, solid storage and dry lot, pasture range and paddock, and other systems). The phase II method of IPCC provides default values for emission factors (% of manure-N that is lost as N_2O for different AWMSs), manure-N production per animal type (kg N animal^{-1} y^{-1}) and the percentage of manure-N that is produced in different AWMSs (% per animal type) for eight regions, among which there are Eastern Europe (including Bulgaria) and Western Europe (including the Netherlands). These default factors for nitrogen excretion in different waste management systems are based on *Ecetoc* (1994), *Safley et al.* (1992), *Vetter et al.* (1989) and *Steffens* and *Vetter* (1990) mainly. The N_2O emission factors are based on a review of experimental studies, listed in *IPCC/OECD* (1997). The only input data needed to calculate N_2O emissions in the IPCC method are animal numbers in the country.

The third agricultural source of N_2O includes the indirect emissions. Indirect emissions of N_2O take place when nitrogen leaves the agricultural fields as gas (ammonia or nitrogen oxides) or as leached nitrogen and is converted to N_2O by bacteria in remote soils or in aquatic systems. The IPCC method estimates indirect emissions as a result of NH_3 or NO_x losses as 1% of the amount of NH_3-N and NO_x-N emitted (Box 1). This is within the range of direct emissions from agricultural soils, and in line with findings by *Bowden et al.* (1991) and *Brumme* and *Beese* (1992). The amount of N from manure and fertilizers that leaches is assumed to be 30% of the total manure and fertilizer nitrogen applied. After leaching, this nitrogen may be nitrified or denitrified, giving rise to emissions of N_2O from rivers and estuaries (*Seitzinger,* 1988, 1990). The emission factor for indirect emissions due to leaching is 2.5% (Box 1), and deduced from extensive literature review (*IPCC/OECD,* 1997).

3.2 Waste

In the IPCC Guidelines two sources of N_2O are included that are related to waste handling: (i) incineration of municipal solid waste (MSW) and (ii) sewage treatment. MSW incineration gives rise to abiogenic N_2O formation (Box 1). Emissions from sewage take place in sewage treatment plants or when the sewage is discharged on surface waters. In the IPCC method the N flux in human sewage is determined on the basis of annual intake of proteins in which the fraction of N is 0.16 (*IPCC/OECD,* 1997). The daily intake per capita in the world varies between 55 and 110 g protein day^{-1}. The related N_2O emissions are calculated as 1% of the amount of N in the sewage (Box 1).

3.3 Energy

The IPCC method provides default emission factors for the stationary combustion of gas, coal and oil (Box 1). However, an emission factor for fluidized bed combustors (FBC) in utility boilers is not provided, while these systems are known to emit more N_2O than conventional coal-fired power plants. In addition, the IPCC method provides emission factors for traffic (listed in *IPCC/OECD,* 1995, 1997).

3.4 Industry

The IPCC method considers process N_2O emissions during production of nitric and adipic acid (*IPCC/OECD,* 1995, 1997). In both Bulgaria and the Netherlands nitric acid is produced, but no adipic acid. The activity data needed are the amounts of HNO_3 produced.

4. Method developed for Netherlands Environmental Outlook (NEO method; Box 2)

The NEO method includes N_2O of both anthropogenic (i.e. resulting from human activities) and natural (i.e. not induced by human activities) origin:

$$\textit{total emissions} = \textit{anthropogenic} + \textit{natural emissions}.$$

In addition, the NEO method distinguishes between biogenic (i.e. of biological origin) and abiogenic emissions. The biogenic emissions are estimated as:

$$\textit{biogenic emissions} = \textit{EFb} \cdot \textit{N-INPUT} + \textit{background},$$

where *EFb* is an emission factor for biogenic emissions, *N-INPUT* is the anthropogenic nitrogen flux to, for instance, soils and waters (kg N y^{-1}), and *background* is the natural plus enhanced background emissions. *EFb* is based on a review of available data, including studies performed in the Netherlands (EF12 and EF14 in *Box 2*). Background emissions may be enhanced due to, for instance, lowering of the ground water level. The total background emissions are calculated as 10 (1–20) and 1 (0.5–5) kg N ha^{-1} y^{-1} for organic and mineral soils, respectively, and the values are mainly based on *Velthof* and *Oenema* (1994b) and *Bouwman* (1996). The natural part of this is, for the Netherlands, estimated from model simulations by *Bouwman* and *van der Hoek* (1991).

Abiogenic emissions are estimated as:

$$\textit{abiogenic emission} = \textit{EFa} \cdot \textit{ACTIVITY} + \textit{abiogenic natural source},$$

Box 2. Summary of NEO method for estimating N_2O emissions (kg N y^{-1}); see for a detailed description *Kroeze* (1994, 1995)

Natural

natural biogenic N_2O = natural background emissions from soils[1]
natural abiogenic N_2O = atmospheric formation = 0.1% of NH_3-N emission[2]

Agriculture

biogenic N_2O from soils and leached N = EF12 · N-INPUT + background emissions[1]

Waste

emissions from waste incineration = EF13 · MSW
emissions from sewage treatment = EF14 · NSEWAGE

Energy

emissions from stationary combustion = EF15 · FUEL
emission from mobile combustion = EF16 · KM

Industry

emissions from adipic acid production = as IPCC method (Box 1)
emissions from nitric acid production = as IPCC method (Box 1)
other chemical industry = in-country estimate

Other

atmospheric formation = 0.1% of NH_3-N emission[2]
N_2O due to non-agricultural N inputs to surface waters = N-INPUT · EF12
atmospheric deposition of non-agricultural NH3 = NH3 emission · EF12
atmospheric deposition of non-agricultural NO_x = NO_x emission · EF12
emissions from anaesthesia = use in anaesthesia

where

EF12 = emission factor (kg N_2O-N per kg N) = 0.1 (0.002–0.125), except for anaerobic storage of manure when EF12 = <0.002; N-inputs to organic soils, manure injected to soils, urine patches and biological treatment of manure when EF12 = 0.2 (0.125–0.25); and nitric acid added to manure and aerobic storage of manure, when EF12 = 0.5 (0.25–0.1)

EF13 = 12.7 (3.2–127) g N_2O-N per ton of MSW (from *Spoelstra* (1993) and IPCC method)

EF14 = 0.1 (0.002–0.125) kg N_2O-N per kg N removal in sewage treatment

EF15 = same as IPCC method (Box 1) except for fluidized bed combustion (FBC) when EF15 = 26.7 (4.4–49) G N_2O-N GJ^{-1} (from *Spoelstra*, 1993)

EF16 = emission factors for several types of vehicles (from *Baas*, 1991)

N-INPUT = Nitrogen flux (kg N y^{-1}): synthetic fertilizer, animal manure, atmospheric deposition of NH_3 or NOx, biological N_2 fixation, nitrogen leaching, sewage

MSW, NSEWAGE, FUEL, KM: see Box 1

---

[1] from *Velthof* and *Oenema* (1994a), *Bouwman* (1996) and *Bouwman* and *van der Hoek* (1991)
[2] *Dentener* (personal communication)

where *EFa* is an emission factor for abiogenic emissions, *ACTIVITY* is the human activity considered, and *abiogenic natural source* include N_2O formation in the unpolluted atmosphere mainly. *EFa* is partly based on IPCC emission factors, and partly on *Baas* (1991, 1994), *Spoelstra* (1993) and *Dentener* (personal communication) (EF13, EF15 and EF16 in Box 2). A detailed description of the NEO method is referred in *Kroeze* (1994, 1995). In the following a description is given of the most important differences between the IPCC and NEO methods.

4.1 Natural emissions

Natural sources include soils, waters and the atmosphere. In soils, bacteria produce N_2O during nitrification and denitrification. These natural background emissions are estimated for the Netherlands by use of model calculations (*Bouwman* and *van der Hoek*, 1991). Natural emissions from aquatic sources could not be quantified. In the atmosphere, N_2O is formed during the oxidation of NH_3. The NEO method assumes that 0.1% of NH_3 emitted is oxidized to N_2O in the Netherlands, of which 10% is natural and 90% is anthropogenic (*Dentener,* personal communication).

4.2 Agriculture

The most important differences between the NEO and IPCC methods for agriculture are caused by differences in emission factors used (Box 1 and 2). For instance, the direct emissions from agricultural soils depend on the type of soil in the NEO method. The NEO emission factors used are 1 (0.2–1.25)% of the N applied for mineral soil and 2 (1.25–2.5)% for organic soil. In the IPCC method differences in soil type are not considered.

Second, emission factors for animal manure in stables differ. The IPCC method is more detailed in this respect (Box 1). In the NEO method only three types of manure storage are considered: anaerobic storage with low emissions, aerobic storage with relatively high emissions, and the manure to which nitric acid has been added in order to avoid emissions of NH_3. Nitric acid addition is nowadays not a common practice in the Netherlands.

Another difference between the two methods is the presumed evaporation of NH_3 from fertilizers and manure (in the NEO method it is mostly based on *Van der Hoek,* 1994). For instance, NEO method assumes that 2% of synthetic fertilizers volatilize as NH_3, as opposed to 10% in the IPCC method. This can be explained by the fact that in the Netherlands virtually no fertilizers are used that give rise to NH_3 emissions (e.g. urea and anhydrous ammonia). The NEO method further assumes that about 8% of the manure N produced in meadows evaporates as NH_3. Of the remaining manure-N about 60% is urine and 40% is

faeces, to which N_2O emission factors of 2 and 1% are applied, respectively (Box 2). Assumptions about NH_3 emissions from stables also differ: the NEO method assumes that about 15% of manure N in stables is emitted as NH_3.

Nitrous oxide emissions related to leaching are calculated differently in the two methods. The NEO method assumes that 20% of the manure and fertilizers applied to soils leaches to the ground water (as opposed to 30% in the IPCC method) and the applied NEO emission factor is 1% (as opposed to 2.5% in the IPCC method). In addition, the methods use different default factors for N excretion by livestock.

Finally, the number of sources included in the two methods differ. The NEO method includes background emissions from both organic and mineral soils. The IPCC method, however, only includes background emissions from cultivated organic soils (histosols). Alternatively, the IPCC method considers crop residues that are left on the field as external N input (Box 1), while the NEO method does not.

4.3 Waste

For municipal solid waste (MSW) incineration the NEO method adopts an emission factor based on measurements in Dutch waste incineration (*Spoelstra,* 1993). This emission factor is 10% lower than the IPCC emission factor. The emission from sewage in NEO is estimated according to the quantity of N removed from the sewage and the nitrogen in the influent and the effluent of the waste water treatment. The applied emission factor is 1%.

4.4 Energy and industry

NEO emissions related to energy use and industrial processes are for most processes estimated as in the IPCC method. Exceptions are fluidized bed combustion and traffic, for which the NEO method uses emission factors that were derived from Dutch studies (*Spoelstra,* 1993; *Baas,* 1991, 1994). In addition, the NEO method includes chemical industries other than adipic and nitric acid production.

5. Nitrous oxide emissions from Bulgaria: IPCC and NEO methods

The emissions of N_2O presented for Bulgaria refer to 1988, since this year was chosen as base year for Bulgaria under the United Nations Frame Convention on Climate Change (UNFCCC). The emissions as calculated following the IPCC method are presented in *Tables 1* and *2* and are from *Bogdanov* (1995, 1996) with the exception of emissions from agriculture and sewage (this study).

Table 1. Nitrogen and nitrous oxide fluxes in Bulgarian and Dutch agriculture (IPCC method[1]) in Gg N y^{-1} (ranges are based on ranges in emission factors)

	Bulgaria		The Netherlands	
	Activity	N_2O emission	Activity	N_2O emission
Direct soil emissions				
Direct soil emissions	N input[2]		N input[2]	
- synthetic fertilizer	385	4.8 (1.0–8.7)	370	4.6 (0.9–8.3)
- animal waste	136	1.7 (0.3–3.1)	521	6.5 (1.3–11.7)
- biological N fixation	11	0.1 (0.0–0.3)	5	0.1 (0.0–0.1)
- crop residue	92	1.2 (0.2–2.1)	25	0.3 (0.1–0.6)
Histosols	Area (ha)		Area (ha)	
- area (ha)	0	0.0 (0.0 – 0.0)	274124	1.4 (0.6–4.1)
Animal production				
	N production			
anaerobic lagoon	4	0.0 (0.0–0.0)	0	0.0 (0.0–0.0)
liquid	59	0.1 (0.0–0.1)	420	0.4 (0.0–0.8)
daily spread	0	0.0 (0.0–0.0)	62	0.0 (0.0–0.0)
solid/dry lot	56	1.1 (0.3–1.7)	122	2.4 (0.6–3.7)
pasture/paddock	151	3.0 (0.8–4.5)	103	2.1 (0.5–3.1)
other	95	0.5 (0.5–0.5)	71	0.4 (0.4–0.4)
Indirect N_2O emission				
	N flux			
NH_3 deposition	116	1.2 (0.2–2.3)	196	2.0 (0.4–3.9)
leaching	238	6.0 (0.5–28.6)	355	8.9 (0.7–42.6)
Total		19.6 (3.8–51.7)		29.0 (5.4–79.3)

[1] see Box 1; input data for Bulgaria are from *FAO* (1990) and for the Netherlands from *Kroeze* (1994, 1995)

[2] Fsn + Faw + Fbn + Fcr (see Box 1)

Table 2. IPCC method: N_2O emissions from Bulgaria and the Netherlands in Gg N_2O-N y^{-1} (ranges are based on ranges in emission factors)

	Bulgaria[1]	**The Netherlands**[2]
Agriculture		
direct soil emissions	7.8 (1.6–14.0)	12.9 (2.9–24.9)
animal emissions	4.7 (1.5–6.8)	5.3 (1.5–7.9)
indirect emissions	7.1 (0.7–30.9)	10.8 (1.1–46.5)
Total	19.6 (3.8–51.7)	29.0 (5.4–79.3)
Waste		
MSW incineration	0.0 (0.0–0.0)	0.1 (0.0–0.4)
sewage	0.6 (0.1–6.9)	0.8 (0.2–9.6)
Total	0.6 (0.1–6.9)	0.9 (0.2–10.0)
Energy		
stationary combustion	3.5 (0.5–26.8)	0.6 (0.0–4.4)
mobile combustion	0.2 (0.1–0.4)	3.7 (1.0–6.3)
Total	3.7 (0.6–27.2)	4.3 (1.0–10.7)
Industry		
nitric acid production	4.9 (2.0–7.8)	10.5 (4.3–16.7)
adipic acid production	0.0 (0.0–0.0)	0.0 (0.0–0.0)
Total	4.9 (2.0–7.8)	10.5 (4.3–16.7)
Total anthropogenic N_2O	28.8 (6.5–93.7)	44.7 (10.9–116.8)

[1] *Bogdanov* (1995), except emissions from agriculture and sewage (this study); ranges are based on ranges in emission factors;
[2] *Kroeze* (1994, 1995), except emissions from agriculture and sewage (this study); ranges are based on ranges in emission factors

Total emissions from Bulgaria calculated using the IPCC method amount to 29 (7–94) Gg N_2O-N y^{-1}. Agriculture is the most important contributor to these emissions, contributing by about two-thirds to total emissions. The input data needed for the IPCC method (Box 1), including fertilizer use, animal numbers and crop production are from *FAO* (1990). In Bulgaria 428 Gg of fertilizer N was used in 1988, mostly as ammonium nitrate (thus Fsn = 385 Gg N). The livestock in the country produced 365 Gg N from which 41% (151 Gg N) was deposited in meadows during pasture and 59% in stables. About 170 Gg of manure-N was used as fertilizer (in-country estimate; thus Faw = 136 Gg N). There are no histosols in Bulgaria, and the area of arable land and permanent crops amounts to 4.1 million hectare (grasslands are not fertilized). Production of pulses and soybeans amounts to 177 Gg, giving rise to 11 Gg of nitrogen added to soils (Fbn). Similarly, 92 Gg of N is input to soils from crop residues (Fcr), as calculated from FAO crop production data and following Box 1. For estimating the emission of N_2O from human sewage following the IPCC method, the annual nitrogen flux in human nutrition is needed as input. In Bulgaria, daily protein intake amounts to 110 g protein^{-1} person^{-1} day (*FAO*, 1990), giving rise to 0.6 (0.1–6.9) Gg N_2O-N emitted annually.

The NEO method estimates Bulgarian emissions at 24 (8–52) Gg N_2O-N. These emissions are found to be largely anthropogenic (*Tables 3* and *4*). The application of the NEO method to Bulgaria required a few additional assumptions, in particular with respect to background emissions from soils. Background emissions are partly natural, and partly a result of agricultural practices (Box 2). For the Netherlands the natural part of the background emissions has been estimated based on country-specific model results, while total current background emissions were estimated from measurements in Dutch soils. For Bulgaria such calculations and measurements have not been performed, so that additional assumptions were needed. For the Netherlands the default emission factor for total background emissions is 10 (1–20) kg N_2O-N ha^{-1} y^{-1} for grassland on organic soil and 1 (0.5–5) kg N_2O-N ha^{-1} y^{-1} for grassland and arable land on mineral soil. Since in Bulgaria there are no organic soils, it is reasonable to assume for Bulgaria that the emission factor for background emissions amounts to 1 kg N_2O-N ha^{-1} y^{-1}, half of which may be natural.

Energy and industry related emissions account for about one-third of Bulgarian emissions according to the NEO method (Table 3) and are calculated from fuel use, car mileage and nitric acid production as presented in *Bogdanov* (1995, 1996). The difference between the IPCC and NEO estimates for Bulgarian traffic emissions is a result of different emission factors used (Box 1 and 2).

Almost two-thirds of Bulgarian emissions are from agriculture according to the NEO method (Tables 3 and 4). The input data on fertilizer use, animal numbers and land area are from FAO (*FAO,* 1990). Animal manure production is calculated by use of the default factors for nitrogen excretion from the IPCC

method. And ammonia emissions are estimated using the emission factors provided by the NEO method: 2 and 20% of synthetic and organic fertilizer use, respectively, and 8% and 15% of manure-N produced in meadows and stables, respectively. In the NEO method nitrogen leaching is estimated as 20% of the N input to soils.

Table 3. Agricultural emissions from Bulgaria (NEO method) in Gg N_2O–N y^{-1} (ranges are based on ranges in emission factors)

	Activity level (Gg N)[1]	N_2O emission (Gg Ny^{-1})[2]
Background	4100000 hectare	2.1 (1.0–10.3)
Synthetic fertilizer (excluding NH_3)		
– on mineral soil	419	4.2 (0.8–5.2)
– on organic soil	0	0.0 (0.0–0.0)
Animal manure (excluding NH_3)		
Produced in meadows		
– urine (60%)	83	1.7 (1.0–2.1)
– faeces (40%)	56	0.6 (0.1 – 0.7)
Produced in stables		
– aerobic storage	47	2.4 (1.2–4.7)
– anaerobic storage	133	0.1 (0.0–0.3)
Applied to soils		
– mineral soils	115	1.2 (0.2–1.4)
– organic soils	0	0.0 (0.0–0.0)
– injection	0	0.0 (0.0–0.0)
NH_3 emissions		
manure	74	0.7 (0.2–0.9)
synthetic fertilizer	9	0.1 (0.0–0.1)
Biological N fixation	11	0.1 (0.0–0.1)
Leaching	113	1.1 (0.2–1.4)
Total		14.2 (4.8–27.3)

[1] except when mentioned otherwise;
[2] ranges are based on ranges in emission factors

Table 4. NEO method: N_2O emissions from Bulgaria and the Netherlands in Gg N y^{-1} (ranges are based on ranges in emission factors); n.q. = not quantified

	Bulgaria[1]	**The Netherlands**[2]
Natural emissions		
soils	2.1 (1.0–10.3)	1.5 (0.5–3.0)
atmospheric form.	0.0 (0.0–0.0)	0.0 (0.0–0.0)
Total	2.1 (1.0–10.3)	1.5 (0.5–3.0)
Anthropogenic emissions		
Agriculture		
background	2.1 (1.0–10.3)	3.0 (0.6–11.1)
fertilizer	4.2 (0.8–5.2)	4.4 (1.2–5.5)
manure meadows	2.2 (1.2–2.8)	2.2 (1.1–2.7)
manure stables	2.5 (1.2–5.0)	0.5 (0.1–0.9)
manure fertilizer	1.2 (0.2–1.4)	3.2 (1.0–4.0)
NH_3 emission	0.8 (0.2–1.0)	1.6 (0.3–2.1)
legumes	0.1 (0.0–0.1)	0.2 (0.0–0.2)
leaching	1.1 (0.2–1.4)	1.8 (0.4–2.3)
Total	14.2 (4.8–27.3)	16.9 (4.7–28.8)
Waste		
MSW incineration	0.0 (0.0–0.0)	0.0 (0.0–0.4)
sewage	0.1 (0.0–0.2)	0.3 (0.1–0.3)
Total	0.1 (0.0–0.2)	0.3 (0.1–0.8)
Energy		
stationary combustion	0.5 (0.0–3.5)	0.7 (0.0–4.5)
mobile combustion	0.3 (0.1–1.0)	3.4 (1.5–11.5)
NO_x emission	1.6 (0.3–2.1)	1.2 (0.2–1.5)
Total	2.5 (0.4–6.5)	5.4 (1.8–17.5)
Industry		
nitric acid	4.9 (2.0–7.8)	10.5 (4.3–16.7)
adipic acid	0.0 (0.0–0.0)	0.0 (0.0–0.0)
other	0.0 (0.0–0.0)	1.1 (1.1–1.1)
Total	4.9 (2.0–7.8)	11.6 (5.4–17.7)
Other		
atmospheric formation	0.0 (0.0–0.0)	0.0 (0.0–0.1)
other N-loading	n.q.	0.6 (0.1–0.7)
other NH_3 emission	0.0 (0.0–0.0)	0.1 (0.0–0.2)
other NO_x emission	0.0 (0.0–0.0)	0.5 (0.1–0.6)
anaesthesia	0.0 (0.0–0.0)	0.3 (0.3–0.3)
Total	0.0 (0.0–0.0)	1.6 (0.6–1.9)
Total anthropogenic	21.7 (7.3–41.8)	35.6 (12.5–66.7)
Total N_2O	23.7 (8.3–52.1)	37.1 (13.0–69.7)

[1] this study; [2] *Kroeze* (1994, 1995)

Waste and the category "other" are moderate sources of N_2O in Bulgaria in the NEO estimate (Table 4). It is assumed here that there is no municipal solid waste (MSW) incineration. The NEO method calculates emissions from sewage treatment plants based on the amount of N removed during treatment of municipal waste water. In Bulgaria, however, data on N removal are scarce and waste water treatment may not be as commonly applied as in the Netherlands. Tentatively assuming equal per capita N removal rates in Bulgaria and the Netherlands, N removal in Bulgaria is estimated at 15.5 Gg N y^{-1}. The related N_2O emissions in Bulgaria are estimated here as 0.1 (0.0–0.2) Gg N y^{-1}. Emissions of N_2O due to non-agricultural N-loading to waters have not been quantified due to the lack of input data.

6. Nitrous oxide emissions from the Netherlands: IPCC and NEO methods

Dutch nitrous oxide emissions in 1990 according to the NEO and IPCC methods have been published in *Kroeze* (1994, 1995), with the exception of agricultural and sewage-related emissions following the IPCC Phase II method (Table 1). Total emissions are 45 (11–117) Gg N_2O-N y^{-1} for the IPCC method and 37 (13–70) Gg N_2O-N y^{-1} for the NEO method (Tables 2 and 4).

The emissions from agriculture are 29 (5–79) Gg N_2O-N y^{-1} according to the revised IPCC method (Table 1). This is based on estimates for total nitrogen input to Dutch soils (N-INPUT in Box 1) amounting to 922 Gg N y^{-1} from synthetic fertilizers (excluding ammonia emissions), animal waste (excluding ammonia emissions), biological N fixation and crop residues. The total use of synthetic fertilizer in the Netherlands is 412 Gg N y^{-1} (*RIVM,* 1993) and according to the IPCC methodology 10% of this is lost as NH_3 (so that Fsn = 370 Gg N; Table 1). Animal manure production amounts to 780 Gg N y^{-1}, of which 20% is lost as NH_3 according to the IPCC method and 13% is produced in meadows (thus Faw = 521 Gg N; Table 1). The nitrogen input from N-fixing crops (Fbn) is calculated as 6% of the dry biomass production of pulses and soybean. In the Netherlands dry pulses production amounts to 83 Gg y^{-1} (*FAO,* 1990); the related N input is therefore 5 Gg N y^{-1} (Table 1). Nitrogen in crop residue (Fcr) is, in the IPCC methodology, estimated as 55% of the total N in crop, where total N in crop is 6% of dry pulses and soybean produced and 3% of dry production of other crops (i.e. 1352 Gg of cereals in the Netherlands (*FAO,* 1990)). Nitrogen input from crop residue in the Netherlands would therefore be 25 Gg N y^{-1} (Table 1). Finally, the area of organic soil in the Netherlands is 274124 hectare (*Van Amstel et al.,* 1994). Other input data used for the Netherlands are presented in detail in *Kroeze* (1994, 1995). This present (phase II) IPCC estimate for agricultural emissions (29 Gg N) is much higher

than the 2.4 Gg N as estimated following the previous (phase I) IPCC Guidelines as a result of more sources included and higher emission factors used (*Kroeze*, 1995).

7. N_2O emissions: IPCC method versus NEO method

The N_2O emissions for both Bulgaria and the Netherlands are summarized in *Figs. 1, 2* and *3*. The IPCC Phase II method results in total N_2O emissions that are about 20% higher than the NEO estimate for Bulgaria and the Netherlands, respectively. These differences in mid-point estimates result from a net effect; for some sources the IPCC method exceeds the NEO method (agriculture, waste and, for Bulgaria, energy) while for others the IPCC estimates are lower than or equal to the NEO estimates (natural emissions, industry, other and, for the Netherlands, energy). The difference between the two methods is larger for Bulgaria than for the Netherlands, because of the difference in N_2O estimates from stationary combustion mainly.

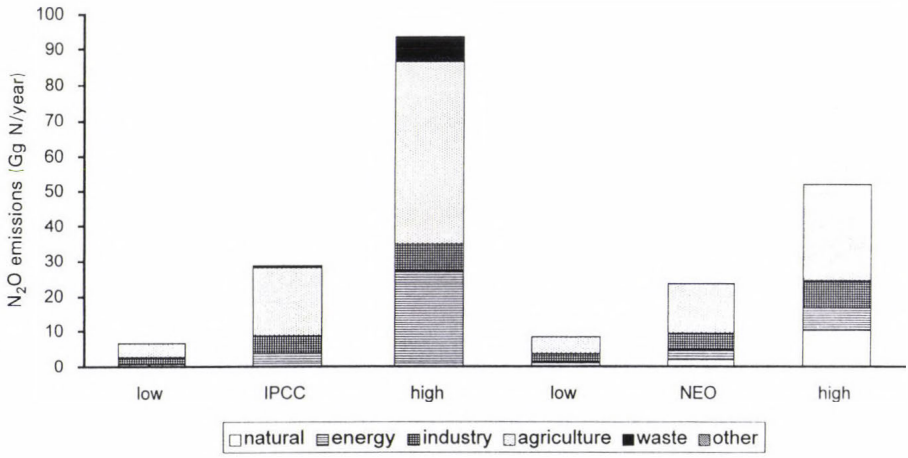

Fig. 1. Bulgarian 1988 emissions of N_2O estimated following the IPCC and NEO methods. Low and high estimates refer to ranges in emission factors (Tables 2 and 4).

Although the IPCC method tends to produce higher mid-point estimates for total N_2O emissions, the ranges of IPCC and NEO emissions show overlap, and the IPCC range exceeds the NEO range (Fig. 3). For instance, the IPCC range for Dutch emissions amounts to 11–117 Gg N_2O-N y^{-1} (Table 2), while the NEO range is 13–70 Gg N_2O-N y^{-1} (Table 4). This is in line with the fact that

the NEO method has been validated against Dutch research where possible, while the IPCC method is considered applicable to any country of the world and thus it is more uncertain. The relatively large ranges reflect the uncertainty in emission factors only.

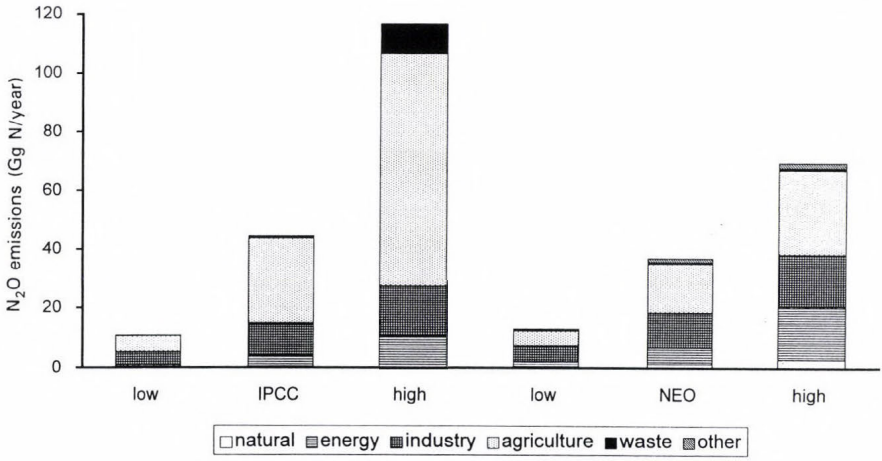

Fig. 2. Dutch 1990 emissions of N_2O estimated following the IPCC and NEO methods. Low and high estimates refer to ranges in emission factors (Tables 2 and 4).

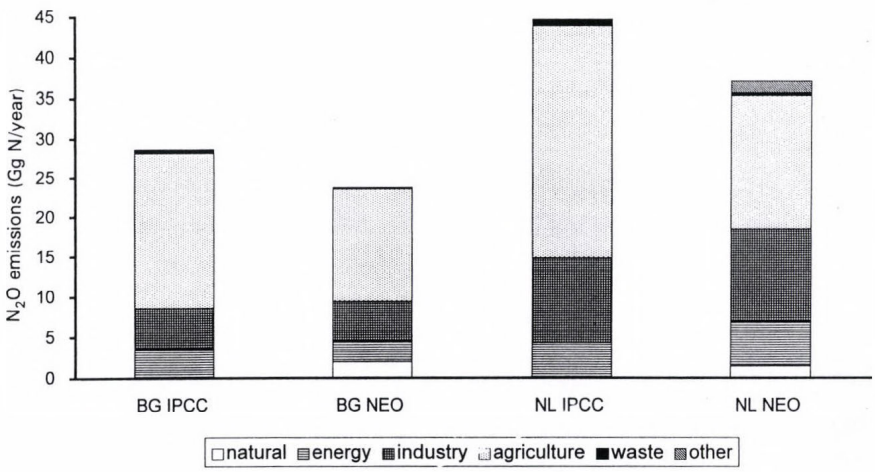

Fig. 3. Bulgarian 1988 and Dutch 1990 emissions of N_2O estimated following the IPCC and NEO methods.

The NEO method includes a number of sources that are not included in the IPCC method. These are natural emissions, enhanced background emissions from mineral soils, N_2O induced by NOx deposition, chemical industries other than nitric and adipic acid, atmospheric formation of N_2O, use in anaesthesia, enhanced emissions due to global warming and aquatic emissions due to non-agricultural N-inputs (see Fig. 3). On the other hand, the NEO method does not account for emissions resulting from crop residues.

Some sources are calculated in different ways in the two methods. For instance, N excretion by livestock in the Netherlands according to the IPCC method (780 Gg N) exceeds the NEO estimate (585 Gg N; *Van der Hoek*, 1994). As a result, there are differences between estimates for N_2O from manure in stables and manure applied as fertilizer. In addition, the enhanced background emissions are estimated differently, as well as emissions as a result of leaching. The net effect of this is that the IPCC estimate for agricultural emissions exceeds the NEO estimate by about 70% for the Netherlands and 40% for Bulgaria.

8. N_2O emissions: Bulgaria versus the Netherlands

Total N_2O emissions from Bulgaria are 29 (IPCC) and 24 (NEO) Gg N y^{-1} and from the Netherlands 45 (IPCC) and 37 (NEO) Gg N y^{-1}. Thus total anthropogenic emissions from the Netherlands are about 15 Gg N higher than those from Bulgaria (Figs. 1, 2 and 3). Dutch emissions exceed Bulgarian for the following sources: agriculture (3–9 Gg N), traffic (about 3 Gg N), nitric acid production (about 6 Gg N), and "other" emissions (about 2 Gg N). These differences mainly result from differences in human activities. For instance, nitric acid production in the Netherlands is about twice of that in Bulgaria. Traffic emissions in the Netherlands exceed those from Bulgaria not only because of a greater number of cars, but mainly because in the Netherlands 3-way catalysts tend to increase N_2O emissions to a larger extent than in Bulgaria.

Dutch agriculture gives rise to more N_2O production than the Bulgarian. This is partly a result of higher nitrogen input to soils in the Netherlands (922 Gg N y^{-1} according to the IPCC method) than in Bulgaria (624 Gg N y^{-1}) (Table 1). Similarly, the Dutch indirect agricultural N_2O emissions are about two times higher than those in Bulgaria. The agricultural N_2O in the Netherlands is largely related to manure produced by relatively large number of animals with relatively high per capita nitrogen excretion, and a relatively large fraction of manure produced in stables. Finally, there are no cultivated organic soils in Bulgaria, while in the Netherlands about 15% of the agricultural soils are classified organic. Organic soils tend to produce more N_2O than mineral.

The estimates for N_2O from stationary combustion vary considerably, mainly because for Bulgaria the IPCC and NEO methods differ (3.5 and 0.5 Gg N,

respectively). This is a result of differences in the applied emission factors for coal combustion. In the NEO method 0.9 g N_2O-N GJ^{-1} is used, except for coal burning in boilers with fluidized bed combustors (FBC) when the emission factor is 26.7 g N_2O-N GJ^{-1}. This is a simplified interpretation of the IPCC Guidelines and partly based on Dutch research. In Bulgaria there is no FBC so that all NEO emissions from coal combustion are calculated using the low emission factor. The IPCC estimate for coal combustion in energy production was calculated using an emission factor of 0.5 g N_2O-N GJ^{-1}, and for combustion outside energy production 36.6 g N_2O-N GJ^{-1} (*Bogdanov*, 1995, 1996) was used. Clearly, validation of these emission factors is desirable.

The emissions of N_2O from mobile sources depend strongly on the presence of cars with 3-way catalyst control. In Bulgaria 3-way catalysts are not commonly applied, because of the absence of legislative regulations and the relatively old car fleet, with a considerable number of cars produced in former socialist countries. In the future, however, emissions from traffic in Bulgaria may increase when 3-way catalysts will be introduced.

9. Conclusions

The purpose of this study is:

(i) to apply both the IPCC and NEO methods to Bulgaria and the Netherlands,

(ii) to investigate differences between the NEO and IPCC methods and

(iii) to compare emissions from Bulgaria to emissions from the Netherlands.

This study shows that the NEO method can be applied to Bulgaria, although for some sources additional assumptions were necessary. These involve estimates for background emissions and emissions from waste water treatment. Further, data on N input to aquatic systems from industries were not available. Validation of the IPCC and NEO method for Bulgaria is difficult, because no experimental data on Bulgarian N_2O emissions exist. Nevertheless, it may be tentatively concluded that the NEO method is applicable to most regions of the world at Northern mid-latitudes, because the most important regional differences may be caused by climatic differences.

For both countries the IPCC method results in about 20% higher mid-point estimates for total emissions than the NEO estimates. The methods differ for several sources, but in particular for agriculture. The IPCC estimate exceeds the NEO estimate for both countries, despite the fact that the NEO method does not account for crop residues as source of nitrogen. The IPCC Guidelines used here (phase II Guidelines) result in higher agricultural emissions than the previous (phase I) IPCC Guidelines, in which agricultural emissions were estimated as a percentage of N input to soils only. For Bulgaria, for instance, the present estimates for agriculture (14 and 20 Gg N_2O-N y^{-1}) are 3–4 times higher than

those based on the phase I IPCC Guidelines (*Bogdanov,* 1995, 1996). The Dutch estimates presented here (17 and 29 Gg N_2O-N y^{-1}) exceed the phase I estimate (2.4 Gg N) even by a factor of 7–10.

Annual emissions from the Netherlands exceed the Bulgarian emissions by about 15 Gg N y^{-1} (mid-point estimates). This is mainly a result of differences in human activities affecting emissions from agriculture, traffic and nitric oxide. A further comparison of emissions from Bulgarian to the Dutch situation reveals that:

(i) the emission factors used for estimating N_2O emissions from stationary combustion in Bulgaria need to be validated, because differences in emission factors used resulted in relatively large differences in estimated emissions from commercial boilers and fluidized bed combustion (FBCs),

(ii) emissions of N_2O from traffic are lower in Bulgaria than in the Netherlands, due to the low number of 3-way catalyst-equipped cars in Bulgaria,

(iii) indirect soil emissions of N_2O induced by atmospheric deposition of NO_x are relatively large in Bulgaria taking into account the total fuel consumption in both countries (further analysis of NO_x emissions would be necessary to validate these estimates),

(iv) enhanced background emission from soils are lower in Bulgaria than in the Netherlands, while the Bulgarian agricultural area exceeds the Dutch by more than a factor of two; this is a result of the absence of histosols in Bulgaria.

The uncertainties in the N_2O emission estimates are large compared to the differences between the mid-point values (Figs. 1, 2 and 3). These ranges only reflect the uncertainties in emission factors, not in activity data. The uncertainties could be reduced through experimental research. This holds for both countries, but for Bulgaria in particular, because there are no N_2O measurements available yet. In Bulgaria, measurements of N_2O emissions from agriculture would be particularly helpful. It is also recommended to establish specific Bulgarian values for annual nitrogen production by livestock, an in-country inventory of animal waste management systems, and a study on the fate of nitrogen in manure. In addition, a more precise estimate of N-flux in crop residues, especially through data for the residues removed from the fields and burned on site would be helpful, as well as an investigation of the practice in municipal, industrial and domestic waste water treatment, additional N-load to surface waters.

Acknowledgements—We would like to thank the International Agricultural Centre (Wageningen, the Netherlands) for financial support.

References

Baas, J., 1991: Literature review of nitrous oxide emissions from transport (in Dutch). *TNO-Rapport* R91/322. TNO Institute of Environmental Science. Delft, The Netherlands.

Baas, J., 1994: Nitrous oxide emissions from road transport in the Netherlands. *TNO-Report* R94/208. TNO Institute of Environmental Science. Delft, The Netherlands.

Bogdanov, S.B., 1995: GHG emissions in Bulgaria 1987-1993. *Report* for Bulgarian Case Study under US Country Studies Program, Sofia, Bulgaria.

Bogdanov, S.B., 1996: Inventory of GHG emissions in Bulgaria: 1987-1993. In *Greenhouse Gas Emissions Inventories (Interim Results from the U.S. Country Study Program)* (ed.: *B.V. Braatz*). Kluwer Academic Publishers, Dordrecht, The Netherlands, pp. 237-252.

Bouwman, A.F. and *Van der Hoek, K.W.*, 1991: Analysis of soil and water borne emissions of nitrous oxide and methane in the Netherlands. *RIVM Report,* No. 736301010. National Institute of Public Health and the Environment, Bilthoven, The Netherlands.

Bouwman, A.F., Van der Hoek, K.W. and *Olivier, J.G.J.*, 1995: Uncertainties in the global source distribution of nitrous oxide. *J. Geophys. Res. 100*, 2785-2800.

Bouwman, A.F., 1996: Direct emission of nitrous oxide from agricultural soils. *Nutrient Cycling in Agroecosystems 46*, 53-70.

Bowden, R.D., Melillo, J.M. and *Steudler, O.A.*, 1991: Effects of nitrogen additions on annual nitrous oxide fluxes from temperate forest soils in the northeastern United States. *J. Geophys. Res. 96,* 9321-9328.

Brumme, R. and *Beese, F.*, 1992: Effects of liming and nitrogen fertilization on emissions of CO_2 and N_2O from a temperate forest. *J. Geophys. Res. 97*, 12851-12858.

Ecetoc, 1994: Ammonia emissions to air in Western Europe. *Technical Report*, No. 26, Brussels.

FAO, 1990: *FAO Yearbook Production, Vol. 44.* FAO Statistic series 99. Rome, Italy.

Houghton, J.T., Meira Filho, L.G., Bruce, J., Hoesung Lee, Callander, B.A., Haites, E., Harris, N. and *Maskell, K.*, 1995: *Climate Change 1994. Radiative Forcing of Climate Change and an Evaluation of the IPCC IS92 Emission Scenarios*. Published for the Intergovernmental Panel on Climate Change, Cambridge University Press.

IPCC/OECD, 1995: *IPCC Guidelines for National Greenhouse Gas Inventories*. IPCC WGI Technical Support Unit, Bracknell, UK.

IPCC/OECD, 1997: *Revised 1996 IPCC Guidelines for National Greenhouse Gas Inventories (Phase II)*. IPCC WG 1 Technical Support Unit, Bracknell, U.K. Nitrous oxide emissions from agriculture revised by *A. Mosier, C. Kroeze, C. Nevison, O. Oenema, S. Seitzinger, O. van Cleemput, L. Bakken, P. Bielek, S. Bogdanov, Y. Bonduki, A.F. Bouwman, R.A. Delmas, F.J. Dentener, R. Francisco, J. Freney, S. Frolking, P. Groffman, O. Heinemeyer, R. Karaban, L. Klemedtsson, P.A. Leffelaar, E. Lin, K. Minami, W.J. Parton, D.C. Parashar, R. Scholes, R. Sherlock, K. Smith, H.G. van Faassen, E. Veldkamp, G.L. Velthof* and *G.X. Xing*.

Kroeze, C., 1994: Nitrous oxide — emission inventory and options for control in the Netherlands. *RIVM Report* 773001004. National Institute for Public Health and the Environment, Bilthoven, The Netherlands.

Kroeze, C., 1995: Comparison of inventory methods for estimating national emissions of nitrous oxide (N_2O). *Időjárás 99*, 209-225.

Mosier, A.R., 1994: Nitrous oxide emissions from agricultural soils. *Fertilizer Research 37,* 191-200.

Mosier, A.R., Kroeze, C., Nevison, C. Oenema, O., Seitzinger, S. and *Van Cleemput, O.*,: Closing the global anthropogenic N_2O budget: nitrous oxide emissions through the agricultural nitrogen cycle. Accepted for publication in *Nutrient Cycling in Agroecosystems*.

Nevison, C.D., Esser, G. and *Holland, E.A.*, 1996: A global model of changing N_2O emissions from natural and perturbed soils. *Climatic Change 32*, 327-378.

Oenema, O., 1995: Direct nitrous oxide emissions in animal production: report of group II of the IPCC/OECD "N_2O Workgroup". Presented at the SENSE Symposium "Broeikaseffect en

Klimaatverandering: invloed van, en gevolgen voor landgebruik, ecosystemen en biodiversiteit". 17 November 1995. Wageningen, The Netherlands.

Prinn, R., Cunnold, D., Rasmussen, R., Simmonds, P., Alyea, D., Crawford, A., Fraser, P. and *Rosen, R.*, 1990: Atmospheric emissions and trends of nitrous oxide deduced from ten years of ALE-GAGE data. *J. Geophys. Res. 95,* 18369-18385.

RIVM, 1993: *National Environmental Outlook 3.* National Institute of Public Health and the Environment. Bilthoven, The Netherlands.

Safley, L.M., Casada, M.E., Woodbury, J.W. and *Roos, K.F.*, 1992: Global methane emissions from livestock and poultry manure. *US-EPA Report* No. 400/1-91/0458. Office of Air and Radiation, Washington D.C., USA.

Seitzinger, S.P., 1988: Denitrification in freshwater and coastal marine ecosystems: ecological and geochemical implications. *Limnol. Oceanogr. 33,* 702-724.

Seitzinger, S.P., 1990: Denitrification in aquatic sediments. In *Denitrification in Soil and Sediment* (eds.: *N.P. Revsbech* and *J. Sorensen*). Plenum Press, New York, pp. 301-312.

Spoelstra, H., 1993: N_2O emissions from combustion processes used in the generation of electricity. *Report* No. 10142-KES/MME 92-4029. KEMA Environmental Service, Arnhem, The Netherlands.

Steffens, G. and *Vetter, H.*, 1990: *Neue Faustzahlen über Nahrstoffgehalte und Nahrstoffanfall.* Landwirtsschaftsblatt Weser-Ems, 3.

Van Amstel, A.R., Albers, R.A.W., Kroeze, C., Matthijsen, A.C., Olivier, J.G.J. and *Spakman, J.*, 1994: Greenhouse gas emissions in the Netherlands 1990, 1991, 1992 and projections for 1990-2000. A background report for the National Communications of the Netherlands for the Climate Convention. *RIVM Report* No. 773001003. National Institute of Public Health and the Environment. Bilthoven, The Netherlands.

Van der Hoek, K.W., 1994: Methodology for calculating ammonia emissions in the Netherlands for the years 1990, 1991 and 1992 (in Dutch). *RIVM report* No. 773004003. National Institute for Public Health and the Environment. Bilthoven, The Netherlands.

Velthof, G.L. and *Oenema, O.*, 1994a: Effect of nitrogen fertilizer type and urine on nitrous oxide flux from grassland in early spring. In *Grassland and Society: Proceedings of the 15th General Meeting of the European Grassland Federation* (eds.: *L. 't Mannetje* and *J. Frame*). Wageningen, The Netherlands, pp. 458-462.

Velthof, G.L. and *Oenema, O.*, 1994b: Nitrous oxide emissions from grassland on sand, clay and peat soils in the Netherlands. In *Non-CO_2 Greenhouse Gases. Why and How to Control?* (eds.: *J. van Ham, L.J.H.M. Janssen* and *R.J. Swart*) Proc. of an International Symposium, 13-15 December 1993. Maastricht, The Netherlands. Kluwer Academic Publishers, London, pp. 439-444.

Vetter, H., Klasink, A. and *Steffens, G.*, 1989: Mist und Gülledüngung nach Mass. *VDLUFA-Schriftenreihe 19*, 41-66.

VROM, 1994: *Netherlands' National Communication on Climate Change Policies.* Prepared for the conference of parties under the Framework Convention on Climate Change. Ministry of Housing, Physical Planning and Environment. The Hague, The Netherlands.

IDŐJÁRÁS

Quarterly Journal of the Hungarian Meteorological Service
Vol. 101, No. 4, October–December 1997, pp. 261–273

Determination of precipitable water for a fixed site using *Global Positioning System* technique

Éva Borbás

Satellite Research Laboratory, Hungarian Meteorological Service,
P.O. Box 39, H–1675 Budapest, Hungary; E-mail: borbas@met.hu

(Manuscript received 1 July 1997; final form 19 August 1997)

Abstract—Water vapor plays an important role in atmospheric processes ranging from global climate change to micrometeorology, therefore its observation is essential for weather and climate research as well as operational weather forecasting. In addition the distribution of water vapor is highly variable in space and time and current numerical models require a better knowledge of this parameter. The resolution of conventional meteorological measurements (radiosonde, remote sensing observations) is limited both in time and space but new methods using data from the Global Positioning System (GPS) in meteorology could provide water vapor measurements as well as other atmospheric parameters such as temperature or pressure profiles with high spatial and temporal resolution. This paper reports about the application of GPS in meteorology and describes the methodology of deriving precipitable water vapor (PWV) from GPS processed data. Comparison with meteorological data (radiosonde, NOAA TOVS) and numerical weather prediction (NWP) model analyses are presented and it is shown that GPS method provides more accurate values of PWV than conventional measurements.

Key-words: ground-based GPS application, zenith tropospheric delay, zenith hydrostatic delay, zenith wet delay, precipitable water vapor.

1. Introduction

An important goal in weather prediction is to improve the accuracy of short-term cloud and precipitation forecast by creating a better initial state for the NWP model. One current limitation is the lack of precise information on the variability of the water vapor distribution both in time and space. *Kuo et al.* (1993) have shown that the assimilation of accurate and high resolution PWV data into a mesoscale model recovers the vertical structure of water vapor with much higher quality than that from statistical retrieval based on climatology and it has a positive impact on the short-range NWP.

A number of different methods have been developed to measure or to derive the vertical and horizontal distribution of water vapor. The radiosondes are in situ measurements providing good vertical resolution of humidity profiles (with accuracy of 3.5%) but because of their high costs, they are launched only twice a day at a limited number of stations. It is possible to estimate the integrated water vapor content (or precipitable water vapor) using a ground based upward looking water vapor radiometer (WVR). This instrument, which provides a good measurement accuracy, is used, in particular, by geophysicists to estimate the tropospheric effects on radio signals. The WVRs measure the background microwave radiation (actually the sky brightness temperature at two or more frequencies) produced by atmospheric water vapor and can estimate the integrated water vapor content along a given line of sight. The method, however, does not provide measurements under all weather conditions and the implementation of a fully meteorological operational system is not feasible. The space-based downward-looking radiometers providing a better spatial but poorer temporal coverage than the ground based instruments are better suited for meteorological application but do not satisfy the full requirement of current models. PWV can also be measured or derived remotely from both geostationary and polar orbiting satellites. Examples of such sounding instruments are the Visible-Infrared Spin Scan Radiometer (VISSR) Atmospheric Sounder (VAS) on NOAA GOES satellites (*Smith,* 1983) or the Tiros Operational Vertical Sounder (TOVS) on NOAA polar orbiting satellites. Their main common disadvantage is that derivation of PWV can be made accurately over cloud-free regions only. At the Satellite Research Laboratory of the Hungarian Meteorological Service humidity and temperature profiles are computed from TOVS data using an International TOVS Processing Package (ITPP) model (*Nieman and Achtor,* 1995) since 1992.

In addition to the above mentioned systems, there are also other space based (SSM/I, AMSU, etc.) and ground based (infrared and solar-optical radiometric technique) instruments used in the determination of PWV. This paper addresses a new and different promising method using the Global Positioning System (GPS).

In the 1970's the number of different navigation systems and associated costs have increased by a large amount. The US Department of Defense (DoD) has therefore decided to create a totally space based navigation system which was called Global Positioning System (*Hoffmann-Wellenhof et al.*, 1993). It was originally designed as a navigation and time transferring system but rapidly a number of other applications making use of the system emerged such as the meteorological one. The first GPS satellite (so-called PRN 4) was launched on 22 February 1978 (*Kleusberg et al.,* 1996). It was the first in a series of 11 so-called Block I satellites. Today satellite PRN 12 is the last of the Block I satellites still alive. The first satellite of the next generation (Block II) of the GPS satellites was launched in February 1989. Twenty-four Block II satellites

are operational today. The GPS satellites which will replace the Block II's are the Block IIR's which have a design life of 10 years. The US GPS consists of 24 satellites orbiting the Earth at an altitude of 20200 km in 6 orbital planes (12 hour orbits), separated by about 60 degrees on the equator, and set with the inclination of about 55 degrees. Four to eight satellites (above 15° elevation) can be observed simultaneously from almost anywhere on the Earth at any time of the day.

There is also a Russian equivalent to GPS called Global Navigation Satellite System (GLONASS). The two systems are very similar, and it is possible to make use of both of them, resulting in a larger number of satellites and more options to chose the best positioning satellites to include in the derivation of the solutions. The combined system is called the Global Positioning and Global Navigation Satellite Systems (GNSS). The signals from the GLONASS satellites can be received since 1996 but the slight differences between the frequencies, altitudes etc. of satellites of the two systems result in the need for improvement in the receiving equipment (*Allan,* 1996). In this study only the data from the GPS (US) satellites were processed.

The GPS satellites transmit radio signals at 1.2 and 1.6 GHz through the Earth's atmosphere to the users equipped with GPS receivers. The ionosphere and the neutral atmosphere affect microwave transmission by slowing down the speed of the radio signals compared to that of the vacuum and curving the ray path. Both effects introduce propagation delays into the travel path length.

The ionospheric delay can be eliminated by using simultaneously two carrier frequencies because its refractivity depends on the frequency. However the neutral atmosphere is a non-dispersive medium for radio waves. The relative errors associated with the behavior of the neutral atmosphere have become more and more significant in the derivation of parameters as the space geodetic techniques were improved. To estimate and eliminate the delay caused by the troposphere especially by the highly variable water vapor above a GPS receiver, the geophysicists and geodesists have developed methods using a network of the ground-based GPS receivers. The delay caused by water vapor — called zenith wet delay (ZWD) — is nearly proportional to the amount of precipitable water vapor (PWV). A precise determination of ZWD and the knowledge of the functional relation between ZWD and PWV should allow the exploitation of a GPS network as a meteorological ground-based observation network for accurate, continuous determination of PWV fields. The application can be referred as "ground-based GPS meteorology" in opposition to "space-based GPS meteorology". In this paper after introducing and describing the techniques of both meteorological applications (Section 2), the evaluation of the ground-based GPS application and results of the test cases are presented and discussed for a fixed geographical site.

2. GPS meteorology

2.1 Space-based GPS meteorology

The branch of GPS meteorology using a GPS receiver spaced on board of a Low Earth Orbiting (LEO) satellite is referred as space-based GPS meteorology. The derivation method uses the radio occultation technique. The history of radio occultation technique started more than two decades ago and was used for studies of the atmospheres of other planets in our solar system. The related experiments have demonstrated the capability of the radio occultation technique to derive profiles of refractivity, neutral density, pressure and temperature for Venus (*Fjeldbo et al.* 1971), Mars (*Fjeldbo and Eshleman,* 1968), Jupiter (*Lindal et al.,* 1981) and some other planets as well as for the Earth.

The radio occultation technique for remote sensing of the neutral atmosphere uses the following approach: the radio signal propagates from the GPS transmitter to the LEO receiver while it traverses the atmosphere from the ionosphere to the limb of the Earth as the satellite moves in its orbits (*Fig. 1).* The propagation path of the electromagnetic wave will be curved and slowed down, as it was mentioned in the previous section. As there is a unique relationship between the total refractive bending angle (α) and the atmospheric refractive index (or refractivity) (*Melbourne et al.,* 1994), the refractivity for each layer can be determined from the measured angle. But the atmospheric refractivity (N) can be approximated (*Smith* and *Weintraub*, 1953; *Thayer,* 1974) by

$$N = 77.6\frac{P_d}{T} + 3.73^{*}10^{5}\frac{P_w}{T^2}, \tag{1}$$

where P_d is the partial pressure of the dry air (in hPa), T is the temperature of the atmosphere (in K) and P_w is the partial pressure of the water vapor (in hPa) in a layer. The effect of humidity and temperature are not separable. The humidity can be retrieved only if the temperature is known and alternatively the temperature can be accurately (better than one degree Kelvin) determined only if the humidity is known, or using the equation of the states for arid region of the neutral atmosphere: stratospheric temperatures globally and upper tropospheric temperatures at middle and high latitudes (*Gorbunov* and *Sokolovskiy*, 1993).

The first LEO satellite with a small radio receiver was launched on 3 April, 1995. More information about this and the space-based GPS application can be read in the report of the GPS/MET team of NCAR (*Ware et al.*, 1994) or in an ESA contract report (*Høeg et al.,* 1996).

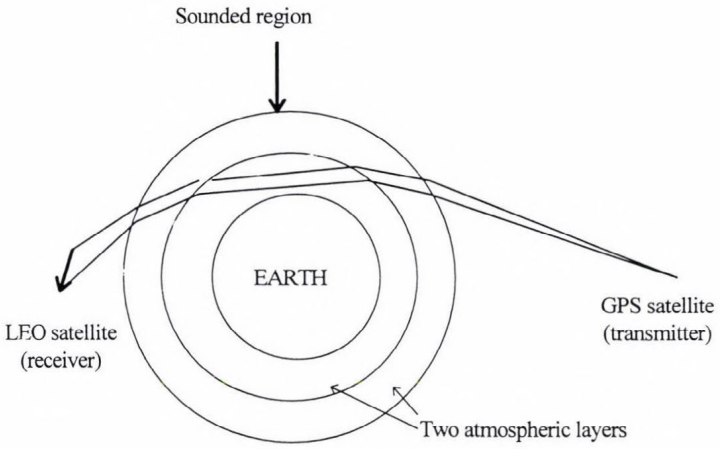

Fig. 1. The radio occultation technique.

2.2 Ground-based GPS meteorology

The radio signals, received by a ground-based GPS receiver, are delayed by water vapor and dry gases of the neutral atmosphere. For this reason the total tropospheric delay (TD) can be partitioned into the wet delay (WD), which is a function of the water vapor distribution and the hydrostatic delay (HD):

$$TD = HD + WD. \tag{2}$$

HD is not considered as dry delay because, unlike dry gases, it includes the nondipole components of the refractivity values of the water vapor. Both delays are the smallest for paths from the zenith direction and increase approximately inversely with the sine of the elevation angle. The mapping function describes the dependence on elevation angle (*Davis et al.*, 1985). The typical value of the HD is 2.3 m at the sea level in the zenith direction and it is about 90 percent of the total tropospheric delay (TD). The value of the zenith wet delay (ZWD) can be less than 1.0 cm in arid regions and its maximum can reach about 40.0 cm in humid areas.

Elgered et al. (1991) used the following equation in an adopted model for the determination of zenith hydrostatic delay (ZHD):

$$ZHD = \frac{(2.2779 \pm 0.0024) P_s}{1 - 0.00266 \cos 2\lambda - 0.00028 H}, \tag{3}$$

where P_s is the total pressure (in hPa) at the Earth's surface, the denominator is the variation of the gravitation acceleration with the latitude (λ) of the station and the height (H) above the ellipsoid. Finally, the precipitable water vapor can be computed by the equation

$$PWV = k\,ZWD,$$

with

$$k = \frac{10^6}{(\rho_w R_v (k_3/T_m + k_2'))},$$

where ρ_w is the density of water, R_v is the specific gas constant for water vapor, $k_2' = 22.1 \pm 2.2$ (K/hPa) and $k_3 = (3.739 \pm 0.0012)\ 10^5$ (K^2/hPa) (*Bevis et al.*, 1994). The weighted mean temperature of the atmosphere (T_m) is defined (*Davis et al.*, 1985) as

$$T_m = \frac{\int (P_v/T)dz}{\int (P_v/T^2)dz}, \tag{4}$$

where P_v is the partial pressure of dry air and T is the absolute temperature. T_m can be estimated by $T_m = 70.2 + 0.72\ T_s$ (K) (*Bevis et al.*, 1992), where T_s is the surface temperature, or computed from a numerical weather prediction model which predicts the three dimensional distribution of temperature.

The zenith tropospheric delay has to be determined or estimated and very accurate meteorological measurements are necessary on site to derive the PWV at the GPS site using the above described GPS technique.

Originally a number of methods were developed to estimate and to eliminate the effects of tropospheric delay on GPS signals. The first and simplest method computes the wet (WD) and hydrostatic delay (HD) from surface pressure (Eq. (3)), temperature and humidity measurements using an atmospheric mapping function (*Saastamoinen*, 1972). This method is very good for the estimation of the ZHD but as ZWD is weakly related to the meteorological surface conditions, it results in bad estimation for our purpose. To avoid the extreme meteorological conditions (inversion, convection), meteorological data of a standard atmosphere are usually used in this method. An alternative method provides the wet delay using Water Vapor Radiometers or radiosondes to measure and determine the precipitable water. The routine operation of these instruments is expensive and WVR is not an "all-weather" instrument. A third method *estimates* the wet delay (or the residual zenith delay = actual ZD – calculated ZD) directly from the GPS data themselves of a network as a part of

the overall least squares inversion for the coordinates of the GPS receivers, the orbital parameters of the GPS satellites, and other geodetic parameters of interest ("deterministic" approach). This method assumes that the ZWD is constant for an interval and hence it causes some constraints on ZWD values, and keeps them within reasonable bounds. Finally, the residual ZD can be estimated by a stochastic model using the Kalman filtering technique where the predicted value will be a time-dependent parameter. The stochastic filtering of the tropospheric delay showed very good results compared to the direct WVR measurements (*Bevis et al.*, 1992). The research group at Jet Propulsion Laboratory was the first to adopt a stochastic estimation method for atmospheric modeling within their GIPSY/OASIS GPS processing package (*Webb* and *Zumberge,* 1993). But a number of GPS processing packages still include the deterministic (Bernese, GAMIT, etc.) rather than the stochastic approach like in the models GIPSY and GAS (*Stewart et al.*, 1995).

2.2.1. Sources of errors

Bevis et al. (1994) showed that the relative error in k depends on the relative error in T_m which can be predicted from only the surface temperature (see the equation above) with a relative rms error of about 2% and from the NWP model with a relative rms error of 1%. Thus the estimation of PWV from ZWD causes a very little error in this process, it introduces errors of less than 5%. The hydrostatic delay can be determined better than 1 mm if the barometer is well calibrated (<0.3 hPa). The hydrostatic delay, however, can be affected by atmospheric dynamics which causes errors of less than 1% (23 mm). Additional errors can be caused by many other conditions as the effects of multipath signals, the effects of incorrect modeling of the elevation angle, the effects of the assumption of the azimuthal symmetry, clock errors etc., but these errors are not significant. *Gutman et al.* (1995) showed that the differences between PWV calculated by using precise orbits and rapid orbits are negligible furthermore there are not significant differences between the results obtained by different GPS processing packages. Thus the major source of the errors in the determination of PWV results from errors of geodetic processing of the GPS data.

3. Determination of PWV values from various measurements for comparison

The aim of the study is to investigate the quality of GPS-derived PWV data for the only Hungarian permanent GPS station, located at Penc (47.789°E; 19.281°N; 247 meters). The data from which PWV amounts can be computed and are available at the Hungarian Meteorological Service are the measurements of the European radiosonde stations twice a day, NOAA TOVS radiances four times a day and forecasts and analyses of a Numerical Weather Prediction model

every three hours. The GPS derived, two hourly zenith tropospheric delays were provided by the Central European Regional Geodynamic Project (CERGOP) Data Center at the Institute of Space Research, Department of Satellite Geodesy in Graz (*Pesec* and *Stangl*, 1995). The comparisons of various derived PWV were made above the GPS station Penc during the period April-May 1996.

The CERGOP Data Center computes zenith tropospehric delay (ZTD) estimates every two hours as a part of the least squares adjustment of a Central European GPS network by using the Bernese software (*Rothacher et al.*, 1990). The network contains 15 Central European GPS sites and the orbits are rapid orbits obtained from the CODE (Center for Orbit Determination in Europe) Center of the International GPS Services for Geodynamics (IGS) in Bern with a three or four day time gap. Because of the "deterministic" approach, the zenith delays are constant during the estimation interval. The baselines between the stations of the network are not too long (less than 500 km), so the receivers view the same satellite at almost the same elevation angles, causing the ZTD estimates to be highly correlated. Therefore the PWV amounts computed from the Central European Network can be considered as relative values. Some techniques are developed to obtain absolute ZTD or PWV amounts. A few other GPS stations need to be added to the network to introduce baselines to be more than 500 km (absolute technique) (*Duan et al.*, 1996) or a Water Vapor Radiometer should be set at the reference station to determine the unknown bias to be applied to the whole network (the bias does not vary in space). The latter method is called WVR levering (*Businger et al.*, 1996).

PWV values were computed and interpolated from the radiosonde data of the European region using linear interpolation with distance-dependent weights. The data of a radiosonde station were considered only if the distance between the GPS site and the radiosonde station was less than 1000 km.

Precipitable Water amounts from NOAA/TOVS data were derived by using the International TOVS Processing Package (ITPP) 5.0 developed at the Cooperative Institute for Meteorological Satellite Studies (CIMSS). The PWV data were interpolated from the values of the nearest clear sky pixels.

The numerical weather prediction (NWP) model which was used in this study is a 12 σ level, primitive equation, limited area model (56×48 grid points, $d \sim 90$ km) developed at the Swedish Meteorological and Hydrological Institute (*Undén,* 1982). The PWV data were interpolated from the four nearest grid points. The model provides 36-hour predictions with three hour analyses.

4. Results

The bias, standard deviation, and rms deviation of the differences between the various PWV products derived from the different measurements and NWP analyses are summarized in *Table 1*. During the study we assumed that the

radiosonde-derived PWV values provided the best data sets. However it should be noted that these values could have been improved using the surface meteorological data in the computation scheme. Referring to the comparisons with radiosondes, the GPS-derived PWV data were better than the TOVS-derived and the NWP PWV amounts. It can also be seen that in the future, further investigations are necessary to figure out the reason of the very high NWP PWV values. The first cell of the table shows that the GPS derived values underestimate the radiosonde PWV amounts (bias is –0.6 mm), which can prove that GPS PWV data are relative values correctable by using the absolute technique or WVR levering technique (see in Section 3).

Table 1. Bias, standard deviation and rms deviation of differences between TOVS-, GPS- and radiosonde-derived precipitable water amounts for April–May 1996

mm		RAOBS	NWP	NOAA-TOVS
GPS	bias	–0.664	–3.140	–1.468
	stdev	1.465	4.243	3.049
	rms	1.610	5.285	3.388
No. of cases		**83**	**153**	**81**
RAOBS	bias		–3.117	–1.422
	stdev		4.173	4.700
	rms		5.217	4.916
No. of cases			**116**	**38**
NWP	bias			2.297
	stdev			4.794
	rms			5.323
No. of cases				**72**

Comparisons of GPS-derived PWV values to radiosonde derived ones at the Penc site for Spring 1996 are shown in *Fig. 2*. The three plots indicate that the GPS derived PWVs follow the trend shown by radiosonde values very well. The reason for the lack of GPS PWV values on the plots is the lack of on-site meteorological observations at the GPS station. The on-site meteorological measurements at permanent stations are not too wide-spread yet or the collection of these types of data is not performed for the moment (but it is currently increasing). This is the reason why it was interesting to examine the effect of using the interpolated surface data from a meteorological observation network instead of using measured values in the PWV derivations (*Table 2*). The use of interpolated meteorological data would introduce an rms error not higher than 0.5 mm in the case of the Penc site. This error depends on the level of the accuracy of the meteorological data, the not well calibrated barometers, and also the high difference between the altitudes of the GPS antenna and the barometer. The bias (–0.4 mm) shows that interpolation underestimates the observation.

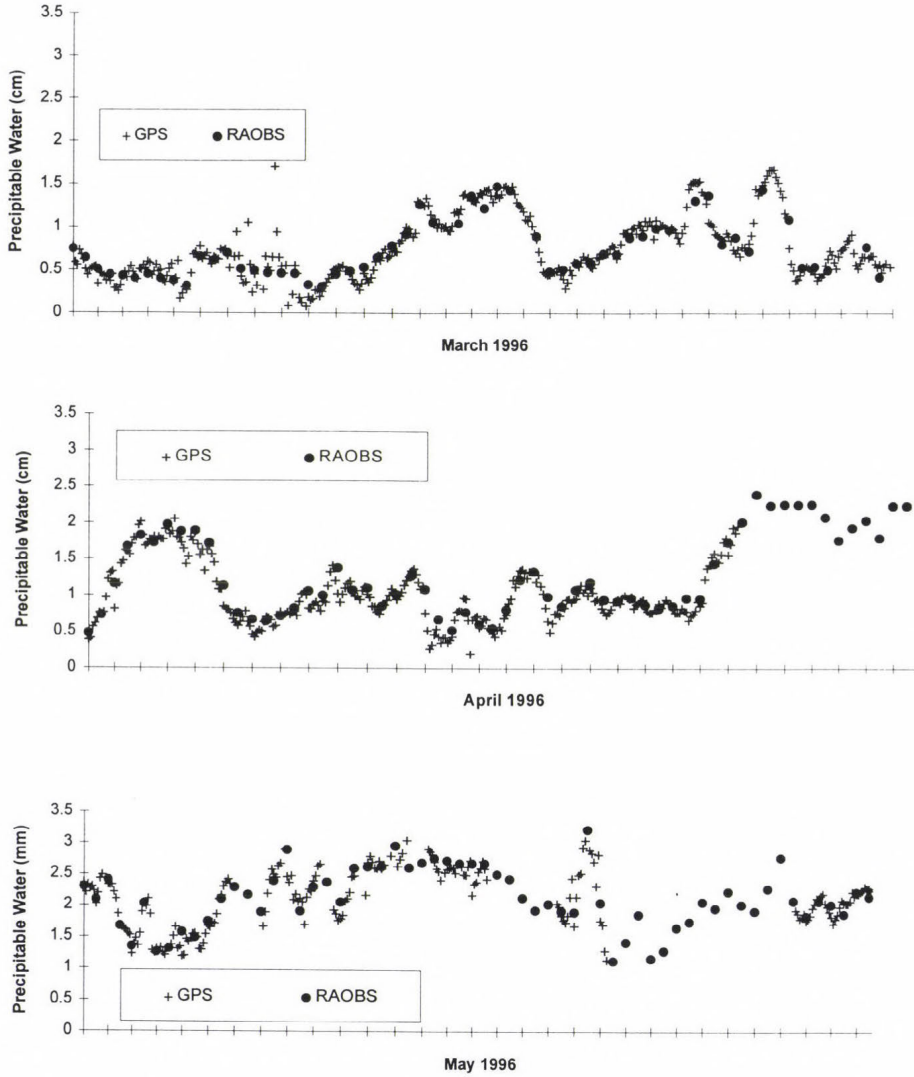

Fig. 2. Comparison of GPS-derived precipitable water amounts to radiosonde-derived values for Spring 1996 at Penc GPS station.

Table 2. Comparison statistics between the GPS-derived PWV values (mm) computed with observed meteorological data and with interpolated ones from the European meteorological observation network

Number of cases	bias	stdev	rms
491	-0.423	0.233	0.483

Our aim was also to examine the variability of the PWV data using a shorter estimation interval in the processing. The scientists of the Satellite Geophysical Observatory at Penc performed 30 minute ZTD estimations during the time period 15 to 18 March 1996. In the computation they used measurements taken at two GPS sites (Penc, Graz (Austria), baseline about 240 km), precise CODE orbits and the Bernese software. Because of the deterministic approach, the PWV values are constants in the intervals. The comparison of the 30 minute PWV amounts with the two-hourly one, using the estimates provided by the Graz center, is presented on *Fig. 3*. It can be observed that the distribution of water vapor is highly variable in time and choosing a 30 minute time interval (or less than 30 minutes) would provide more and useful information about the water vapor amount.

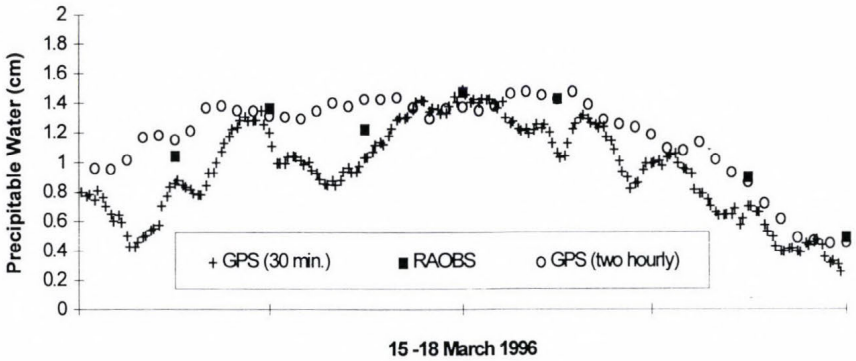

Fig. 3. The use of different time intervals (30 minutes and two hours) in the GPS processing to obtain precipitable water amounts. Comparison to each other and to the radiosonde-derived PWV values during the time period between 15 to 18 March 1996 at Penc site.

5. Conclusions and future plans

In this study we examined the quality of GPS-derived precipitable water amounts. For this reason, we compared them to values derived from other meteorological measurements and NWP analyses or forecasts for April and May 1996. It is shown that the GPS method provides more accurate values of precipitable water amounts than the NOAA TOVS radiances or NWP analyses and forecasts and the method has a much better temporal resolution. The use of interpolated meteorological data instead of on-site measurements in the computation of GPS PWV values was also examined. It introduced an 0.5 mm rms error in case of Penc site.

The results showed that GPS technique can provide accurate estimates of PWV with sub-hourly temporal resolution but the current problem is that results are not available in real time. The main problem of getting near real time PWV estimates is the acquisition of the real time precise orbit data. The real time precise orbit processing is currently under development.

In the future we are planning to improve the accuracy of the GPS derived PWV data by computing the T_m mean temperature from the NWP analyses. Our main purpose is to examine the impact of the GPS-derived PWV data on the NWP analyses and on the forecast, hence we intend to assimilate accurate GPS-derived PWV values of an European GPS network into the LAM NWP model which was adapted from the Swedish Meteorological and Hydrological Institute. For this purpose, we will have to apply the method which was described in this paper for a more extended European GPS network.

Acknowledgements—I would like to acknowledge the role of, and thank the scientists at the Satellite Geodesy Observatory in Penc and the Department of Satellite Geodesy at the Institute for Space Research in Graz for providing the processed GPS data. This study was partially supported by State Scientific Research Fund (OTKA F 015963) and by the National Committee for Technological Development (OMFB TP 063).

References

Allan, D.W., 1996: Harmonizing GPS and GLONASS. *GPS World 7*, No. 5, 51-53.

Bevis, M., Businger, S., Herring, T.A., Rocken, C., Anthes, R.A. and *Ware, R.H.*, 1992: GPS meteorology: Remote sensing of atmospheric water vapour using the global positioning system. *J. Geophys. Res. 97*, 15787-15801.

Bevis, M., Businger, S., Herring, T.A., Anthes, R.A., Rocken, C., Ware, R.H. and *Chiswell, S.R.*, 1994: GPS meteorology: Mapping zenith wet delay onto precipitable water. *J. Appl. Meteor. 33*, 379-386.

Businger, S., Chiswell, S., Bevis, M., Duan, J., Anthes, R.A., Rocken, C., Ware, R.H., Exner, M., Hoven T., and *Solheim, F.S.*, 1996: The promise of GPS in atmospheric monitoring. *Bull. Amer. Meteorol. Soc. 77*, 5-18.

Davis, J.L., Herring, T.A., Shapiro, I.I., Rogers, A.E. and *Elgered, G.*, 1985: Geodesy by radio interferometry: Effects of atmospheric modelling errors on estimates of baseline length. *Radio Sci. 20*, 1593-1607.

Duan, J., Bevis, M., Fang, P., Bock, Y., Chiswell, S., Businger, S., Rocken, C., Solheim, F., VanHove, T., Ware, H.R., McClusky, S., Herring, T.A. and *King, R.W.*, 1996: GPS meteorology: Direct estimation of the absolute value of the precipitable water. *J. Appl. Meteor. 35*, 830-838.

Elgered, G., Davis, J.L., Herring, T.A. and *Shapiro, I.I.*, 1991: Geodesy by radio interferometry: Water vapor radiometry for estimation of the wet delay. *J. Geophys. Res. 96*, 6541-6555.

Fjeldbo, G. and *Eshleman, V.R.*, 1968: The atmosphere of Mars analyzed by integral inversion of the Marine IV occultation data. *Planet. Space Sci. 16*, 1035-1059.

Fjeldbo, G., Kliore, A.J. and *Eshleman, V.R.*, 1971: The neutral atmosphere of Venus as studied with the Marine V radio occultation experiments. *Astnonom. J. 76*, 123-140.

Gorbunov, M. E. and *Sokolovskiy, S.V.*, 1993: Remote sensing of refractivity from space for global observations of atmospheric parameters. *Report*, No. 119. Max-Planck-Institute for Meteorology, Hamburg, Germany.

Gutman, S.I., Wolfe, D.E. and *Simon, A.*, 1995: Development of an operational water vapor remote sensing system using GPS: a progress report. *FSL Forum*, December 1995, 21-32.

Hoffmann-Wellenhof, B., Lichtenegger, H. and *Collins, J.*, 1993: *GPS-theory and Practice* (second edition). Springer-Verlag, Wien, New York.

Høeg, P., Hauchecorne, A., Kirchengast, G., Syndergaard, S., Balloul, B., Leitinger, R. and *Rothleitner, W.*, 1996: Derivation of atmospheric properties using radio occultation technique. *DMI Scientific Report*, 95-4. Danish Meteorological Institute, Copenhagen, Denmark.

Kleusberg, A. and *Teunissen, P.J.G.*, 1996: *GPS for Geodesy*. Lecture Notes in Earth Sciences 60. Springer-Verlag, Berlin, Heidelberg.

Kuo, Y.-H, Guo, Y.-R. and *Westwater, E.R.*, 1993: Assimilation of precipitable water measurements into a mesoscale numerical model. *Mon. Wea. Rev. 121*, 1215-1238.

Lindal, G.F., Wood, G.E., Levy, G.S., Anderson, J.D., Sweetnam, D.N., Hotz, H.B., Buckles, B.J., Holmes, D.P., Doms, P.E., Eshleman, V.R., Typer, G.L. and *Croft, T.A.*, 1981: The atmosphere of Jupiter: An analysis of the Voyager radio occultation measurements. *J. Geophys. Res. 86*, 8721-8727.

Melburne, W.G., Davis, E.S., Duncan, C.B., Hajj, G.A., Hardy, K.R., Kursinski, E.R., Meehan, T.K., Young, L.E. and *Yunck, T.P.*, 1994: The application of spaceborn GPS to atmospheric limb sounding and global change monitoring. *JPL Publication*, 94-18, Pasadena, CA, USA.

Nieman S. and *Achtor, T.*, 1995: *ITPP-5.0 User Guide*. Cooperative Institute for Meteorological Satellite Studies, University of Wisconsin-Madison. ftp://winds.ssec.edu/www/tovs/userman.-html.

Pesec, P. and *Stangl, G.*, 1995: Current status of the CERGOP Processing Center Graz. *Proc. of the 3rd CERGOP working conference, Sződliget, Hungary, 8 May 1995 and 3rd International Seminar on "GPS in Central Europe", Penc, Hungary, 9-11 May, 1995*, 101 p.

Rothacher, M., Beutler, G., Gurtner, W., Schildknecht, T. and *Wild, U.*, 1990: *Documentation for Bernese GPS Software Version 3.2*. CODE Analysis Center of IGS, Univ. of Bern, Switzerland.

Saastamoinen, J., 1972: Atmospheric correction for the troposphere and stratosphere in radio ranging of satellites. In *The Use of Artificial Satellites for Geodesy. Geophys. Monogr.* Ser. 15. American Geophys. Union, Washington D.C., 247-251.

Smith, E.K. and *Weintraub, S.*, 1953: The constants in the equation of atmospheric refractive index at radio frequencies. *Proc. of the Institute of Radio Engineers 41*, No. 8, 1035-1037.

Smith, W.L., 1983: The retrieval of atmospheric profiles from VAS geostationary radiance observations. *J. Atmos. Sci. 40*, 2025-2035.

Stewart, M.P., Foulkes, G.H., Ochieng, W.Y. and *Shardlow, P.J.*, 1995: GAS: GPS Analysis Software, Version 2.32. *User Manual, Publication IESSG*. The University of Nottingham, United Kingdom.

Thayer, D., 1974: An improved equation for the radio refractive index in air. *Radio Sci. 6*, 803-807.

Undén, P., 1982: The Swedish limited area model. *SMHI Report*, RMK 35. Swedish Meteorological and Hydrological Institute, Stockholm.

Ware, R.H., Exner, M., Herman, B.M., Kuo, Y.-H., Meehan, T.K. and *Rocken, C.*, 1994: *Summary: GPS/MET Program, Phase I: Proof of Concept*. GPS/MET Workshop, NOAA, Boulder, USA, September 1994.

Webb, F.H. and *Zumberge, J.F.*, 1993: An introduction to the GIPSY/OASIS-II. *JPL Publ. D-11088*, Jet Propulsion Laboratory, Pasadena, California.

IDŐJÁRÁS

Quarterly Journal of the Hungarian Meteorological Service
Vol. 101, No. 4, October–December 1997, pp. 275–288

Measurement of mean stomatal resistance in maize

A. Anda, J. Páll and **Zs. Lőke**

Pannon University of Agricultural Sciences, Georgikon Faculty of Agronomy, P.O. Box 71, H-8361 Keszthely, Hungary; E-mail: and5536@ella.hu

(Manuscript received 26 May 1997; final form 15 September 1997)

Abstract—Field trial on maize stomatal resistance behavior was carried out at the research area of the Pannon Agricultural University of Keszthely, Hungary in the growing seasons of 1992–1996. The measurements had two purposes: first the investigation of the divergence in stomatal resistance of two epidermises in opened maize stand (May and June) and the second goal was to map the distribution of stomatal resistance inside a leaf and, later on, within a well developed maize plant. To verify mean stomatal resistance assumption a modified model of *Goudriaan* (1977) was used. Agreement between the simulated and measured resistances of two different water supply levels was quite good (8–12%), but only on completely clear days. At disturbed radiation conditions the differences between measured and simulated values sometimes exceeded 30%. To improve results more investigation is needed on maize stomatal resistance, mainly under variable radiation conditions.

Key-words: stomatal resistance distribution, resistance simulation, maize, modeling.

1. Introduction

The climate change in the past decades in the Carpathian basin resulted in about 10% decrease in yearly rainfall sum drawing the attention of researchers and farmers to the importance of water in the soil-plant-atmosphere continuum. There are several methods to investigate water supply state of crops; measuring precipitation amounts or available soil moisture from the most simple gravimetrical way to the application of more or less sophisticated instruments (for example neutron probe) etc. As the purpose of the study is tending towards plant-water relations, those measurements aimed directly at plant behavior must take priority. One of the plant features being in direct connection with plant water supply is the stomatal resistance. According to the importance of diffusive resistances in plant water balance, huge amount of papers dealt with its application together with the arising problems when it is used in field trials. Our

goal was to complete earlier information about maize stomatal resistance behavior in field conditions. Parallel with resistance measurements we tried to interpret resistance results as well.

2. *Theoretical consideration*

The transpiration rate (E) in the simplest form expressed by Fick's law of diffusion is the ratio of the rate of gradient of water vapor from the intercellular spaces inside the leaf to the atmosphere (ΔW) to the sum of resistances on the way of water from the soil to the open air (Σr):

$$E = \frac{\Delta W}{\Sigma r}. \tag{1}$$

Since the air in intercellular spaces is assumed to be saturated, the transpiration driving force (ΔW) is equal to the difference between saturation vapor pressure at given leaf temperature (w_2) and actual vapor pressure of the ambient air (w_1):

$$\Delta W = (w_2 - w_1). \tag{2}$$

Because of the complexity of diffusive resistances occurring on water pathway from the soil to the air, the approach of calculating the denominator of fraction (Eq. (1)) is not as simple as calculation of ΔW. Soil moisture content determines hydraulic conductivity of the soil, whose inverse is the soil resistance (r_{soil}). In moist soils the r_{soil} is considered to be very small. Plant water uptake depends on the extent of root system (r_{root}) and sap movement of the xylem's vascular system (r_{xylem}). Roots are supposed to offer the largest resistance of the whole soil-plant-atmosphere system. The stem together with leaves nearly matches the resistance of roots. In leaves the water vapor diffuses from wet mesophyll cell walls surrounding the intercellular air spaces to the stomata, to "intercellular windows" allocated between two specialized guard-cells. Resistances of cuticle (r_{cu}) are in a parallel circuit with stomatal resistance (r_s) at the whole leaf resistance (r_{leaf}) calculation:

$$\frac{1}{r_{leaf}} = \frac{1}{r_{cu}} + \frac{1}{r_s}. \tag{3}$$

When stomas are open, r_{cu} is much higher than r_s, for this reason its value used to be ignored. Practically at amphistomatous plants the determination of true cuticular resistance is very complicated (almost impossible).

Stomatal resistance consists of individual but hardly approachable parts connected in series:

$$r_s = r_m + r_i, \tag{4}$$

where r_m is the resistance of mesophyll cell walls, and r_i is the resistance of intercellular spaces.

Using a theoretical consideration resistance of intercellular spaces is very small. The neglect of this component involves an error of 2–5% in the total r_s (*Kozlowsky,* 1976). Determination of r_m is difficult and a considerable uncertainty is still exist. Under normal outdoor conditions "general" resistance of mesophyll cell walls was assumed to be about 0.2 sec/cm (neglecting this means a 5% error at stomatal resistance estimation). As nowadays there is no way to measure r_s components distinctly, when porometer is applied the measured resistance is assumed to be equal to stomatal resistance. On the pathway of water vapor after leaving leaf surface 2 other resistances have left; resistance of boundary layer (r_b) and of turbulent air (r_a). These latter two are calculated from measuring plant (leaf) dimensions and wind characteristics.

Amphistomatous plants have two evaporating surfaces with more or less different resistances on abaxial (r_{su}) and adaxial (r_{sl}) leaf-sides being connected in parallel:

$$\overline{r_s} = \frac{r_{su}\, r_{sl}}{r_{su} + r_{sl}}. \tag{5}$$

In case of maize Eq. (5) must be applied during May and June. Later on measurement at one side is enough to characterize mean stomatal (leaf) resistance as the number of stomata is almost the same at both leaf surfaces.

Hence the key resistance to plant water loss is stomatal resistance — except when canopy is wet, — *Monteith* (1965) suggested to initiate the concept of canopy or surface resistance (r_c) characterizing water loss of the whole plant stand:

$$r_c = W_0/E \cong \overline{r_s}/LAI \quad \text{or} \quad r_c = \overline{r_s}/2\, LAI, \tag{6}$$

where W_0 is the vapor density deficit for given canopy surface temperature, $\bar{r}_s$ is the mean stomatal resistance for the whole plant, *LAI* is the leaf area index.

Choice depends on leaf stomatal distribution; at amphistomatous plants the second version is appropriate. One of our aims connected to Eq. (6), were to find the probable place of "mean stomatal resistance" inside a leaf and a fully developed maize plant.

3. Instrumentation to measure stomatal resistance and test model description

There are three different types of diffusion porometer (*Table 1*) to measure stomatal resistances (*Pearcy et al.*, 1991):

(1) The earliest porometers are the transient type ones, the closed chambers attached to the leaf. They measure "response" time required to increase humidity between two selected categories.

(2) Null-balance porometers keep the chamber humidity constant by introducing a varied flow of dry air into the chamber to balance the water vapor being lost by transpiration.

(3) Constant flow porometers measure a steady-state increase in humidity at constant air mass introduction after closing the leaf into the chamber.

Table 1. Comparison of different porometer types

Porometer type	Advantages	Disadvantages
Transient	Relatively simple to use Cheap Very good for "higher" resistances	Leaf size and shape limitations High temperature response Laborious calibration necessity Errors due to water sorption
Null-balance	Minimum water sorption Easier calibration Wide variety of leaf shape and size Best for "lower" resistances Complexity	Expensive
Constant flow	Both CO_2/H_2O exchange results in the same time	Error at high difference in ambient humidity (water absorption or desorption) Price increase (extra IR gas analyzer!) Less portable

In our experiments we applied an improved version of transient porometers manufactured by Delta T Devices in Great Britain (version AP 4). The AP 4 porometer has got a capacitance type humidity sensor, that makes possible more precise transit time determinations. The manufacturer applied new materials

(polypropylene etc.) to minimize vapor sorption in sensor head. There is an extra (built up) microprocessor connected to the instrument that helps to achieve easy repeatable and considerably quick calibration results increasing the reliability of the improved porometer version.

The calibration of porometers has of primary importance because its accuracy determines the validity of all the resistance measurements. In most cases (in case of AP4 type porometer also) the following equation is adopted to construct a known resistance value:

$$r_s \text{ (sec/cm)} = \frac{L}{\alpha} 4A\left(Lo + \frac{\pi d}{8}\right) / \alpha n \pi d^2, \tag{7}$$

where L effective diffusion pathlength,
α diffusivity of water vapor at given temperature,
Lo actual length of each hole (on calibration plate),
A aperture area of the vapor cup,
n number of holes,
d diameter of the holes.

To test our field stomatal resistance observations a modified version of the Crop Simulation Model of *Goudriaan* (1977) was used. Modification was made by *Chen* (1984). Basis of assumption of stomatal resistance simulation is that mass transport processes — both water vapor and CO_2 — occur via stomata, so that the ratio between their resistances is equal to the ratio between their diffusivities. In case of maize plant a linear relationship exists between net CO_2 assimilation and inverse leaf resistance at constant CO_2 concentration of substomatal cavity. This connection served to simulate the leaf resistance, since net CO_2 assimilation can be deducted precisely from the absorbed short wave radiation *(Goudriaan,* 1977). Exceeding the saturation point of CO_2 assimilation (200 J m^{-2} s^{-1} for sunny maize leaves) the leaf resistance approaches its minimum value *(Stiger et al.,* 1977). Rate of net CO_2 assimilation was considered empirically by *Van Laar et al.* (1977) as follows:

$$F = (F_m - F_d)\,[1/\exp(R_v \varepsilon / F_m)] + F_d, \tag{8}$$

where F_m maximum rate of net assimilation,
F_d dark respiration,
R_v absorbed short wave radiation (per LAI),
ε slope of the curve of F–R_v at low light intensities, *or* efficiency (17.2×10^{-9} kg/J light in maize).

At calculation of F_m the influence of leaf age and ambient CO_2 concentration were simplified and their average values were applied. Dependence of leaf temperature was considered as a dependence on ambient air temperature. Dark respiration was at about –0.1 of F_m (*Goudriaan*, 1977). To calculate maize leaf (stomatal) resistance Eq. (8) can be written as:

$$F = \frac{1.83 \times 10^{-6} (C_e - C_r)}{1{,}66 r_{leaf} + 1.32 r_{b,h}} \quad \Rightarrow \quad r_{leaf} = \frac{1.83 \times 10^{-6} (C_e - C_r)}{1.66 F.} - 0.795, \quad (9)$$

where $r_{b,h}$ boundary layer resistance for heat,
1.66 is the ratio between diffusivities (for CO_2 and H_2O),
1.83×10^{-6} converts CO_2 concentration into kg CO_2/m^2 at 20°C,
C_e external CO_2 concentration,
C_r assumed as "regulatory" CO_2 concentration,
1.32 originates from calculation of boundary layer resistance for CO_2.

The r_{leaf} was assumed to be equal to the resistance measured by porometer, to stomatal resistance.

4. Material and methods

Investigations on stomatal resistance of maize were carried out at the research area of the Pannon Agricultural University of Keszthely, Hungary, in the growing seasons of 1990–1996. Although we had different aims in different years, the subject of the study was the same: investigation of maize diffusive resistance behavior in field conditions. In the time of measurements *Pioneer hybrids* served as test plants which have a short growing season. Two water supply levels were used:

- maize grown at non limited water supply in lysimeter growing chambers,
- control plants with natural rainfall only.

The surface area of the chambers of Thornthwaite type compensation evapotranspirometers was 4 m^2, and the depth of them was 1 m. We filled the chambers with Ramann type brown forest soil, characteristic soil type in the surroundings of Keszthely. Daily sum of evapotranspiration was given by the change in the volume of soil water in the chamber, by additional water supply (irrigation) through the compensation pot and by precipitation values.

Stomatal resistance was measured with transient type porometers. We used a LI-COR 60 version between 1990–1992, and later on an improved model of Delta T Manufacturers, an AP4 type porometer was applied. We constructed

daily course of stomatal resistances by using hourly values. In general, the number of repetitions was 3 to 5. In the beginnig of the growing seasons (May–June) both abaxial and adaxial leaf sides were sampled. Later on the lower epidermis was applied for resistance determinations. Place of stomatal resistance samples depended on the purpose of observation: at determination of stomatal resistance variability within a leaf we separated three leaf sections of each blade, at vertical profile observations the bottom — or top — third line of leaves served as sites of measurements. More details on methodology can also be found in the *Result* section.

Plant parameters as plant height, leaf area index, phenological phases and meteorological observation were also made. (The Agrometeorological Station is located on the same place where field trial was conducted.)

6. Results and discussion

In spite of constant 13.3% difference in pore numbers between two leaf sides of maize — 52 and 68 pieces mm^{-2} on upper and lower epidermises, respectively, — measured divergence in stomatal resistance between two leaf surfaces was not the same during the whole growing season. In the beginning of measurements, size of change in resistance between two leaf sides was much higher than the constant distinction of pore numbers would admit. Independently on investigated years in the series between 1992–94, during May and June the stomatal resistance measured on the upper epidermis of plants grown in lysimeters was 28,3% higher than that resistance of the lower leaf side. The resistance variability within canopy with non limited water supply was about 10% higher than resistance change determined in control plant stands (39%). A likely reason of measured decrease in stomatal resistance of lower epidermis can be attributed to special environmental conditions caused by the canopy structure. In May and June the maize stand is "opened" letting a better radiation penetration into the plant stand and serving more light for pore opening of lower epidermis than after the plant canopy closure. Lower epidermises are known to be more sensitive to light than the upper ones (*Burrows* and *Milthrope*, 1976). After canopy closure, because of mutual shading of leaves, light intensity close to lower epidermis decreases and causes a moderate increase in the stomatal resistance compared to resistance values of the lower epidermis of opened canopies. Independently of water supply level, a linear relationship was determined in maize stomatal resistances between two leaf sides of three investigated years during the early '90-es (*Fig. 1*). This result substitutes earlier knowledge about amphystomatous maize resistance behavior in the very beginning of the growing seasons: before canopy closure both leaf surfaces must be sampled and taken into account when average resistance is calculated.

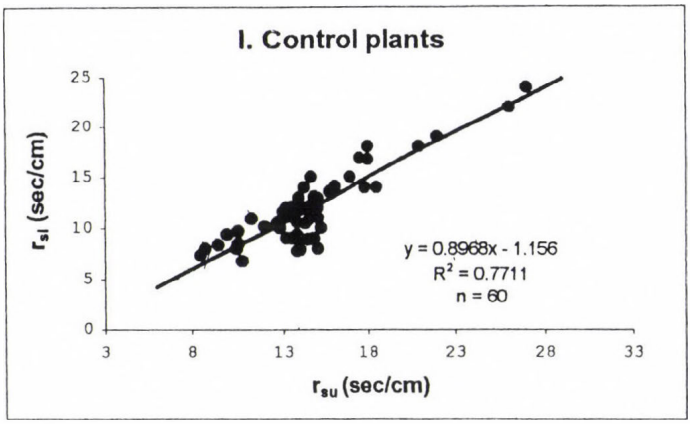

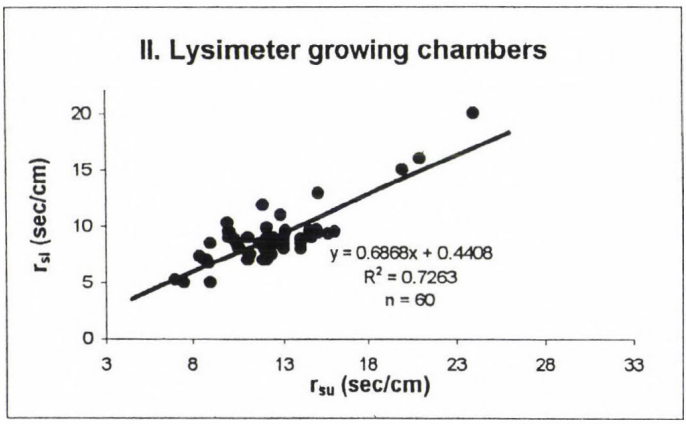

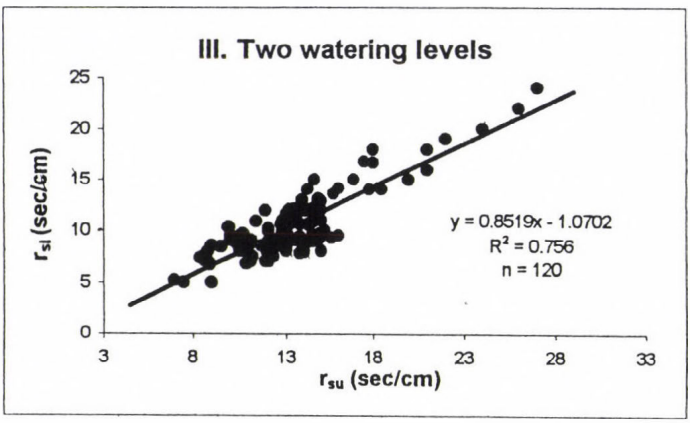

Fig. 1. Relationship of stomatal resistances measured on the upper r_{su} and lower r_{sl} epidermises.

6.1 Distribution of stomatal resistance within maize plant (Where and how to measure "average" stomatal resistance in the field?)

Investigation on error at taking stomatal resistance samples was made on six days between 22 July–1 August 1996. We adopted a traditional procedure in stomatal resistance measurements when sample leaves were well insulated, approximately same aged (the youngest) located on top third of the plant height. The mean stomatal resistance for half an hour time period together with statistical parameters of six selected days in the end of July 1996 are presented in *Table 2*. Among sample days there were 4 cloudless and two fully overcast days. Daily number of repetitions (*n*) depended on time necessity of measurements: we repeated observations until the half an hour sample time has finished. On cloudless conditions there were more samples because transit time is shorter than under overcast weather conditions. Plants were grown in lysimeters to decrease the influence of changing water supply on stomatal resistance values. To neglect the influence of altering radiation on pore movements, daily sample times were chosen close to each other, approximately at the same sun angles.

Table 2. Errors in stomatal resistance measurements when samples are taken "accidentally"

Name of measurements Day/Month/Year Sample time (hours)	r_s (sec/cm)	SD*	VC** (%)	No. of sample plants***
Cloudless days				
24/07/1996 10.00–10.30	2.88	1.635	56.64	44
25/07/1996 10.00–10.30	2.61	0.983	37.71	42
31/07/1996 9.40–10.10	3.05	1.096	36.00	45
1/08/1996 11.00–11.30	2.65	0.995	37.55	35
Overcast days				
26/07/1996 10.30–11.00	12.17	9.112	74.84	38
30/07/1996 10.30–11.00	9.97	6.952	69.70	36

SD* : Standard Deviation
VC**: Variation Coefficient
*** : one resistance value per sample plant

Although on completely clear days there was no significant difference in average resistance during the end of July, statistical parameters as SD and VC were not acceptable, mainly during overcast conditions (VC: 69.7–74.84%). These results drew our attention to look for a better place to take resistance samples, to the importance of directed sample taking.

With the better knowledge about stomatal resistance distribution, the likely place of average value can be approximated more precisely and with less energy investments than earlier.

In the first step the sample leaves were chosen accidentally after tasseling, when maize reached its final height. As this method did not produce any valuable result — because of high resistance deviations —, later on the experimental leaves were separated into two categories: for totally sunlit and for completely shaded leaves. This was important, because the influence of radiation seemed to have a more vigorous effect on stomatal resistance than that of the leaf age, that is equivalent to its position on plant level. Fully sunlit approximately same aged (and oriented) leaves are mainly in the top third of plant height. On three to five sample days yearly in July–August of 1992–1996, 10–10 blades were measured around midday (11.00 -15.00 LMT) to neglect the effect of changing radiation on pore movements. The number of sampled days has changed from year to year (finally we had results about 120 leaves). One blade were separated into 6 parts, 3–3 on the right and on the left side from the main rib. Stomatal resistances in 3 to 5 repetitions were registered for each section. Measured leaf section was signed earlier, approximately site of border lines was drawn where significant difference in stomatal resistance had occurred. Finally we had left 3 leaf sections only (360 resistance data) with altered stomatal resistances, because on the right and on the left sides from the rib the resistances differed only casually. Although absolute values of stomatal resistances changed from day to day, their distribution in percentage of whole leaf's mean showed the same tendency: lowest stomatal resistances were measured in the middle of the leaves. The average values of this leaf part were at about 40–45% less, than means of the total leaf area. Reasonable, but always less than 20% increase in resistance was determined on the bottom third of leaf, closest to the stem. The highest resistances can be found on the top of blades, where change in leaf average exceeded 30–35%. A likely reason of this latest increase might have been associated with "self-shading" of maize leaf sections because of their special inclination. (Variation Coefficients were 22, 14 and 31% on the bottom, in the middle and on the top of blades, respectively.)

Completely shaded leaves are positioned on the lower third of plant height close to the soil surface. During our investigation period significant difference in resistance distribution between different blade sections was not measured because of the high deviations of samples, but, like a tendency, a moderate increase in resistances from the stem to the top of blades was registered. Stomatal resistance distribution inside a single shaded leaf was more balanced

than resistance distribution of sunny blades, but the variability in resistances between differently oriented (aged) leaves exceeded the variance determined among sunny ones.

After drawing the stomatal resistance distribution of differently positioned leaves, likely site of "average" stomatal resistance — inside a sunny leaf — can be found close to the two border lines dividing the total leaf area into 3 parts. At completely shaded leaves the lower half of the nearest blade third seemed to be the best place for mean resistance measurements. The vertical profile of stomatal resistance of a completely developed maize plant was also drawn (*Fig. 2a*). Each level contains the mean resistance of one leaf. The highest leaf resistances with largest standard deviations occurred in the bottom third of plant height close to soil surface, where shaded leaves are located. The place of the least resistances with a moderately increased standard deviation can be found around the cobs in the middle of plant height. On top level the stomatal resistance showed a reasonable increase compared to the resistance of cob leaves, but this expansion never reached the resistances closest to the soil surface. The vertical profile of resistances and mainly its deviation explain the earlier selection of researchers: top third of height is the place of well-insolated, sunny leaves where the repetition of measurements still gives "acceptable" result with low deviations. But when the purpose of determination is average leaf- (plant-) or mainly crop resistance, a more precise approach should be adopted.

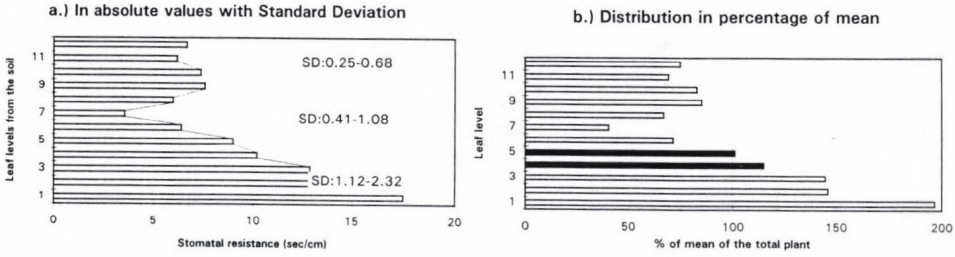

Fig. 2. Vertical profiles of stomatal resistances in maize.

Stomatal resistance of the 2nd or 3rd leaf levels just below the cob seem to be the nearest to the whole plant's average (*Fig. 2b*).

6.2 Verification of the assumption of "average" stomatal resistance

Hourly change in stomatal resistances was simulated under ten soil water potential conditions from –0.1 to –14.0 bars on 25 July 1995 *(Fig. 3)* by using

a modified model of Goudriaan. Modification was done by *Chen* (1984), and as a result of this simplification the program was applicable on PC as well. In the same time, in the root zone of lysimeters and control plots –0.28 and –4.3 bars soil water potentials were measured, respectively. During our selected sample day the weather conditions were the best for stomatal resistance measurements, since the sky was completely cloudless and there was no wind.

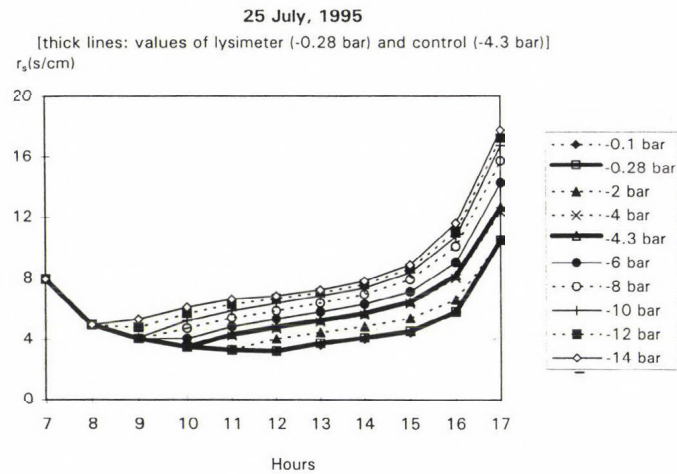

Fig. 3. Daily change in simulated resistances (25 July 1995).

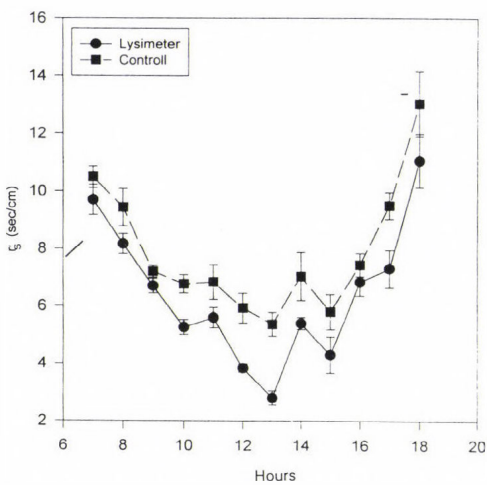

Fig. 4. Daily change in measured stomatal resistances (25 July 1995).

Daily change in measured stomatal resistance of two water supply levels differed significantly *(Fig. 4)*. Highest alteration in hourly resistance values appeared around solar noon. Moderate increase in SD was registered at the beginning and at the end of the measurement period, at low sun angles. Average stomatal resistance of maize plants grown in lysimeters was 21.1% less than the daily mean of control treatments. Change in daily mean of measured and simulated stomatal resistances differed on higher extent, than the averages of two water supply levels (*Fig. 5*). Independently on water supply, in most cases measured resistances can be found below the 1:1 lines: the simulation procedure produces higher resistances than that of the measured ones at high insolation. Simulation of maize stomatal resistance in lysimeters gave better agreement than in case of the control plots. Differences in daily mean stomatal resistances were 8.1% and 12.0% at non limited water supply and the control treatments respectively. Although the values of simulated and measured stomatal resistances were very close to each other for 25 July 1995, at undisturbed radiation and calm weather, then under variable radiation conditions, when the sky is cloudy, the differences in hourly values of simulated and measured stomatal resistance increase, sometimes exceeding 30–40%. However these results are not of universal validity yet, and need further investigations.

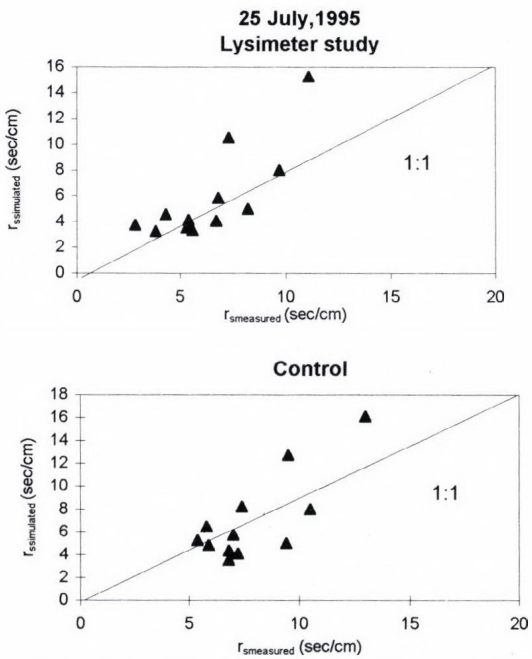

Fig. 5. Comparison of measured and simulated resistances.

References

Burrows, F.J. and *Milthrope, F.L.*, 1976: Stomatal conductance in the control of gas exchange. In *Water Deficit and Plant Growth* (ed.: *T.T. Kozlowski*). Vol. IV. Academic Press, New York-San Francisco-London, pp. 103-147.

Chen, J., 1984: Mathematical analysis and simulation of crop micrometeorology. *Ph.D. Thesis*. The Netherlands.

Goudriaan, J., 1977: *Crop Micrometeorology: A Simulation Study*. Simulation monographs. Pudoc, Wageningen.

Kozlowsky, T.T., 1976: Water deficits and plant growth. In *Soil Water Measurement, Plant Responses, and Breeding for Drought Resistance*. Vol. IV. Academic Press, New York–San Francisco–London.

Monteith, J.L., 1965: Evaporation and environment. *Symp. Soc. Exp. Biol. XIX.*, 205-234.

Pearcy, R.W., Ehleringer, J., Mooney, H.A. and *Rundel, P.W.*, 1991: *Plant Physiological Ecology*. Chapman and Hall, London-New York-Tokyo-Melbourne-Madras.

Stiger, C.J., Goudriaan, J., Bottemanne, F.A., Birnie, J., Lengkeek, J.G. and *Simba, L.*, 1977: Experimental evaluation of a crop microclimate simulation model for Indian corn (Zea mays). *Agric. Met. 18*, 163-186.

Van Laar, H.H., Kremer, D. and *De Vit, C.T.*, 1977: Maize. In *Crop Photosynthesis: Methods and Compilation of Data Obtained with a Mobile Field Equipment*. Agric. Res. Rep. 865. Pudoc, Wageningen, pp. 12-22.

IDŐJÁRÁS

Quarterly Journal of the Hungarian Meteorological Service
Vol. 101, No. 4, October–December 1997, pp. 289–305

Constant pressure balloon–satellite observing system simulation experiments

R. Randriamampianina[1] and **E. P. Borisenkov**[2]

[1]*Hungarian Meteorological Service, Satellite Research Laboratory, P.O. Box 39, H-1675 Budapest, Hungary; E-mail: roger@met.hu*

[2]*Main Geophysical Observatory, 7 Karbisev str., 94018 St. Petersburg, Russia*

(Manuscript received 11 October 1997; final form 14 November 1997)

Abstract—In order to get meteorological information from remote areas, satellite observations are the only available tools. Since satellite observations produce *indirectly* measured data, *a priori* information is required for the retrieval. We studied the possibilities of using an observation system that contains constant pressure balloons together with satellites (CPB-satellite complexes). Mathematical model has been worked out for the estimation of the coverage level of CPBs in the studied area (the Northern Hemisphere). A good distribution of CPBs was found and recommendations have been given about an optimal CPB launching system which can guarantee the necessary level of coverage. Methodological principles and algorithms have been worked out for the synchronization of CPB-satellite complex data in space and time, including: (a) the study of the vertical extrapolation method of the meteorological values; (b) the study of the dynamical initialization method; (c) the development of a new method for the assimilation of the retrieved discretely measured data; (d) the statistical analysis of the horizontal field structure of the meteorological values. Numerical experiments have been carried out to examine the possibilities of CPB and satellite data assimilation. The possibilities and the accuracy of the 4-dimensional data assimilation based on a Numerical Weather Prediction (NWP) model have been estimated. The simulation experiments showed a weak positive impact of simulated CPB data on forecasts.

Key-words: constant pressure balloon, trajectory calculation, optimization problem, data assimilation, dynamical initialization, optimum interpolation, vertical extrapolation.

1. Introduction

For the further development of the World Weather Watch it is necessary to improve the quality of observations over oceans and territories that are difficult to access. However further development of the conventional observation systems for these territories does not seem to be promising.

Therefore satellites and other, non-conventional observation systems (balloons, ships etc.) perform special interest. Remote sensing is a powerful tool to get information from far off territories. In order to retrieve remotely sensed geophysical parameters (e.g. vertical temperature profiles) initial or first guess values (i.e. initial or first guess temperature profiles in the mentioned case) are needed (*Smith et al.*, 1985; *Eyre*, 1989). In practice, climatological data, statistical regression or output of an NWP model are used as initial profiles. This kind of information can be supplemented with data observed by CPBs — e.g. tetrons — equipped with temperature sensors that transmit information through satellites (*Borisenkov et al.*, 1982; *Lally et al.*, 1967). Since the CPB data are independent from the satellite data, a new task has to be solved, namely the simultaneous assimilation of synchronous (conventional) and asynchronous (non-conventional, like balloons, satellites etc.) information.

Since the realization of experiments using a CPB-satellite complex is a very expensive and complicated task, the method of numerical simulation of the CPB observations on the basis of a hydrodynamical model of the atmosphere was chosen as the main research method.

The next section of the paper will introduce a short review of the use of balloons in meteorology. The third section will describe the experiments about the trajectory analysis and the spatial-temporal coverage by CPBs over the Northern Hemisphere. The observation system simulation experiments will be described in section 4 while section 5 contains the results and conclusions.

2. The application of CPBs in meteorology and related research

Balloons have been used as scientific tools from the end of the 18th century. Since the tracing of balloons as well as the transmission of the information from the balloons to the Earth became possible using satellites, the utilization of balloons for meteorological purposes gained more perspective. In particular, the idea of a global observation system containing a large number of balloons together with other systems came up.

In *Borisenkov et al.* (1982), the use of meteorological balloons in different international meteorological and environmental projects is well described. Thus, the meteorological balloons were used in several investigations for the following purposes:

- To study the atmosphere over the Pacific Ocean;
- For the vertical sounding of the atmosphere: projects EOLE, TWERLE and GHOST (*Lally et al.*, 1967);
- To study the atmospheric circulation in the Tropics: project TWERLE;
- To study the dynamics of monsoon: project TWERLE and exp. Balsamine.
- For trajectory forecast and hindcast over Australia (*Mills et al.*, 1994);
- To derive tracer plume trajectories during ETEX (European Tracer Experiment) (*Koffi et al.*, 1997).

3. Design of the numerical experiments with simulated CPBs

In the present study two numerical experiments were accomplished to examine the behavior of the CPBs in the atmosphere:

Exp. 1. The calculation of the trajectories of the balloons.

Exp. 2. The study of the most appropriate balloon-launching method for getting the optimum coverage of the territory.

When studying the behavior of the balloons, we used the GARP (Global Atmospheric Research Program) data which include:

- data of geopotential, temperature, wind speed components and dew-point temperature for levels 1000, 850, 700, 500, 300 and 100 hPa;
- relative humidity data for levels 1000, 850, 700, 500 and 300 hPa.

The data were presented on a regular grid in the spherical coordinate system. We carried out the transformation of the data into the Cartesian coordinate system using polar stereographic projection on latitude 60°.

3.1 Analysis of the trajectories of CPBs

The goal was to study the path of the balloons to decide whether they can fly separately from each other or just follow the jet stream.

The trajectories of 17 balloons, theoretically launched from different latitudes and longitudes of the Northern Hemisphere were calculated according to Eq. (1) (*Fig. 1*).

$$X_\eta^{t+\Delta T} = X_\eta^t + m_{\varphi\eta} \cdot \Delta t \cdot U_\eta^t, \tag{1}$$

where $X_\eta^\alpha = \left(x_\eta^\alpha, y_\eta^\alpha\right)$ is the coordinate vector of the balloon in the Cartesian co-ordinate system; $U_\eta^\alpha = \left(u_\eta^\alpha, v_\eta^\alpha\right)$ is the wind speed; $\alpha = t$ or $t + \Delta t$ is the index of time; $m_{\varphi\eta} = 1.866/(1 + \sin \varphi_\eta)$ is the mapping parameter; η is the index of CPB.

For this experiment we used the data received from the GARP project for the summer and winter period of 1979. For the summer period the starting day was 5 June 1979, for winter — 1 January 1979. In both cases data of 20 days were used.

According to the results (Fig. 1), one complete turn of CPBs around the globe required about 20 days. The balloons did not cross the Equator and the tendency of displacement to higher or lower latitudes was not significant. A good agreement between the behavior of the balloons and the zonality of the atmosphere was obtained during the flight in summer and in winter as well — accumulation of balloons could not be observed.

Since CPBs can fly over territories that are difficult to access they can assure a good coverage of the Northern Hemisphere. Therefore the next experiment was to examine the spatial-temporal distribution of the CPBs over the Northern Hemisphere.

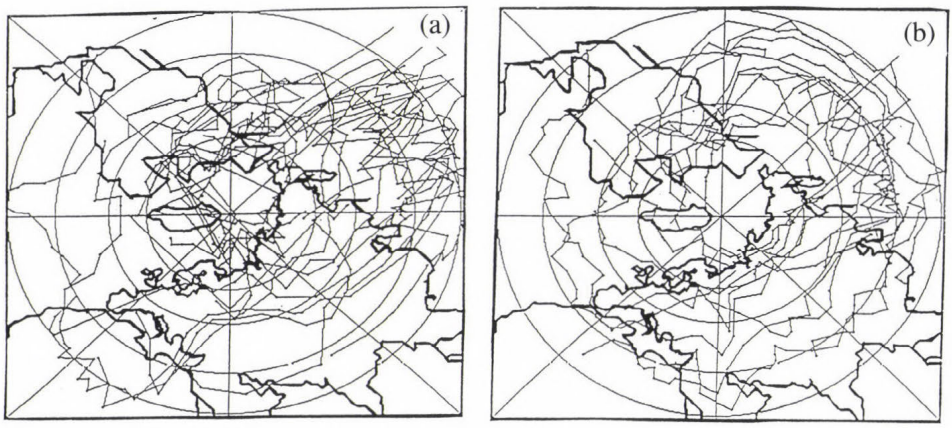

Fig. 1. The trajectory of CPBs (*a*) in winter, (*b*) in summer.

3.2. Study of the spatial-temporal coverage of the investigated area

The main task of the observation systems is to detect the state and the evolution of the meteorological elements and the physical parameters of the surface. Perturbations of the meteorological fields are caused by atmospheric motion systems characterized by their intensity, geometrical size and life time. On this basis atmospheric motion systems are often identified with and called as perturbations. The spatial-temporal characteristics of the observation system determine the accuracy of measurements of different scale perturbations. The "ideal" observation system should be able to detect the whole cycle of any perturbation from the moment of its arising till the end of its existence. In practice, this criterion applies only to synoptic scale or larger perturbations ($L \geq 5000$ km).

One of the methods to establish the minimum required density of a radiosounding network is to determine the influence radius of synoptic-scale atmospheric perturbations. According to the calculations (*Reshetov,* 1973) the required density of sounding on stratospheric levels (200–10 hPa) should be around 500–1000 km, which corresponds to the demands of the World Meteorological Organization. In the GARP project the recommended resolution of a CPB system on 200 hPa level was 500 km (*Bengtsson,* 1975). In this case the minimum number of balloons would be around 220–320 when investigating the Northern Hemisphere — excluding any accumulation of balloons resulted by either flux convergence, diffusion or vertical movement.

The estimation of the degree of accumulation of the balloons on 200 hPa level in the Southern Hemisphere was one of the goals of the EOLE project in 1971–72 (*Sitbon,* 1975). According to the experiments the distribution of the balloons over the Southern Hemisphere was almost uniform.

The aim of our study was to decide whether it is possible using a smaller amount of periodically launched CPBs to reach the *minimum required* coverage level of the Northern Hemisphere.

Since the number of balloons as well as the launching points were not identified at the beginning of this rather complicated investigation, several series of experiments were accomplished. Therefore, a certain number of CPBs were launched 12 hourly:

(1) 140 balloons in 2 days (*Fig. 2* and *Fig. 3a*);

(2) 40 balloons in 3 days (*Fig. 2* and *Fig. 3b*).

The space resolution of sounding (P) was determined based on the distances between the balloons. In case of 140 balloons the mean space resolution of sounding for the "model area" (due to the stereographic projection, it is smaller than the Northern Hemisphere area) was 480 km.

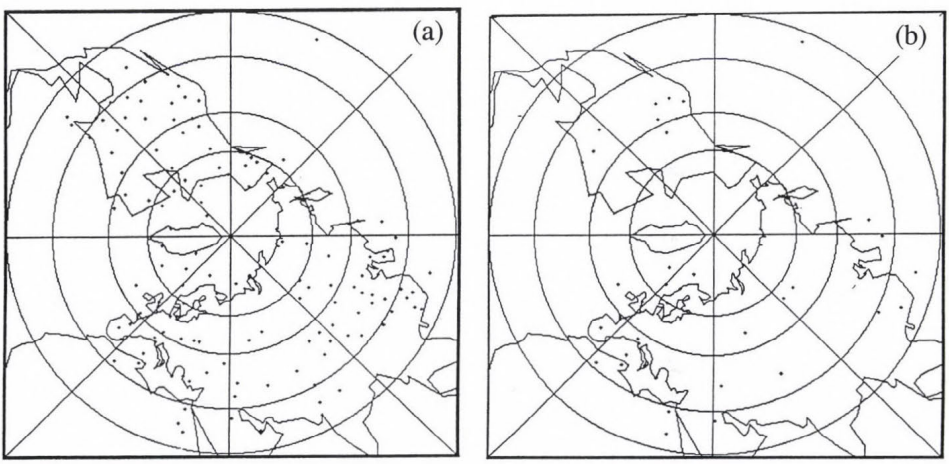

Fig. 2. Launching positions of CPBs; (*a*) 140 CPBs, (*b*) 40 CPBs.

By increasing the number of CPBs we could decrease the frequency of their launch. The period between the launches at the beginning can be chosen freely — 6 hours, 12 hours or 24 hours etc. —, but as soon as the coverage of the studied area reaches the necessary level for the concrete task, we can increase the interval between the launches up to 24 hours, 36 hours etc. According to our calculations, for example, in case of launching 140 CPBs at the beginning, we can increase the intervals between their launches on the third day (mean P about 480 km), while starting only with 40 CPBs (mean P about 640 km, after the second day) we need at least 4–6 days to obtain the same amount of information as in the first case.

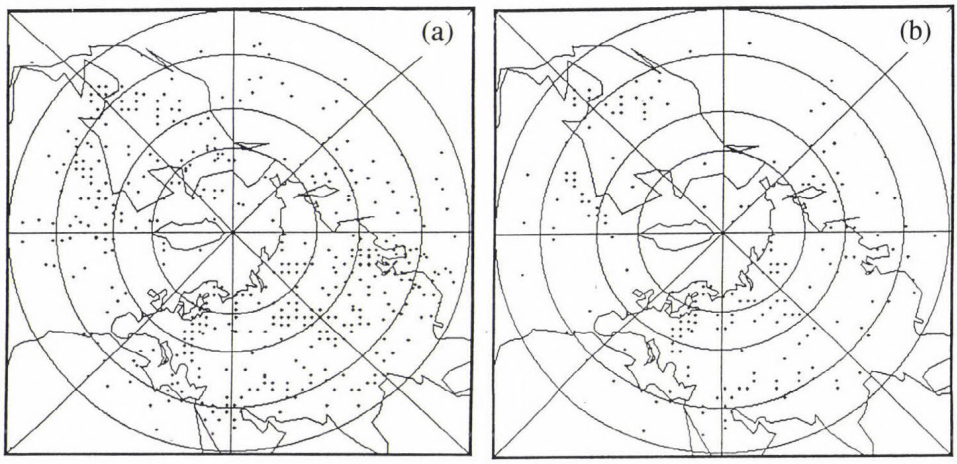

Fig. 3. Position of CPBs after the second day of launching using (*a*) 140 pieces, (*b*) 40 pieces.

The optimum number of CPBs strongly depends on the objective of the study. For example, when studying the synoptic situation in the atmosphere some dozens of CPBs could turn out to be enough and the frequency of their launching could be decreased in 3–4 days after starting. Such results are comparable with the results of other investigations (*Borisenkov et al.*, 1982). However, for applying CPB data as a *first guess* to assimilate satellite data (e.g. TOVS) one should use a greater number of CPBs (about 100), having about a 4-day *preliminary launching*[1] from places well separated from each other.

Based on the results discussed above, the realization of a CPB-satellite observation system which includes CPBs transmitting information through satellites (for example geostationary orbital satellites) seems to be feasible. The offered CPB system could be realized by using light weight balloons and could prove to be considerably cheaper than using the same amount of radiosondes. Some economic calculations are published in *Borisenkov et al.* (1982). The presented method, applied and realized on computer permits to model any kind of CPB-launching strategy based on real data.

[1] By preliminary launching we mean the period during which we reach the necessary coverage and after which we can decrease the frequency of launching.

4. Observing System Simulation Experiments (OSSE)

All simulation experiments have been performed by applying the adiabatic version of the hemispheric prognostic NWP model developed at the Russian Hydrometeorological Centre (Moscow, Russia) with the contribution of the Russian State Hydrometeorological Institute (St. Petersburg, Russia). This model is based on the dynamical equations of the atmosphere in quasi-static approximation (*Berkovitch,* 1982; *Berkovitch et al.,* 1982, 1985; *Kritchak*, 1981).

In order to perform the four-dimensional analysis, we used the geopotential, temperature, humidity and horizontal wind vector data taken from TEMP and SATEM information. We could not use TOVS radiance data because even if we had been able to get them we would have had a computer memory problem. Since we could not use real data measured by CPBs the calculation of balloon paths as well as the calculation of data that could have been measured by CPBs were carried out.

To analyze the impact of CPBs on the observing system the following numerical experiments (A, B, C) for four-dimensional data assimilation have been accomplished using the *continuous* data assimilation system (*Fig. 4*):

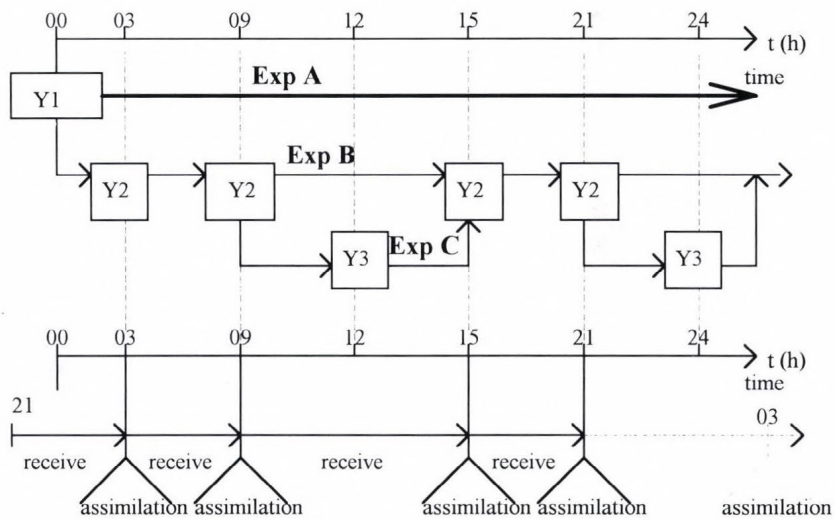

Fig. 4. Time steps of the data assimilation scheme.

Exp. A: 24 hour forecast.

Exp. B: Assimilation of SATEM and balloon data:

B1: run with SATEM data only;

B2: run with SATEM and balloon data (supposing "on level" measurements);

B3: run with SATEM and balloon data (supposing vertical profile measurements).

Exp. C: Assimilation of all available (SATEM, TEMP, balloon) data:

C1: run with TEMP, SATEM and balloon data (supposing "on level" measurements);

C2: run with TEMP, SATEM and balloon data (supposing vertical profile measurements);

C3: run with TEMP and SATEM data only.

This way of carrying out the experiments allowed us to estimate the impact of the balloon data on the assimilated fields.

4.1 Data assimilation schemes

Usually the data assimilation cycle is performed every 6 hours: 00, 06, 12 and 18 UTC. In the scheme applied in these analyses (see Fig. 4) there is a time displacement between the assimilation of the remotely sensed data (Y2) and the conventional ones (Y3). Such a structure allows to separate the asynchronous data from the synchronous ones (TEMP) and makes it possible to evaluate the impact of balloons on the forecast. Hereafter we give detailed description of **the important steps** in the different blocks of the assimilation scheme.

Y1. (Fig. 4): Initial data processing includes data interpolation to the grid.

Y2. (*Figs.* 4, 5): Assimilation of asynchronous (SATEM and CPB) data.

Step 1. The model uses Arakawa C grids, but it is more convenient to use uniform grids when assimilating the data.

Step 2. Simulation of the data of CPB measurements.

The simulated observation errors were calculated as a sum of two types of errors: random error and systematic error. If we assume that we can measure two variables, the air temperature and the geopotential height, we can model them as:

$$T_\eta^M = (\beta_T)_\eta + (E_T)_\eta + (E_T)_s \tag{2}$$

$$H_\eta^M = (\beta_H)_\eta + (E_H)_\eta + (E_H)_s \tag{3}$$

where β denotes the background values; H and T are the indices of the background values of the geopotential height or temperature; M is the index of the simulated values; s is the index of the systematic error; η is the index of CBP.

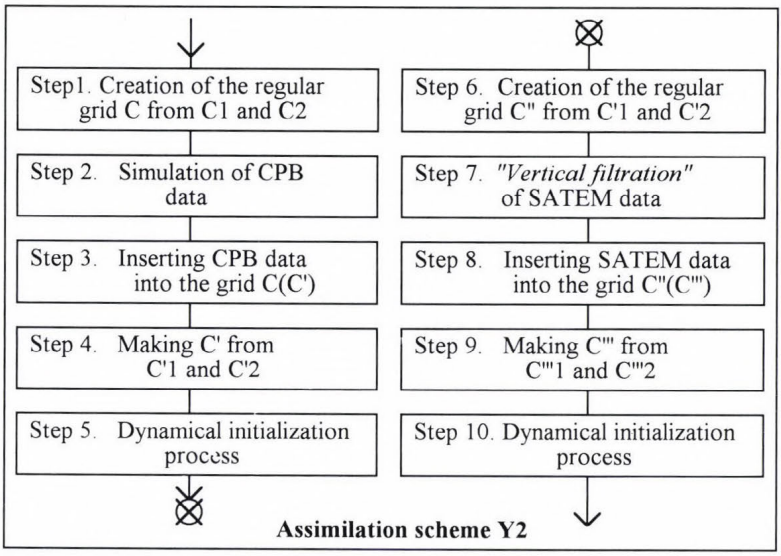

Fig. 5. Assimilation scheme for asynchronous data.

The generator of the random error is a random variable ξ for which:

$$-1 \le \xi(\sigma) \le 1, \tag{4}$$

where σ is an arbitrary random event. For an arbitrary error E_η:

$$-E_x \le E_\eta \le E_x, \tag{5}$$

where $E_\eta = \xi_\eta(E_x)$; E_x is the maximum possible error; x is a meteorological variable.

In case of vertical profile observations from balloons we have to simulate the "measured" profiles as well taking into account the profile of the systematic error of the geopotential height and the temperature. The following scheme was used to extrapolate data from the level of measurement in order to establish the profile in case of "on level" observation with balloons:

$$\gamma_\eta = \frac{1}{4} \sum_{i}^{i+1} \sum_{j}^{j+1} \gamma_{i,j}, \tag{6}$$

$$\gamma_{i,j} = \frac{\beta^T_{i,j,k+1} - \beta^T_{i,j,k}}{\beta^H_{i,j,k+1} - \beta^H_{i,j,k}}, \tag{7}$$

$$H^M_{\eta,k+1} = H^M_{\eta,k} + \frac{\overline{\beta^T_{\eta,k}}}{\gamma_\eta}\left[\left(\frac{P_{k+1}}{P_k}\right)^{\frac{-R\gamma_\eta}{g_0}} - 1\right] \quad \text{if} \quad \gamma \neq 0, \tag{8}$$

$$H^M_{\eta,k+1} = H^M_{\eta,k} + \frac{\overline{R\beta^T_{\eta,k}}}{g_0} \ln\left(\frac{P_{k+1}}{P_k}\right) \quad \text{if} \quad \gamma = 0, \tag{9}$$

where R is the gas constant for dry air; i, j are indices of the nearest grid point; k is the index of the model level; g_0 is the average value of the force of gravity on sea-level; $\overline{\beta^T}$ is the average grid background value.

$$\overline{\beta^T_{\eta,k}} = \frac{1}{4}\sum_{i}^{i+1}\sum_{j}^{j+1}(\beta_T)_{i,j}. \tag{10}$$

$T^M_{\eta,k+1}$ is calculated as below:

$$T^M_{\eta,k+1} = T^M_{\eta,k} + \gamma_\eta\left(H^M_{\eta,k+1} - H^M_{\eta,k}\right). \tag{11}$$

Step 5. For the dynamical assimilation the forward-backward method has been chosen.

Step 7. For the assimilation of satellite data we used the method described in *Lorenc* (1986). The assimilation of the relative humidity data was performed according to *Filiberti et al.* (1994) for levels 300, 500 and 700 hPa. For the other levels (where we did not have data of precipitable water amount) we used the equation given by *Tarakanova* in *Czelnai et al.* (1976) for the calculation of relative humidity. The assimilation of geopotential data was carried out by using the following algorithm:

(1) Geopotential thickness between 1000 hPa and P_k:

$$\Delta H_{g,k} = -(H_{1000} - H_k). \tag{12}$$

(2) Mean virtual temperature between P_0 and P_k:

$$T_{m,k} = \frac{g_0 \Delta H_{g,k}}{R \ln \frac{P_0}{P_k}}. \tag{13}$$

(3) Control: $$D_k = \Delta H_{g,k} - \Delta H_{s,k}.$$

Profiles were not taken into account if $P_0 < 1000$ hPa;

For $D_k > 500$ m: $$\hat{T}_{m,k} = T_{m,k}.$$

(4) $$\hat{T}_{m,i} = T_{m,i} + CK^T(KCK^T + E)^{-1} \cdot (\Delta H_{s,i} - \Delta H_{g,i}). \tag{14}$$

(5) $$\Delta \hat{H}_k = \frac{R\hat{T}_{m,k}}{g_0} \cdot \ln \frac{P_0}{P_k}, \tag{15}$$

(6) $$H_k = \Delta \hat{H}_k + H_{1000,g}, \tag{16}$$

where k is the index of the level, i is the index of the profile, g is the index of the background value, C is the error covariance matrix of T_m, s is the index indicating the satellite data, E is the observation error covariance matrix and K is a diagonal matrix, consisting of the elements $\frac{R}{g_0} \cdot \ln \frac{P_0}{P_k}$, $k = 1, 2 \ldots$

Y2'. (*Figs.* 4, *6*): Corrected version of the scheme Y2.

When applying scheme Y2, data were put on the grid in such a way that the nearest point on the grid had been identified for each data and its value had been given directly to that point. Simulation results demonstrated, however, that such an approach disturbs the horizontal structure of the meteorological fields (Fig. 8a). Therefore we decided to apply scheme Y2' (Fig. 6). In Y2' optimum interpolation (*Gandin et al.*, 1976) was included for assigning the data to the grid points.

Y3. (*Figs.* 4, *7*): This scheme was used when including the TEMP data into the analysis.

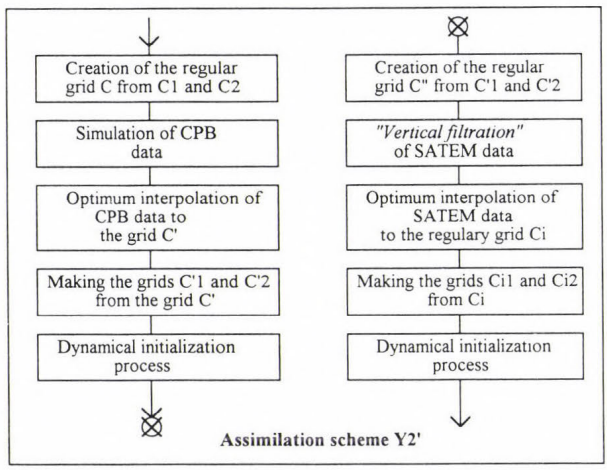

Fig. 6. Corrected assimilation scheme for asynchronous data.

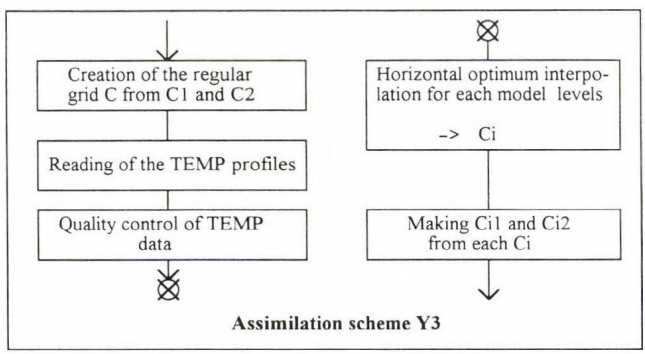

Fig. 7. Assimilation scheme for conventional data.

5. Results and conclusions

Evaluating briefly each of the methods that have been used, we can conclude the following:

(1) The dynamical initialization method has been tested on the basis of specially created noise[2]. The evaluation has been carried out using the results of the assimilation after four cycles of pseudo-forecast forward and

[2] The noises were created by adding non-realistic random values to the geopotential fields (see Eqs. (2) and (3) without systematic part of the errors) at randomly chosen points of the Northern Hemisphere.

backward (*Fig. 8a, 8b*). We can note a positive change of the structure of meteorological fields.

(2) The bias of the optimum interpolation of TEMP data (geopotential field for the 500 hPa level, at 12.00 UTC on 24.09.1993) into the grids is presented on *Fig. 9*. The results show that inside the observation area the error of optimum interpolation is small and it increases towards the edges.

(3) The improvement of the relative humidity field retrieved using the quantity of precipitable water (SATEM) is presented on *Fig. 10* for the 700 hPa level. Comparing the maps we can note that after the assimilation the relative humidity field changed in a positive way. We can observe analogous changes in the case of the retrieval of the geopotential using Step 7 of the block Y2 (*Fig. 11*) in the assimilation scheme.

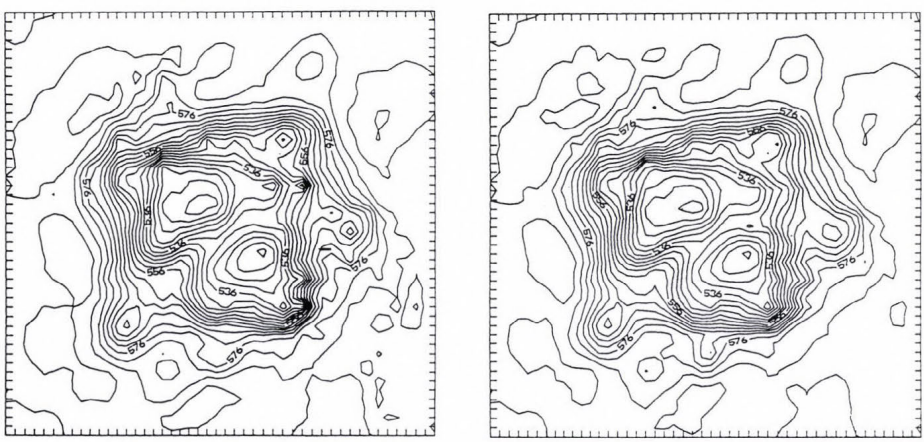

Fig. 8. 500 hPa geopotential field: before (*a*) and after (*b*) dynamical initialization (Y2); (03.00 UTC 24.09.1993; unit is 10 m).

From the assimilation results of the CPB-satellite complex the following conclusions can be made using quantitative evaluation (see Fig. 12 and Fig. 13):

(1) The impact of SATEM data on the forecast (exp. B1) is slightly positive. This result does not contradict the conclusions of earlier studies (*Eyre,* 1989; *Eyre et al.*, 1989; *Filiberti et al.*, 1994; *Riley et al.*, 1995) according to which it is difficult to show the positive impact of the satellite data in the Northern Hemisphere. On the other hand, using variational technique, a bigger impact of SATEM data in the Northern Hemisphere was found with the French forecasting system (ARPEGE) (*Randriamampianina et al.*, 1997). The accuracy of the analysis is outstanding for the 1000 hPa level field.

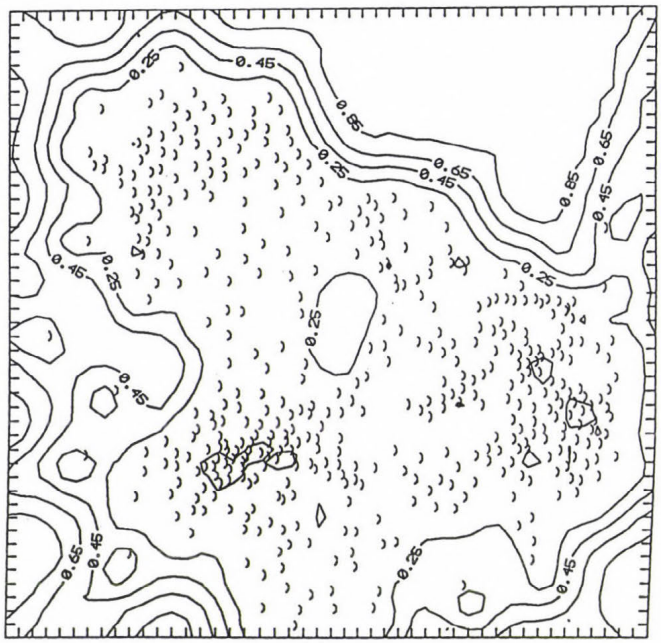

Fig. 9. Relative error of OI of TEMP data to the grid (geopotential field for the 500 hPa level at 12.00 UTC 24.09.1993).

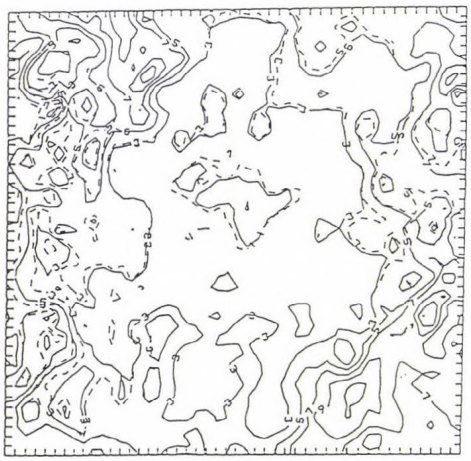

Fig. 10. 700 hPa relative humidity field before (dashed) and after (solid) the assimilation; (21.00 UTC 24.09.1993; unit is g/kg).

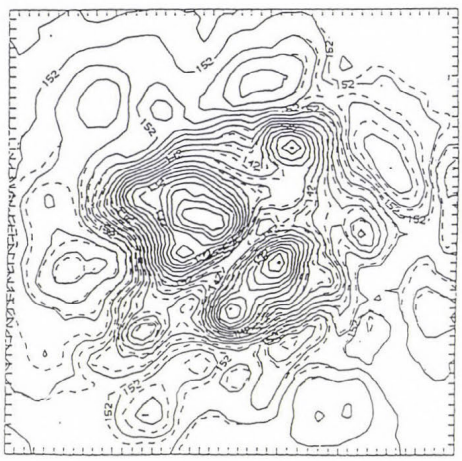

Fig. 11. 850 hPa geopotential field before (dashed) and after (solid) the assimilation; (21.00 UTC 24.09.1993; unit is 10 m).

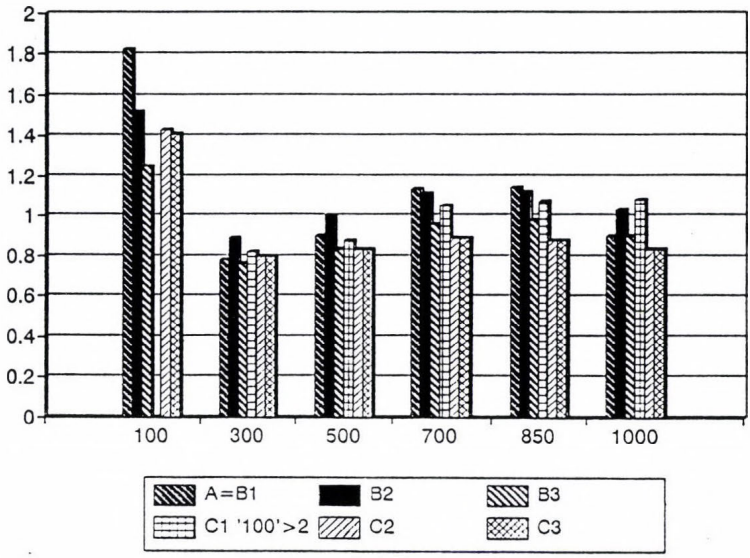

Fig. 12. Root mean square error of geopotential after 24 hour assimilation on the 100, 300, 500, 700, 850 and 1000 hPa levels.

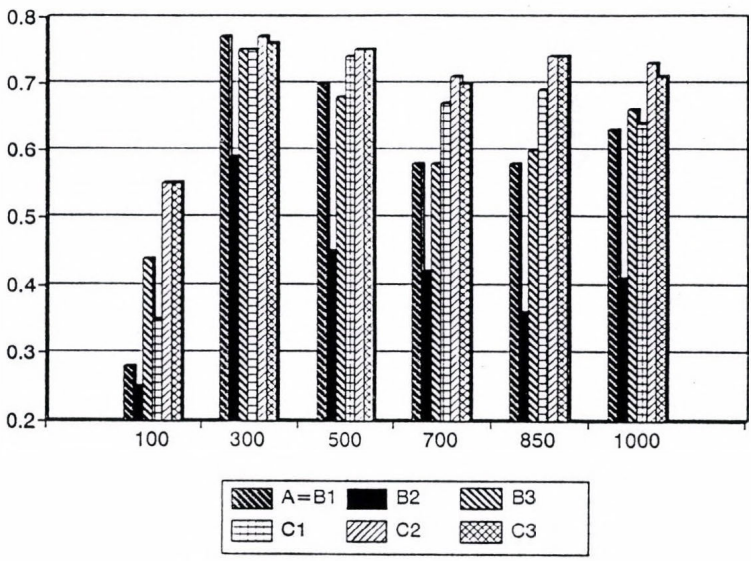

Fig. 13. Correlation between NMC and our analyses after 24 hour assimilation on the 100, 300, 500, 700, 850 and 1000 hPa levels.

(2) The chosen vertical extrapolation method is very poor. As a consequence, analysis B2 became even worse than B1, with the exception of the 300 hPa level. Therefore, it is necessary to improve the extrapolation method.
(3) All results of the assimilated fields improved in case of the assumption that CPBs can make measurements of vertical profiles of meteorological elements — see exp. B3 (the correlation for the 100 hPa level, for example, was around 0.44, while it was 0.25–0.28 in the other cases).
(4) In case of experiments of the third group (C) we could reach a considerable improvement by adding TEMP data to the assimilation. However the problem of data extrapolation still exists in this case of assimilating all available data. We also received the best results when we used vertical CPB measurements (C2).

Therefore, applying the CPB-satellite measurement complex with vertical CPB measurements one can improve the quality of the analyses of asynchronous data. In the case of "on level" CPB measurements however, the improvement of vertical data extrapolation is very important as well.

The perspectives of efficiently using a 4D assimilation based on balloon-satellite observation system seem to be the following:

(1) The model-assimilator used in the present study is a quite simple one — a hemispheric adiabatic model with 300 km resolution. It would be necessary to add non-adiabatic factors to get more reliable results.
(2) When starting this study we intended to use more observation types in the assimilation. However, we faced a lot of problems related to the available data and computer memory limit; so only the TEMP and SATEM data were used. It is necessary to mention here that we were given data only for a two-day period (24 09 1993–25 09 1993). In order to be able to draw more valid conclusions when studying the impact of CPB data on the analysis of synchronous and asynchronous observations, a longer experimental period is required.
(3) In *Borisenkov et al.* (1982) CPBs were assumed to be suitable for performing vertical profile measurements. It would be interesting to consider the possibility of using CPBs that could carry out vertical profile measurements based on LIDAR or RADAR principles.
(4) It would be interesting to perform the same experiments treating the satellite–CPB system as an autonomous source of all measured data in 4D assimilation.

Acknowledgements—Partial support for this work has been provided by Hungarian Scientific Joint Foundation F015963 and T014933. The authors wish to thank *B. D. Panin, T. Práger, G. Major, J. Pailleux, Yu. A. Pichugin, O. M. Pokrovski* and *Zs. Ruzsbatzky* for helpful discussions.

References

Bengtsson, L., 1975: 4-dimensional assimilation of meteorological observation. *GARP Publication series*, No. 15. 75 p.

Berkovitch, L.V. and *Tkachev, Yu.V.*, 1982: A non-adiabatic hemispherical model of atmosphere for forecast of meteorological elements up to some days (in Russian). *Trudy GMC USSR*, edition 242.

Berkovitch, L.V and *Tkachev, Yu.V.*, 1985: The evolution of the hemispherical atmospheric model (in Russian). *Trudy GMC USSR*, edition 277.

Berkovitch, L.V., 1982: A six levels scheme of forecast based on completes equations for a large territory (in Russian). *Trudy GMC USSR*, edition 100.

Borisenkov, E.P., Alter-Zalik, Yu.G. and *Kuznitsov, A.D.*, 1982: *Atmospheric Sounding with Meteorological Balloon* (in Russian). Gidrometeoizdat, Leningrad, 176 p.

Czelnai, R, Gandin, L.S. and *Zachariew, W.I.*, 1976: *Statistical Structure of Meteorological Fields*. Hungarian Meteorological Service.

Eyre, J.R., 1989: Inversion of cloudy satellite sounding radiances by nonlinear optimal estimation. I: Theory and simulation for TOVS. *Quart. J. Roy. Meteorol. Soc. 115*, 1001-1026.

Eyre, J.R. and *Lorenc, A.C.*, 1989: Direct use of satellite sounding radiances in numerical weather prediction. *Meteorological Magazine 118.*

Filiberti, M.A., Eymard, L. and *Urban, B.*, 1994: Assimilation of satellite precipitable water in a meteorological forecast model. *Quart. J. Roy. Meteorol. Soc. 122*, 486-506.

Gandin L.S. and *Kagan, R.L*, 1976: *Statistical Interpolation Methods of Meteorological Fields*. Gidrometeoizdat, Leningrad, 356 p.

Koffi, E., Nodop, K. and *Bénech, B.*, 1997: Constant volume balloon model used to derive tracer plume trajectories (ETEX experiment first release). *ETEX symposium on long-range transport, model verification and emergency response*, 13-16 May 1997, Vienna Austria.

Koffi, E., Nodop, K. and *Bénech, B.*, 1997: Constant volume balloon model used to derive tracer plume trajectories (ETEX experiment second release). *ETEX symposium on long-range transport, model verification and emergency response*, 13-16 May 1997, Vienna Austria.

Kritchak, S.O., 1981: A non-adiabatic model of atmosphere based on primitive equations to forecast the meteorological elements above Europe (in Russian). *Met. and Hydr.*, edition 7.

Mills, G.A., Downey, W.K. and *Whitby, F.*, 1994: Trajectory calculations in support of meteorological planning and forecasting for two transcontinental balloon flights. *Aust. Met. Mag. 43*, 29-39.

Lally, V.E. and *Rickel, A.B.*, 1967: Project GHOST. *Science*, 1967 June, 60-65.

Lorenc, A.C., 1986: *Technical Proceedings of the Second International TOVS Study Conference*. 18-22 Feb 1985, Igls, Austria, pp. 224-253.

Randriamampianina, R., Pailleux, J., Thépaut, J.-N. and *Moll, P.*, 1997: The impact of the satellite TOVS data in 3D variational analysis at Météo France. *Technical Proceedings of the ninth International TOVS Study Conference*, 20-26 Feb 1997, Igls, Austria.

Riley, P., Steinle, P., Hart, T. and *Kelly, G.*, 1995: The impact of 1DVAR TOVS retrievals compared to NESDIS retrievals on 5 day global forecasts. *Technical proceedings of the eighth international TOVS study conference*, Queenstown, New Zealand.

Reshetov, V.D., 1973: *Variability of Meteorological Elements* (in Russian). Gidrometeoizdat, Leningrad.

Sitbon, P., 1975: Platform location and data collection by satellite systems. The EOLE experiment. *IEEE Trans. Geosci. Electron. 13*, No. 1, 2-17.

Smith, W.L., Woolf, H.M., Hayden, C.M. and *Schreiner, A.J.*, 1985: *Technical Proceedings of the Second International TOVS Study Conference*, 18-22 Feb 1985, Igls, Austria, pp. 224-253.

BOOK REVIEW

Ernő Mészáros: **Atmospheric Chemistry** (in Hungarian). *Issued by:* Veszprémi Egyetemi Kiadó. 57 figures and 22 tables, 167 pages.

The principal goal of the book is to discuss the chemical processes and related phase transitions occurring in the Earth's atmosphere. They are in close connection with the biogeochemical cycle of elements and the consequences of anthropogenic activity. The book contains 8 *Chapters* and 4 *Annexes*.

Chapter 1 summarizes the basic characteristics of the atmospheric radiation transfer, photochemical and thermal reactions as well as the formation of free radicals in the atmosphere. In *Chapter 2* the chemistry of upper atmosphere is described including the structure of the ionosphere (E, F and D layers). *Chapter 3* is dedicated to the ozone problem in three sub-chapters: Homogeneous chemistry of the stratosphere; Heterogenous processes in the stratosphere (with special attention to the formation of ozone hole); Tropospheric ozone. In *Chapter 4* reader is provided with the explanation of gas-phase reactions of carbonaceous components. Reduced and oxidized sulfur compounds are discussed in *Chapter 5*, including the emission, chemical transformation and deposition of these species. *Chapter 6* describes the characteristics, dynamics and chemical composition of aerosol particles. Effects of particles on climate control are also discussed in this chapter. The role of water in the control of chemical processes, including cloud and precipitation formation, deposition processes of trace components as well as chemical composition of cloud and precipitating water is presented in *Chapter 7.* Basic atmospheric transport models and their applications are introduced in the last chapter. It is also emphasized here that modeling can only be a powerful tool in the case if it is applied together with high quality measurements. More than 100 references are cited for the eight chapters.

The textbook is proposed to read first of all for students studying chemistry, meteorology, environmental engineering and environmental sciences, however, it will be useful for scientist who are interested in a young science between meteorology and chemistry, in close connection with the problems of environmental protection. Most recent and widely published atmospheric issues like stratospheric ozone hole formation or tropospheric ozone formation in pollutant air are explained in details in the book.

László Bozó

NEWS

Second Conference on Forest and Climate (SCFC) Sopron, Hungary 4–6 June 1997

Hungarian meteorologists, foresters, biologists and ecologists held a common meeting for the second time in order to discuss the interrelation of the forest and climate as well as the impact of global warming first of all on the ecosystem and on the modification of the radiation-, heat- and water-budget of the forest. The responsible experts, as participants of the First Conference on Forest and Climate (FCFC) in Noszvaj (Hungary) from 1–3 June 1994, agreed to announce that such common scientific meeting should be organized in the future, as well. They thought that every three years so much new results would gather in our country in the research of the interrelation system of forest and climate that these could be discussed in a common meeting by the interested specialists.

In the spirit of the above mentioned thoughts the SCFC was held in Sopron, Hotel "Siesta" located among the beautiful "Lővérek" (pine forests), 4-6 June 1997.

The unusually successful, effective and very instructive scientific conference was organized by the Meteorological Department of Kossuth Lajos University of Debrecen and the Department of Science of Knowledge for the Arable Site of the Forestry University of Sopron with the support of the Debrecen Team of the Hungarian Meteorological Society, the National Forestry Assembly and the Meteorological Working Group of the Territorial Commission in Debrecen of the Hungarian Academy of Sciences.

The papers delivered at the conference were focused on discussing the newest results reached in the field of the following three main subjects:

- new results in Hungary in the topic of a possible climate change (global warming),
- development possibilities of the forestry climate classifying methods,
- interrelations between the forestal ecosystem and the atmospheric processes near the ground.

These topics show that the forestry climatology (whose founder in our country was *Károly Botvay*, professor of the University of Sopron) covers a wide range of relations between forestal and environmental factors, implies environmental changes on micro- and macro-scales, as well as local and regional environmental problems. When having defined the subjects of the conference, the role of meteorological transfer processes in the formation of micro-climate of the forest stand, as a new investigational branch, was stressed.

As it is known, these processes are based on a self-adjusting system of dynamical processes of the radiation-, heat- and water-balance in the forestal ecosystems (stands) and between the forest and atmospheric layers near the ground, as well.

Since the microclimate of the forest is controlled by processes of energy balance, when the call for papers was issued the conference organizers emphasized that the processes of energy transformation of the forest stand should be studied, known and understood with an increasing intensity. Namely, the expected and also under way modifications of forest climate, which are produced by the joint effect of the global environmental changes (warming, acid rain, ozone layer depletion, concentration increase of air pollutants, modification of global circulation systems, decrease of diversity of fauna and flora species, consequences of global social and economical changes, etc.) and the local forest management (cultivation, deforestation, afforestation) can be modelled and forecasted only if we know these processes.

Nearly hundred participants listened to 43 papers about the mentioned topics. Besides papers treating general relationships, information was given about numerous investigational results based on in situ measurements in some forests (Sopron Hills, Síkfőkút, Mátra, Park Forest of Pilis, Zala Hills), while directing an outstanding attention to oaks, beeches, spruces and mixed forest stands in lowlands. Similarly to the FCFC, at this meeting several papers were also concerned with the role of noxious insects depending on climate. The relation between the forest management and climate change, the damage done by sleet, mapping of environmental evaluation as well as energetic utilization of the forestry waste were also mentioned.

Meteorological "output" of the conference were a survey of regional consequences of global climate change in terms of scenarios, the establishment of possibilities and limitations of genetical and migration conditions of the forest adaptation, and the assessment of the rate of spatial and temporal variations of trends and extremes in the time series of precipitation and temperature.

More than ten presentations dealt with the changes of radiation-, heat- and water-budget components and temperature, precipitation and soil moisture conditions within the forest stand, moreover with nitrogen budget and the exchange conditions of trace gases in the forestal ecosystems. Furthermore, the audience could get information about a few new measuring and calculating techniques, which have been applied by Hungarian scientists to discover the microclimatic and ecological system of the forest. Some papers discussed the causes of the forest degradation and outlined the tasks of forestry for saving and meliorating the forest stands.

As it was already emphasized by the speakers and contributors at the FCFC the hygienic state of our forests has been gradually deteriorating in which the drought, occurring with greater frequency and greater intensity in the last two

decades than earlier, has played a significant role. The more frequently observed, prolonged and considerable lack of precipitation has caused that the forestal ecosystems is becoming feebler and consequently there is a degradation of individuals of some species. This process is accelerated by the acid rain water and the multiplication of pathogens due to the more extreme weather phenomena. It seemed to be proved that as a consequence of the anthropogenic activities the forestal ecosystem became more sensitive and more vulnerable. This tendency is certainly strengthened by global changes (among others global warming) and it may be assumed that these variations are faster than the acclimatization ability of biocenosises of forests — as it was established by the participants of the conference.

The investigational achievements in topics discussed at the SCFC not only increase the scientific knowledge but can contribute to the scientific foundation of a more modern forest management, to the planning of the afforestation, considering environmental conditions of the next century, and to the professional foundation of the expansion of our forested areas (in the future decades a new afforestation in an area of about one million hectare is planned in Hungary, which will increase the forested area of our country by one-third part of the present extension). The participants of the SCFC also expressed their desire that the newest forestry investigational results should be considered and utilized when the Hungarian Parliament will codify a new forest law in the future. For this reason the conference formulated proposals, and a working group was deputed to compile their final version. The organizers are intending to publish the papers presented at the conference, including the proposals as well.

On the first afternoon of the conference the participants, professionally guided by *Péter Víg* first assistant, could study the radiation-, heat- and water-balance measuring station of the University of Sopron on the site in the forests of Sopron Hills region. It was an outstanding program of the conference, when a statue of *Prof. Károly Botvay* was inaugurated in the Botanical Garden of the University of Sopron.

The successful organization of the SCFC may be owed to *Dr. Károly Tar* university lecturer, the leader of the Meteorological Department (Kossuth Lajos University of Debrecen) and *Dr. Péter Víg* first assistant (University of Sopron) as well as their co-workers who performed really cautious, tiring and altruistic work. On behalf of the conference participants I would like to express my congratulations and thanks to the above mentioned colleagues for the excellent organizing of this meeting which was very useful and enjoyable for all participants.

Emánuel Antal

The 1997 EUMETSAT Meteorological Satellite Data Users' Conference Brussels, Belgium 29 September–3 October 1997

The 1997 EUMETSAT Meteorological Satellite Data Users' Conference was held in Brussels from 27 September to 3 October. Earlier the Meteosat and NOAA Users' conferences were organized separately in every two years, but from the previous year they are joined into one common conference. In this year the conference was organized and sponsored by the European Organization for Exploitation of Meteorological Satellites (EUMETSAT) and the Belgian Royal Meteorological Institute.

The conference began with the opening remarks by the Minister of Sciences of Belgium, the head of the Belgian Royal Meteorological Institute and *Dr. Tillmann Mohr*, the director of EUMETSAT.

The conference gave good opportunity for the users of data of the meteorological satellites to exchange experiences. New methods, applications and algorithms were presented mainly for Meteosat and NOAA data, but there were also presentations on GOES satellite data and application of microwave instrument SSM/I of DMSP American satellite. We obtained useful information on other geostationary satellites as well, like the Russian GOMS, INSAT of India and technical characteristics of the Chinese meteorological satellite to be lunched soon.

The presentations were separated into five sessions: Operational applications, Data processing, Pre-processing for products, Derivation of geophysical parameters and Current and future satellite systems. Two additional sessions were organized, one on Calibration and the other on Satellite Application Facility (SAF) groups. In addition to the oral sessions, a poster session, including software presentations, was also held; this, concerning the principal importance of the visualization of satellite imagery, proved to be highly useful and efficient. The posters were hanged in the foyer of the auditorium during the whole week, and all poster authors held a 3-minutes verbal presentation as well.

The short-wave spectral bands of Meteosat and NOAA satellites do not have in-flight calibration. The 1. and 2. channels of NOAA/AVHRR instrument have pre-launch calibration but the visible cannel of Meteosat does not have any. A special session was held on methods of the indirect after-launch calibration and the cross-calibration of the different satellites.

A large number of presentations reported on cloud detection and cloud classification. For NOAA satellites these methods are mostly threshold methods like the APOLLO (for the region of the Alps) and the SCANDIA (developed for Sweden), but methods based on statistical investigations were also shown. For the region of the Alps a cloud coverage statistics for a five year period was presented. The SCANDIA method applies more thresholds, it is not only for

cloud detection but also for cloud classification. For Meteosat images a method called MET'clock was presented for cloud detection and cloud top height retrieving.

Several talks discussed the methods for detection of meso-scale convective systems and estimation of the expected rainfall.

Other papers presented methods for identification of clouds giving a large amount of precipitation and for rainfall estimation. For the mid-latitudes these methods apply simultaneously SSM/I and NOAA/AVHRR data.

The operational cloud motion wind vectors are among the most important products retrieved from Meteosat data. Many presentations were held on this topic, on the accuracy of the vectors and on further developments.

Other papers presented methods for the application of satellite information in vegetation monitoring and crop yield estimation. Investigations were shown on fire detection mostly for the tropics but also for Spain.

In the last session the plans for the main further developments were presented. The expected launch time of the Meteosat Second Generation (MSG) is October 2000. The SEVIRI, the imagery system of the MSG will be ready in February 1999. EUMETSAT plans to launch two new own quasi-polar orbiters called METOP. The new version of American NOAA satellites will be launched in 1998 working with 6 or 7 channels.

In the Education Program of EUMETSAT an interactive program package is elaborated, some parts of that is already working on the Internet in field of satellite meteorology and numerical prediction (http://eumetsat.meteo.fr).

Dr. Anikó Rimóczi-Paál presented a paper titled 'Mapping of Radiation Balance Components for Hungary Using Meteosat Data' in the session Derivation of Geophysical Parameters. *Dr. Mária Putsay* presented a poster titled 'Atmospheric correction of NOAA/AVHRR visible and near-IR channels in Hungary'. Both presentations drew a great interest, and some scientists asked for reprints.

The presented papers will be published in the conference proceedings.

The next conference in this field will be organized in Paris, in May 1998 by METEO-France.

Mária Putsay
Anikó Rimóczi-Paál

ATMOSPHERIC ENVIRONMENT

an international journal

To promote the distribution of Atmospheric Environment *Időjárás* publishes regularly the contents of this important journal. For further information the interested reader is asked to contact *Prof. P. Brimblecombe*, School for Environmental Sciences, University of East Anglia, Norwich NR4 7TJ, U.K.; E-mail: atmos_env@uea.ac.uk

Volume 31 Number 14 1997

The Lower Fraser Valley oxidants/Pacific '93 field study

Volume 31 Number 15 1997

Volume 31 Number 16 1997

Special Issue on the Great Dunn Fell Clad Experiment 1993, Eurotrac sub-project Ground-based Cloud Experiment (GCE)

Volume 31 Number 17 1997

IDŐJÁRÁS

VOLUME 101 * 1997

BUDAPEST, HUNGARY

AUTHOR INDEX

TABLE OF CONTENTS
I. Papers

II. Book review

III. News

Contents of journal Atmospheric Environment, 1997

IV. SUBJECT INDEX

The asterisk denotes book review or news

NOTES TO CONTRIBUTORS

The purpose of *Időjárás* is to publish papers in the field of theoretical and applied meteorology. These may be reports on new results of scientific investigations, critical review articles summarizing current problems in certain subject, or shorter contributions dealing with a specific question. Authors may be of any nationality but papers are published only in English.

Papers will be subjected to constructive criticism by unidentified referees.

* * *

The manuscript should meet the following formal requirements:

Title should contain the title of the paper, the names(s) of the author(s) with indication of the name and address of employment.

The title should be followed by an *abstract* containing the aim, method and conclusions of the scientific investigation. After the abstract, the *key-words* of the content of the paper must be given.

Three copies of the manuscript, typed with double space, should be sent to the Editor-in-Chief: *P.O. Box 39, H-1675 Budapest,* Hungary.

References: The text citation should contain the name(s) of the author(s) in Italic letter or underlined and the year of publication. In case of one author: *Miller* (1989), or if the name of the author cannot be fitted into the text: *(Miller,* 1989); in the case of two authors: *Gamov* and *Cleveland* (1973); if there are more than two authors: *Smith et al.* (1990). When referring to several papers published in the same year by the same author, the year of publication should be followed by letters a,b etc. At the end of the paper the list of references should be arranged alphabetically. For an article: the name(s) of author(s) in Italics or underlined, year, title of article, name of journal, volume number (the latter two in Italics or underlined) and pages. E.g. *Nathan, K. K.,* 1986: A note on the relationship between photosynthetically active radiation and cloud amount. *Időjárás 90,* 10-13. For a book: the name(s) of author(s), year, title of the book (all in Italics or underlined with except of the year), publisher and place of publication. E.g. *Junge, C. E.,* 1963: *Air Chemistry and Radioactivity.* Academic Press, New York and London.

Figures should be prepared entirely in black India ink upon transparent paper or copied by a good quality copier. A series of figures should be attached to each copy of the manuscript. The legends of figures should be given on a separate sheet. Photographs of good quality may be provided in black and white.

Tables should be marked by Arabic numbers and provided on separate sheets together with relevant captions. In one table the column number is maximum 13 if possible. One column should not contain more than five characters.

Mathematical formulas and *symbols:* non-Latin letters and hand-written marks should be explained by making marginal notes in pencil.

The final text should be submitted both in manuscript form and on *diskette.* Use standard 3.5" or 5.25" DOS formatted diskettes for this purpose. The following word processors are supported: WordPerfect 5.1, WordPerfect for Windows 5.1, Microsoft Word 5.5, Microsoft Word 6.0. In all other cases the preferred text format is ASCII.

* * *

Authors receive 30 *reprints* free of charge. Additional reprints may be ordered at the authors' expense when sending back the proofs to the Editorial Office.

Published by the Hungarian Meteorological Service

Budapest, Hungary

INDEX: 26 361

HU ISSN 0324-6329